Overtopping Breaching of Rock-Avalanche Dams

A thesis

submitted in partial fulfilment of

the requirements for the degree of

Master of Engineering

at the

University of Canterbury

by

Jeremy Scott Wishart

UNIVERSITY OF CANTERBURY

2007

Abstract

River blockages formed by rock avalanches appear to pose a higher hazard potential than other landslide dams, given the extreme run-out distances and volumes of rock avalanche deposits. Recent research has identified rock avalanche deposits to have internal sedimentology consisting of a coarse surficial material (carapace) and a finer fragmented interior (body) potentially of critical importance to rock-avalanche dam stability. Physical scale modelling of overtopping failure and breach development in rock avalanche dams was used to quantify the influence of this sedimentology on critical breach parameters, and their prediction using existing embankment dam breach technologies. Results from this study indicate that the time to failure for rock avalanche dams is approximately twice that observed for homogeneous dams due to the armouring properties of the carapace; and that peak discharge is not significantly affected by sedimentology. While application of empirical, parametric, dimensional and physically based models indicated that uncertainty associated with predicted dam break discharges could range from ±19% to ±107%, no modelling technique was able to simulate the armouring phenomenon adequately. Comparison of actual and simulated breach evolution shows linear assumptions of breach depth and width development (as observed in homogeneous dams) to be incorrect. In the context of hazard management, the results suggest that empirical regression relationships should be used for rapid assessment of potential dam break flood magnitude.

Acknowledgements

Completion of this research has been extremely challenging, yet hugely rewarding. The physical testing requirements for this study extended both human and lab resources to their limits dragging unprecedented volumes of sediment through an immaculately kept Fluids Lab (much to Ian's horror). The influence of sediment volumes on equipment alone was evident in the technical failure of 3 video cameras, the drying oven and transport crane. I am therefore indebted to the indispensable assistance of Ian Sheppard, Kevin Wines, Peter McGuigan and Richard Newton for their continual service, incredible patience throughout ongoing changes to model design and friendship during the five months I spent testing in the lab.

I am especially grateful to Assoc. Prof Tim Davies for his guidance, discussion and immense patience throughout the course of this study. This study also benefited from the assistance of Dr. David Painter, Dr. Vern Manville (GNS) and Murray Gillon (Damwatch).

The opportunity to study as a postgraduate would not have been possible without the financial support from the Todd Foundation for Excellence and the New Zealand Freemasons to whom I am both extremely thankful.

To my family, thanks for the continual support throughout my time at university. To my wonderful officemates in E324, Thorbjoerg (for all the support, the "real" coffee and endless conversation on Iceland), Per (for your hunting stories) and Jodie (always in defence of Timaru) thanks for making my time in engineering so memorable. For all the bluegrass, basketball and tennis - thanks so much Greg; it preserved my sanity. To Desiree, Jess, Dave, Josiah, Gloria, and the Americans, thanks for being wonderful friends. All the Tragedy boys; cheers for letting me turn up late to gigs and miss countless practices. Thanks also to Monique and Ranee for their invaluable assistance.

And finally, Philippians 4:13; it took this masters for me to realise its significance.

Contents

List of Figures

List of Tables

Notation

a	*regression coefficient*
A_s	*surface area of lake at level of dam crest*
B	*average breach width*
B_{eb}	*base level for breach erosion*
c_v	*velocity correction for exiting flow upstream of breach*
C	*coefficient*
C_d	*drag coefficient*
C_{max}	*cross sectional profile at the breach inlet (crest maximum)*
d	*lake depth*
d_{30}	*grain-size than which 30 % of the total material is finer*
d_{50}	*grain-size than which 50 % of the total material is finer, median grain-size*
d_{90}	*grain-size than which 90 % of the total material is finer*
d_B	*depth of breach*
d_c	*critical flow depth*
d_m	*mean roughness height (approximated by $d_s/3$)*
d_s	*equivalent stone diameter (d_{50})*
D	*total drop in lake level during flood*
D_c	*dam height relative to crest*
f	*breach shape factor*
F_r	*Froude number*
F_{r^*}	*grain size Froude number*
g	*acceleration due to gravity*
h	*elevation of the lake surface*
h_b	*elevation of the breach bottom*
h_d	*water depth over the base of the breach (feet)*
H_b	*head over the breach*
k	*breach erosion rate*
k^*	*dimensionless breach erosion rate*
k_s	*tailwater submergence correction factor*
k_o	*failure mode constant*
K_r	*the bed grain roughness*
K_s	*Srickler coefficient for no wall drag*

m *lake hypsometry factor*

n *Manning roughness (friction) coefficient*

P *perimeter of breach*

q *volumetric water discharge per unit width (m^3/s)*

q_{sb} *volumetric sediment discharge per unit channel width*

q_c *critical unit discharge per unit width (m^3/s)*

Q_b *breach discharge*

Q_e *estimated breach discharge (cusecs)*

Q_p *peak discharge*

Q_p* *dimensionless peak discharge*

r *ratio of basal breach width to breach depth*

R_e *Reynolds' number*

R_{e*} *Reynolds' grain size number*

S *channel slope*

t *time*

t_b *breach development time*

u *flow velocity*

y_m *mean water depth relative to slope*

v_c *critical velocity*

V_* *shear velocity*

V_o *excess volume of lake*

V_o* *dimensionless excess volume of lake*

V_r *excess volume of lake (acre-ft)*

W_B *breach basal width*

W_T *breach top width*

W_m *minimum width cross sectional profile (breach outlet position)*

X *lake or dam characteristic*

z *breach sidewall slope*

τ *bed shear stress*

τ_c *critical shear stress*

γ_s *specific weight of sediment*

γ_w *specific weight of water*

λ *scaling factor*

η *dimensionless parameter*

α *bedslope angle*

θ *angle of dam upstream and downstream face (inclination to horizontal)*

θ_r *the critical dimensionless shear stress*

δ *angle of repose of bed material*

σ *aeration factor*

ϕ *dimensionless sediment transport rate*

ρ *density*

ρ_s *density of sediment*

ρ_w *density of water*

μ *dynamic viscosity*

υ *kinematic viscosity*

Chapter 1 Introduction

1.1 Introduction

Rock avalanches are catastrophic mass movements derived from the failure of a volume of > $1x10^6$ m^3 of bedrock in regions of predominantly steep terrain worldwide. The deposits of these events often cause temporary or permanent blockages of mountain drainage networks due to their high volume and ability to run-out for considerable distances both across- and along-valley. Of the many landslide types that generate natural dams, rock-avalanche deposits pose perhaps the greatest hazard, given their runout distances, volumes and elevations.

Many landslide dams are ephemeral features on the geo(morpho)logical timescale owing to their rapid formation and generally short lives; they are usually initiated by excessive precipitation, snowmelt or seismicity. The temporary blockage of river channels by landslide dams can pose a substantial hazard to infrastructure and settlements downstream due to the potential for catastrophic failure (usually from overtopping). Failure often occurs a short time after formation; 50% of breached landslide dams documented worldwide failed within 10 days of formation (Costa and Schuster, 1988). Very large natural dams however, can remain intact for millennia: life expectancy of natural dams has therefore ranges from several minutes to several thousand years, depending on factors including valley shape, volume, size, shape, composition and sorting of blockage material, rates of seepage through the blockage and rates of sediment and water flow into the newly formed lake. When a dam is emplaced it is very difficult to predict when, or whether, it will fail; hazard management must be based on the conservative assumption that it will fail. Consequently, understanding how the characteristics of natural dams influence the peak outflow of resulting dambreak floods is of critical importance for effective hazard management.

Managing hazards such as landslide dams requires an understanding of the temporal and spatial scales on which such phenomena operate. Much previous work on landslide dams has been mainly descriptive in character, and has produced a multitude of documented case studies and inventories (e.g. Costa and Schuster, 1988; Costa and Schuster, 1991). More recent work has focussed on quantitative methods of determining the post-formation development, in particular the controls on dam longevity (Ermini and Casagli, 2003; Manville, 2001; Korup, 2004, 2005; Schuster, 2000).

Although the failure mechanisms of landslide dams are relatively well understood (overtopping, piping, seepage, etc) from extensive engineering research on artificial dams, little is known about the actual processes involved given the few direct observations of and data on landslide dam failures. Landslide dam failure is still frequently modelled as a homogenous earthen dam failure, because the mechanism of

breach formation is considered very similar, despite obvious differences in dam geometry and material properties.

Lithological composition and barrier geometry have been found to influence landslide dam longevity (Dunning, 2005), and grain-size distribution influences the primary failure mechanism (overtopping). Estimating breach development rate and shape, particularly in large volume rock avalanche barriers, is also problematic given the heterogeneous internal fabric.

With the potential for catastrophic failure shortly after emplacement, management of dambreak flood hazards requires rapid forecasting of potential peak discharge based on minimal parametric information such as dam and lake geometry and inflow rates. Given the severity of downstream flooding from dam breaching, affecting both natural and human environments, a model may be considered effective if estimates of peak discharge (Q_p) and breach development time (t_b) lie within ± 30% of the actual values. Obtaining such accuracy from rapid processing of limited parametric data, even without consideration of the dam sedimentology, presents a major challenge. Estimation of the potential flood hydrograph from a breaching dam is complicated by dependence on four inter-related factors; the volume of the lake, the height of the dam, the average width of the breach, and the breach development time. Four main techniques have been developed in the past two decades to assess the magnitude of potential dam break floods: (a) empirical regression relationships; (b) parametric models; (c) dimensionless analysis and (d) physically based computer models. This research aims to identify models which best simulate breach development in landslide dams for the prediction of peak outflow, using a dataset of failures obtained from scaled physical modelling.

The purpose of this thesis is to investigate the effect of rock avalanche material heterogeneity and structure on dam stability, peak discharge and breach development time. This research will attempt to characterise the influence of variable grain size and sedimentology on the breach development process and resultant peak outflow. This will be achieved through physical scale modelling of overtopping failure in non-cohesive, heterogeneous landslide dams.

1.2 Local Context

Landslide dams occur in high alpine environments and therefore pose considerable hazard to human systems in New Zealand. New Zealand occupies a complex geological setting, derived from convergence of the Australian and Pacific plates, promoting rapid uplift and high seismicity within mountainous terrain. These conditions, combined with high precipitation levels, are conducive to the development of large scale slope instability and stream blockages in the Hawkes Bay, Northwest Nelson, North Westland, South Westland, Western Canterbury and Fiordland regions (Perrin and Hancox, 1992). Within the past

decade, four short-lived landslide dammed lakes have been recorded (Figure 1.1) occurring on the Poerua, Greenstone, Waitotora and Turakina rivers (Manville, 2001).

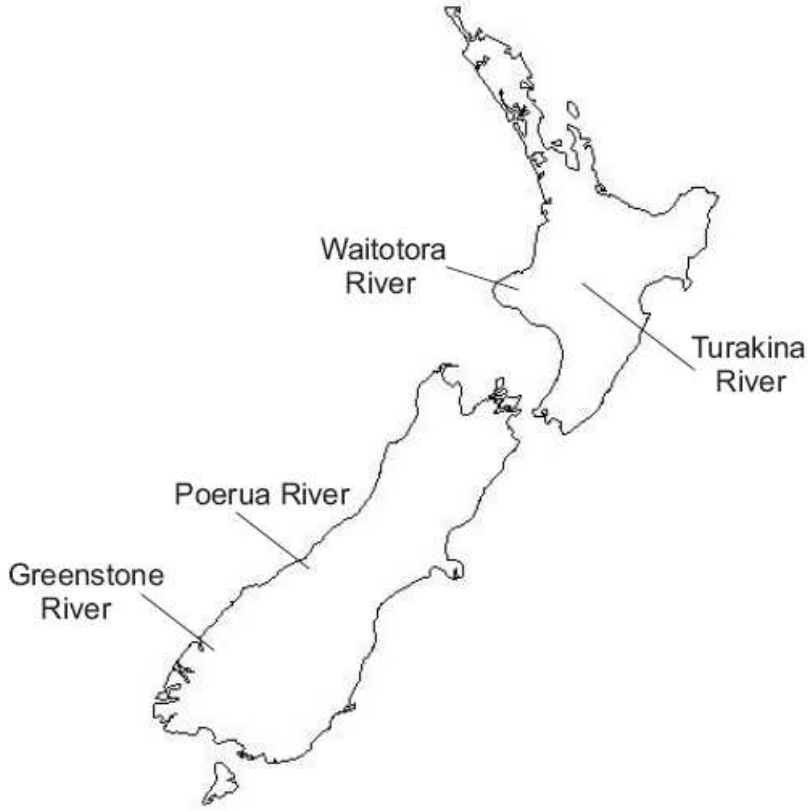

Figure 1.1 Recent landslide dams in New Zealand

The recent formation and failure of the 1999 Mt Adams rock-avalanche dam on the Poerua River (Hancox *et al.*, 1999; 2005) highlighted the susceptibility of foreland communities in South Westland to an intrinsic alpine geomorphic process which may recur with higher magnitude and frequency in the future.

1.2.1 Poerua Landslide Dam

On 6 October 1999 an estimated 10-15 million m^3 of schist and colluvium fell 1800m from the northern peak of Mt Adams into the Poerua River valley on the West Coast of the South Island, New Zealand. The landslide formed a dam ~10 x 10^6 m^3 in volume, 85m high with a crest length of 450m impounding a lake 1200 m long and 80 m deep, and holding 5 – 7 million m^3 of water (Hancox, 1999).

Dam material consisted of large boulders (up to 4m in diameter) observed to armour the dam surface, spillway, and outflow channel. The average block size diameter for the whole dam (d_{50}) was ~ 6mm (Hancox *et al.,*2005). Initial overtopping of the dam crest occurred approximately 24 hours after formation. Rapid breach development was triggered 6 days after initial overtopping, during a rainfall event in which 80mm precipitation was recorded over a 12 hour period (Hancox *et al.,*2005). This event caused partial failure of the dam, eroding a 300m long trapezoidal breach channel, to a depth approximately half the original dam height and reducing the original lake volume by approximately 75%. The resulting flood peaked between 500-1000 m^3/s ~ 8km downstream of the dam causing significant channel aggradation proximal to the gorge exit, but no casualties (Hancox *et al.,*2005).

1.3 Hazard Management; The Physical and Legal Context

The potential hazard posed by the emplacement of a rock avalanche into a valley upstream of human settlement and infrastructure is subject to management under two pieces of legislation in New Zealand; the Resource Management Act (1991) and the Civil Defence and Emergency Management Act (2002).

1.3.1 The Resource Management Act

The Resource Management Act 1991 (RMA) promotes the sustainable management of New Zealand's natural and physical resources at local, regional and national scales. These three levels have different responsibilities to assume, depending on the resources being managed (Appendix B1, RMA Sections 24, 30, 31). Section 2 of the RMA defines a natural hazard as

…any atmospheric, or earth, or water related occurrence (including earthquake, tsunami, erosion, volcanic and geothermal activity, landslip, subsidence, sedimentation, wind, drought, fire or flooding), the acting of which adversely affects or may affect human life, property or aspects of the environment.

The RMA states that regional councils have primary responsibility to avoid and mitigate natural hazards. Local authorities are also required to maintain data such as fault line mapping, flood plains and natural disaster history on property documents. The RMA also binds development through a resource consent and consultation processes. The RMA is linked to the CDEMA in a requirement to consider natural hazards.

1.3.2 The Civil Defence Emergency Management Act

In December 2002, the Civil Defence Emergency Management Act 2002 (CDEMA) replaced the Civil Defence Act 1983. The CDEMA creates a framework within which New Zealand must address hazards and prepare for, deal with, and recover from local, regional and national emergencies. The new approach integrates traditional civil defence (response and associated planning) with risk reduction as provided by the RMA. The CDEMA encourages coordination between a wide range of agencies (central government, local authorities, emergency services and lifeline utilities) providing clear specification of their individual roles and responsibilities.

The CDEMA requires Regional Councils to identify specific hazards and sustainably manage them to achieve acceptable levels of risk and plan and prepare for emergency response and recovery by forming regional Civil Defence Emergency Management (CDEM) Groups. The CDEMA (s48) states that each CDEM Group "must prepare and approve a civil defence emergency management plan". The Regional CDEM Plan must also have the ability to be integrated into the National CDEM Strategy (CDEMA s37 (1) and s53 (1).

A hazard is defined in the Civil Defence Emergency Management Act 2002 as

"any happening, whether natural or otherwise including, without limitation, any explosion, earthquake, eruption, tsunami, land movement, flood, storm, tornado, cyclone, serious fire, leakage or spillage of any dangerous gas or substance, technological failure, infestation, plaque, epidemic, failure of or disruption of emergency service or lifeline utility, or actual or imminent attack or warlike act which may occur and causes or may cause loss of life or injury or illness or distress or in any way endangers the safety of the public or property"

Inconsistency between the definitions used for hazard in the RMA and CDEMA may also hinder management.

1.3.3 Dam Management Legislation

As landslide dams are largely ignored by definition in current legislation, NZSOLD dam safety guidelines and the Building Act have little legal relevance to their management. Such guidelines could however be applied to landslide dams to describe the hazard in the context of current dam management policy, in the absence of specific regulations for landslide dams.

1.3.3.1 NZSOLD Safety Guidelines

The acceptable level of risk to a downstream community from landslide dam break flooding is put in perspective by comparison with acceptable levels of risk for dam design in New Zealand. The New

Zealand Society of Large Dams (NZSOLD) considers the hazard potential of a dam to be influenced by the dam height, storage volume, downstream conditions (degree of habitation, public assets) and surrounding environment (ie. precipitation, seismicity of a region).

The NZSOLD *Dam Safety Guidelines* (2000) for classification of potential impact from dam failure (Table 1) primarily consider dam height and reservoir volume in the assessment of damage potential.

Table 1.1 Classification of Potential Impact from dam failure (NZSOLD Safety Guidelines).

Potential Impact Category	Potential Incremental Consequences of Failure	
	Life	Socio-economic, Financial, & Environmental
High	Fatalities	Catastrophic damages
Medium	A few fatalities are possible	Major damages
Low	No fatalities expected	Moderate damages
Very Low	No fatalities	minimal damages beyond owner's property

NZSOLD designates a **high potential impact** classification for dams impounding water to a height greater than 20m and a storage volume exceeding $10^6 m^3$. All landslide dams fall into this category since their average height ranges between 40-80m and reservoir volume usually exceeds 5 x $10^6 m^3$.

Suggested guidelines for societal risk with regard to dam safety have been published by several organisations including USBR (1997) and ANCOLD (1998). Finlay and Fell (1997) report similar ranges for acceptance of risk from landslides, concluding that for a risk to be perceived as low or very low, the annual loss of life frequency would need to be between 10^{-5} and 10^{-6}**.**

Such studies can be used to define the acceptable level of societal risk with regard to outburst flood hazards. A recent study commissioned by the Ministry of Civil Defence and Emergency Management (Optimex, 2003) investigating the societal risk to the Franz Josef Township from an outburst flood resulting from breaching of a landslide dam, concluded that the current probabilities of fatalities range from 2 x 10^{-3} to 10^{-2}, allowing for the current warning and response systems. These probabilities are significantly greater than the acceptable ANCOLD limit of 10^{-5}.

However, it is emphasised that the use of acceptable risk guidelines to convey the hazard potential of landslide dam outbreak floods on downstream communities and infrastructure, particularly in a legislative context is limited given there are as yet **no** societal risk criteria for natural hazards widely endorsed by any regulatory agency in New Zealand.

1.3.3.2 The Building Act (2004)

Section 161 of the Building Act (2004) requires all regional authorities to adopt a policy on dangerous dams. A dangerous dam is defined in section 153 as:

(a) a high potential impact dam or a medium potential impact dam; and

(b) likely to collapse -

(i) in the ordinary course of events; or

(ii) in a moderate earthquake; or

(iii) in a moderate flood; or

(c) a leaky dam.

Industry best practice has been assessed in terms of design of dams to cope with earthquake events using the annual exceedence probability (AEP). This is an accepted concept for describing earthquake or flood events and has been found suitable for consistent application across New Zealand.

A moderate earthquake (s153) is defined according to **AS/NZS 1170.0 2002** *Structural Design Actions* (Appendix A) which requires a 1 in 2500 AEP earthquake shaking to be used for structures with importance **level 3**. While high potential impact dams (importance **level 5**) are not covered by this standard, studies of the regional seismic hazard in New Zealand suggest that such dams should be designed to withstand a 1 in 10,000 AEP seismic hazard (an event 1.3 times larger than the 1 in 2500 AEP seismic hazard event).

A moderate flood (s153) is defined for a high potential impact dam as a flood flowing into the reservoir created by the dam that is associated with 1.4 x 1 in 100 annual exceedence probability (AEP) flood flow. This definition is based on the requirement for high impact dams to pass a minimum design flood usually between 1 in 10,000 AEP and the probable maximum flood (PMF). A 1 in 100 AEP flow or high intensity rainfall distribution is also commonly used in hydrological designs.

Non-engineered natural barriers are only subject to *dam* management legislation (Building Act, 2004), if "*a natural feature has been significantly modified to function as a dam" (Section 7)*. Currently, only the Waikaremoana landslide dam, due to its use as a hydropower facility is subject to Dam management legislation specified in Subpart 7; s134-162 of The Building Act (2004). Dam owners and operators must also comply with NZSOLD Dam Safety Guidelines (2000).

1.4 Issues affecting the management of landslide dam hazards

The CDEMA is the only piece of legislation that requires specific identification of hazards by councils. However, the scope of this identification is limited to the hazards already identified through the Resource Management Act (RMA) process and for which building works have been undertaken in hazard zones. Hazard identification can only be inferred from other pieces of legislation such as the Building Act and RMA. Development control outside recognised hazard zones is limited; therefore unless hazard identification and zonation is frequently evaluated, the provisions of the various acts concerning land use cannot be effectively applied.

Complication exists in the designation of responsibility for management of natural barrier type natural hazards (as defined by the RMA Section 2). Occurrence of such a natural hazard within the boundary of a National Park (i.e Crater Lake Tephra Barrier, Mt Tongariro National Park) requires the Department of Conservation (DOC) to assume responsibility and co-ordinate hazard management. All other areas are subject to hazard management by a Regional Council. The interpretation of who is responsible for constructed dam safety is inconsistent at both District Council and Regional Council levels and also varies between regions.

While hazard categorisation of dams for statutory management in public arenas is necessarily simplistic, current approaches generalise hazard potential using broad assumptions on the impact of a failure for a given dam, which are not always supported by science.

To adequately classify and manage the potential hazard from landslide dam failure, ongoing estimates of; failure mechanism, potential flood hydrograph, event probability, CDEM response methodology, and overall social, economic and environmental impact forecasting are required. The development and refinement of technical methods for the analysis of dam failures is therefore important to public safety, enabling better classification of dam hazard potential.

1.5 Thesis Format

As increasing land pressures force human settlement and development into upland regions, the risk of human fatality and damage to assets and infrastructure from the rapid failure of large stream blocking events increases.

This research investigates the applicability of contemporary embankment dam technology to modelling overtopping failure in a non-cohesive rock avalanche dam. To communicate the findings, the thesis will be laid out in the following format:

Chapter 2 backgrounds the formation and failure of landslide dams based on published research in both global and local contexts. Particular emphasis is given to the recent identification of specific facies within rock avalanche deposits and the implications of internal structure and heterogeneous fabric for dam behaviour under overtopping conditions.

Chapter 3 outlines the methodology of the research design and the necessity for Froude-scale modelling. The criteria for the model design and its inherent limitations are presented.

Chapter 4 details the experimental design used to represent prototype conditions. Descriptions of the resources and instrumentation used in the modelling are provided. Six different dam structures with a range of internal sedimentologies are tested under different inflow and saturation conditions.

Chapter 5 provides an overview of the key observations and results from scale modelling of the breaching process. Results are presented for each dam type tested, in the form of outflow hydrographs and evolving cross sectional area profiles for two specific cross sections within the breach. Investigation into the breach formation mechanism is presented through a description of the failure chronology.

Chapter 6 backgrounds the current state of dam breach modelling technology, in the context of selecting models applicable to breach development in rock avalanche dams. To date most information on breach development in landslide dams has been derived from engineering research on artificial earthen or rockfill dams, without consideration of grainsize distributions and sedimentology of non-engineered dams.

Chapter 7 critically reviews breach development models commonly used to predict both peak discharge and breach development time, using the dataset obtained from physical modelling. Limitations to the accuracy and applicability of empirical, parametric, dimensionless and physical methods are presented. Uncertainty analysis of the physical model dataset is also presented.

Chapter 8 presents the models most applicable to primary and secondary rapid response for effective hazard management of rock avalanche dams.

Chapter 9 summarises the main objectives and results from this study.

Chapter 2
Literature Review of Rock Avalanche Dams

2.1 Introduction

Rock avalanche dams are a particular type of landslide dam. They often pose a higher hazard potential than other landslide dams, given the extreme volumes and runout distances of rock avalanche deposits. Research into landslide dams and their associated phenomena has only recently become established as a critical component in understanding the interaction between fluvial and hill slope systems (Korup, 2002), often requiring a multidisciplinary approach involving the application of both geomorphic and engineering principles. The effects of landslide dams can be subdivided into short and long-term impacts. Short term impacts involve upstream and downstream flooding; downstream flooding is the most hazardous to populated areas and infrastructure in the potential flood path and therefore receives significant attention. Rapid initial assessment of a landslide dam to identify the probability of catastrophic failure associated with impounded water is essential for emergency management. Current research is therefore focussed on predicting a dam's post-formation development for early identification of its potential for catastrophic dam failure through use of dam break modelling techniques. Long-term impacts receive less attention because they concern the effects of landslide dam has on sediment transport and overall hydrological impacts, which do not pose any immediate threat to populated areas downstream of the landslide dam.

Much previous work on landslide dams has been descriptive in character, and has produced a number of documented case studies (Korup, 2002). This reflects not only the difficulty of data acquisition, but the diversity of its application. This chapter attempts to summarise and evaluate the current state of knowledge of rock avalanche emplacement, landslide dam formation and failure characteristics, dam breach hydraulics and available technology.

2.2 Rock Avalanches

Rock avalanches are high magnitude, low frequency mass movements involving the failure of over 10^6 m^3 of bedrock and weathered mountainside. These events are often triggered by localised seismicity, high intensity or prolonged rainfall, human activity or accelerating creep, but the trigger mechanism apparently has no influence on the form of the resulting deposit (Korup, 2002). Rock avalanches have been reported

to transport material remarkable distances, beyond that expected from the normal laws of friction; the precise mechanisms operating during motion and emplacement are still poorly understood.

2.2.1 Definition of the Phenomena

The term "*Sturzstrom" (rock-fall stream)* was first used by Albert Heim to describe the observed behaviour of the mass movement event which destroyed the town of Elm, Switzerland in 1881 (Hsu, 1978). McConnell and Brock (1904) applied this description of motion to the Frank slide in Alberta, Canada, labelling the event as a *rock avalanche.* This has since become a common term describing the process (Evans, *et al.,* 1989).

Classification schemes have been used by various researchers, notably Varnes (1996; see Table 2.1) and Hutchinson (1965; 1988) to describe landslides, however the variation in definitions and terminology between these schemes contributes to ambiguity in a universal working definition. Smith (2003) highlighted that a rock avalanche is not derived from remobilization of debris as inferred by Varnes (1996) *rockfall / rock slide debris avalanche*, but rather from first-time failure of a relatively large (> 10^6 m^3) *in-situ* intact rock mass (Whitehouse and Griffins, 1983). Failure generally initiates along pre-existing defects, a process Davies and McSaveney (2002) refer to as *collapse*; however the subsequent behaviour involves intense comminution of rock debris to grains as small as nanometres.

Table 2.1 Varnes and Cruden (1996) landslide classification scheme

Type of Movement	***Type of Material***	***Engineering Soils***	
	Bedrock	*Predominantly Coarse*	*Predominantly Fine*
Fall	*Rockfall*	*Debris Fall*	*Earth Fall*
Topple	*Rock Topple*	*Debris Topple*	*Earth Topple*
Slides -rotational	*Rock Slump*	*Debris Slump*	*Earth Slump*
-transitional	*Rock Slide*	*Debris Slide*	*Earth Slide*
Lateral Spreads	*Rock Spread*	*Debris Spread*	*Earth Spread*
Flows	*Rock Flow*	*Debris Flow*	*Earth Flow (soil creep)*
Complex	*Combination of two principal types of movement*		

Although velocity classes give poor division of landslide type, Hungr *et al.,*(2001) suggested that velocity is the most important measure of hazard intensity to people. Therefore human response has been incorporated into both classification and definition. Table 2.2 illustrates human vulnerability to a rock avalanche (velocity class 7).

Table 2.2 Probable human response with regard to variable landslide velocity

Velocity Class	*Description*	*Velocity mm/sec*	*Typical Velocity*	*Human Response*
7	*Extremely Rapid*	$5x10^{3}$	*> 5m / sec*	*Nil*
6	*Very Rapid*	$5x10^{1}$	*3m / sec*	*Nil*
5	*Rapid*	$5x10^{-1}$	*1.8m / hr*	*Evacuation*
4	*Moderate*	$5x10^{-3}$	*13m / month*	*Evacuation*
3	*Slow*	$5x10^{-5}$	*1.6m / year*	*Maintenance*
2	*Very Slow*	$5x10^{-7}$	*16 mm / year*	*Maintenance*
1	*Extremely Slow*	$< 5x10^{-7}$	-	-

Based on the description proposed by Hungr *et al.*,(2001) the preferred definition of a rock avalanche in this investigation is as follows *"A rock avalanche is an extremely rapid, massive, mobile, flow- like motion of fragmenting rock derived directly from a large bedrock failure."*

2.2.2 Triggering Mechanisms

Rock avalanches can be triggered by rock weathering, earthquakes, storm events, removal of toe support and human interference. A primary requirement for the formation of a rock avalanche is the rapid detachment of rock mass, as can be caused by the propagation of seismic energy within the epicentral area of $M_w > 6$ magnitudes (Eisbacher and Clague, 1984). Seismic shaking can widen fractures and defects within a rock mass reducing cohesion or shear strength of failure surface asperities and roughnesses. In of areas prone to frequent, smaller earthquakes, shear strength can be progressively reduced to increase susceptibility to fatigue-related failure mechanisms (Erismann and Abele, 2001). Furthermore, studies of topographic amplification (Zaslavsky and Shapira, 2000) document the effect relief has on the amplification of seismic waves. A tendency exists to assign the triggering of a rock avalanche to a seismic source rather than precipitation (Voight, 1978).

In the Southern Alps of the Central South Island, New Zealand, oversteepening of valley sides by glacial erosion has resulted in relaxation within the rock mass and a redistribution of stress and strain causing joint dilation, crack enlargement. While Whitehouse and Griffith (1983) consider oversteepening to be a precondition rather than a trigger of failure, climate change has been postulated as a destabilisation mechanism that may initiate some rock avalanches in isolated cases (McSaveney, 2002). The distressing and disaggregation of rock mass is often attributed to periglacial activity, however Erismann and Abele, (2001) and McSaveney (2002) consider freezing to be a fatiguing process and argue that ice also protects mountain faces, acting as a barrier against erosion.

While the role of precipitation in slope destabilisation processes is well documented (usually associated with soils and superficial failures, Kilburn (1998), Melosh (1987) noted that few historic rock avalanche

events are actually triggered by precipitation. Collapse can occur as a deep-seated brittle failure, with instability occurring when gravity loading and fracture growth exceed the shear strength within the rock body. Often such weakening of asperities is assisted by high internal water pressures and chemical weathering.

2.2.3 Diagnostic Characteristics of Rock Avalanches

The rock avalanche process exhibits characteristics which distinguish it from other forms of landslide and types of flow. The mass volume is often dry, displaying high mobility and extremely rapid velocity (Varnes and Cruden, 1996; Hungr *et al.,*2001). Such properties enable the debris to travel abnormal distances and overrun topographic obstacles, with super elevation where impeded or deflected. Entrainment of surface material on the run out path combined with dilation of the rock mass during collapse and fragmentation, often cause rock avalanche deposits to generally exceed their 'source' volume.

The volume of the displaced mass has significant influence on the geometry and spread of the resultant deposit (Davies and McSaveney, 1999). Runout simulations conducted by Okura *et al.,* (2000), demonstrated that runout distance (spread) is directly related to the volume of the displaced mass. Okura *et al.,* (2000) concluded that long runout could be attributed to inter-block impacts causing increased dispersion of kinetic energy rearward of the debris front while resulting in a retreat of the centre of mass, preservation of stratigraphy and ultimately an increase in the distance reached by frontal blocks. These results are consistent with the conclusions of Davies *et al.,*(1999) concerning fragmenting granular avalanches where increased dispersive stresses caused amplified spreading, runout and desposition thickness in proximal areas. Davies *et al.,* (1999) chose to normalise fall height, length and volume ratios and interpreted a size effect occurring at volumes greater than 10^7 m^3. This was attributed to the onset of rock fragmentation driving the mass, suggesting fragmenting induced long runout occurred at volumes $\geq 10^6$ m^3.

The initial phase of motion has been termed collapse (Eisbacher, 1979, McSaveney and Davies 2002), where the trigger releases a volume of bedrock that dilates along preexisting discontinuity surfaces such as jointing or foliation during the initial fall and / or slide to the valley floor. The mechanism of motion driving the dispersion and runout of the rock avalanche at high speeds remains controversial. Previous explanations for long runout of rock avalanches have focused on reducing basal friction or internal friction, however neither has been successful in explaining the phenomenon as it occurs in nature (Davies *et al.,*1999) The dynamic fragmentation hypothesis proposed by Davies and McSaveney (2002) is consistent with the observed pulverized internal sedimentology of rock avalanche deposits. This theory involves a confined explosive disintegration of rock occurring at a smaller scale than that of insitu

jointing or structural discontinuities; a process very similar in mechanism to an explosive failure of an unconfined compression tests (Davies and McSaveney, 2002). The confinement of the high kinetic energy released from innumerable continuous explosions on surrounding clasts causes dilation of the rock mass, resulting in exceptional spreading and longer run out. The boundary between static-dynamic fragmentations is a function of the size of the fracturing mass, and decreases in size exponentially as the volume of mass increases (Davies and McSaveney, 2002).

2.2.4 Rock Avalanche Deposits

Detailed sedimentological data for rock-avalanche deposits are sparse. Recent work has attempted to characterise the sedimentology of rock-avalanche deposits using either a facies approach or direct measurement (Hewitt, 1999; Casagli and Ermini, 2003). Direct measurement of rock-avalanche deposits has been hindered by both natural impediments such as internal exposure availability and accessibility and, crucially, sampling methodology (Dunning, 2005). Previous sedimentological data have been collected as part of other rock avalanche research and so have often, necessarily, been limited to single small samples (McSaveney, in press; Hewitt, 1999) from the main body of deposits without detailed study of the surrounding exposure to set the sample in a structural context.

Grain-size distributions of rock avalanches from New Zealand and worldwide (Table 2.3) have a fractal dimension close to 2.58, a value found by Sammis *et al.,*(1987) to correspond to a three-dimensional geometry that equalises and minimises the probability of fracture of all particles. Thus all grains present in a rock avalanche are equally likely to fragment at any given time.

Figure 2.1 Falling Mountain Rock Avalanche deposit, New Zealand

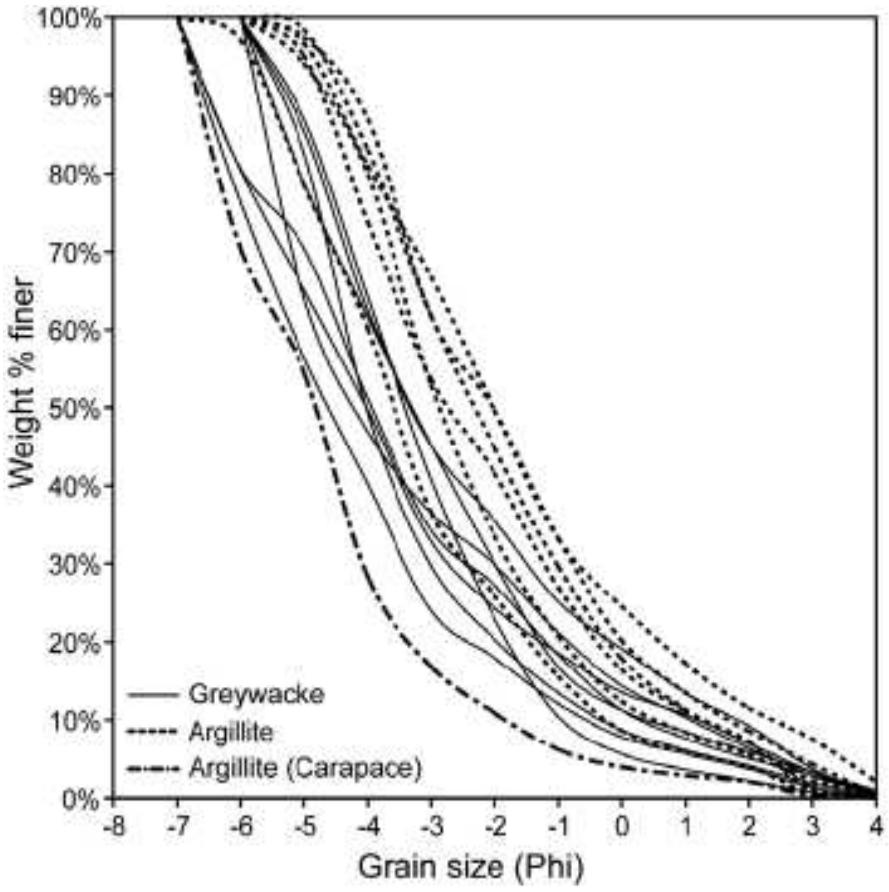

Figure 2.2 Grain Size Distribution for the Falling Mountain Rock Avalanche deposit (Dunning et al., 2005)

Table 2.3 The range of values for selected descriptive statistics based on five rock avalanche deposits in varied lithologies (Dunning, 2005).

	N	Minimum	Maximum	Mean	Standard Deviation
Mean (Phi)	89	-.13	-5.69	-2.63	1.31
Median (Phi)	89	-.82	-6.19	-3.24	1.36
Sorting (Phi)	89	1.46	3.69	2.60	0.48
Gravel (Wt %)	89	46.97	98.65	75.85	0.10
Fractal (d)	89	1.95	3.04	2.44	0.20

2.2.5 Sedimentology

The deposit resulting from a rock avalanche is sedimentologically distinctive and can thus form an important basis for classification (Dunning, 2004). Common results based on both observation and direct measurement indicate the presence of highly fragmented but undisaggregated clasts (McSaveney, in press), preservation of original source stratigraphy (Strom, 1999) interactions with the deposit substrate and accounts of crude inverse grading (Cruden and Hungr, 1986), which Dunning *et al.,* (2005) attribute to lithological variation.

McSaveney *et al.,* (2000) describe the deposit of the 1929 Falling Mountain rock avalanche in Arthur's Pass National Park, New Zealand (Figure 2.1). About 55 x 10^6 m^3 of rock fell from the north face of the 1900m mountain, bulking to a volume of 60 x 10^6 m^3 before travelling 4.5 km down valley. Detailed field investigations at Falling Mountain in combination with grain size distribution of interior samples (Figure 2.2) by Dunnning (2004) and Dunning *et al.,* (2005) reveal that the deposits are not inversely graded but show three distinct facies composed of angular, highly fragmented clasts reflecting source stratigraphy with variation only due to lithology. McSaveney *et al.,* (2000) noted that at Falling Mountain, upper deposits are collapsed and clast supported, but not fragmented, while underlying deposits are matrix supported with extensive fragmentation. The grain-size distributions segregate based on lithological variation (Figure 2.2) and become finer with distance travelled from the source. Dunning (2004) proposed a facies model consisting of the surficial, coarse, *Carapace facies*: a fragmented interior *Body facies;* and the *Basal facies* of entrained debris.

2.2.6 A Facies Model of Internal Structure

The *Carapace facies (surface/near-surface material)* is an assemblage of large, angular interlocking blocks created during the collapse of the bedrock slope and transported near the surface of the rock avalanche (Figure 2.3). The geometry of the carapace material is controlled by original rock properties such as strength and discontinuities, and runout distance. The carapace is the coarsest unit of a rock-avalanche deposit accounting for as much as 30 % of deposit thickness, but for considerably less by mass

due to void spacing and clast-supported fabric (Dunning *et al.,* 2005). Consequently the carapace is characterised by high hydraulic conductivities, in the region of 0.1 ms^{-1} for a relatively fine carapace of argillite (Falling Mountain, New Zealand). The facies is clast-supported and retains source stratigraphy as discrete bands without mixing. The *Carapace facies* is potentially of critical importance to rock-avalanche dam stability because it is the material forming the dam surface (Figure 2.4), and the only visible basis for rapid hazard assessment (Dunning *et al.,* 2005a). The high permeability of the carapace has also been reported to inhibit overtopping failure (Hewitt, 1999); on the other hand, turbulent free-surface flow between large blocks of carapace at the interface between the carapace and body facies can cause internal erosion and the carapace destruction.

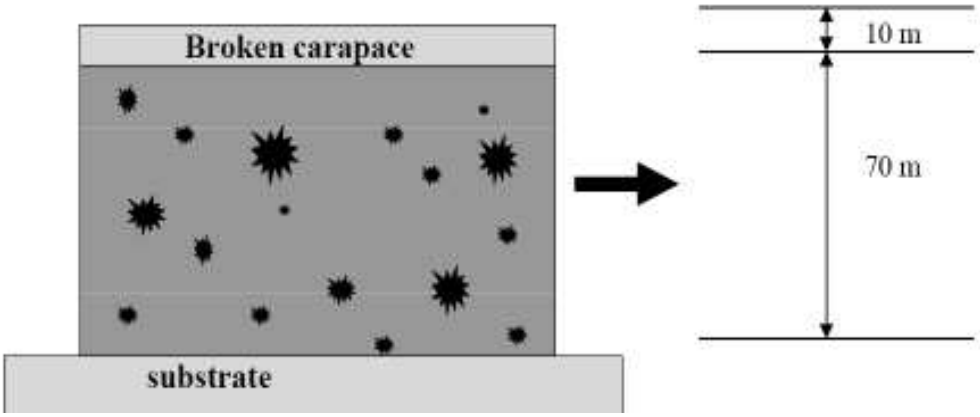

Figure 2.3.Diagram of fragmentation in rock avalanche; dimensions refer to Falling Mountain situation (Davies et al., 2002)

Figure 2.4.The coarse carapace observed at the dam crest (left) and downstream toe (right) at the Tsatichhu rock avalanche dam Bhutan (Dunning et al., 2005)

The *Body facies* (Figure 2.5) has been identified as a "graded" boundary underlying the *Carapace* below which material is intensely fragmented but relatively undisaggregated, matrix supported and showing fragmentation derived features (Dunning *et al.,*2005b; McSaveney *et al.,*2000). This unit accounts for the greatest thickness within rock-avalanche deposits and is usually the most voluminous in valley-confined deposits. Dunning *et al.,* (2005a) report bands of fragmented material showing preserved stratigraphy relative to the source to be intrinsic features of rock avalanche deposits. Due to preservation of stratigraphy, grain-size distribution and material properties such as hydraulic conductivity for the interior vary based upon the lithology. For the basis of comparison an argillite sample in the body facies of the Falling Mountain rock-avalanche deposit yielded hydraulic conductivity values of around 3×10^{-3} ms^{-1} and porosity of around 20% (Dunning, 2005b).

The *basal facies* is the smallest unit by volume within a rock-avalanche deposit, and represents material altered by the passing rock avalanche that has interacted with the substrate. This includes entrainment of soft, erodible valley fills and surface vegetation into the base of the moving event, and also subsequent deposition of modified mixes of substrate and rock-avalanche material, which can cause superficial erosion to bedrock. The boundary between the *Basal facies* and the *Body facies* is often indistinct and variable in its height.

With more accurate knowledge of the sedimentology of rock-avalanche dam deposits, the failure of landslide dams can be modelled with more certainty. The information gained from sedimentological investigation, geomorphic data and landslide inventories allows distinct categories of dam geometry, sedimentology and associated failure styles and timing to be identified.

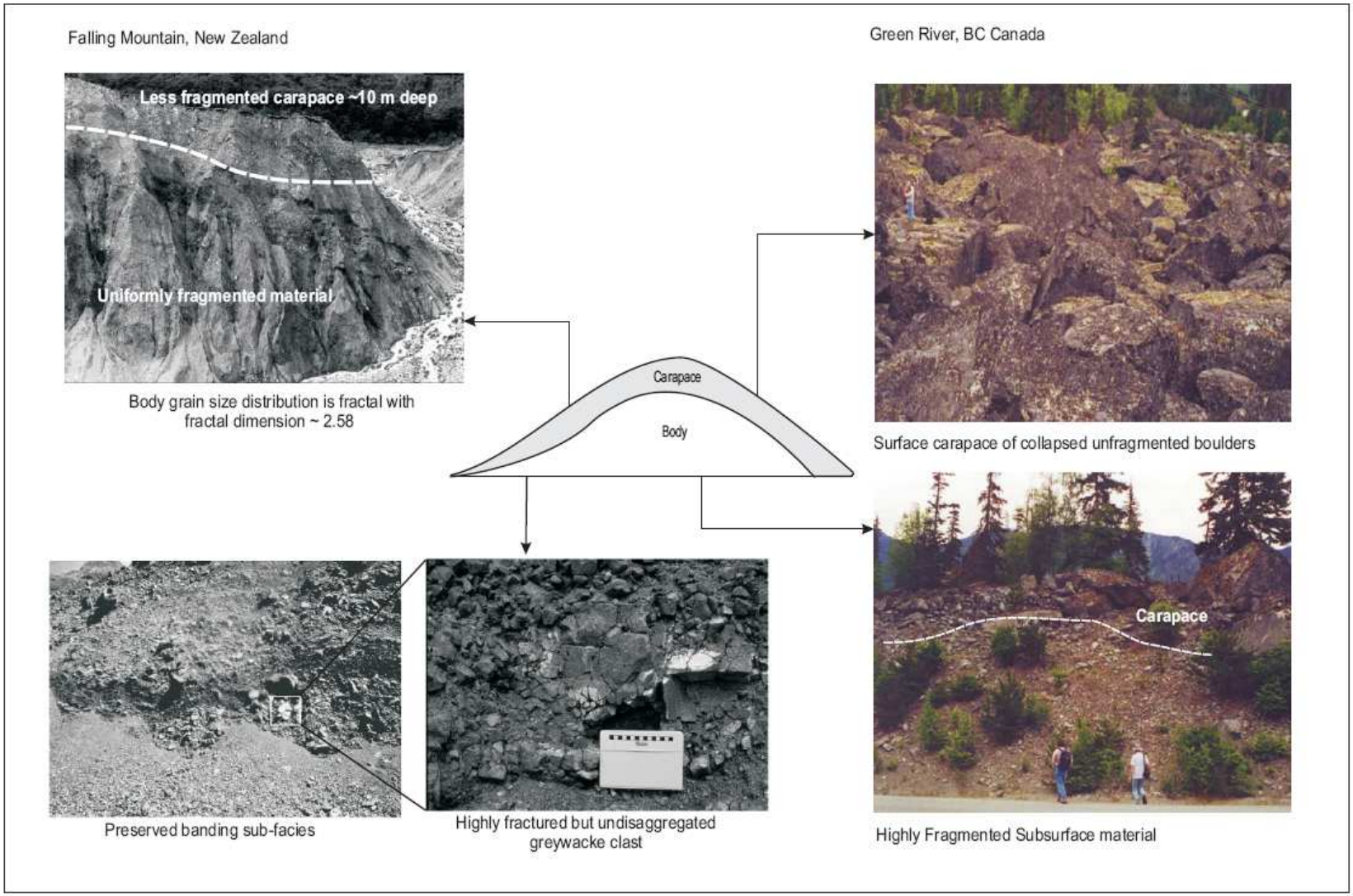

Figure 2.5. Rock avalanche deposits indicating the presence of different sedimentological facies (Source; Dunning et al., 2005 and T. Davies)

2.2.7 Rock Avalanche Dam Morphology

Rock avalanche dam morphology has been documented to be largely a function of lithology and the valley geometry into which the deposit is emplaced, (Strom, 1999). Ollett (2001) used small scale physical modelling to assess the influence of bed slope, valley geometry and angular drop height, on the geometry of the rock avalanche dam. Valleys with moderate geometries (slopes between 40-48%) were found to produce a higher dam crest, whereas shallow (<40%) and steep (>48%) geometries encouraged deposition concentration on the release side of the channel, and a lower dam crest. Upstream dam slope was observed to decrease linearly with increasing bed slope, for all channel slope angles. Similarly the downstream slope was observed to increase linearly with increasing bed slope. Correct modelling of slope roughness promoted batter steepening by up to 9%. The volume of displaced material did not influence geometry. The model closely simulated the geometric characteristics of well documented case studies.

2.2.7.1 Classification

The landslide dam classification most commonly used (Ermini and Casagli 2003) is that of Costa and Schuster (1988), in which six morphologies of possible valley blocking landslides are described, of which four are commonly formed by rock avalanche. Using cross-sectional profile and the distribution of mass, (Strom 1999) developed a classification system based upon *Stalled*, *Secondary Two-Phase*, and *Spread* morphological types. Both the Costa & Schuster (1988) and Strom (1999) classifications consider entry of a rock avalanche at near right angles into the main river drainage, and its subsequent effect on that major drainage. This research will focus on modelling the breaching potential from impoundments typical of *stalled* rock avalanche morphologies characteristic of Type II and III blockages.

2.2.7.2 Stalled Morphologies

Stalled rock avalanche deposits are generated through the restriction of radial spread by direct impact (at near right angles) on opposing valley slopes, consequently *freezing* the mass due to the high rate of energy dissipation. Such impacts have also been observed to produce super-elevation of debris, which can collapse back onto the deposit causing the initial surface texture to be obscured by finer material. Lobate features from progressive phases of failure can significantly affect the pathways available for overtopping water before discharges are reached whereby carapace blocks cannot resist erosion.

2.3 Landslide dams

2.3.1 Background

The term “landslide dam” refers to a natural blockage of a drainage basin caused by slope movements (Casagli and Ermini, 1999). The river blockage may be complete or partial; in both instances, an impoundment may be formed upstream. Hazards from landslide dams are related to their rapid failure and

variable longevity. The temporal variation associated with the stability of landslide dams is highlighted by Costa and Schuster (1988), who sampled 73 landslide dams with known time to failure and found 85% to fail within a year of formation. In contrast, blockages can also impound sediment and water for millennia due to their natural stability and resistance to erosion (Adams, 1981; Hewitt 1996). In general, however, landslide dams have a low resistance to both internal erosion and overtopping by the impounded water. In many cases failure may be catastrophic, causing major downstream flooding, or in others, it may be slow resulting in minimal downstream damage (Schuster, 2000). Additional hazards, such as backwater flooding, occur upstream of a landslide dam as the impoundment fills; filling is generally a slow process depending on the size of the catchment above the point of the blockage; however, it can potentially inundate communities and valuable agricultural land (Costa and Schuster, 1986).

2.3.2 Spatial Distribution of Landslide Dams

Schuster *et al.,* (1998) listed four groups of factors that govern the spatial distribution of landslide dams: (1) seismic intensity (peak acceleration, duration of strong shaking), (2) slope gradient and topography, (3) lithology and weathering properties and (4) soil moisture and groundwater content. Figure 1.1 (previous chapter) outlines the spatial distribution of recent New Zealand landslide dams.

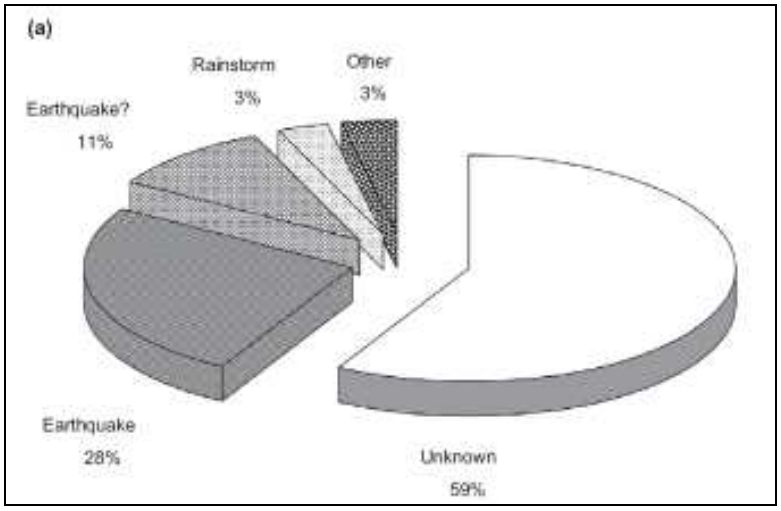

Figure 2.6. Trigger mechanisms involved with the formation of landslide dams in New Zealand (Korup, 2004).

Dam forming landslides are generally initiated by mechanisms that act to reduce the internal strength of the rock mass. Analysis of 394 historical cases of landslide dam formation with a known triggering mechanism by Schuster (1993) suggests that the most important natural processes influencing the initiation of dam forming landslides are excessive rainfall, snowmelt and earthquakes which, when combined represent 90% of the landslide dams investigated. Korup (2004) suggests 39% of New Zealand landslide dams are seismogenically triggered (Figure 2.6).

2.3.3 Dam- Forming Landslides

Rock and debris avalanches form 19% of landslide dams worldwide (Ermini and Casagali, 2003), with generally larger volumes and higher velocities than earth slumps or debris/ earth flows. In addition there is often a continuum between a rock or earth slide and a rock and debris avalanche, with the former disintegrating into the later upon down slope movement (Nash, 2003). In New Zealand extremely rapid landslides involving rock avalanching are the most common type and account for 27% of the data (Figure 2.7).

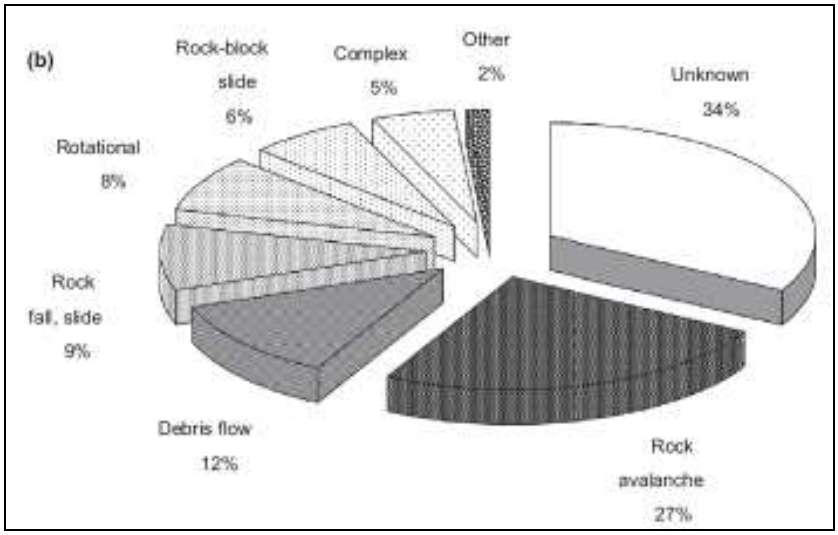

Figure 2.7. Landslide types involved with the formation of landslide dams in New Zealand (Korup, 2004)

2.3.4 Geomorphic Classification of Landslide Dams

The potential for landslide induced blockage of a drainage basin is a function of the lithological type, volume and distribution of displaced material as well as the channel width and flow velocity. Swanson *et al.,* (1986) proposed a geomorphic classification scheme for landslide dams based on geometric relations with the valley floor. This classification was further modified by Costa and Schuster (1988) who were able to distinguish six types of landslide dam from a dataset of 184 case studies. Based on their relations with the valley floor Costa and Schuster (1988) classified landslide dams into six types of dams (Figure 2.8):

Type I: Partial obstruction of channel forming shallow non hazardous dams.

Type II: Complete obstruction of channel, spanning valley floor, high hazard potential.

Type III: Complete obstruction of channel, highest material volumes with extensive runout distances, impounding large hazardous lakes and blocking valley tributaries.

Type IV- V: Simultaneous failure of material from two sites in the same valley to obstruct the channel. Potentially hazardous if large volumes are emplaced in narrow valleys. The Poerua Landslide Dam was of this type.

Type VI: Dams of this type have a failure surface that extends under the river channel. They pose least threat of downstream flooding because a complete blockage seldom results. Water storage is small and rapid incision of the dam unlikely.

The most frequently documented types of landslide dam are types II (44%) and III (41%).

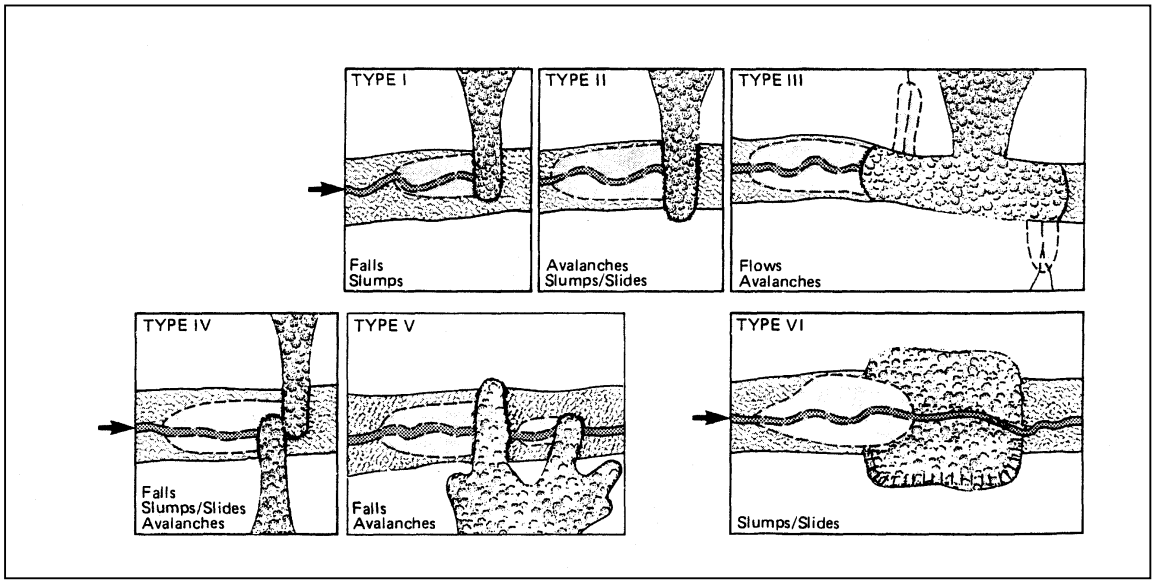

Figure 2.8. Types of Landslide dam (Costa and Schuster, 1988)

2.3.5 Geomorphological considerations

In addition to the classification systems outlined above, a number of indices and statistical relationships based upon geomorphic parameters are available to provide information on the configurations that create an 'unstable' or 'stable' landslide dam (Casagli and Ermini 1999, Ermini and Casagli 2003, Korup 2002). Such an empirical approach provides no indication of the possible future evolution of 'stable' dams into the 'unstable' field. Instead, they are a measure of simply of whether the dam is stable or unstable at the time of measurement. The approach is, however, deemed useful (Korup, 2002) for the first approximation of the stability of landslide dams and as a comparison of the conditions necessary for the formation of stable dams between regions with varied geomorphic and bounding conditions.

Casagli and Ermini (1999) developed a set of geomorphic indices using a combination of dam volume, dam height, lake volume and catchment area above the point of blockage to predict the post-formation development of a landslide dam. While such systems are useful in providing approximations of dam stability, they do not consider the influential role of material properties and the grain size. Nash (2003)

attributes the poor performance of the applied geomorphic indices for stability prediction in landslide dams in the Nelson Region, New Zealand, to the inability of the index to account for dam composition and resistance to erosion, thus highlighting the importance of material heterogeneity and material 50% finer by weight (d_{50}) as critical parameters in dam stability. Furthermore Nash (2003) found the Casagli and Ermini (1999) index to incorrectly assign stability to failed dams based on an inability of parameters used in the indices to represent the erodibility of the landslide debris.

2.3.6 Critical Breach Parameters

Nash (2003) identified the critical parameters required for assessment and modelling of landslide dams for pre (Figure 2.9) and post breach (Figure 2.10) conditions.

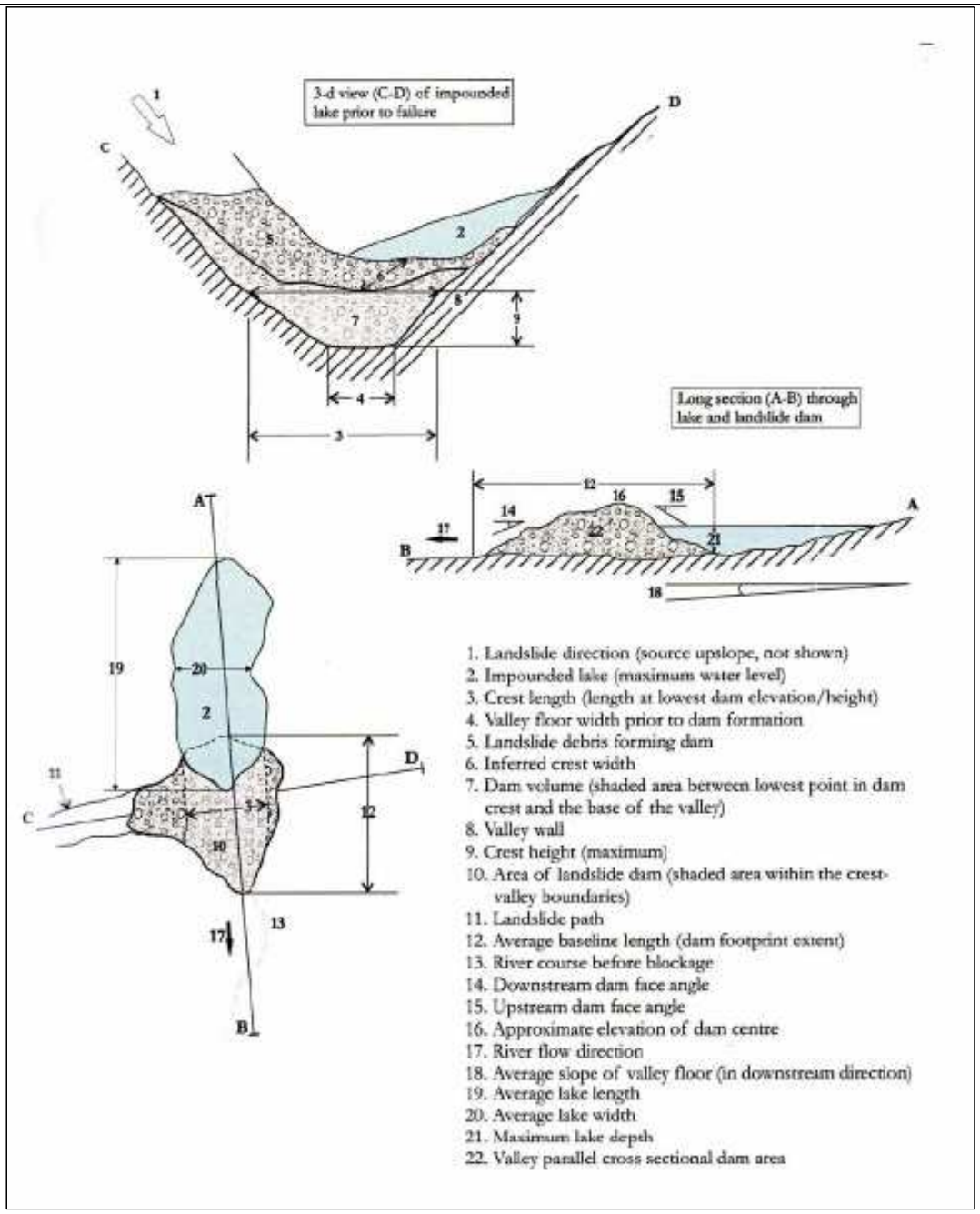

Figure 2.9. Pre-breach landslide dam parameters in plan and sectional view (Nash, 2003)

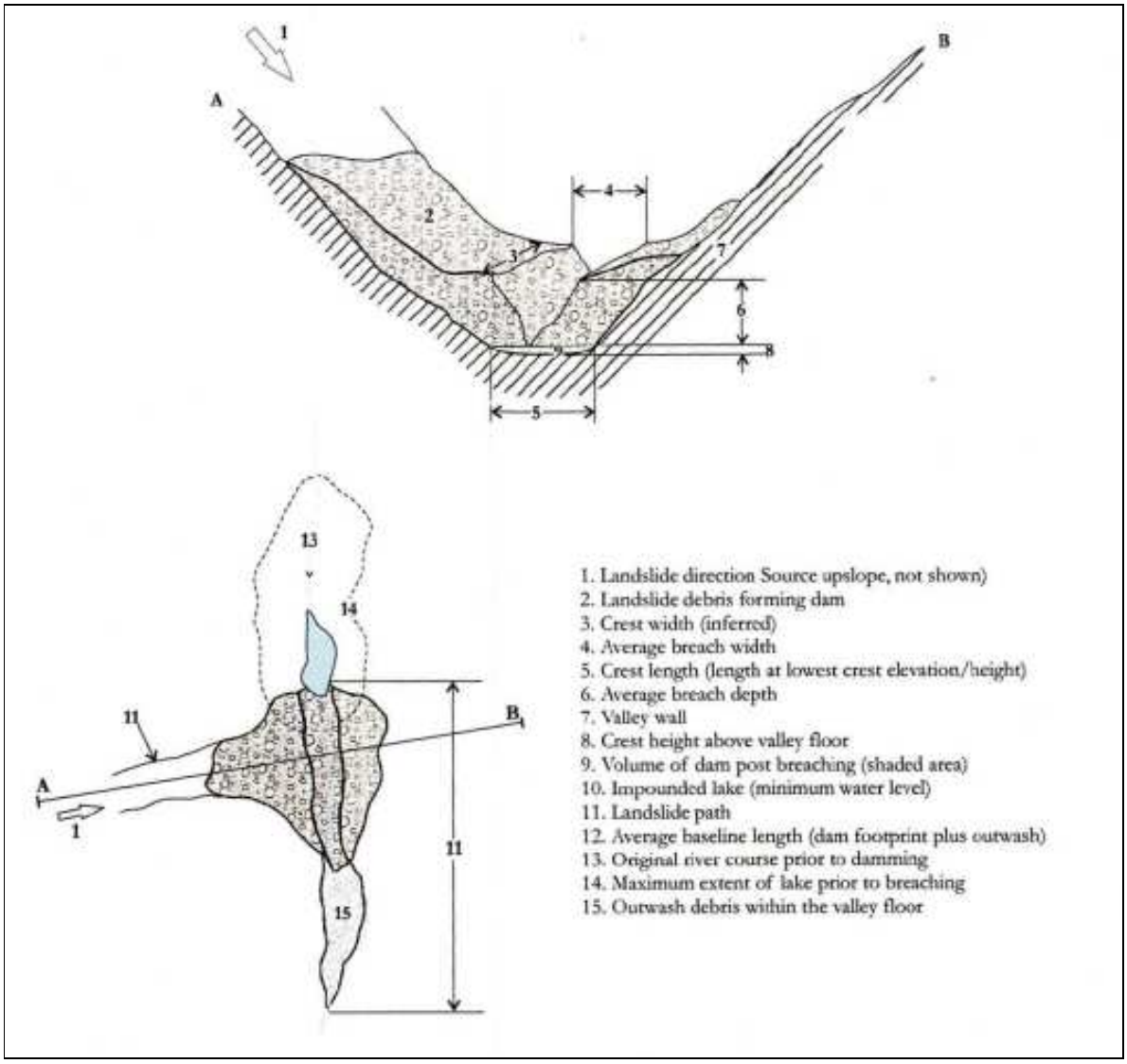

Figure 2.10. Post-breach landslide dam parameters in plan and sectional view (Nash, 2003)

2.3.7 Geotechnical Properties of Landslide dams

The physical properties of the material comprising the landslide dam are critical to correctly simulate dam breaching in numerical models.

- There is significant variation between the median particle size (d_{50}) within a rock avalanche deposit, ranging from 10-10 000 mm (Davies, *pers. comm*) within the carapace and 0-9mm within the body. The d_{50} from documented rock avalanche deposits can be highly variable, ranging from 0.35-200mm (Dunning *et al.,* 2005).

- Cohesive Strength (kPa); The rock avalanche material does not undergo compaction and therefore has low cohesion; cohesive strength may be in the region of 20 kPa.

- Porosity is also variable throughout the rock avalanche deposit due to the internal structure. Turner and Schuster (1996) suggest an average swell factor of 33%, to account for bulking processes in rock avalanches. From the physical scale modelling, the silica sand used to simulate the body facies had a porosity of 45%. The high void density of the carapace produced higher porosity values of 60%.

2.4 Longevity and Stability of Landslide Dams

As indicated in Figure 2.11, landslide dam longevity is highly variable ranging from minutes to millennia (Costa and Schuster, 1988). Two examples illustrate this variability; a dam-forming debris flow on the East Fork Hood River, Washington, breached in 12 minutes, to cause US $13 million damage (Korup, 2002). In contrast, a dam created by a rock avalanche on the Tegermach River, Kyrghizstan, which formed Lake Yashingul in 1835, failed 131 years after formation to cause widespread downstream damage (Korup, 2002).

Schuster (1993) reported that 35% of the 187 investigated breached landslide dams failed within one day of formation while 89% failed within one year. Ermini and Casagli (2003) found similar results upon investigating 205 failed landslide dams; c.20% failed within one day and c.80% within one year of formation.

The longevity of a landslide dam depends on factors such as (1) the rates of sediment and water flow into the upstream reservoir; (2) physical characteristics of the dam and valley such as geometry, volume and the geotechnical properties; and (3) the amount of water loss via seepage through the dam, evaporation and groundwater recharge into abutment rocks.

Rock avalanche dam longevity is directly proportional to its ability to resist erosion (externally from overtopping or slope heave and internally from piping). At the grain size scale, resistance to erosion within a rock or soil material is dictated solely by geotechnical properties (d_{50}, cohesion and friction angle) and mass characteristics such as weathering, strength and grading of the rock material. However, it is the volume and distribution (spatial variation) of such materials within the structure of the rock avalanche deposit that determines stability. Field-based recognition of various run-out based morphologies producing variable carapace thickness and distribution, influence the ability of the rock avalanche deposit to impound water indefinitely (Dunning *et al.,* 2005).

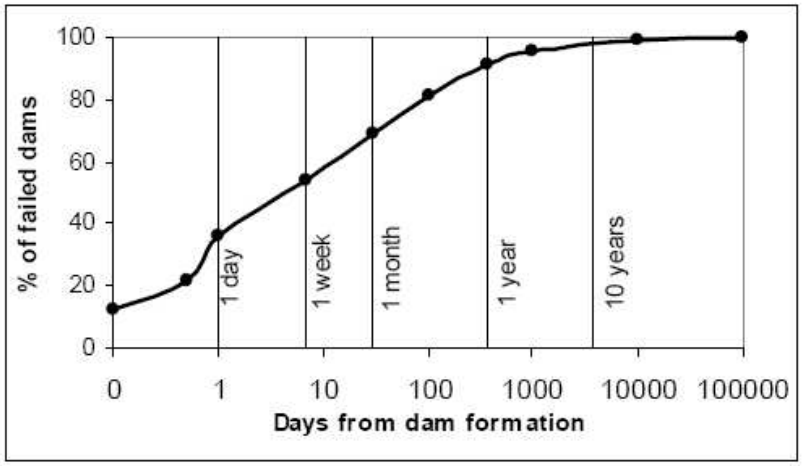

Figure 2.11. Age of dams at time of failure (Costa and Schuster, 1988)

2.4.1 Conditions promoting stability

Case studies show examples of stable to limited overflow conditions, where flow confined to the *Carapace facies* does not erode internally to failure, but acts to lower the reservoir level behind the dam crest, promoting stability by maintaining equilibrium between inflow and outflow (Dunning *et al.,*2005; Hancox *et al.,*1999). In such cases the role of seepage becomes critical to dam stability, and thus exemplifies the importance of correctly modelling the morphology and internal sedimentology.

Hydraulic conductivity and intrinsic permeability (Figure 2.12) can be calculated from the grain size distribution (Dunning, 2004). From sampling carried out at the Poerua landslide dam (Dunning, 2004) hydraulic conductivity was found to range between 1.24 x 10^{-1} m/s in the *Carapace facies* to 3.69 x 10^{-4} for the *Body facies*.

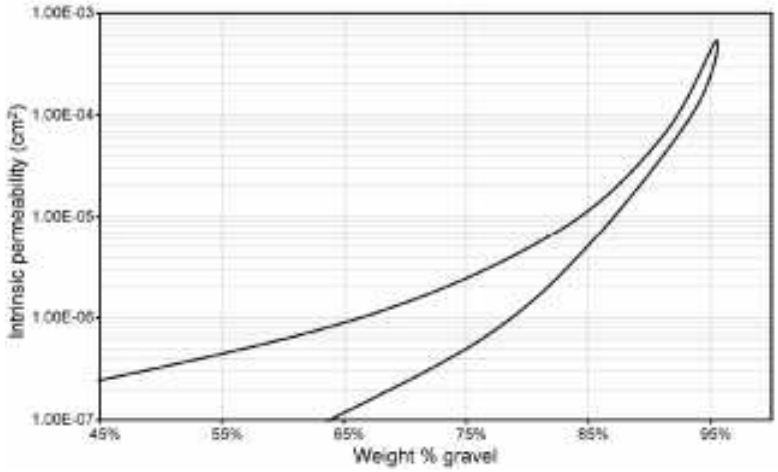

Figure 2.12. Intrinsic Permeability for rock avalanche deposits based upon a measure of weight percentage gravel (Dunning, 2005)

Dunning *et al.,* (2005a) claimed the higher hydraulic conductivity of the carapace to be crucial in the rapid destabilisation of natural dams. Modelling of reservoir infilling behind a homogenous dam using SLOPE/W and SEEP/W, produced a time to failure of 18.75 days. A realistic sedimentology, characteristic of a rock avalanche dam, caused failure within 48 hours (Figure 2.13). Such variation in failure time has serious consequences for hazard assessment and consequent evacuation procedure. Furthermore, Dunning *et al.,* (2005a) suggested visual observation of phreatic migration on the downstream dam face could be a key indicator to confirm internal sedimentology of the dam and lead to subsequent predictions of its stability.

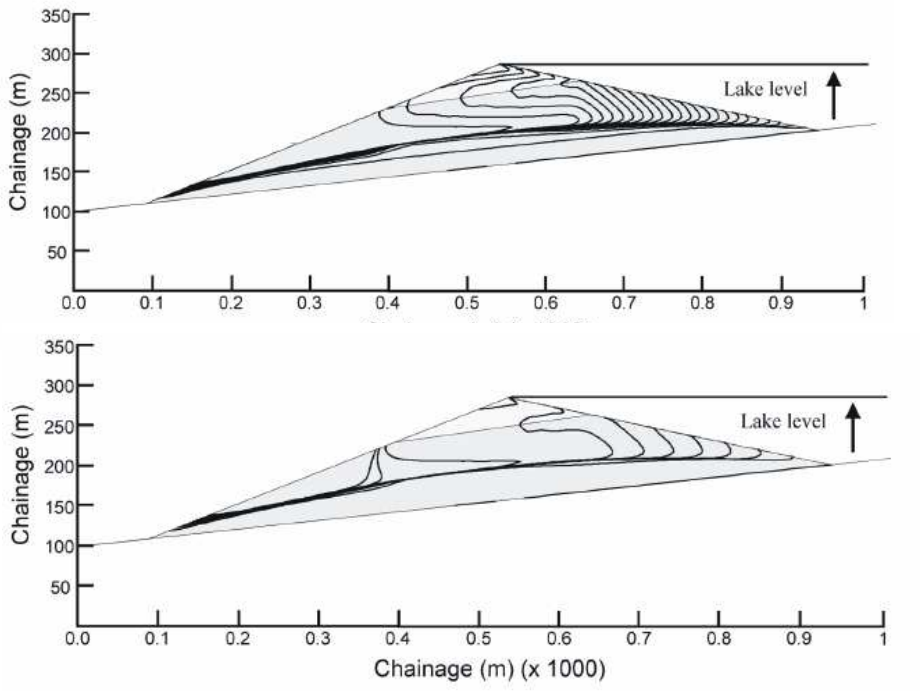

Figure 2.13. Geoslope simulations of seepage through heterogeneous rock avalanche deposit at 2-hourly (48hr) and 6 hourly (60 hr) simulations (Dunning, 2005)

Slope failure on the downstream face has been found to be prevalent in deposits that do not overtop – i.e. those that are stable to low overflow conditions. Many researchers attribute the stability of prehistoric damming to events to '*effective boulder armour*' and no apparent seepage, combined with the sheer dimensions of the blockage (Hewitt, 1999; Costa and Schuster, 1988). However predictions on formation and stability of a landslide dam are likely to be only applicable for dataset from which they were derived.

2.5 Failure of Landslide Dams

Natural dams differ from artificial dams in composition, construction and geometry. They are typically composed of unconsolidated and poorly sorted material with no engineered features designed to prevent piping, seepage or saturation, or channelised spillways or other outlets to control overflows. The time to failure of landslide dams can therefore range from minutes to thousands of years, depending on factors including lithology and hydrologic conditions within the catchment. However four factors appear to primarily control failure;

1. Rates of sediment and water inflow into the impounded reservoir
2. Dam and valley geometries
3. Dam sedimentology and surface morphology
4. Geotechnical properties of the dam materials

Dam height and valley geometry determine the maximum impoundment volume at lake full level, but ultimately it is the local hydrologic characteristics and the catchment area that control the inflow/outflow which in turn determine the actual rate of filling and ultimate stability. If the river inflow exceeds seepage outflow the lake can fill to crest level, resulting in overtopping, breach formation and potential dam failure.

Breach processes operating within artificial structures provide a useful analogue for quantifying the response of similar processes in the heterogeneous materials characteristic of rock avalanche dams. Documented earth dam disasters indicate gradual and progressive modes of failure. Loukola *et al.,* (1993) noted that 98% of all dam failures in China (87,000 failed dams) are associated with earth dams. The main cause of failure was overtopping due to heavy rainfall and floods exceeding spillway design parameters. Middlebrooks (1953), in an investigation into rockfill dam failures, related failure to the age of the structure. Similarly in earth dam structures, susceptibility to failure by sliding, seepage or conduit leakage is greatest within the first five years of operation (Singh, 1996).

Assigning a classification of ‘stability’ to landslide dams has to be treated with caution, since it is not time-invariant (Korup, 2004). Seemingly stable landslide barriers were reported to fail years or even decades after their formation without any obvious relationship to their dam or reservoir dimensions (Figure 2.14). Even a barrier that may satisfy basic geomechanical requirements such as internal cohesion or resistance to shear stress by the volume of the impounded water body, may be subject to failure by excess stress from earthquake-induced ground acceleration or landslide induced displacement wave.

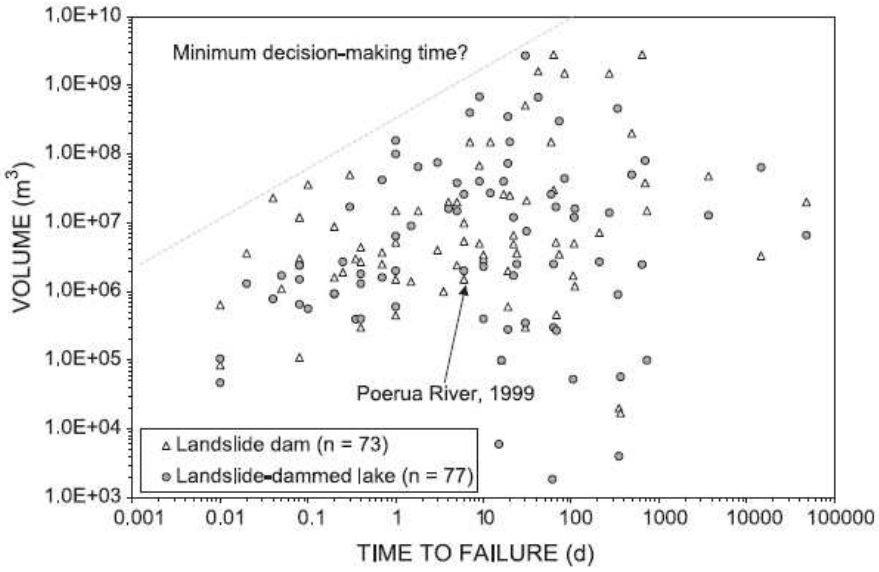

Figure 2.14. Estimated volumes of landslide dams and related lakes versus the time to dam failure, based on the NZ dataset (Korup, 2004)

2.5.1 Rockfill dams as an Analogue to Failure in Rock Avalanche dams

Rockfill embankments with impermeable cores have been the subject of investigations by Skoglund and Solvik (1995) in Norway, where approximately 170 large rockfill dams exist. It was found that the degree of overtopping of the core had little influence on the extent of damage to the core by internal erosion processes. Pugh (1985) studied zoned and rockfill embankments as fuse plugs for the controlled release of high return period floods over auxiliary spillways. His findings identified material gradation in the sand filter and embankments to be a key element contributing to the control of erosion rates, including lateral erosion.

Observations from the pre-construction failure of the Hell Hole rockfill Dam (US) demonstrated the high permeability of the lower zone of dumped rockfill and its lack of stability under high throughflow (Kollgaard *et al.,*1988).

A naturally formed spillway may resist erosion during normal overflow conditions; higher discharges during periods of intense rainfall, may overcome the channel materials erosional resistance initiating the erosion process leading to failure (Hancox, 1999). Slow migration of a phreatic front through the dam, to daylight at the downstream face some time after formation, may also cause long-delayed failure. Similarly if reservoir inflow and outflow are in equilibrium due to evaporation, or seepage through the dam material, the lake level can stabilise below the crest level without overtopping.

Dodge (1988), reporting on embankment tests assessing crest and face protection schemes that would permit overtopping flow without causing dam breach, concluded that material placement controlled the

erosion process (Wahl, 1998). Overtopping flow was described to evolve from planar sheet flow to chute-pool flow, characterized by reduced erosion rates.

2.5.1.1 Critical Velocity for armouring failure

Non-Darcy flow conditions can develop for flow through a rockfill dam with a wide profile (Li, 1998). Such conditions are due to seepage flow with a high Reynolds number in rockfill and the interaction between normal pressure seepage flow and overtopping flow. The stability of the rockfill then decreases with increasing slope caused by the increasing flow velocity and therefore increasing destabilising forces. Rathgeb (2000) suggests that rock sliding occurs at low discharges due to hydrodynamic uplift forces reducing the normal force on the sublayer and therefore the activated friction force (Figure 2.15). Movement of multiple rocks promotes the expansion of an upstream gap, causing higher dynamic forces on the rock behind the gap and, therefore the reduction of the erosion stability of the stone.

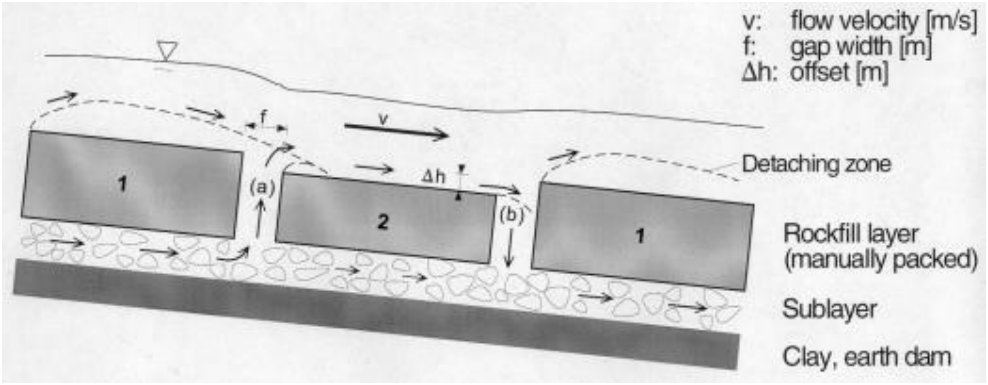

Figure 2.15. Incipient Motion in Rockfill layering (Rathgeb, 2000)

Several investigators have attempted to apply the Shields parameter to the design of riprap and the prediction of riprap failure thresholds. The Shields parameter is the dimensionless ratio of inertial forces (due to bed shear) and gravitational forces on a riprap particle, expressed by Wittler (1994) as:

$$T = \frac{\tau}{(\gamma_s - \gamma_w)(\cos\alpha)d_s(\cos\alpha\tan\delta - \sin\alpha)}$$

where: T = Shields parameter
τ = bed shear stress
α = bed slope
δ = angle of repose of the bed material.

Equation 2.1

γ_s = unit weight of stones
γ_w = unit weight of water

d_s = equivalent stone diameter, d50

For large boundary Reynolds numbers (>10^3), most investigators have found the critical value of Shields parameter at incipient motion to be a constant. Wittler (1994) hypothesised that the correct critical value of Shields parameter is 0.047, even for shallow, highly aerated flows down rough, steep slopes. Wittler (1994) and Abt *et al.,* (1987) also studied the influence of riprap gradation uniformity, reporting that well graded mixtures (less uniform) had significantly lower failure thresholds.

Coleman *et al.,* (2002) suggest that the critical velocity for incipient motion at the breach crest can be related to breach slope S by;

$$V_c = 0.7334e^{-3.11S} \qquad \textit{Equation 2.2}$$

Hartung and Scheuerlein (1970) proposed a relation for fully-developed flow velocity over the downstream face of a rockfill dam as a function of the flow depth, slope, rock size, a particle packing factor, and an aeration factor.

The aeration factor is given by;

$$\sigma = 1 - 1.3\sin\theta + 0.08\frac{y_m}{d_m} \qquad \textit{Equation 2.3}$$

where: d_m = mean roughness height (approximated by $\frac{d_s}{3}$)
y_m = mean water depth normal to the slope
θ = angle of the slope

The critical velocity for incipient motion is then given as

$$v_c = \sqrt{\frac{2g(\gamma_s - \gamma_w)}{\sigma\gamma_w}}\sqrt{d_s\cos\theta}\sqrt{\frac{2}{3}(\tan\delta - \tan\theta)} \qquad \textit{Equation 2.4}$$

2.5.2 Seepage

Seepage forces exist whenever there is a pressure gradient in permeable material that allows water movement. They induce many different types of geomorphic change described by several terms in the literature such as artesian sapping, tunnel scour, mass wasting, rilling and seepage induced transport.

Seepage in a rock avalanche dam is usually free surface flow. While seepage flow is laminar in fine to medium grain size materials (clays and fine sands), subsurface flow may become very turbulent in rock

fill dams (or rock avalanche deposits). The analysis of flow through a rock avalanche deposit is thus complicated by the non-linear relationship between discharge velocity and the applied hydraulic gradient. Seepage flow through landslide dams will therefore depend mainly on the geometry of the rock particles and the voids within the deposit.

2.6 Implications of Rock Avalanche Dam Failure

2.6.1 Flooding

With increasing population growth and land use pressure encouraging development in steep, marginal alpine valleys, the temporal disruption of river channels by landslide dams can pose substantial hazards. Catastrophic outburst floods from naturally dammed reservoirs causing loss of lives, housing and infrastructure have occurred repeatedly in many upland regions of the world (Costa and Schuster, 1988; Casagli and Ermini, 2003). The seismogenic landslide dam that blocked the Dadu River, China in 1786, breached to produce a flood wave that travelled 1400km killing 100,000 people (Li, 1989). More recently, the 1967 Tanggudong landslide (68×10^6 m^3), which dammed a major tributary of the Yangtze to an elevation 175m above its natural valley floor, produced a peak discharge of 53,000 m^3/sec upon breaching,. The scale of such events can also lead to significant economic loss, exemplified in the backwater flooding of the Spanish Forks River (1983), inundating the town of Thistle, Utah to cause US$400 million damage (Costa and Schuster, 1988).

The failure process is specific to each dam, dictated primarily by the volume, distribution and geotechnical properties of the displaced material and the rate of inflow behind the impoundment. While most outburst events are initiated by a combination of climatic and hydrologic variables, failures may also be initiated by landsliding or ice-fall into the reservoir. The severity of downstream flooding may depend on 1) dam material composition; 2) volume and rate of outburst flows; 3) volume of lacustrine sediment behind the impoundment; and 4) the character of the downstream valley, particularly the volume of loose, easily erodible material available for the bulking process (ie entrainment of loose materials) (Schuster, 2000).

Various researchers (e.g. Costa 1985; Evans, 1986; Froehlich, 1987) have attempted to establish empirical relationships among key parameters such as dam height, reservoir volume and breach. These relationships often result in the segregation of dams according to type (Figure 2.16, after Costa and Schuster, 1988) or inferred failure mechanism (Casagli and Ermini, 2003). Dam breach technologies will be treated in more detail in Chapter 6.

Rock avalanche dams have a bimodal overall grain size distribution resulting from material heterogeneity and therefore differ significantly from constructed dams. This difference is observed in the comparison of peak discharges from natural and artificial structures (Figure 2.16).

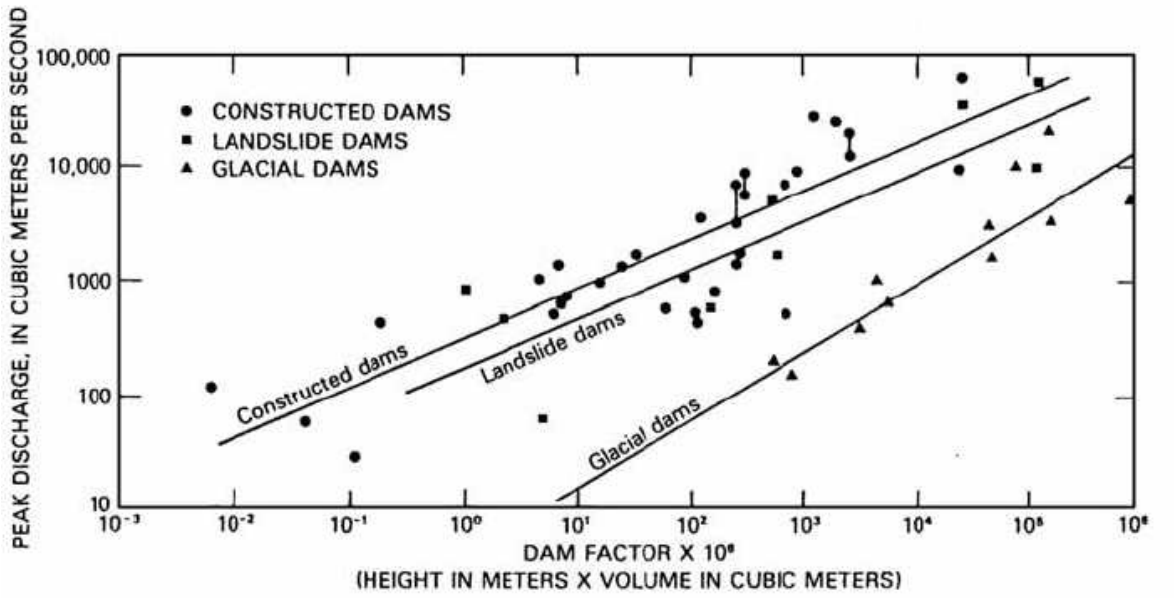

Figure 2.16. Flood peak discharge versus dam factor for constructed, landslide, and glacial dams (Costa, 1985)

Peak outflow rates from failed landslide dams appear to be a little smaller than those for constructed dams with the same dam height and reservoir volume. This can be attributed to the higher volumes of sediment present in the formation of a landslide dam, prolonging the breach-erosion process (more sediment and debris to be eroded before a full breach is developed). The emplacement of large sediment volumes also cause landslide dams to have a larger footprint than constructed dams (Figure 2.17), resulting in significant elongation of the breach channel.

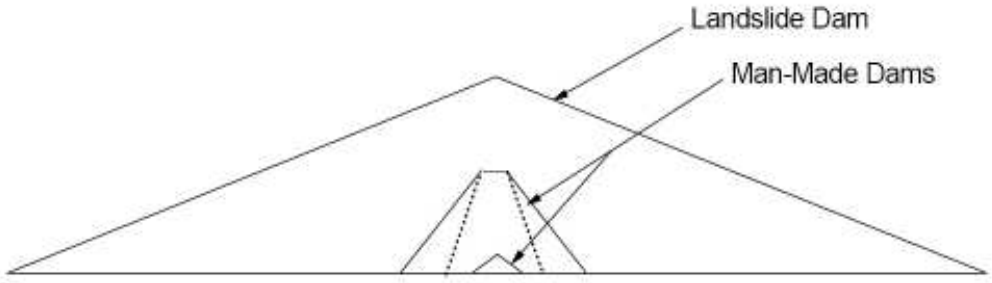

Figure 2.17. Comparative Geometries of Landslide Dams and Constructed Dams (Fread, 1988)

2.6.2 Geomorphic Change

The geomorphic change in the downstream reach of a valley below the point of rock avalanche dam failure will vary with the amount of sediment transported, velocity of the peak discharge, duration of the flooding and river bed slope (Costa and Schuster, 1988). Channel degradation resulting from breach discharges may remove the support at the toe of a slope leading to collapse of the valley side. Similar valley side destabilisation processes have been observed to also occur through aggradation-induced lateral erosion (*Davies, pers comm.).*

Significant geomorphic change may occur upstream also through rapid reservoir drawdown behind the impoundment, initiating valley wall instability (a secondary hazard), from removal of lateral support immediately following lake drainage (Hancox, 1999).

Failure of a landslide dam generates large increases in sediment transport, promoting localised bed aggradation through gradient reduction and consequent avulsion in the downstream channel. Bathurst and Ashiq (1998) observed localised bed aggradation to seriously affect the medium and long term channel morphology and stability. Comparison of downstream, post breach channel profiles on the Poerua River reveal a maximum bed level increase of 4 m, (Hancox *et al.,* 2005) with the most severe channel instability occurring proximal to the gorge exit (Figure 2.18).

Generation of hyperconcentrated/debris flows as reported by King *et al.,* (1989) and Cruden and Lu (1992) pose a significantly higher geomorphic impact potential than mere water floods given sufficient entrainment and concentration of reservoir sediment, dam material or downstream channel alluvium by bulking Schuster (2000).

Figure 2.18. Aerial photos of the Poerua River fan showing the post failure geomorphic features A, October 1999, 2 days after the dam B, August 2001, after 22 months of sediment aggradation and erosion. (Hancox et al., 2005)

2.7 Mechanisms of Failure

Failure of the dam structure most commonly results from erosion of embankment material by the flow of water either over or through the dam. The former results from overtopping of the dam crest and subsequent erosion. The latter gives rise to internal erosion or piping. Overtopping it is the most common cause of failure in natural dams (Figure 2.19).

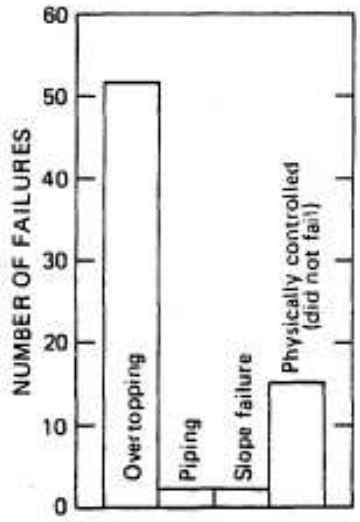

Figure 2.19. Most common modes of failure (Costa and Schuster, 1988)

2.7.1 Overtopping Failure

Overtopping failure is caused by water spilling over the dam crest subsequently eroding a channel along the downstream face of the dam (Manville, 2001). Growth of the breach generally involves erosion of the channel base via sediment entrainment and knick-point retreat in conjunction with mass failure of the channel sidewalls and downstream dam face.

Armouring of the breach channel (Figure 2.20) (particularly in dams with d_{50} > 1mm), and sediment accumulation immediately downstream of the dam, will restrict the depth to which the breach erodes. Costa and Schuster (1988) in a study of 73 landslide dams from around the world, found 50% failed due to overtopping. In a later study of 202 landslide dams by Schuster (1993), 97% failed by overtopping.

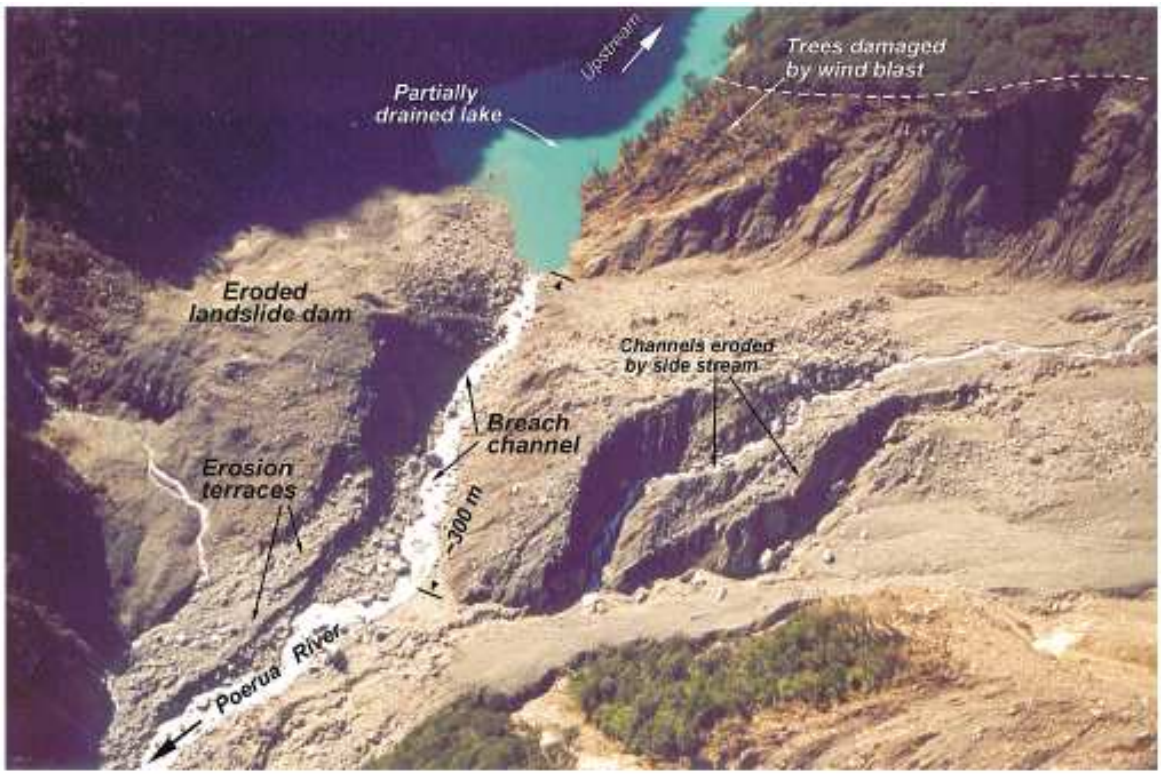

Figure 2.20 Overtopping Breach Incision of the Poerua Landslide dam (Hancox et al., 2005)

2.7.2 Piping failure

Piping is a significant mechanism of initiating dam failure, often leading to a similar breach erosion process as overtopping. Singh (1996) defines piping as subsurface erosion initiated by percolating which removes solid particles and produces tubular underground conduits that appear initially as springs or seepage on the downstream face. Piping is usually initiated low on the dam, due to the higher hydrostatic pressure gradient there. Once sufficient particles have been removed to form a conduit for water, the flow regime is changed from seepage to pressure flow in a closed conduit. As the pipe grows laterally and vertically, support for the dam crest is removed initiating collapse and the development of an open breach (Manville, 2001). Although multiple pipes may be active early in the breach, they are ultimately superseded by the conduit with the highest discharge and without intervention, erosion continues at an increasing rate as the cavity widens.

Landslide dams are particularly susceptible to piping due to their heterogeneous nature - unlike man made structures such as embankment dams, which have undergone systematic design and compaction to reduce permeability which minimises the potential for piping (Meyer *et al.,*1994). In artificial dams, piping can be initiated by; intrinsic soil properties, hydraulic fracturing from internal stresses in specific layers becoming lower than hydrostatic pressures, impacts of bioturbation, and differential settlement. Piping can also result from leaking caused by inadequately compacted or pervious layers in an embankment,

inferior compaction adjacent to concrete outlet pipes, or poor compaction and bond between the embankment and the foundation or abutments.

The formation of conduits from internal erosion in landslide dams is a function of the material composition of the dam. Because of their composition, landslide dams are not particularly subject to failure by internal erosion (Costa and Schuster, 1988). Within their inventory Costa and Schuster only accredit 2 failures to piping related processes. Davies and McSaveney (2004) attribute the low frequency of seepage, slumping or piping related landslide dam failures to a wide grain-size distribution and the minimal average void size of dam materials which act as an impermeable barrier when saturated. Following emplacement of the dam, seepage rates will be low and therefore slumping on the downstream dam face due to daylighting of the phreatic surface is likely to require a long time to occur, and is therefore relatively unlikely prior to overtopping. It can however reduce the ability of a spillway channel to resist erosion by surface flow.

2.7.3 Piping-Related Failure Mechanisms

2.7.3.1 Sloughing

If the downstream face of the dam becomes saturated, sloughing (or raveling) may occur, whereby erosion at the downstream toe may cause a slide in the material just upslope, thinning the embankment.

2.7.3.2 Slope failure

Slope failure is commonly associated with both piping and overtopping when vertical erosion oversteepens the breach sidewalls leading to gravitational collapse (Manville, 2001). Dam failure is initiated when the hydraulic pressure exerted by the impounded water overcomes the dam materials' frictional resistance to shear. Dunning *et al.,* (2005a) suggest that slope failure, particularly on the downstream face, may be prevalent in dams that appear stable due to the ability of the carapace to allow overflow without internal erosion (equilibrium inflow/ outflow).

2.7.3.3 Human Intervention

When a landslide blocks a tributary, leading to the formation of a large lake upstream of populated areas or major infrastructure, there is a need to minimise the impact of an outburst flood. This is often best achieved by reducing the capacity of a dam to store water by lowering the dam crest through construction of a spillway over the dam. Other methods include blasting of the dam using explosives; however this technique is not as controlled as spillway construction. Alternately stabilisation of the reservoir to a maximum freeboard can be achieved through tunnelling into abutment rocks below the minimum crest height allowing drainage of lake water. The requirements of good access, high cost and plentiful time precludes the use of this approach for many rock avalanche dams.

2.8 Overtopping Flow Regimes

Overtopping erosion of a rock avalanche dam is a multivariable, multidisciplinary problem. Poweledge *et al.,* (1989) provided clear descriptions of the initial hydraulic and erosion zones relating to the three flow regimes set up across a typical embankment during the initiation of overtopping. These zones indicate approximate positions for the transition of flow across the embankment from subcritical to the critical and supercritical flow regimes (Figure 2.21).

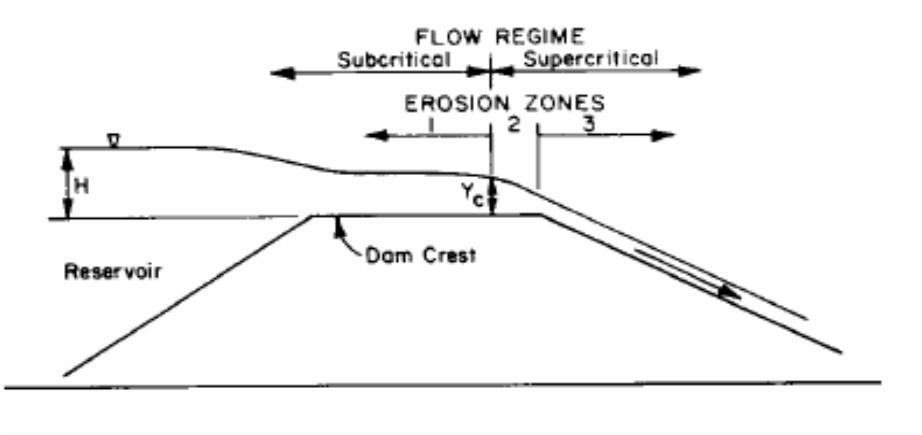

Figure 2.21. Flow and erosion regimes in embankment overtopping (Powledge et al.,1989)

In the subcritical flow region on the dam crest, energy slopes, velocities, and tractive stresses are relatively low. A transition to supercritical flow occurs on the downstream side of the crest. Energy slopes and tractive stresses are higher in this region, and erosion is sometimes observed as formation of a knickpoint at the downstream edge of the crest. The third flow regime involves supercritical flow and erosion on the downstream face of the dam. The energy slope is steep causing higher velocities. Shear stress also varies through horizontal and vertical flow convergence (Figure 2.22).

2.9 Flow Regimes in Steep Channels

When slope exceeds critical slope - that is when the Froude number exceeds unity - much higher velocities result (Jarrett, 1984). Most analysts model large discharges through high gradient reaches as supercritical flow (Trieste, 1992). While this assumption may be valid for man-made channels of smooth, non erosive materials and uniform bedrock natural channels, it is questionable for most natural channels modelled. However, Grant (1997) suggests that high-gradient streams with beds ranging from sand to boulders typically achieve an equilibrium adjustment between the flow, sediment transport, and channel morphology at or near critical flow.

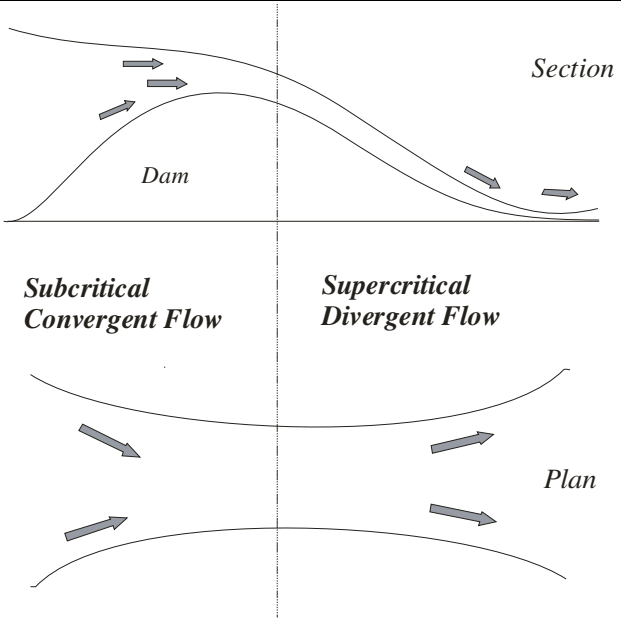

Figure 2.22. Flow Convergence (Davies pers comm.)

Within high gradient channel reaches, supercritical flow may occur for very short distances, but it normally changes back to subcritical flow because of extreme energy dissipation such as hydraulic jumps, turbulence and obstructions. Therefore, both large and small flows in steep natural channel reaches may alternate between sub critical and supercritical. Studies by Jarrett (1984) and Grant (1997) have suggested that supercritical flow does not occur extensively in most natural high-gradient channels. This has important implications for the modelling of natural and artificial dam break events because, if applied over long channel reaches, assuming supercritical flow could cause error in predicted flood depths and widths, velocities and travel times. The assumption of critical flow in steep channel floods would simplify many existing unknown sediment transport relationships (particularly at high slopes) and would allow resistance equations such as Manning's to be replaced with $v = (gd)^{0.5}$ (Trieste, 1995).

2.10 Erosion Mechanics During Overtopping Flow

The mechanism of erosion involved is described by Singh (1996, p.34) as "*complex and governed by the structure of the material and the nature of the interaction between the pore and eroding fluids"*. Erosion will occur when local shear stress exceeds a critical value, after which particles are set in motion (Singh, 1996). The rate at which the erosion process occurs is dependent upon both the erodibility of the dam forming material and the intensity of the water flow. In non-cohesive materials, erodibility depends primarily on grain size distribution, density, grain shape and arrangement. The main resistance to erosion by water is offered by the submerged weight of sediment, ie. gravity and friction forces (Singh, 1996).

For embankment dams, Powledge *et al.,* (1989) listed the following factors having a strong influence on the initiation and rate of erosion:

1. Embankment configuration, types and densities of materials
2. Maximum velocity attained by the flow
3. Discontinuities, cracks or voids in the slope and anomalies at the toe
4. Presence and height of tail water on the downstream slope
5. Flow concentration at low points along the embankment

During overtopping, seepage daylighting at the toe of the downstream face accelerates bed slope erosion due to uplift on bed grains. As overtopping flows accelerate down the downstream face, the highest kinetic energy is achieved towards the base; the point where the materials shear stress is most likely to be exceeded by the flow (Singh, 1996). Tractive stresses are very high, and changes in slope or surface discontinuities can concentrate stresses and initiate erosion causing head cutting and upstream migration of a widening scour hole.

2.10.1 Breach Erosion Mechanisms

Breaching in embankments may develop by tractive or headward erosion. Headcut erosion is the process of fluvial erosion extending in an upstream direction. A headcut may be defined as a steep drop in channel bed elevation. The headcut retreats progressively headward as the base of the headcut deepens and widens (Figure 2.23). Failure and breaching occurs when the headcut migrates through the upstream crest of the dam (Hanson *et al.,* 2003).

Figure 2.23. Headcut erosion of a cohesive embankment (Hanson et al.,2003)

Alternatively a breach may also develop by down cutting, a channel incision process caused by erosion of a channel, usually characteristic of non cohesive granular material. Down-cutting behaviour is commonly observed in the breaching of sand dikes (Visser, 1998) where it requires preferential flow in a zone of weakness to initiate vertical and lateral incision of the embankment.

2.10.2 Physical Modelling of Erosion Mechanisms

Observations of earth-dam failures such as those reported by Ralston, (1987) and laboratory experiments (AlQaser, 1991) indicate that the process of breach formation involves both tractive erosion of sediment and collapse of large masses of sediment from the breach walls, which are subsequently entrained and removed by the flowing water.

There are several physically-based embankment dam breach models that simulate the erosion processes with time, based on the fundamental assumption that the primary erosion mechanism is sediment transport (Lou, 1981; Singh and Scarlatos, 1985). In such models both tractive and mass-wasting erosion processes are assumed to operate simultaneously.

Recent research has continued to emphasise sediment transport and breach channel incision (rather than headcut advance) as the critical erosion process in breaching of non-cohesive sediments. From studies of breach growth in sand dikes, Visser (1998) provides a detailed description of the erosion processes occurring during non-cohesive embankment failures, relating the rate of retrograde slope erosion and widening to sediment transport concepts. Coleman *et al.,* (2002) in a study of overtopping failure in homogeneous embankments reported erosion to evolve from vertical to lateral in nature, with the breach channel initially eroding the downstream face with an invert slope parallel to the face, before flattening to a terminal value by rotating about a fixed pivot point along the base of the embankment

2.10.3 Breach Position

Predicting the size, shape and exact location of the initial breach is very difficult. Overtopping is often induced by settlement within the dam sediment. If the largest settlement occurs at the centre of the dam, the greatest depths occur during overtopping at this point leading to a central failure. The heterogeneity of landslide material is likely to exert a variable resistance to shear on top of the dam. Therefore due to local weakness, erosion may be initiated under less than maximum stress (Singh, 1996).

2.10.4 Breach Shape

Previous researchers have typically approximated breach cross-sectional shapes as simplified trapezoids or triangles (MacDonald and Langridge-Monopolis 1984). To a lesser extent, rectangular, parabolic, semicircular, cosine, and curved regime channel cross sections have also been used in breach

development analyses (Singh 1996). The predominant presumption of trapezoidal and rectangular breach shapes is based on observation of final breach shapes, given the difficulty of establishing dimensions during breaching. In a review of recent work, Manville (2001) states that values for the ratio of breach width to breach depth vary between 1-5 (Johnson and Iles, 1976), (Walder and O'Connor 1997). Andrews (1998) argues that these final shapes have been influenced by falling reservoir levels reflecting limited reservoir volumes as the breach has developed and do not represent the true shape below the water surface of the developing breach.

Various researchers have derived empirical relationships and numerical models (e.g. BossBREACH, OUTFLOW3) to link lake and dam characteristics to total breach development time and breach geometry (presented in Section 7.2) for a variety of natural and constructed dam types, including landslides (Costa 1985; Costa and Schuster 1988; Walder and O'Connor 1997).

2.10.4.1 Trapezoidal Breach

Most dam breaches are trapezoidal in final form (MacDonald and Langridge-Monopolis 1984); they may possibly also have this geometry during their development. MacDonald and Langridge-Monopolis (1984) in their analysis of the failure of 42 US dams, concluded that breach geometry evolved from a triangular shape (2V:1H), to a trapezoid (2V:1H) assuming the breach had reached the base of the embankment and discharge was sufficient to continue eroding the breach laterally. Houston (1985), using the same dataset, also favoured generation of a trapezoidal geometry with 1V:1H side slopes and base width equal to the depth of the breach. The extent of lateral erosion was given as a function of reservoir size and volume of stored water.

2.10.4.2 Triangular Breach

While a triangular final breach profile is rarely documented in current literature, this geometry represents an important stage in breach development and may reflect the restriction of lateral erosion by a small reservoir volume (Johnson and Iles 1976), or the failure to reach a non-erodible foundation.

2.10.4.3 Rectangular Breach

Rectangular breach shapes have not been reported for observed dam failures. Fread (1988), however, used rectangular cross sections to represent various stages of a developing breach. Singh and Scarletos (1988) also successfully used a rectangular geometry to model the 1976 Teton failure.

2.10.4.4 Curvilinear Breach

Several options for the assumption of curved breach shapes have been developed by various researchers. A parabolic breach shape was assumed by Harris and Wagner (1967) and Andrews (1998).

2.11 Breach Hydraulics

Singh (1996) considers flow over a dam as being comprised of three elements;

- Flow over the crest
- Flow through the breach; and
- Flow through the breach channel on the downstream face.

Assuming low tailwater conditions at the downstream face, the hydraulics associated with flow in the developing breach can be simplified. Flow at the upstream end of the breach will become critical, causing it to behave hydraulically as a broad-crested weir, where the breach discharge is given by (Henderson, 1966):

$$Q_b = g^{0.5} H^{2.5} f(\text{shape}) \qquad \textit{Equation 2.5}$$

Fread (1987) incorporated this assumption into calculation of flow over the breach crest and into the breach channel. Singh and Scarlatos (1988), Pugh (1985) and Cristifano (1965) use the broad-crested weir equation to describe flow through the breach which enables breach flow to be expressed as a function of reservoir and crest level.

Singh (1996) outlined the governing equations for flow over a dam which incorporates the continuity, broad-crested weir, breach shape geometric relation, resistance to flow equations. While the dam-break problem involves unsteady non-uniform flow, the steep gradients and short channel lengths involved justify the assumption of quasi-steady flow, allowing the methods of flow approximation described above.

Flow through a breach channel was calculated by Fread (1988) using the Manning Formula, where the Manning friction factor *n* was derived from the Strickler equation. Alternately, the Chezy formula was used for breach channel flow by Guiseppetti and Molinaro (1989). The Strickler equation was also used to determine the Chezy C parameter in the Chezy formula.

Analyses based on the full development of unidirectional free surface flow (de Saint Venant equations) have been used by Ponce and Tsivoglou (1981) and Macchione and Sirangelo (1988).

The breach development process is highly dynamic so breach flow analysis is extremely difficult. Unsteady flow conditions combined with uneven bed geometry invalidate the use of the Manning equation. Similarly the de Saint Venant equations are invalidated by the fact that streamline curvature is not small, hence vertical accelerations may not be negligible, and the slope of the downstream face of the embankment is considered steep in hydraulic terms. Although the broad-crested weir equation represents

an approximate measure, it provides reasonable results and can be incorporated into an approximate relationship for breach width as a function of breach depth (Jack, 1996).

2.12 Sediment Transport

Sediment transport by breach flows reflects the flow rate, material composition and channel gradient. The amount of channel erosion may be directly related to the channel gradient, roughness and the flow regime, which will determine the size of the material being transported and resultant breach size. Because sediment supply is unlimited, sediment transport capacity equations can be used.

The problem of defining critical flow conditions associated with the inception of sediment transport is of fundamental importance to understanding mechanisms associated with fluid erosion in channels of variable gradient. Tractive shear theory remains the basis for sediment discharge in low gradient alluvial streams. For coarse bed materials, the critical unit tractive force necessary to initiate bedload movement is a function of bed-sediment size. Tractive shear theory is therefore also applied in sediment discharge calculations for dam breaching (Singh, 1996). The sediment transport relationships proposed by Schoklitsch (1962) and Smart and Jaeggi (1983), are particularly relevant to breach development in rock avalanche dams because they were derived for steep slopes from laboratory and field studies.

2.13.1 Smart and Jaeggi (1983)

The Smart and Jaeggi (1983) relationship, an extension of the Meyer-Peter and Müller formula; (Equation 2.6) is applicable to steep bed slopes in the range of 0.04-20% and sediment sizes of d_{50}>0.04mm and therefore useful in the study of sediment transport in a dam breaching event.

$$\phi = 8\left[\left(\frac{K_s}{K_r}\right)^{1.5}\theta - 0.047\right]^{1.5} \qquad \textit{Equation 2.6}$$

In which ϕ = dimensionless sediment transport rate $\left[q_{sb}\left[(s-1)gd^3\right]^{-0.5}\right.$

$\frac{K_s}{K_r}$ = a correction factor for bed roughness; and

θ = dimensionless bed shear stress $HS/\left[(s-1)d\right]$

Where q_{sb} = volumetric sediment discharge per unit channel width;

K_s = Srickler coefficient for no wall drag

K_r = the bed grain roughness

For bed plane conditions Equation 2.6 has the form (Smart, 1984);

$$\phi = 8(\theta - \theta_{cr})^{1.5} \qquad \textit{Equation 2.7}$$

Where θ_{cr} = the critical dimensionless shear stress introduced by Shields (1936)

The resulting relationship, unlike the Meyer-Peter - Müller formula, accounts for the effect of non-uniformity in sediment grain size using the ratio d_{90}/d_{30}, therefore giving it specific application to the modelling of a breaching rock avalanche deposit with extreme material heterogeneity. Smart and Jaeggi (1983) also replace the bed roughness correction factor K_s/K_r with a resistance factor (C), defined as the ratio of mean velocity to shear velocity, to give;

$$\phi = 4\left[\left(\frac{d_{90}}{d_{30}}\right)^{0.2} S^{0.6} C\theta^{0.5}(\theta - \theta_{cr})\right] \qquad \textit{Equation 2.8}$$

Modelling the transport of large sediment inputs down steep channel systems using equations established by Meyer-Peter and Muller (1948) and redefined by Smart and Jaeggi (1983) are useful for understanding fluid erosion in steep channels but are often hampered by unreliable sediment discharge functions and linkages with the geometry, friction, and armouring of erodible channels.

2.13.2 Schoklitsch (1962)

Corrado *et al.,* (2006) consider that bed-load transport rate within the breach channel can be adequately simulated using the Schoklitsch (1962) tractive force formula. This equation furnishes the best results under conditions of unlimited supply and for mountain rivers (coarse grain-size and steep slopes; Bathurst *et al.,* 1996).

Bed load transport is calculated as follows;

$$m_s = 2500 S^{1.5} (q - q_c) \qquad \textit{Equation 2.9}$$

$$q_c = 0.26 \left(\frac{\rho_s}{\rho} - 1 \right)^{5/3} d_{40}^{3/2} S^{-7/6} \qquad \textit{Equation 2.10}$$

Where m_s = *transport rate per unit width (kg/s);*

S = *channel slope;*

q = *volumetric water discharge per unit width (m^3/s);*

q_c = *critical volumetric water discharge per unit width (m^3/s);*

ρ_s = *specific mass of sediments (kg/m^3),*

ρ = *specific mass of water (kg/m^3)*

d_{40} = *diameter for which 40% of sediments are finer (m).*

2.13 Physical Scale Modelling

The relationships between fluvial process and form are often extremely difficult to quantify using conventional field and analytical techniques. Physical modelling provides a complementary technique to these methods and may be used to simulate complex processes and feedbacks in many geomorphic phenomena (Peakall *et al.,*1996).

Through this technique, the formative processes can be observed, usually in a reduced time-frame, within a controlled and manageable laboratory environment to produce valuable quantitative information. Physical models may allow incorporation of variables which have markedly non-linear effects on the resultant dynamics or morphology.

Historically, small-scale embankment failure research was considered to be qualitative due to the difficulty of adequately reproducing the complex processes of erosion and sediment transport in steep, shallow flows at small scales; research in large-scale facilities was considered more quantitative (Singh, 1996). Random influences can be substantial, and thus repetition of model tests is critical.

Physical scale modelling to verify the role of the carapace facies in overtopping induced breach development appears to be a potentially useful approach, owing to the scale and cost of the structures under investigation. Several researchers have previously used this approach to identify and examine the factors affecting the temporal evolution of overtopping breaching phenomena.

2.13.1 Studies using Physical Scale Modelling

Donadini and Kunz (2001) and Davies *et al.,*(2006 in press) successfully used physical scale modelling to verify the failure sequence of the Poerua rock avalanche dam, in Westland, New Zealand, and collect data on the hydrograph shape generated by overtopping failure of a homogeneous dam of this type. After testing various dam geometries in a tilting v-shape flume, they concluded that higher peak discharges were characteristic of smaller dam volumes and larger water volumes. Although the highest peak discharges were generated by the steepest dam geometries, the gradient of the upstream valley bed slope appeared to exert the greatest control on peak discharge, due to its critical influence dam volume. Furthermore channel gradient was found to exert significant control on peak discharge, with recorded Q_p rates from a valley bed slope of 5° appearing 20-30% lower than those recorded on a bedslope of 3.5° (a smaller peak discharge for steeper valley bed slopes).

A constant inflow rate of 3 L/s was used in the model to fill and overtop the dam, corresponding to 800 m^3/s in the prototype (equivalent to a 2-year flood in the Poerua River). Using a linear scale ratio of 1:150 ($\lambda = 150$), the recorded breach outflow from the model achieved a high degree of similarity to outflow and temporal rates inferred during the prototype event. Application of regression-based peak discharge estimations (Costa, 1988) were also in agreement with the modelled rates.

Investigation of breach development in overtopping non-cohesive embankments by Coleman *et al.,* (2002) reveals that erosion primarily evolves from vertical to lateral, involving the processes of tractive shear and turbulence. The breach channel initially erodes the downstream face of the embankment with an invert slope parallel to the face; the breach invert slope then progressively flattens to a final value by rotating about a fixed pivot point along the base of the embankment, the location of this pivot point being a function of the size of the embankment material.

In terms of hydraulic performance, Coleman *et al.,* (2002) also concluded that breach development was consistent with the principle of minimum rate of energy dissipation for streams, whereby a stream is

assumed to change its channel geometry in a manner that tends towards producing a minimum rate of energy dissipation (Chanson, 1999). Such channel geometry has been observed to correspond to maximum sediment transport conditions (Davies and McSaveney, in press 2007).

Chapter 3 Model Similitude

3.1 Introduction

Scaled reproduction of processes and forms resulting from the overtopping of heterogeneous non-cohesive rock avalanche deposits requires adherence to correct geometric, kinematic and dynamic scale ratios between the model and prototype. Often, all relations cannot be satisfied simultaneously and therefore a systematic procedure for selecting the similitude requirements that minimise the scale effects is required. Using dimensional analysis, similarity relations can be derived and relationships between geomorphic forms and processes established and interpreted in the context of the assumptions used. Scale models are based on similarity theory, which produces a series of dimensionless parameters that fully characterise the phenomena.

Scale models have two advantages over mathematical models (Peakall *et al.*,1996);

1. The formative processes can be observed, usually in a reduced time frame, within a controlled and manageable laboratory environment.
2. They allow incorporation of variables which are not known a priori and may have markedly non-linear effects on the resultant dynamics or morphology

3.2 Hydraulic Similarity

The success of any physical scale model depends on the proper choice of similitude requirements and the extent to which they are satisfied. For any set of similar phenomena, all the corresponding dimensionless characteristics (dimensionless combinations of dimensional quantities) have the same numerical values. As the hydraulics are principally concerned with the forces that affect fluid and sediment motion, hydraulic similarity requires dynamic similarity between a model and its prototype.

Three degrees of similarity are required between a model and its prototype.

Geometric Similarity requires a constant ratio of length dimensions.
Kinematic Similarity requires constant ratios for both length and time dimensions to give a similar velocity.
Dynamic Similarity requires constant ratios for length, time and mass to ensure similarity of forces; note that this incorporates geometric and kinematic similarity.

Overtopping failure is a free surface, gravity dominated phenomenon, and therefore Froudian model scaling laws apply, requiring that the ratios of gravity to inertia forces correspond between model and prototype (Andrews *et al.,* 1999). In an idealised situation, every variable should be perfectly scaled in the model, requiring unity between Reynolds, Euler, Froude and Weber numbers in both the model and prototype; however due to experimental limitations, fulfilment of this requirement is never possible.

3.3 Dimensionless Parameters

Using dimensional analysis, the several parameters which describe a given system can be combined into a smaller number of dimensionless groups (Young and Warburton, 1996). Assuming a non-cohesive, homogenous material, two phase flow over a mobile bed can be completely described by;

- properties of the fluid; the dynamic viscosity (μ) and density (ρ)
- properties of the sediment; grain size *(D)*, density (ρ_s) grading coefficient (Ø)
- the nature of the flow; bed slope (*S*), flow depth (*d*) and gravity (*g*)

$$\gamma_s = g(\rho_s - \rho) \qquad \textit{Equation 3.1}$$

$$V^* = \sqrt{Sgd} \qquad \textit{Equation 3.2}$$

Substitution of independent parameters such as gravity into Equation 1 to give the *specific weight of the granular material* (Eq. 3.1) and flow characteristics into Equation 2 to calculate the *shear velocity* (Eq. 3.2) produces the four dimensional groups (Equations 3.3-3.6) after Young and Warburton (1986).

$$\mathrm{Re}^* = \frac{V^* D}{\nu} \qquad \textit{Equation 3.3}$$

$$Fr_* = \frac{\rho V_*^{\,2}}{\gamma_s D} \qquad \textit{Equation 3.4}$$

$$d_{relative} = \frac{d}{D}$$ *Equation 3.5*

$$\rho_{relative} = \frac{\rho_s}{\rho}$$ *Equation 3.6*

If the linear scale ratio between prototype and model is kept constant for all four of these terms, the model can only satisfy full dynamic similarity with a length scale of unity, thus requiring a full scale model (scale ratio 1:1).

When modelling dam breaching, the model grain size must be large enough to ensure rough turbulent flow (R_e* >70; Young and Warburton, 1996) necessitating the use of gravel and sand sized particles. As flow in the prototype is entirely turbulent, so must flow in the model. The criterion for turbulent flow in open channels is the Reynolds Number (Equation 3.7).

$$\mathrm{Re} = \frac{Vd}{v} \geq 500$$ *Equation 3.7*

3.4 Key Requirements for Dynamic Similarity

Warburton and Young (1996) specify five requirements to be met in order for dynamic similarity to be achieved;

- sediment density is equal in both model and prototype
- grain sizes are scaled directly by length scale
- water is used as the model fluid
- flow is rough-turbulent in the model
- bed slopes are equal in model and prototype

In the present case the grain-size Reynolds number criterion is relaxed, while ensuring that flow remains in the fully turbulent regime, but the Froude number is scaled correctly. Relaxation of the grain-size Reynolds number allows more flexibility in the model scaling than variation in the Froude number which must be more tightly constrained. This technique is known as Froude scale modelling (FSM) and is

commonly used successfully in moveable–bed modelling. In free-surface flows, most laboratory studies are based upon a Froude similitude (Henderson, 1966; Chanson, 1999).

Flow through a developing breach in a landslide dam can be simplified by the assumption that there is no back-water effect at its downstream end. In such a case the flow at the upstream end of the breach will become critical (Fr = 1), causing it to behave hydraulically as an undrowned broad-crested weir (Walder and O'Connor, 1997).

Froude scaling using a length scaling ratio of $\lambda = 400$ was chosen. The principal criterion for choosing the optimal length scale for an FSM study is a function of the ratio between the prototype R_e* and the minimum R_e* for turbulent conditions in the modelled flow. The practical limitations are usually size of the available flume facility, or the limits of space, time and money available when constructing a new flume. A length scale of $\lambda = 400$ also allows the average geometry of prototype landslide dams to be matched from linear scaling of model geometries. Mention that prototype dams have height ~ 100 m, models usually <1 m; is shows where the 400 comes from.

All model dimensions and hydraulic data outlined in Table 3.2 (kinematic and dynamic similitude) can be scaled to prototype values using the relationships derived from Froude Scaling outlined in Table 3.1. The geometric, kinematic and dynamic scaling ratios for the Froude model are shown in the following equations, where λ equals the model to prototype scaling ratio for the property *x*.

Table 3.1 Froude Scaling Ratios

Parameter	***Ratio***	***Scaling X_p X_m***
Length	$Xp/Xm = \lambda$	*400 1*
Time	$tp/tm = \lambda = \lambda^{1/2}$	*20 1*
Volume	$Vp/Vm = \lambda^3$	$64x10^6$ *1*
Flow	$Qp/Qm = \lambda^{5/2}$	$32x10^5$ *1*
Force	$Fp/Fm = \psi = \lambda^3$	$64x10^6$ *1*
Cohesion	$Cp/Cm = \lambda$	*400 1*

A key factor in similitude is the model roughness. Turbulent flow in the model can be assured by specifying a minimum Reynolds number for the model flow. Therefore, the Reynolds number similarity is relaxed, with the proviso, R_e remains within a fully turbulent flow regime (R_e>500). Turbulent flow implies that the friction factor is independent of the Reynolds number.

Table 3.2 Summary Table of scaled model design parameters and conditions

Parameter	*Prototype Value*	*Model Value*	*Scale*
Flow depth (m)	*~8*	*~0.02*	*400 1* Ł
Mean flow rate (m^3/s^{-1})	*~3400*	*~1.08 x10^{-3}*	*3200000 1*
Sediment d_{50} (m)	*0.1-1.0*	*6x10^{-3} - 6x10^{-4}*	*400 1*
Reynolds number	*~17x10^6*	*~2000*	*400 1*
grainsize Reynolds	*2 x 10^5*	*~ 107*	*400 1*§
Assumed Froude	*1*	*1*	*1 1*¶
Weber number	*43*	*0.1*	*400 1* jj
Relative Density (kg/m^3)	*2.6*	*2.6*	*1 1* ŁŁ

Ł Assumed flow depth

§ Usual requirement is for both model and prototype values to be >70 (rough turbulent flow).

¶ Usual requirement is for model and prototype vales to be identical (free surface flow)

jj Usual requirement is for model value to be >10–100.

ŁŁ Usual requirement is for model and prototype vales to be identical

3.5 Scale Effects in Steep Channels

Scale effects (discrepancies between model and prototype) generally arise from imperfect modelling of geometric and kinematic conditions rather than a flaw in basic theory of dynamic similitude (Young and Warburton, 1996).

3.5.1 Model flow Conditions

Model dissimilarity occurs when parameter values become inconsistent between model and prototype (usually caused by use of a small scale). Correct modelling of shear stresses is a vital component of the successful modelling of the transport rate of non-cohesive sediments. Owing to turbulence, the tractive stress, and consequently the drag force on the particle, is subject to fluctuations. The choice of scale for modelling erosion process, is restricted by a requirement for rough turbulent flow. Yalin (1971) suggests this critical value for R_e* lies between 70-150. The scatter of incipient motion values derived from different studies however suggests that transitional and rough turbulent flow conditions may prevail at lower R_e* (Young and Warburton, 1996).

Pugh (1985) also suggests that models operated solely according to Froude scaling do not accurately simulate the tractive forces (sediment erosion) and therefore should maintain a R_e* >70. In this case, the relative magnitudes of viscous forces will be approximately correctly simulated in the model.

In rough-turbulent flow, grain detachment and motion are independent of fluid viscosity and therefore R_e* itself. Flow with R_e between 500 and 2000 is transitional and has some characteristics of laminar flow, but some turbulence as well. Laminar flow also occurs locally in turbulent flows right at the contact between the fluid and a smooth surface it is flowing over as velocity decreases. This has important implications for transport of fine sediments.

Several problems arise in attempting to quantify bed load transport, especially in highly dynamic erosion environments, non-representative of the conditions used to derive many sediment transport relations. Yalin (1971) demonstrated that if R_e* is below the critical threshold for a fully turbulent boundary while fluid and temperature characteristics are maintained for both model and prototype, dynamic similarity of sediment transport can never be achieved. Studies from river modelling also indicate that the inclusion of a high proportion of fine sediment in grain size distribution or local sorting in the model can vary and often increase bedload transfer, causing overestimation of bedload transport rates.

3.6 Surface Tension

The forces caused by surface tension are very important in hydraulic models with lower flow velocities or small dimensions where the surface area to volume ratio is large, and the radii of curvature of the liquid surface, and the distances from the solid boundaries, are very small. Surface tension forces are negligible in field-scale rivers and should be kept negligible in hydraulic models also.

$$We = \frac{\rho . d . V_*^2}{\sigma} \qquad \textit{Equation 3.8}$$

Defining a critical Weber number (Equation 3.8) for small hydraulic models has to date been largely based on operator experience. The calculated model Weber number of 43 for the present study is within the suggested range of critical values (10-120) which suggests that surface tension induced distortion may be minimal. Henderson (1966) advises that, as long as channel depths and widths are greater than *0.025-0.05m* capillarity and surface tension can be ignored. Novak and Cabelka (1981) suggest three minimum operating conditions to reduce surface tension effects:

- The length of a surface wave on the model is > *0.017m*
- The velocity at the water surface of the model is $>0.23ms^{-1}$ so that gravity waves are free to develop
- The depth of flow in the model is > *0.015m*

As the current model adheres to the recommendations of both Henderson (1966) and Novak and Cabelka (1981), surface affects are assumed to be negligible and no adjustment using additives or rescaling is required.

Chapter 4 Experimental Study

4.1 Experimental Objectives

The objectives for modelling the role of the carapace facies in breach development within rock avalanche deposits were as follows:

1. To obtain data on the overtopping of a rock avalanche dam constructed of non-cohesive heterogeneous materials for the purpose of investigating the influence of the carapace in the stability of rock avalanche dams. This includes determination of the following parameters:

    - Breach outflow hydrograph
    - Evolution of breach geometry with time
    - Migration of the phreatic front during lake filling and overtopping

2. To observe peak discharges and the rates of breach development for rock avalanche dam failure so as to assess the ability of contemporary engineering applications to represent the phenomena processes of catastrophic failure of rock avalanche dams.

3. To quantify the uncertainty associated with peak discharge prediction from overtopping breaching of rock avalanche dams using four different modelling techniques.

4.1.2 Model Assumptions

In modelling events such as landslide dam formation and failure, a conservative approach or *worst case scenario* is the most appropriate for hazard management and emergency planning.

- The presence of a carapace has been documented to act as a permeable spillway (as designed in various rockfill dams) promoting equilibrium conditions between inflow and outflow. A key assumption in modelling such phenomena would require a threshold condition (such as inflow rate, or lake level) to be exceeded to produce overtopping failure.

- As landslide dam failure is most likely to be induced by excessive precipitation (Section 2.2.2); a storm hydrograph entering the impounded reservoir would cause inflow to increase to a definable

peak before subsiding. For this investigation the reservoir inflow rate was assumed to be constant. This approach accounts for the following conditions:

1. The peak discharge of the inflow storm hydrograph occurs before emplacement of the rock avalanche impoundment.

2. The storm event volume is insufficient to completely fill the impounded reservoir.

3. Flow through a developing breach is simplified in assuming minimal back-water effects at the breach outlet, in turn causing flow at the breach inlet to become critical (Fr = 1), and behave hydraulically as a broad-crested weir (Chow, 1959; Henderson, 1956). Walder and O'Connor (1997) claim this simplification strictly valid only if the breach length is sufficient to promote the development of a critical flow regime. Frictional resistance to flow may be more prevalent in breach channels of natural dams which incorporate a broad geometry, resulting in an overestimate of outflow discharge.

4. Given the inherent difficulty in modelling the dynamic and rapidly varied hydraulic processes observed in landslide dam failure, breach development is oversimplified using uniform steady-flow hydraulics. Such hydraulic regimes are a convenient "best guess" and therefore severely limit the applicability of various sediment transport models to dam breaching.

4.2 Principal Parameters

4.2.1 Inflow

The influence of inflow conditions on rock avalanche dam stability was a key objective of this research. From extensive preliminary studies (outlined in Figure 4.2), failure was assessed for both a high and low reservoir inflow condition. From these studies it was noted that a reservoir inflow of 0.001m^3/s represented the minimum critical inflow capable of initiating failure in carapace dams (under laboratory conditions). Therefore a low inflow condition of 0.001m^3/s was sufficient to reliably initiate failure, without overwhelming the intrinsic behaviour of the failing dam. Due to the nature of the scaling factor, the low inflow condition of 0.001m^3/s in the laboratory is represented by an inflow of 3200 m^3/s in the prototype. This is extremely conservative and of low probability, representing a 10 year flood or alternately a 100 year rainfall event within a 100 km^2 catchment, produced by inundation of the catchment with >100 mm falling in 24 hours. The high inflow condition of 0.0035 m^3/s (10,000 m^3/s at the prototype scale) was only representative of a condition whereby multiple landslide dams had formed in a river

valley and a cascading outburst flow had been generated from an upstream collapse. All simulations used a constant inflow throughout the duration of breaching. Flow rates were measured with a Dall™ tube flowmeter.

4.2.2 Saturation

A second objective was to assess the influence of dam material saturation on dam stability. Saturated conditions could result from slow rates of reservoir filling leading to complete saturation of the dam base before the reservoir level reaches the dam crest. Saturation may significantly influence dam stability.

4.3 Experimental Design for Dam Failure Modelling

4.3.1 Experimental Design

Physical scale modelling of breach development processes in the overtopping failure of rock avalanche dams was carried out in the Fluid Mechanics Laboratory of the Civil Engineering Department at the University of Canterbury, Christchurch, New Zealand.

The experimental procedure used for the Physical Scale Model (PSM) dataset (Figure 4.1) was refined from an extensive background study program (summarised in Figure 4.2). Over 100 dams were tested in this study, 60% of which constitute those used in background studies to refine the both the materials being tested and the research methodology used to generate appropriate relationships between breach geometry and the outflow hydrograph.

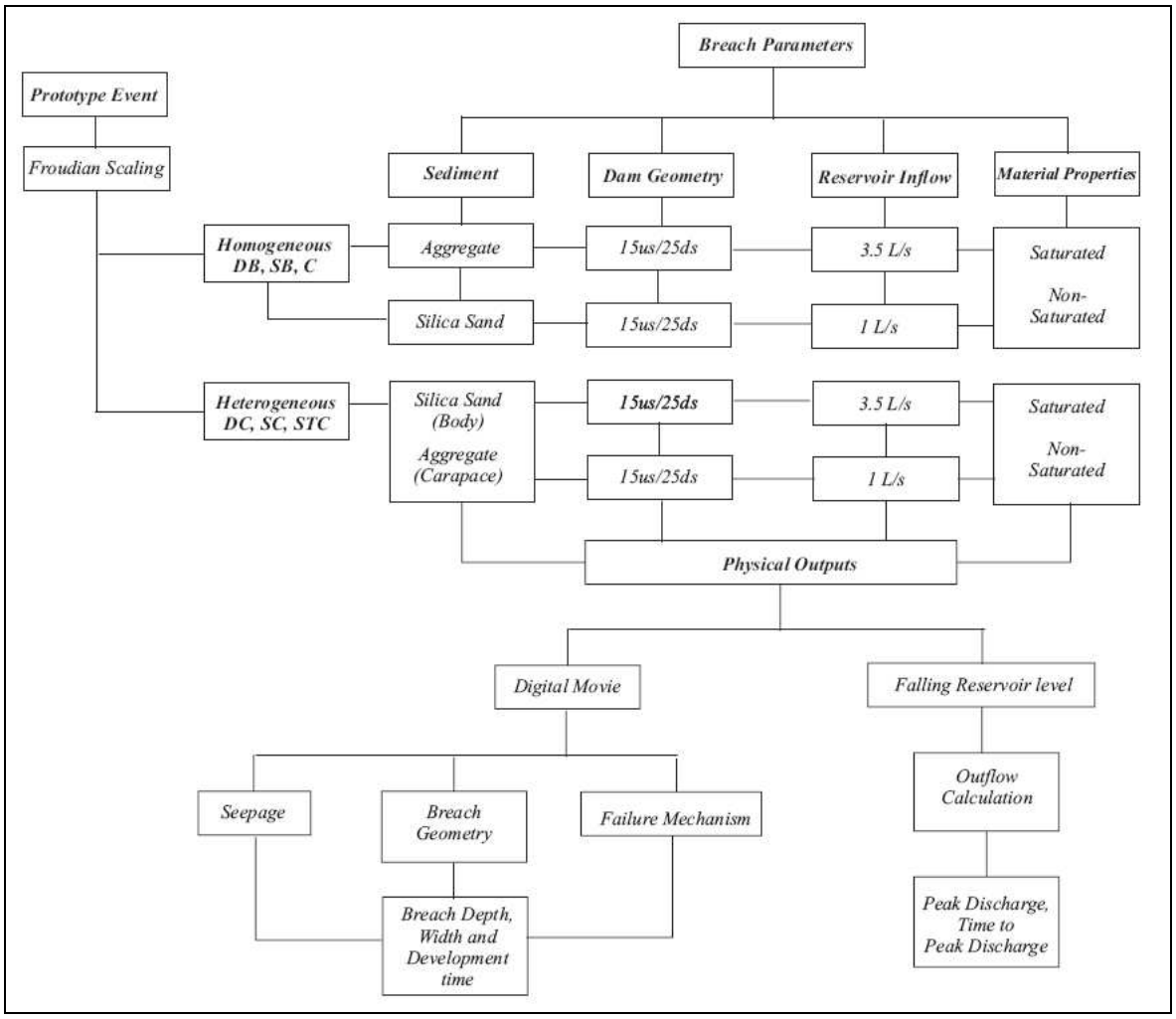

Figure 4.1. Experimental Procedure for Physical Scale Model dataset

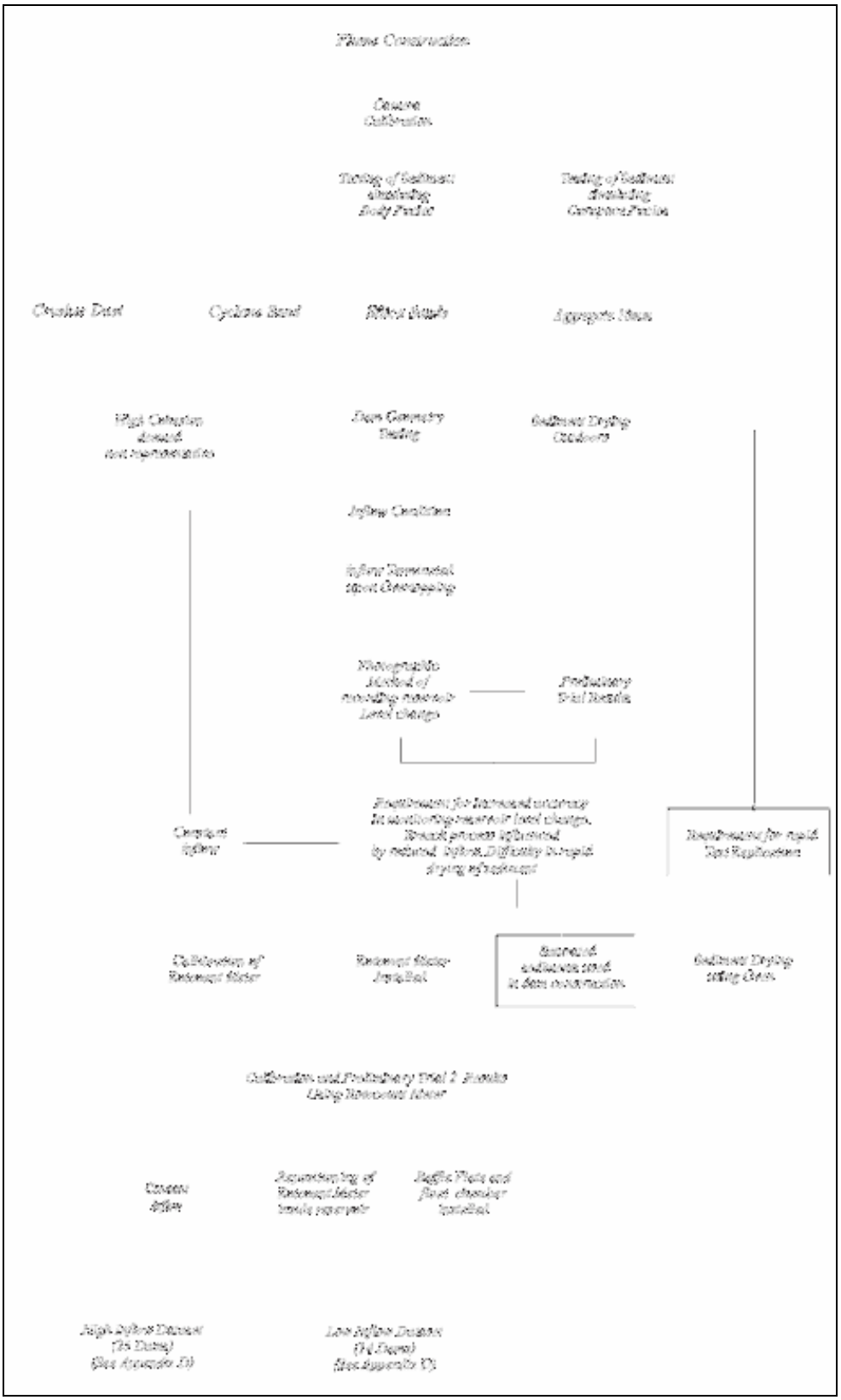

Figure 4.2. Background Study Program

4.4 Experimental Set-up

4.4.1 Flume

A purpose-built flume (Figure 4.3 and 4.4) was constructed for this research, to allow complete visibility of the breach development in longitudinal profile, in addition to accessibility for sediment retrieval. Water was sourced and collected from the laboratory constant head supply system.

The flume incorporated a rectangular storage reservoir (simulating an impounded lake or water body), channelised flow through a flume to discharge into a sediment retrieval structure. The 0.5m deep, 0.5m wide and 4m long flume also had a 0.02m thick glass panel on one side to allow complete recording of the breaching process. The reservoir was 1.5 x 2.2m in plan, with a maximum storage volume of ~ 0.82 m^3 (behind a 0.25m high dam). A 1m long sheet metal extension to the timber flume fed the discharged sediment and water to temporary storage; this was pumped to an external drain (Figure 4.4).

The volume of the reservoir was selected to give a relatively long-duration outbreak event, so that the erosive processes occurring in the breach channel could be adequately monitored. This resulted in some dissimilarity with field situations in steep mountain terrain, where the lake volume is likely to be smaller relative to dam volume due to the steep valley slope and narrow valley width. Thus the peak discharges from the model are likely to be much higher than would be expected from a similarly-sized dam in a more realistic reservoir setting such as that observed for the Poerua event.

4.4.2 Digital Recording Cameras

The flume was specifically designed for visualisation of the breach process. Video captured the failures of dams of variable composition for measurement of breach development and seepage rates. Three digital cameras recorded the breach development process for overhead, longitudinal and frontal profiles (Figure 4.4).

- The overhead profile was filmed using a Canon™ MV30i (speed: 25 frames/sec, shutter: 1/4 to 1/10,000 sec: sand mode, lens F/4.1-4.9 zoom: 1:12) located 3m above the dam crest.

- The longitudinal profile was filmed using a digital video-camcorder Canon™ XM2 (speed: 25 frames/sec, shutter: 1/4 to 1/16,000 sec., lens F/1.6-2.9, zoom: 1:20; 1488x 1128 pixels) positioned perpendicular to the dam crest at a distance of 1.3m.

- The frontal profile was filmed with a Sony™ Digital Handycam DCRTRV740E (speed: 25 frames/sec, shutter: 1/4 to 1/10,000 sec: sand mode, lens F/4.1-4.9 zoom: 1:12). Positioned 2.5m from the dam crest.

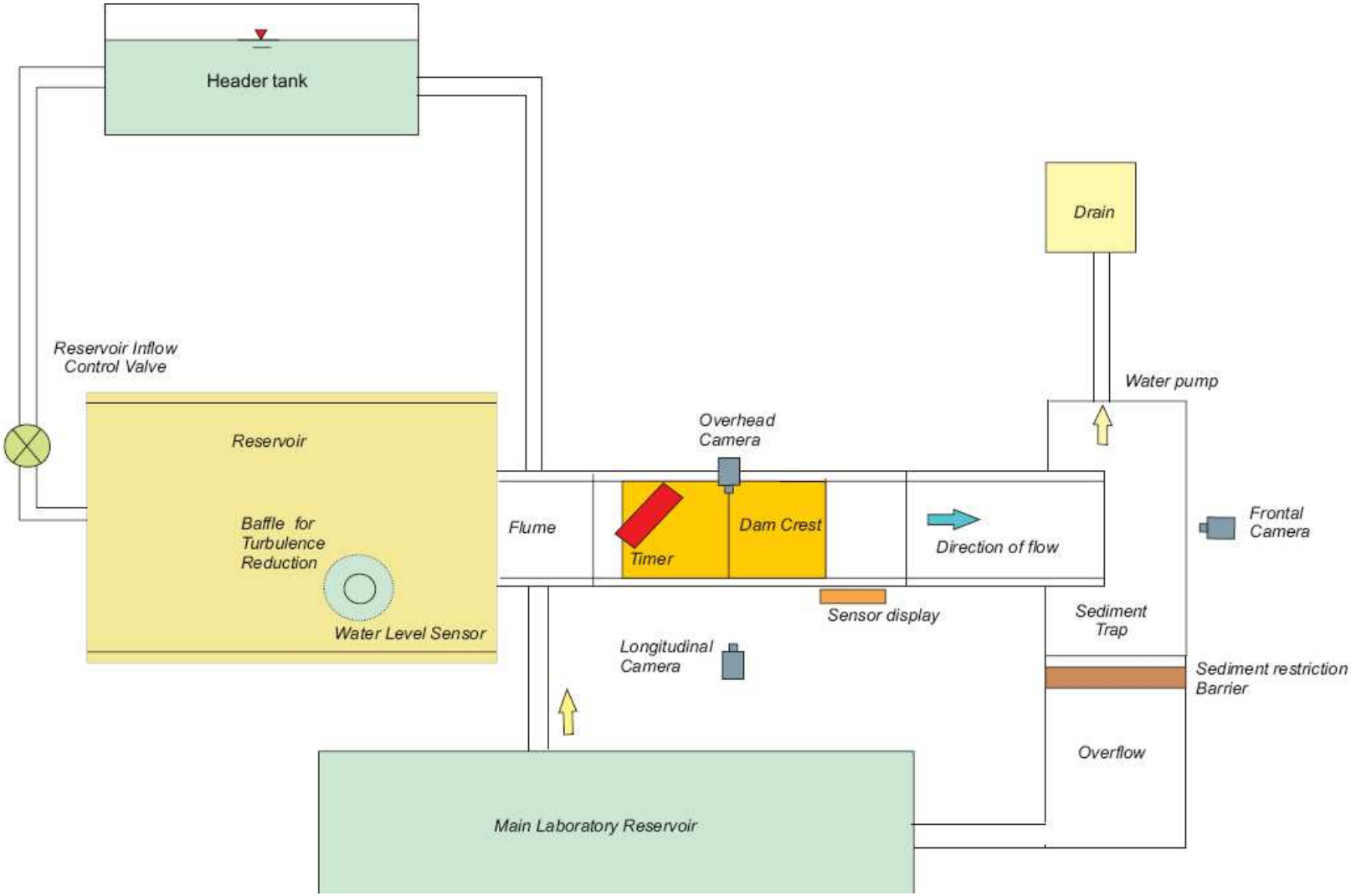

Figure 4.3. Experimental Flume Set up

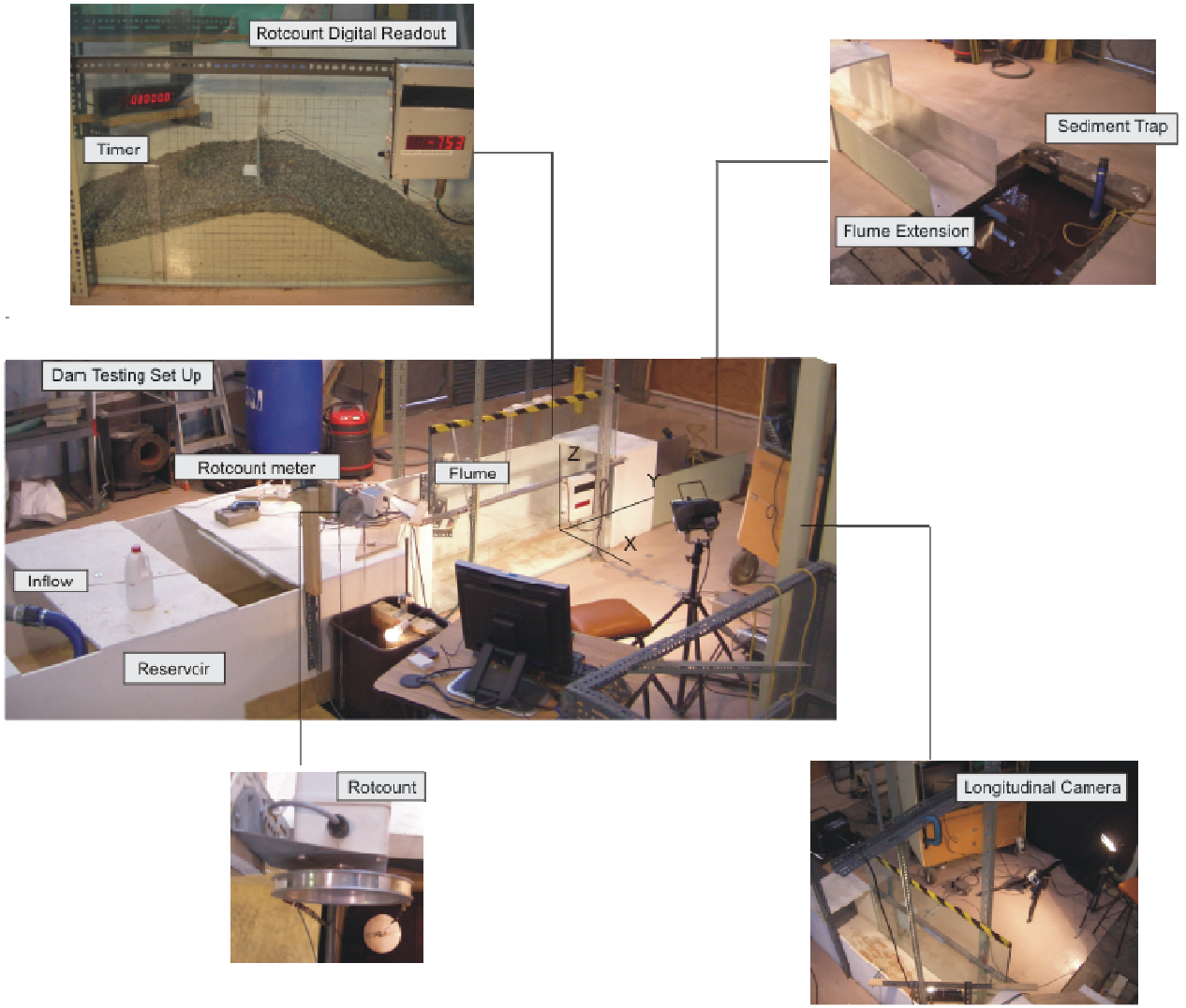

Figure 4.4. Laboratory Setup

4.4.3 Water Level Recording

When dam failure starts, the reservoir surface level starts decreasing and at the same time the outflow increases. By measuring the decrease of the water surface level, change in volume can be calculated, and thus the outflow discharge.

During this experiment a *rotcount meter* (Figure 4.5) was used to measure the variations of the water surface level with a count rate of 5 seconds in "pulses". The pulses were then converted into millimetres. One pulse was the 4000^{th} part of one complete turn of the rotcount-wheel, which has a perimeter of 0.37m. This measuring apparatus had a very high precision (1 pulse = 0.0925 mm) and was able to record the transition from a rising to falling water level in the critical period following overtopping and breach incision.

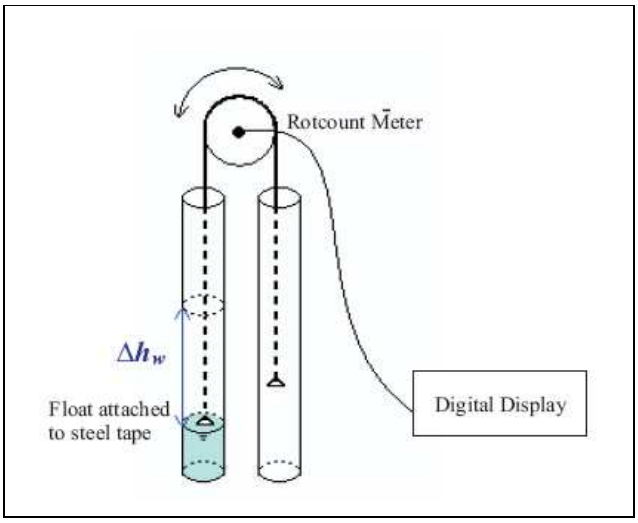

Figure 4.5.Rotcount meter

The water level was recorded by a float, housed in a permeable chamber constructed from 0.15m diameter PVC piping within the reservoir itself. This chamber was designed to reduce the influence of wave action on the water surface being measured and increase the accuracy of the readout. The float resting on this water surface was attached to a steel tape which rested on the pulley wheel of the rotcount meter. Upon breaching at the dam crest, the float would fall with the falling reservoir level, with the rotcount meter recording the pulse count as the pulley wheel rotated. The pulse count was then electrically transmitted from the rotcount meter to a digital display output mounted on the flume wall. The breach discharge $Q_{out}(m^3/s)$, was calculated by subtracting the reservoir inflow Q_{in} (m^3/s) from the total breach outflow $Q(m^3/s)$.

4.5 Dam Construction

This study incorporated a half-width simulation of overtopping failure. Preliminary studies outlined in Figure 4.2 indicated that due to settlement, overtopping would be concentrated at the central part of the dam crest to produce a breach which remained pseudo-symmetrical throughout development. Half breach simulations were found to accurately reproduce breach widths generated in full breach simulations for similar sediment and inflow conditions. Therefore half breach measurements can be extended to represent the full breach condition.

Dam geometry and volume were held constant. Each dam was constructed to a predefined geometry marked on the exterior of the flume walls. The construction method varied depending on the dam type being modelled. Table 4.1 outlines the 6 types of dams constructed.

Table 4.1 Structures Tested

Trial	*Abbreviation*	*Definition*	*Repetitions*	
			1 Litre/sec	**3 Litre/sec**
Heterogeneous				
Carapace	*DC*	*Dry Carapace*	*2*	*4*
	SC	*Saturated Carapace*	*5*	*7*
	STC	*Saturated Thickened Carapace*	*2*	*5*
Homogeneous				
Carapace	*C*	*Carapace*	*2*	*3*
Non-Carapace	*DB*	*Dry Body*	*2*	*3*
	SB	*Saturated Body*	*3*	*6*

4.5.1 Dam Geometry

The model dams were constructed to represent the average geometry and sedimentology of rock avalanche dams recorded in several inventories (Costa and Schuster 1988; Walder et al., 1997) . The dam was constructed with a downstream face slope of 25° and an upstream face slope of 15°, to produce a dam volume of 7.2×10^{-3} m^3. This longitudinal section resembles that of the landslide dam which blocked the Poerua River valley in 1999 (Figure 4.6). The dam crest was maintained at a height of 0.25m above the flume base, with the breach pilot channel incised to a depth and width of 0.02m adjacent to the glass flume wall prior to reservoir filling.

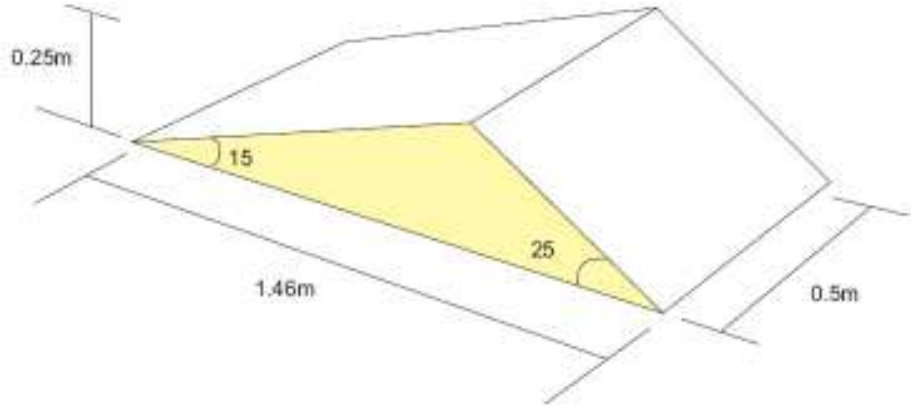

Figure 4.6. Dam Geometry

4.5.2 Dam Materials

Field observations of rock avalanche deposits (Dunning *et al.,*2005) have led identified distinct zonations or facies, notably the *carapace facies* which is highly angular, boulder-sized and porous with a high hydraulic conductivity. The underlying *body facies* consists primarily of finely crushed material matrix containing larger clasts of all sizes, with a higher susceptibility to erosion.

The construction materials were selected to accurately simulate the influence of material heterogeneity on breach development during overtopping failure of a rock avalanche dam. The selected material needed to be relatively impermeable and also non-cohesive. Cohesion in actual rock avalanche deposits is usually very low (*Davies pers. comm.)* and therefore in the model the cohesion of the dam material, which has to be reduced by the scaling factor (λ) is likely to have a negligible influence on the breaching process.

Overtopping and down cutting, promoting breach enlargement through sidewall failure are the most prominent failure mechanisms at the prototype scale. The representation of these processes requires approppriate model material.

In preliminary studies materials including crusher dust and cyclone sand were tested to simulate body facies; however all had too much cohesion, particularly under saturated conditions. Silica sand was selected as the simulation material because of its low permeability, zero cohesion (when dry) and availability. Simulation of the carapace was achieved using crushed roading aggregate (10mm metal chip) derived from greywacke river gravels. The body facies was simulated using a mixture of four parts silica sand to one part aggregate. Standard sieve analysis tests were carried out for both the silica sand mixture and the aggregate to determine grain size distribution (Figures 4.7 to 4.8). The properties of the test material are listed in Table 4.2.

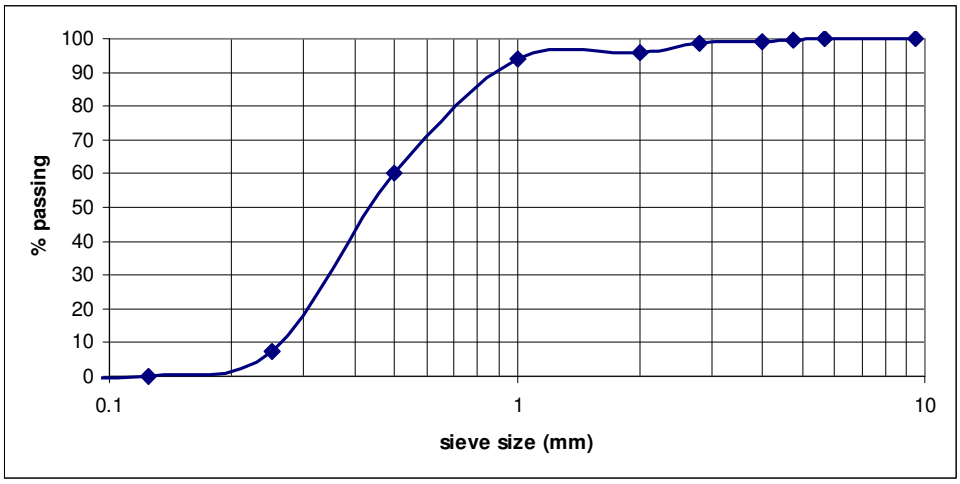

Figure 4.7.Grading curve for silica sand mixture used to simulate the body facies

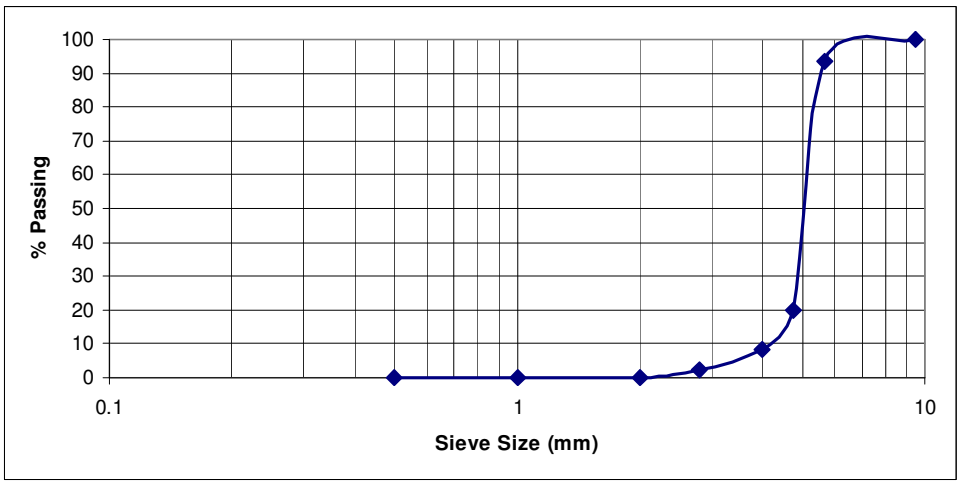

Figure 4.8.Grading curve for aggregate used to simulate the carapace facies

Table 4.2 Material Properties

Sediment	d_{50} *(mm)*	*Bulk dry density* (kg/m^3)
Silica Sand Mixture	*0.043*	*1505*
Aggregate	*5*	*1353*

4.5.3 Construction Sequence

The dam was constructed within the flume, with *body* sediment mixed to a standard ratio of 4:1 (silica sand mixture: aggregate) externally before emplacement. Construction of the dry dams incorporated a multiple stage system, to ensure a maximum degree of uniformity throughout the deposit. Each dam building stage involved placement of an equal material volume using the homogenised mixed sediment. A

spade was then used for compaction and surface smoothing. Material compaction was assessed by hand and considered adequate when a firm response to applied pressure was felt without shear of the material.

Construction of dry carapace (DC type) dams incorporated the emplacement of a carapace over the body material (Figure 4.9). The aggregate was deposited by shovel over the dam in a mantled morphology of uniform thickness. The thickness of the carapace layer required for saturated thick carapace (STC) dams, made uniformity difficult to maintain. No attempt was made to simulate the lobate morphologies of real rock avalanche deposits on the carapace structure. Apart from ensuring adherence to geometrical and volumetric constraints, the aggregate was not compacted or smoothed after placement.

Figure 4.9. Dry Carapace (DC) and Dry Body (DB) dams after construction

Saturated dams were built differently due to the change in geotechnical properties of the model material. Such tests were conducted following the completion of a non-saturated trial and involved collection and recycling of the sediment used in the previous trial. Consequently sediment/aggregate ratios in the model material for SC and STC trials were higher (3:1) due to the incorporation of the carapace aggregate into the body material on dam failure.

Saturated dams were of standard geometry and volume. Compaction and smoothing were restricted to the downstream face. On contact with water, silica sands tended to bond to the aggregate and make visual distinction of carapace thickness and uniformity difficult.

Homogeneous dams; Dry body (DB), Saturated Body (SB), and body composed of carapace (C) were constructed/ emplaced with adherence only to dam geometry and volume constraints.

4.6 Pre Run Check

Prior to the commencement of any trial, the following steps were required.

- Removal of surface water in flume with wet/dry vacuum.
- Longitudinal Camera, focused with display to audiovisual unit (aid for construction).
- Dam construction.
- Pilot channel cut.
- Positioning and clamping of dam crest scale.
- Timer turned on and reset to zero.
- Remove foreign objects and obstructions to downstream flow.
- Raise and secure the reservoir drainage pipe (inhibit reservoir drainage).
- Sieve and basket positioned under flume extension for sediment retrieval.
- Electronic readout for rotcount switched on and in view of camera.
- Lighting (spot and focused) switched on and positioned (reflection management).
- Longitudinal Camera, focused and in standby mode with feed to video capture on computer initiated.
- Overhead Camera, focused and in standby mode.
- Frontal Camera, focused and in standby mode.
- Hazard barrier in place to redirect lab foot traffic.
- Positioning of light restriction screen using lab crane.
- Main laboratory pump switched on(feed from header tank).
- Flow meter on, clear air from reservoir inflow valve.
- Addition of premixed red food colouring (flow visualisation).
- Lower polystyrene wave baffle sheet to water surface height.

4.7 Experimental Personnel

During the background studies, 2 people were required to operate the experimental setup modelling the breach process, due to the initial study requirement of zero inflow upon dam overtopping. A technician was required to activate the main laboratory pump, and then control the reservoir inflow to a constant rate. The second person monitored the change in water surface elevation adjacent to the upstream dam crest. When the reservoir had reached the maximum crest height and overflow had initiated erosion on the

downstream face, the second person signalled the technician to terminate the inflow. The second person then took still-frame photos of the changing water surface elevation.

To run the constant inflow experiments only 1 person was required after the technician had activated the main laboratory pump. The individual could monitor the inflow until the constant rate was achieved.

4.8 Reservoir Filling

The filling of the reservoir required particular care to minimise the influence of wave development and the potential for overtopping from a displaced or turbulent water profile. Wave reduction was achieved by the positioning of the inflow pipe behind a baffle plate, the use of a polystyrene wave sheet in the reservoir and the permeable housing for the rotcount float.

4.9 Identifying Critical Breach Parameters

For the purposes of this study, the term breach parameters will include the parameters needed to physically describe the breach (breach depth, breach width, and side slope angles) as well as parameters that define the time required for breach initiation and development. These parameters are summarised below.

Breach depth (d_B) is defined for this study as the vertical extent of the breach, measured from a datum, usually the dam crest down to the invert of the breach (breach channel).

Breach width is defined for this study as the breach width at the top (W_T) and bottom (W_B) of the breach opening. As outlined in Section 4.10, this study adopted the use of two cross sectional profiles for breach development analysis.

Breach side slope factor is defined for this study as the angle of repose of the landslide material (approximately 45°). Accurately predicting the breach side slope angles is generally of secondary importance to predicting the breach width and depth.

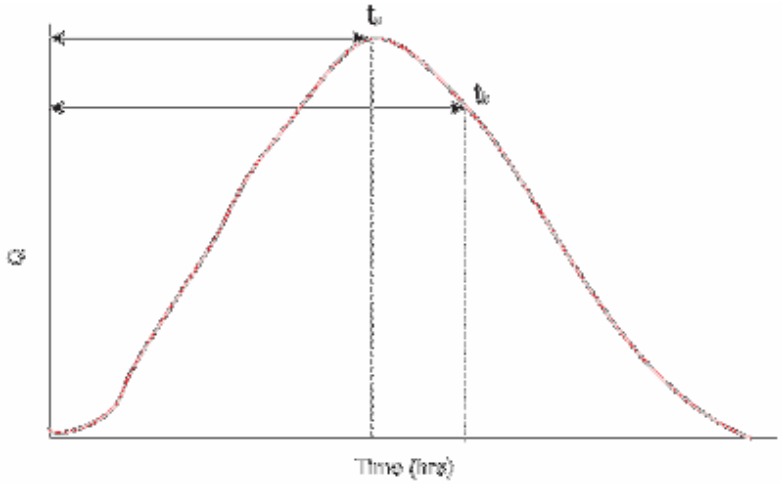

Figure 4.10. Temporal Breach Parameters

The only other key physical parameter is that already identified as;

Peak discharge (Q_p) represents the highest recorded outflow to pass through the breach channel, signified by a point of inflection on the hydrograph and the transition from a rising to falling limb.

Time related parameters are also required in modelling breach development. These are;

Time to Peak Discharge (t_p) for this study is defined as the time required for the outflow to reach its peak discharge (Figure 4.10).

Breach Initiation Time for this study is defined as the time from when initial flow over or through a dam is identified to the first breaching of the upstream face. The use of a pilot channel is this study makes the duration of this stage significantly shorter than that observed for prototype events and therefore is not considered.

Breach Development Time (t_b) for this study is defined as the duration of time between the first breaching of the dam upstream face and the time at which;

1. sidewall collapse into the breach channel ceased or

2. flow velocity through the breach was insufficient to erode the breach bed or readily transport sediment through the breach channel (evaluated from flow depth).

Identifying two distinct time parameters recognises that there are two phases in which the mechanics and rate of erosion can be dramatically different. This is discussed further in Section 5.7.2.

4.10 Measurement of Breach Parameters

All breach parameter data was collected using digital video in x, y and z axes and analysed at the completion of each simulation. From each axis, 2 dimensions of the breach event were captured. The x axis (longitudinal profile) provided breach *length* and *height*, while the z axis (plan profile) provided breach *width*. Although the frontal profile in the y axis was captured, it was used specifically for verification of both x and y axes and identification of key failure mechanisms.

From observation during testing, the breach evolved differently at the breach inlet (head) and outlet (toe). To describe the different breach behaviours, two key cross sections through the breach channel were identified. A primary cross section called C_{max} was used to represent the breach inlet or *crest maximum width* position. This cross section was not fixed, but migrated upstream during breach development. A second, fixed cross section called W_m representing a *minimum breach width* position was used to characterise the outlet zone of the breach. All width measurements were made at these two cross sections (Figure 4.11).

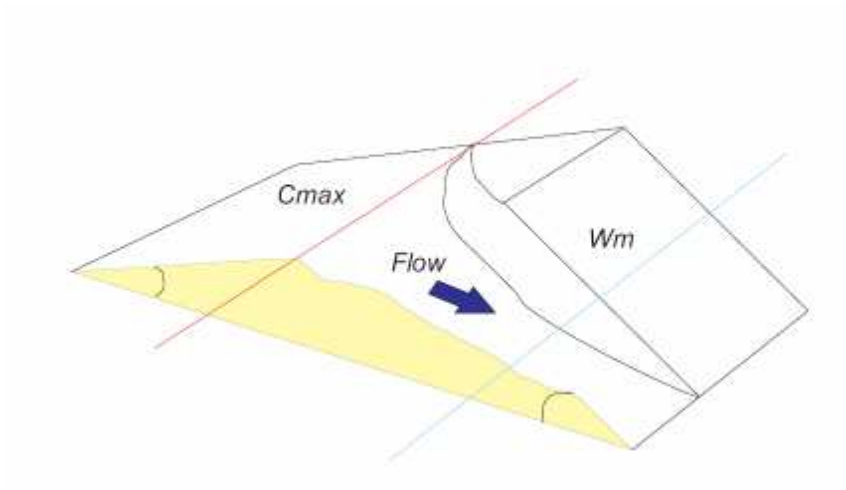

Figure 4.11. Specific cross sectional profiles established for collection of parametric data

Breach width (W_T and W_B), breach water surface elevation (h), elevation of the breach bed (H_b), carapace thickness and crest migration were measured at both C_{max} and W_m profiles, at 5 second intervals using a transparent overlay during the digital playback of longitudinal and overhead profiles. The complete datasets are given in Appendix F.

The collection of depth data from both the C_{max} and W_m cross sections in the longitudinal profile provided a high level of accuracy for verifying breach depth at the breach channel inlet and outlet positions. Cross sectional depths from C_{max} and W_m profiles however, could not be integrated to produce an average breach depth. As d_B is critical to the development of breach geometry, its estimation became an integral part of this investigation.

4.11 Presenting Breach Parameters

In the real-life event of overtopping failure of a landslide dam, only a few parameters may be available. Dam height can usually be estimated accurately and is therefore a known parameter from which other variables such as breach depth, length and width (parameters with significant uncertainties) may be derived or presented. Contemporary empirical analysis techniques used in dam breach modelling (outlined in Chapter 6) also adopt the method of presenting unknown parameters as a function of known parameters.

The method used to characterise the depth of the breach relates the final surface elevation of the breach channel (d_B) below a predefined datum (usually the dam crest) to the original dam height (H).

In terms of the unknown parameter d_B, the base level for the breach erosion process is usually represented by the former riverbed, or the original valley topography can be inferred from field observation. This level, outlined in Figure 4.12, is important in the consideration of a maximum d_B, as peak discharge from large lakes is very sensitive to breach geometry (Walder *et al.*, 1997). While peak discharge from small lakes displays higher sensitivity to breach development time (t_b), breach depth is still a relevant parameter given the observation that breach development initially proceeds from vertical to lateral erosion. Partial failure in landslide dams has also been reported (Hancox *et al.,*2005; Costa and Schuster, 1988) to produce a higher elevation of the final breach channel (smaller d_B) and therefore presentation of breach depth (d_B) as a function of dam height (H) enables full consideration of the above mentioned scenarios.

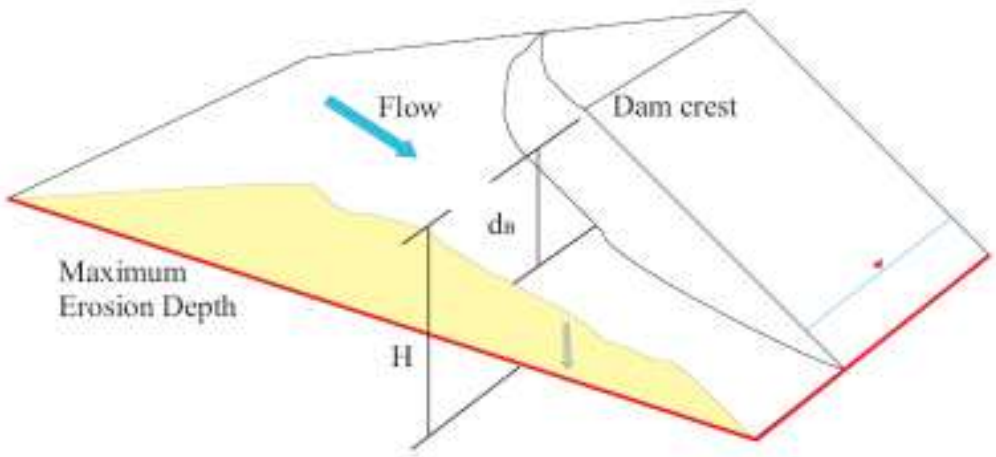

Figure 4.12. Defining the uncertain parameter breach depth (d_B) as a function of the known parameter dam height (H), which is measured from the dam crest to the base level for breach erosion (indicated by the red line)

Although the results obtained from this study were generated specifically for testing numerical models for predicting peak discharge and breach development time, some of these preliminary results indicated potential new research directions.

Chapter 5 Results and Observations

5.1 Introduction

The output data from the Physical Scale Model (PSM) study are initially presented at laboratory scale. For the scaling up peak discharges, the following equation was used:

$$\frac{Q_P}{Q_M} = \frac{x_P^3}{x_M^3} \Big/ \frac{t_P}{t_M} = \lambda^{5/2} \qquad \textit{Equation 5.1}$$

Q_P *flow in the prototype* (m^3/s)

Q_M *flow in the model* (m^3/s)

Table 5.1 Key Results from Physical Scale Modelling of natural dam internal sedimentology at high inflows

Dam type		*Average Outflow*	Q_p	t_p	*Dam Height*	*Breach Depth*	*Breach Depth/ dam height*	*Top Breach Full Width**	*Bottom Full Width*	*Rectangular Area*	*Trapezoidal Area*
		(m^3/s)	(m^3/s)	(hr)	(m)	(m)	(%)	(m)	(m)	(m^2)	(m^2)
DC	Model	0.006	0.011	0.01	0.25	0.2	80	0.91	0.50	0.18	0.14
	Prototype	19200	35200	0.25	100	80	80	364	204	29120	22720
SC	Model	0.006	0.01	0.01	0.25	0.18	75	0.88	0.50	0.16	0.12
	Prototype	19200	32000	0.22	100	75	75	352	202	26400	20775
STC	Model	0.005	0.01	0.01	0.25	0.17	70	0.93	0.60	0.16	0.13
	Prototype	16000	32000	0.25	100	70	70	372	232	26040	21140
C	Model	0.005	0.007	0.01	0.25	0.17	70	0.82	0.50	0.14	0.11
	Prototype	16000	22400	0.22	100	70	70	328	188	22960	18060
DB	Model	0.004	0.008	0.02	0.25	0.212	85	0.96	0.61	0.20	0.16
	Prototype	12800	25600	0.32	100	85	85	386	245	32844	26825
SB	Model	0.006	0.012	0.01	0.25	0.21	85	0.95	0.70	0.20	0.17
	Prototype	19200	38400	0.28	100	85	85	380	282	32300	28131

*Width dimensions doubled to simulate full breach failure

Table 5.2 Key Results from Physical Scale Modelling of natural dam internal sedimentology at low inflows

Dam Type		*Average Outflow*	Q_p	t_p	*Dam Height*	*Breach Depth*	*Breach Depth/ dam height*	*Top Breach Full Width**	*Bottom Full Width**	*Rectangular Area*	*Trapezoidal Area*
		(m^3/s)	(m^3/s)	(hr)	(m)	(m)	(%)	(m)	(m)	(m^2)	(m^2)
DC	Model	0.003	0.007	0.03	0.25	0.20	80	0.92	0.50	0.20	0.10
	Prototype	9600	22400	0.62	100	80	80	366	206	29312	22912
SC	Model	0.003	0.006	0.03	0.25	0.19	75	0.84	0.50	0.20	0.10
	Prototype	9600	19200	0.66	100	75	75	335	185	25140	19515
STC	Model	0.003	0.007	0.03	0.25	0.18	70	0.86	0.50	0.20	0.10
	Prototype	9600	22400	0.5	100	70	70	345	205	24136	19236
DB	Model	0.004	0.008	0.01	0.25	0.21	85	0.79	0.40	0.20	0.10
	Prototype	12800	25600	0.25	100	85	85	315	174	26792	20774
SB	Model	0.004	0.008	0.02	0.25	0.21	85	0.76	0.50	0.20	0.10
	Prototype	12800	25600	0.36	100	85	85	305	207	25908	21739

*Width dimensions doubled to simulate full breach failure

5.2 Outflow Hydrographs

outflow discharge was calculated as a function of time from the changing surface elevation of the reservoir and the reservoir surface elevation and the constant inflow.

Simple variation of base parameters (inflow, saturation) cause the physical scale models of a breaching natural dam to produce significant variability in outflow. Trials were first carried out using a constant inflow of 3.5 L/s (Figure 5.1), but the output parameters were relative insensitive due to the overwhelming influence of inflow rate, and a further set of trials was carried out at an inflow rate of 1 L/s (Figure 5.2), to better reveal some inherent differences between homogeneous and heterogeneous dams.

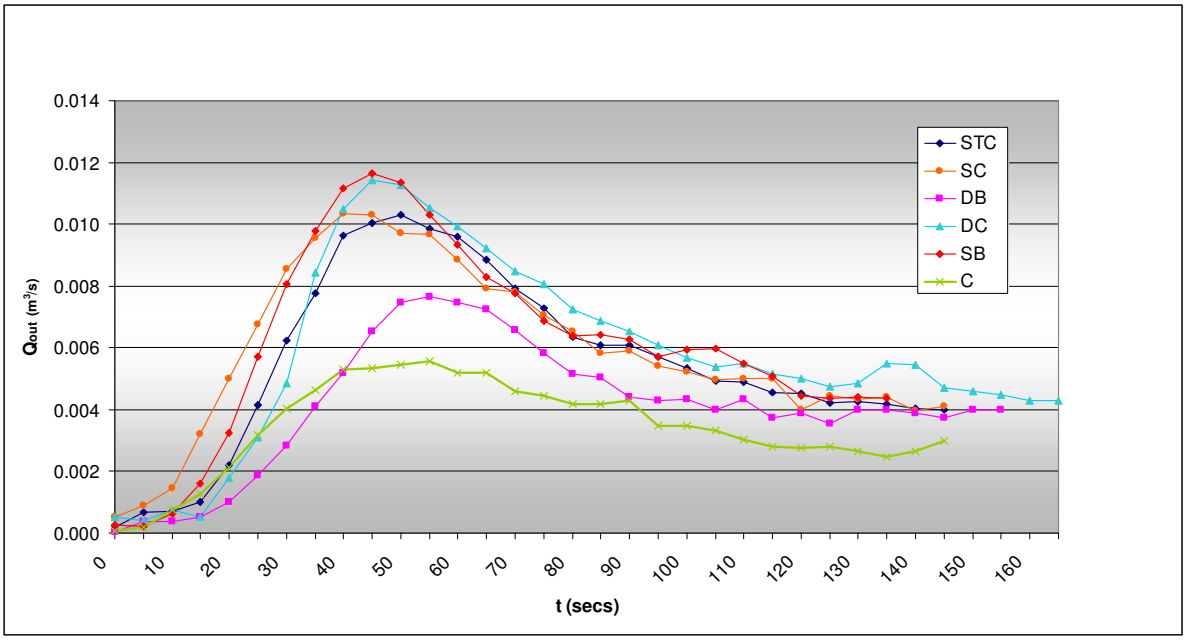

Figure 5.1. Outflows from 3.5 litre/sec inflow models.

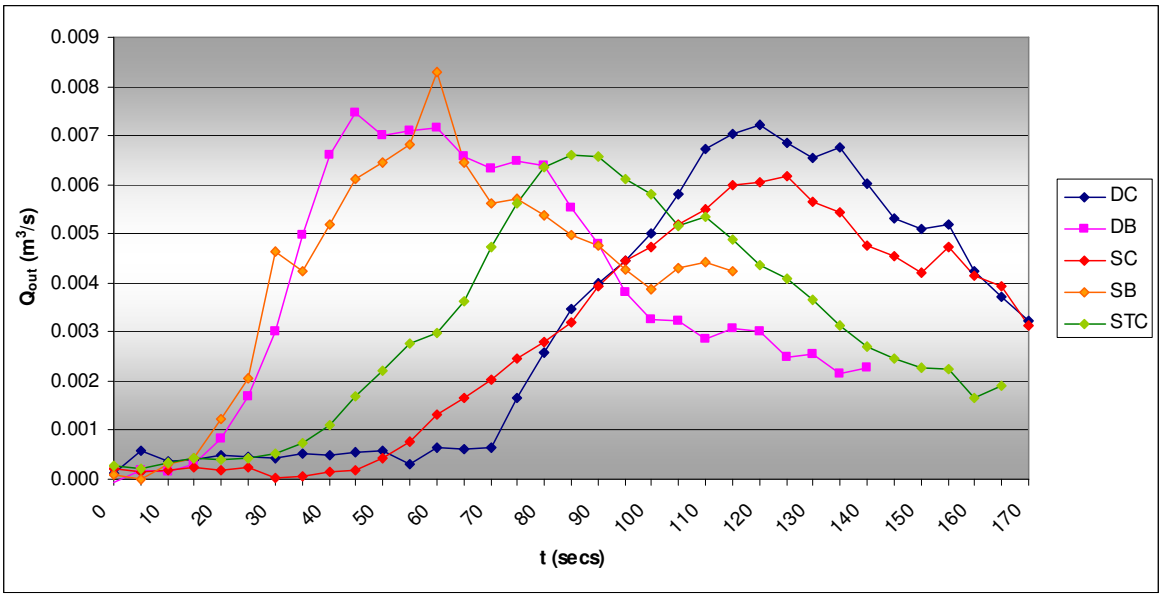

Figure 5.2. Outflows from 1 litre/sec models. The higher sensitivity of the outflow due to reduction of the constant inflow, reveals the effects of the carapace

5.3 Geometry and Hydrology of Breach Development

In order to characterise the evolution of the breach, its incision and geometric enlargement were analysed using width and depth measurements, from which a cross sectional area was derived (Section 4.9). Breach length is only relevant to the maintenance of critical flow in the breach (significance of backwater effects) so it was not considered in this study.

Superposition of the outflow hydrograph onto the cross-section development rate for each dam type links the hydraulic processes observed during failure to the physical enlargement of the breach area through erosion. The C_{max} and W_m profiles are shown in each hydrograph to represent breach development at the breach inlet and outlet respectively. Data are presented for each dam type, at both high and low inflows.

5.3.1 Dry Carapace

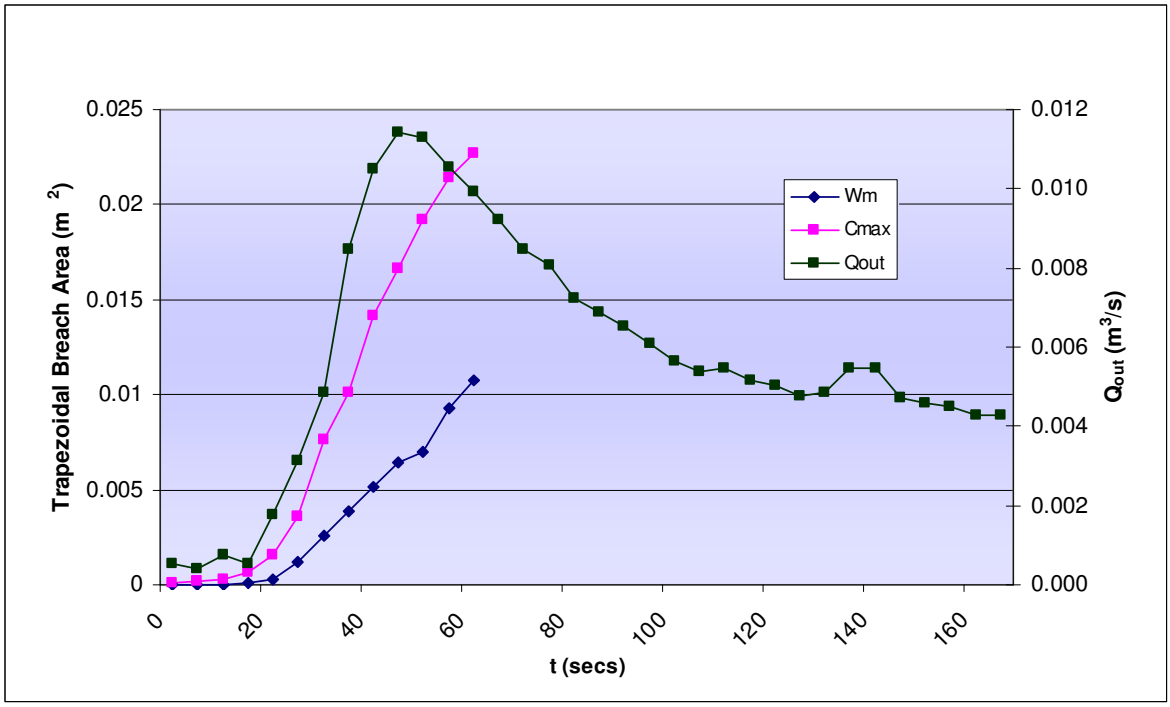

Figure 5.3. Dry Carapace High Inflow

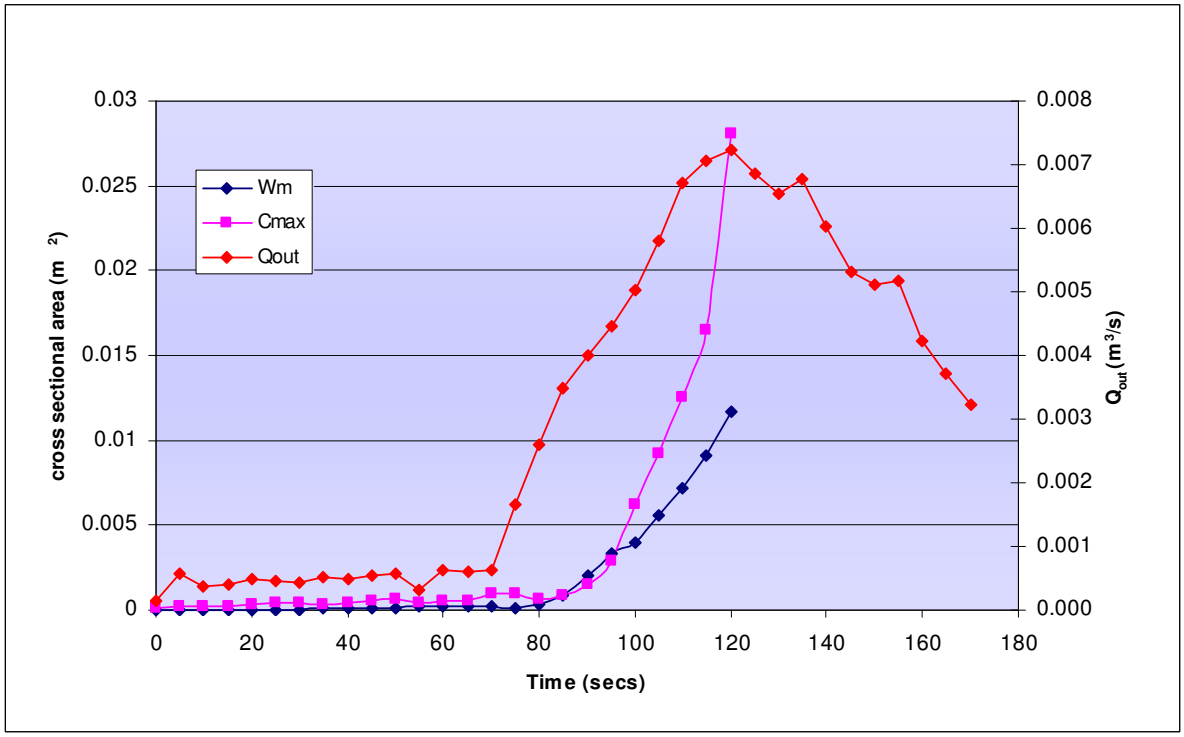

Figure 5.4. Dry Carapace Low Inflow

5.3.2 Saturated Carapace

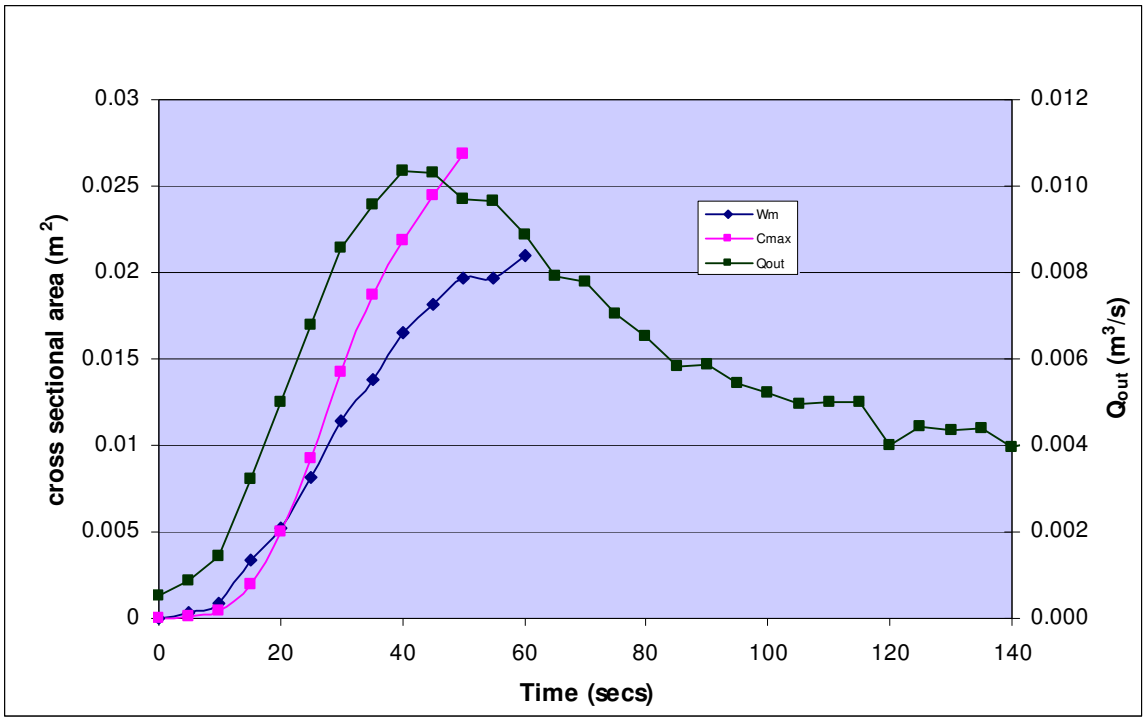

Figure 5.5.Saturated Carapace High Inflow

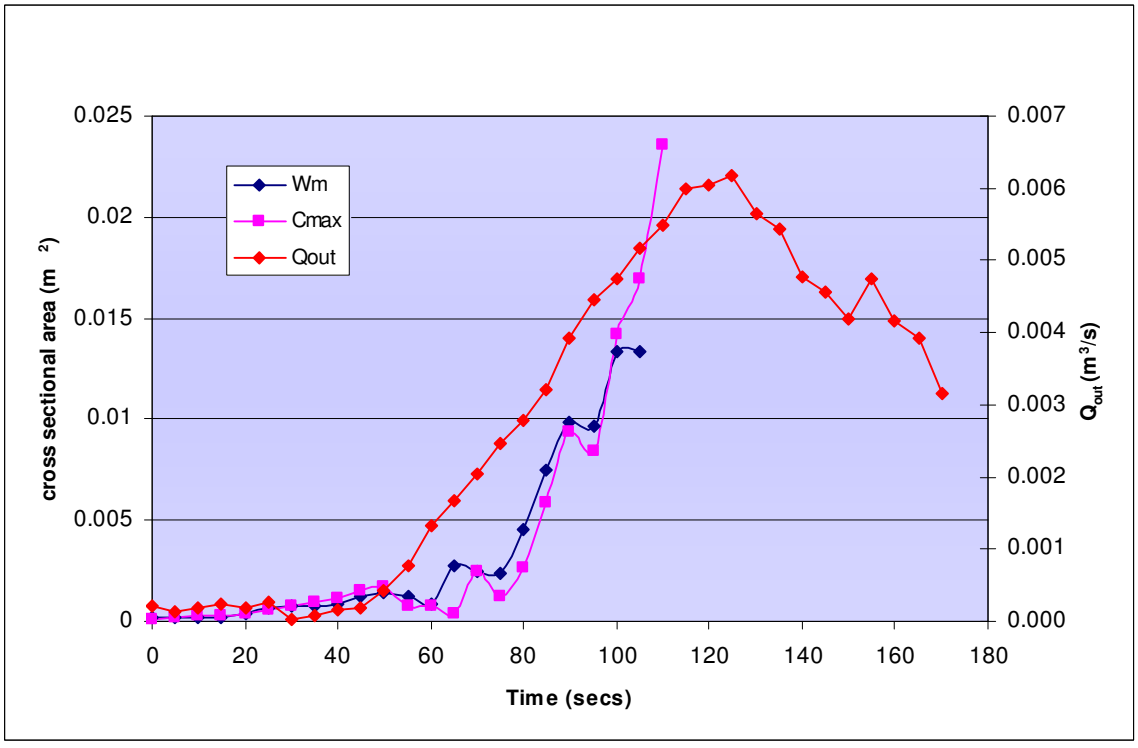

Figure 5.6. Saturated Carapace Low Inflow

5.3.3 Saturated Thick Carapace

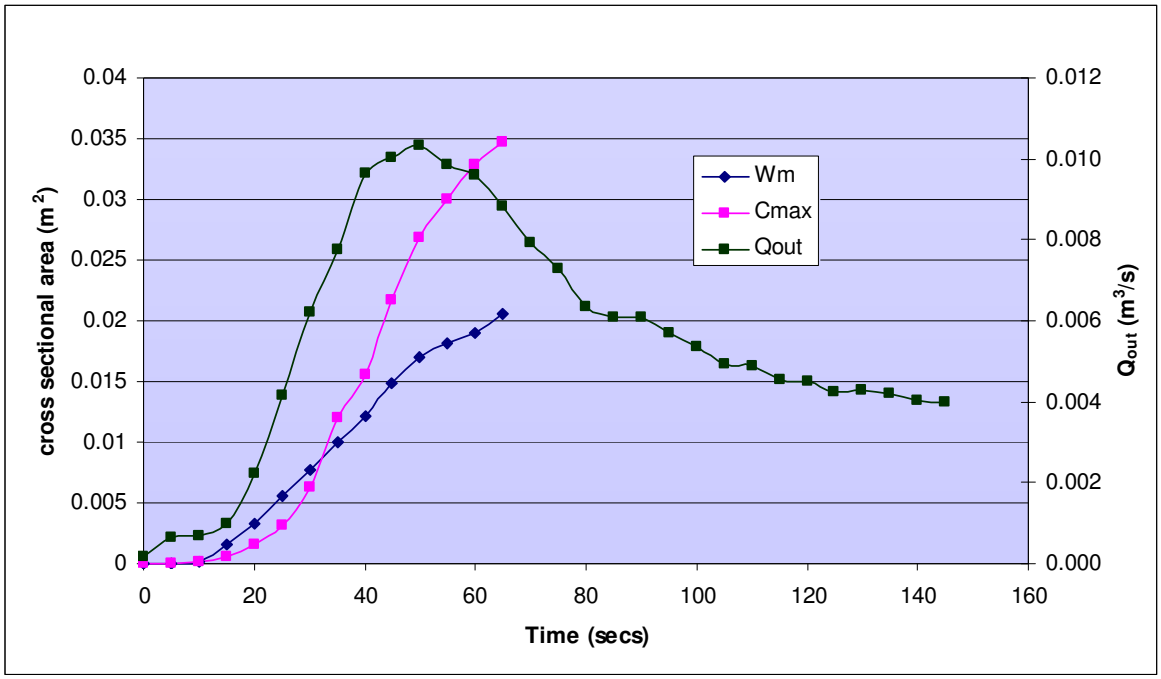

Figure 5.7. Saturated Thick Carapace High Inflow

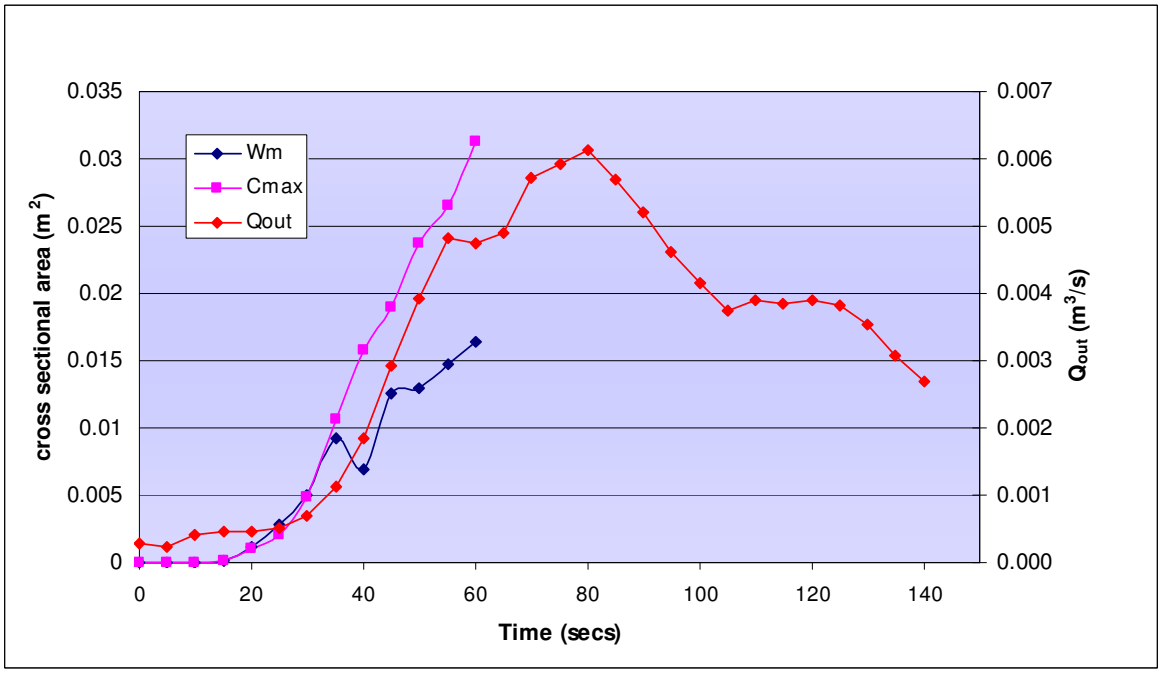

Figure 5.8 Saturated Thick Carapace Low Inflow

5.3.4 Dry Body

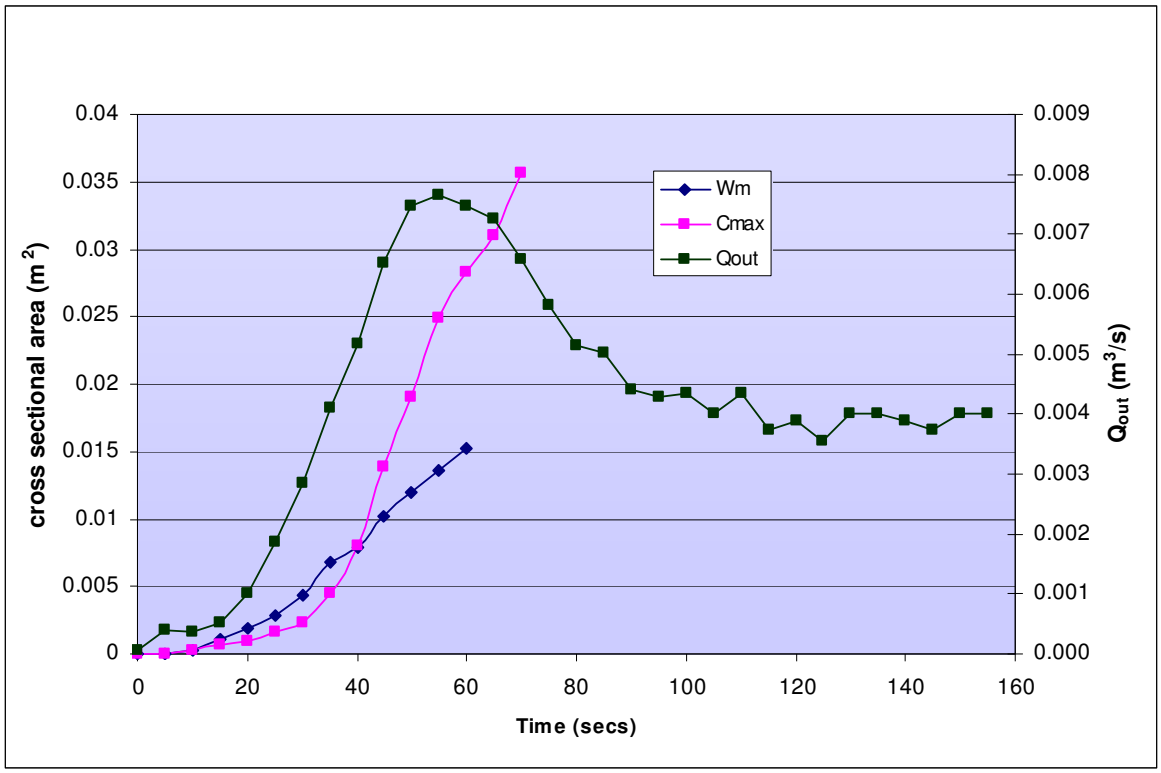

Figure 5.9. Dry Body High Inflow

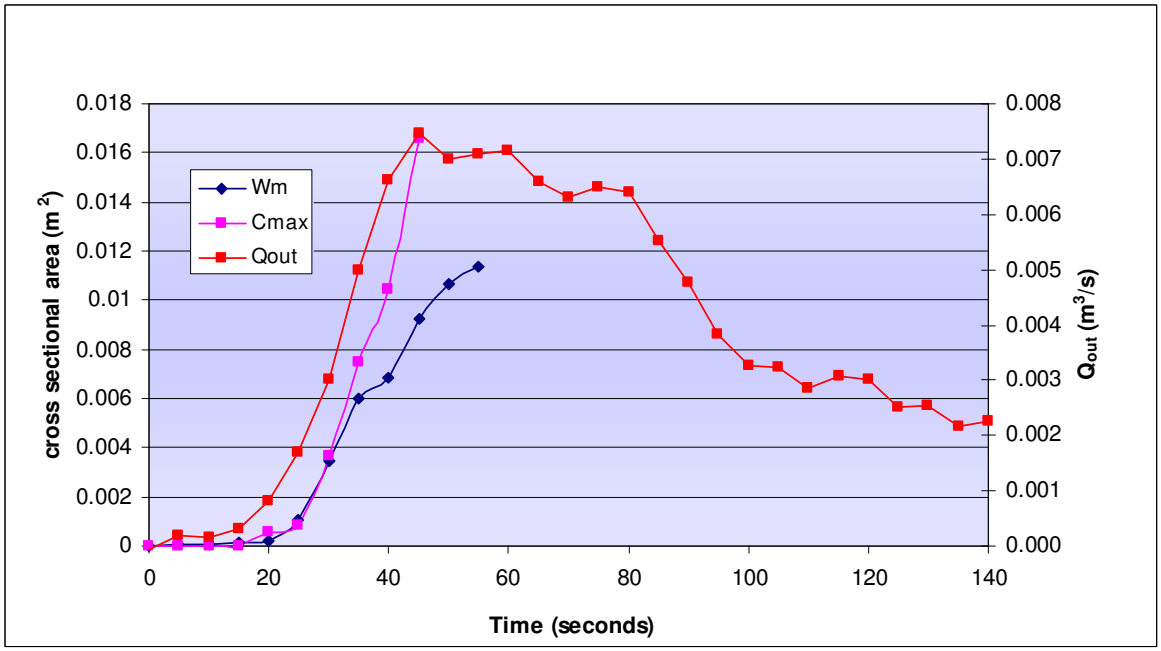

Figure 5.10. Dry Body Low Inflow

5.3.5 Saturated Body

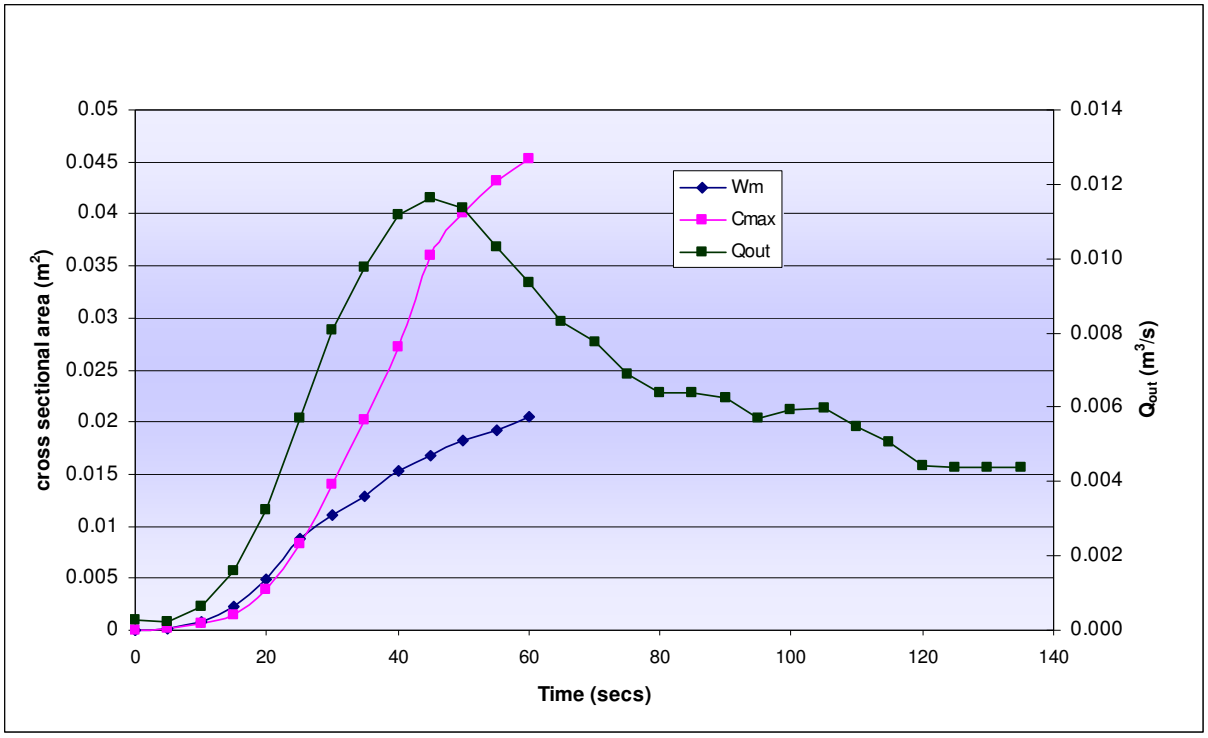

Figure 5.11. Saturated Body High Inflow

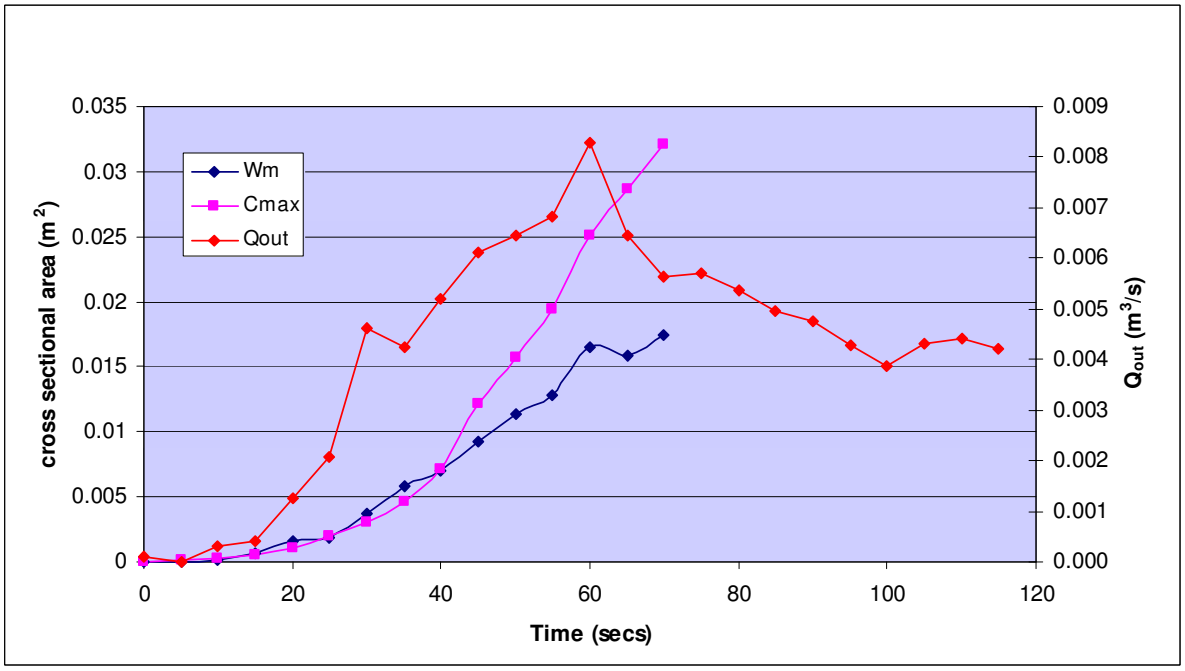

Figure 5.12. Saturated Body Low Inflow

5.3.6 Carapace Body

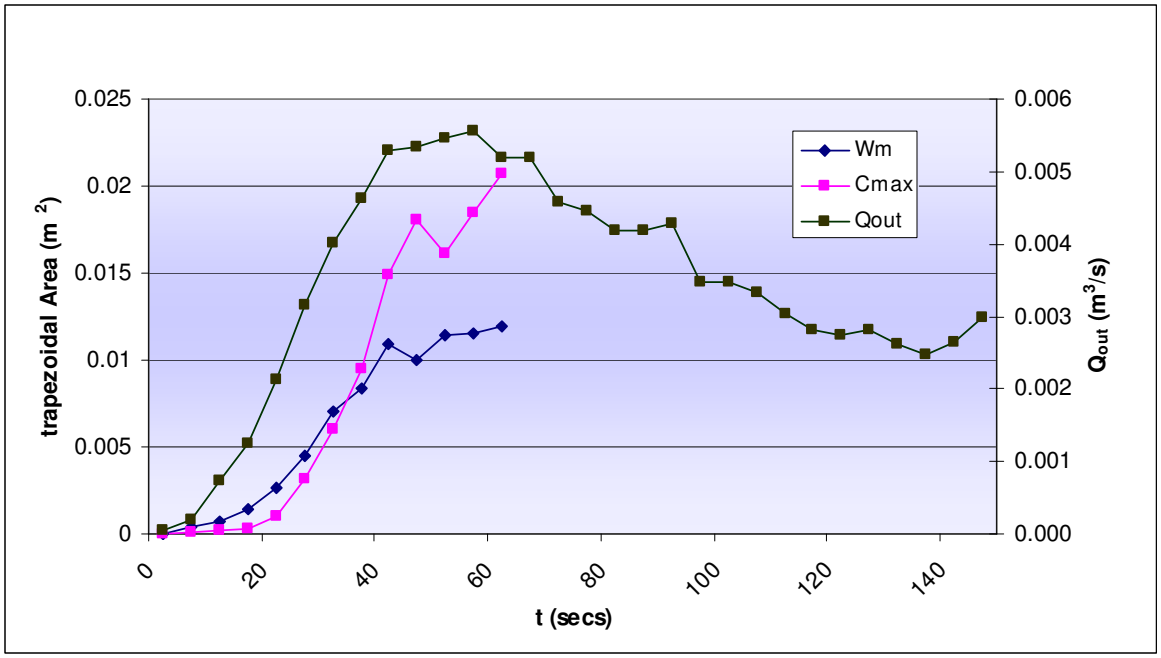

Figure 5.13. Carapace Homogeneous Body High Inflow

5.4 Peak Discharge

A key objective of this research was to understand the influence of the internal structure of a rock avalanche dam not only on the breach development rate, but ultimately on the outflow hydrograph and peak discharge. To extrapolate the laboratory model results to a prototype condition, inflow and outflow discharges recorded in model were scaled up by $400^{(2..5)}$ to produce discharges representative of the prototype condition. The prototype inflows of 3200 m^3/s (low) and 10,000 m^3/s (high) were subtracted from the total discharge to give the true outflow discharge (equivalent to that with zero inflow) through the breach. Outflow discharge is often presented against a variable known as the *dam factor* which incorporates both dam height and impounded lake volume. Using the dam factor (HV_o), Figure 5.14 indicates that the peak discharge for the prototype condition of the PSM study lies within the range of observed peak discharges from both landslide and constructed dam failures.

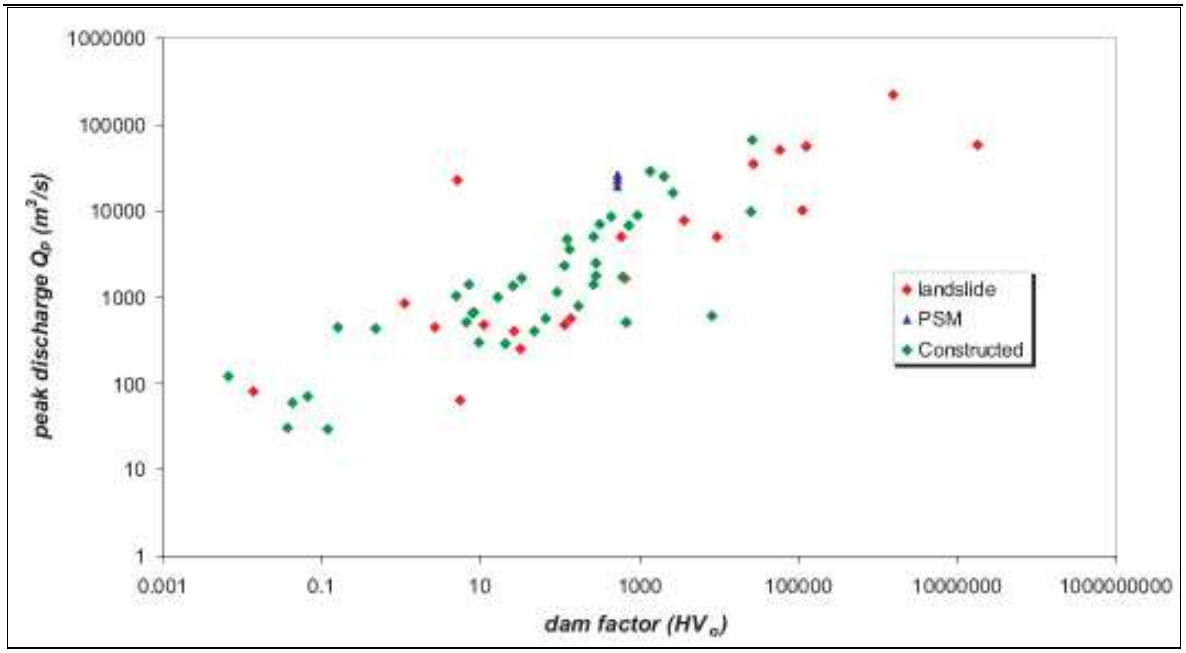

Figure 5.14. Comparison of the PSM dataset to prototype conditions recorded from natural and constructed dam failures (dataset obtained from Manville, 2001)

Tables 5.1 and 5.2 show the influence of variable internal structure and sedimentology on the potential peak outflow at a prototype scale of 400:1. As Q_p is a function of breach geometry and dam/lake volume, it provides a useful indicator of the magnitude of an overtopping failure of a rock avalanche deposit impounding a lake of uniform depth with an approximate volume of 50 x 10^6 m^3 and vertical walls. While Table 5.3 indicates that the highest outflows are generally recorded from saturated homogeneous impoundments, the inclusion of a carapace reduces the outflow by 10-15%. Table 5.3 indicates that the carapace (comparative to a dam of homogeneous nature) does not have a large effect on the peak discharge.

Table 5.3 Summary of Prototype Peak Discharges

High Inflow		*Low Inflow*	
Type	*Q_p (m^3/s)*	*Type*	*Q_p (m^3/s)*
SB	*38400*	*SB*	*25600*
DC	*35200*	*DC*	*22400*
SC	*32000*	*SC*	*19200*
STC	*32000*	*STC*	*22400*
DB	*25600*	*DB*	*25600*
C	*22400*		

Under high inflow conditions however, when the emplaced material is dry prior to reservoir infilling, the inclusion of the carapace produces a 28% *increase* in peak outflow. The physical properties of the carapace differ from those of the body, with larger, more angular grain sizes and a higher hydraulic

conductivity, leading to enhanced failure, through accelerated propagation of the phreatic front. A homogenous dam constructed using only the carapace material produced a peak discharge 36% lower than in the carapace model. Such a result is indicative of the high intrinsic permeability of the carapace facies and its ability to transmit a large amount of the outflow through seepage. Saturation is a parameter which may reduce time to failure of a rock avalanche dam. At high inflows, saturation of dam materials prior to infilling produced outflows 36% higher in homogeneous dams, but only 10% higher in heterogeneous dams.

At lower inflow rates, the influence of specific material properties became more pronounced; carapace-type structures slowed breach development by armouring the dam crest and breach channel to produce an outflow 13% lower than that observed from non-carapace dams. The influence of material saturation on the reduction of peak discharge appears to be independent of inflow conditions.

5.4.1 Time to Peak

The development of the outflow hydrograph rising limb requires the active development of the breach channel and therefore also provides significant insight into the potential rate of breach enlargement.

Under conditions of high inflow, t_p is between 0.22 and 0.32 hours. All carapace (heterogeneous) dams reached peak discharge 20-30% faster than the non carapace (homogeneous) dams of the same material properties. Under high inflows, the carapace facies appears to reduce the time to peak outflow. These results also suggest that no correlation exists between Qp and t_p under high inflow.

Under low inflow conditions, t_p varies much more, ranging between 0.25 and 0.66 hours. Under low inflows, the carapace facies appears to increase the time to peak outflow by up to 60% when the dam is unsaturated. Even under conditions of pre-saturation, the presence of a carapace increases t_p by 54%, strongly supporting the proposition that the carapace acts as armouring mechanism resisting erosion under low inflow conditions. Dam saturation prior to infilling at lower inflows appears to increase t_p by up to 30% in homogeneous dams compared to 7% in heterogeneous dams. At low inflows a correlation exists between high Q_p and low t_p.

5.5 Armouring

Armouring refers to the process of resistance to erosion usually due to selective erosion of fine particles, leaving large grain sizes which require higher critical velocities for entrainment. Armouring inhibits breach bed incision leading to a smaller final breach section area therefore reducing peak discharge. Simulation of the carapace facies using angular aggregate in the PSM allowed the armouring properties of

the carapace to be observed. Figure 5.15 indicates the influence of the carapace armouring of the dam crest in the DC trial to increase t_p by 54% when compared to the homogeneous DB trial. The armouring phenomenon was observed to only operate under low inflow conditions.

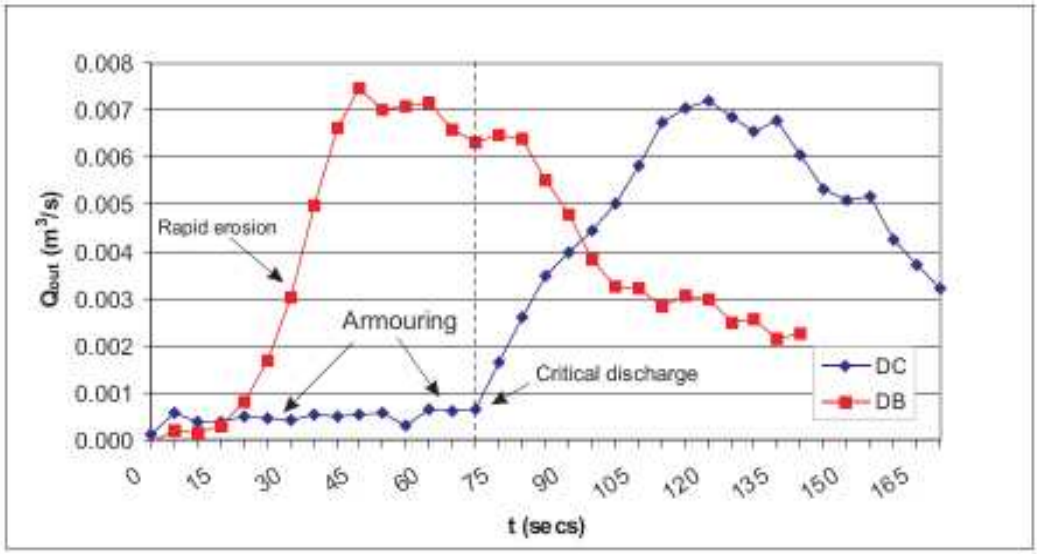

Figure 5.15. The armouring phenomena visible in the comparison of DC and DB dam hydrographs for low inflow conditions

5.6 Breach Geometry

From the methods outlined in Chapter 4, dimensional data were compiled to produce a mean dataset for each dam structure modelled. The data were all derived from physical scale modelling of a half breach and therefore all width dimensions are doubled to make the data applicable to a full breach scenario. All dimensions presented in Table 5.1 and 5.2 were generated from the *crest maximum* profile (Figure 4.11), a position representative of the breach head or inlet. The breach outlet geometry is characterised separately by the *minimum width* cross section.

5.6.1 Breach Depth

The rate at which vertical erosion takes place in the breach has been identified by many researchers as a key factor influencing t_p, t_b and Q_p. Breach depth was found to be insensitive to inflow conditions (see Appendix F). Armouring within the breach channel was frequently observed in the carapace dams modelled, tending to reduce bed erosion and depth development. Non-carapace dams produced breach depths greater than 85% the original dam height, whereas carapace dam breach depths ranged from 70-80%.

5.6.2 Breach Width

Breach width is a key constraint on Q_{out} and therefore both t_p and Q_p. Breach width is calculated from the top and bottom widths of the channel measured at the crest (or breach inlet position). The *breach top width* (W_T) was the only visible dimension in overhead video view. The base width of the breach (W_B) was calculated using observed breach sidewall slope angles. For all carapace dams, a sidewall angle of 45° was assumed; in non-carapace dams the sidewall angle was observed to increase to 60° under saturated conditions and 50° under non saturated conditions.

Under high inflow conditions, the DB model recorded the largest W_T yet produced a minimum peak discharge. W_T was generally observed to be largest in non-carapace dams, approximately 5% larger than in carapace dams. Saturation appears to increase breach width. Although W_B was synthetically generated, the largest dimensions were recorded in non-carapace dams. W_B reduces as the ratio of carapace to body increases, recording the smallest width in the C model. Reduced W_B in carapace models were also observed in final breach configurations in the physical model.

At low inflows W_T was generally observed to be largest in carapace dams. This result contrasts with the behaviour observed for carapace dams under high inflow conditions, suggesting parameter insensitivity may be a function of an unrealistic inflow condition. The DC model recorded a W_T 15% larger than the DB model. The largest W_B is observed in the SB model, 15% higher than the DB model, again indicating that saturation increases breach width.

5.6.3 Breach Walls

The ratio of carapace to body material used in the model strongly influenced the slope angle of the breach walls. The lowest sidewall angle (30°) was observed in the homogeneous dam composed purely of the carapace material. With the inclusion of body material, carapace type dams (Figure 5.16) produced side walls with an angle close to the material angle of repose (45°). On saturation of dam materials prior to infilling, the steepest side walls were recorded (50-60°), in non carapace type dams (Figure 5.16), due to apparent cohesion where pore pressure is <0

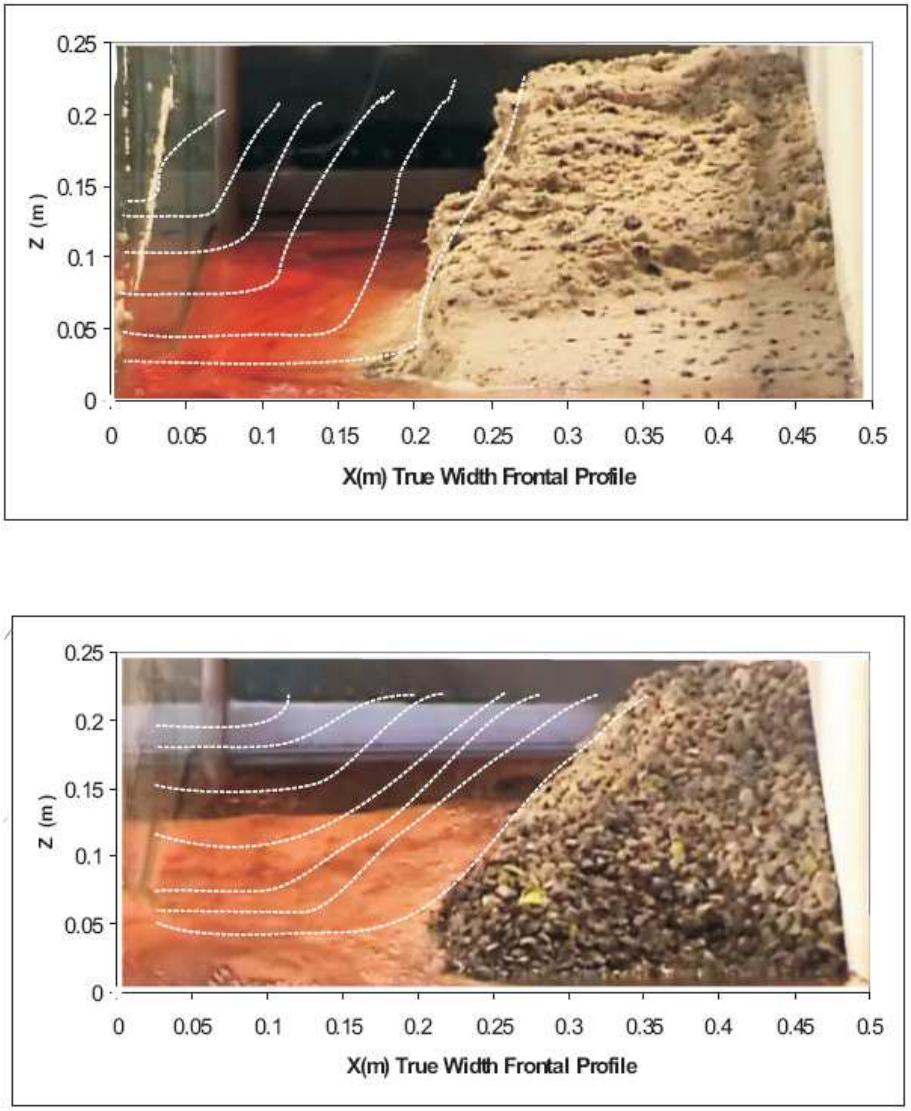

Figure 5.16. Breach Enlargement at 10 sec time intervals for SB (top) and DC (bottom) dam types under low inflow conditions as observed from downstream. Note the DC dam has a 45° sidewall and the SB dam has a 60° sidewall

5.6.4 Breach Cross Sectional Area

Breach area was calculated as a trapezoid, with assumed sidewall angles of 45° for carapace dams and 60° for non carapace dams as observed from Figure 5.16. At high inflows, non carapace models generated the largest trapezoidal breach area, approximately 20% larger than carapace models. Saturation-enhanced enlargement of the breach area appears to be characteristic only of homogeneous models, whereas saturation appears to *restrict* breach area growth in carapace type models. With the exception of the DB model, there is direct correlation between the trapezoidal breach area and Q_p. At low inflows the largest breach area was generated by the DC model. Despite this, the trend of non carapace dams developing larger breach areas was also observed at low inflows.

5.7 Breach Development

5.7.1 Breach Development Time

Where dam volume is small relative to lake volume, peak outflow occurs at about the time breach development is complete (Wahl, 1998). Many researchers define breach development time t_b in terms of the outflow hydrograph, usually as the sum of time to peak (t_p) and time to fall (t_f), however breach development during testing was frequently observed to terminate either prior to, or shortly after the occurrence of t_p. Therefore the relevance of t_f is questioned, when the breach profile may have already reached its maximum dimensions before or at t_p.

Breach development time (t_b) in this study was obtained from video analysis of breach enlargement, using plan and longitudinal views (Table 5.4). The parameter t_b represents maximum breach geometry and defines the time at which;

1. sidewall collapse into the breach channel ceased or

2. flow velocity through the breach was insufficient to erode the breach bed or readily transport sediment through the breach channel (evaluated from flow depth).

The time at which the "dam failure" occurs is therefore considered synonymous with the parameter t_b (the time required for the maximum breach cross sectional area to develop).

Table 5.4 Comparison of model $_{(m)}$ and prototype $_{(p)}$ breach development time (in hours) for each dam type

	Low Inflow			*High Inflow*		
	$t_{b(m)}$ *hrs*	$t_{b(p)}$ *hrs*	$t_{p(p)}$ *hrs*	$t_{b(m)}$ *hrs*	$t_{b(p)}$ *hrs*	$t_{p(p)}$ *hrs*
DC	*0.03*	*0.66*	*0.62*	*0.02*	*0.39*	*0.25*
DB	*0.01*	*0.28*	*0.25*	*0.02*	*0.44*	*0.32*
SC	*0.03*	*0.61*	*0.66*	*0.02*	*0.31*	*0.22*
SB	*0.02*	*0.39*	*0.36*	*0.02*	*0.31*	*0.28*
STC	*0.03*	*0.56*	*0.50*	*0.02*	*0.33*	*0.25*
C	-	-	-	*0.01*	*0.28*	*0.22*

Time to Peak outflow (t_p) is also displayed to allow consideration of the influence of lake volume on t_b

Comparison of temporal breach parameters in Table 5.4 reveals that under low inflow conditions, t_p will occur on average at $0.94t_b$ while under high inflow conditions t_p was observed to reduce to to $0.75t_b$. The generation of maximum breach geometry prior to t_p was only observed in SC dams under low inflow conditions, however in all other dams the breach appeared to continue developing after Q_p. Table 5.4 also indicates that the time required for maximum breach geometry to develop (complete failure) under low inflow conditions, in rock avalanche dams, is approximately twice that observed for homogeneous dams due to the armouring properties of the carapace.

Increased inflow conditions caused t_b values to reduce by 55% in carapace dams, but only 25% in non carapace dams, suggesting that t_b may be a function of material geotechnical properties such as average grainsize (d_{50}) and friction angle of the dam.

5.7.2 Breach Development

Breach geometry and development time (t_b) are important parameters that influence Q_p. Although breach depth was not generated from the C_{max} and W_m cross sectional data, such information allows both the enlargement rate and geometry of the developing breach to be calculated for both the inlet and outlet of the breach.

Due to the observed disparity in the breach development rates at the C_{max} and W_m cross sections, trapezoidal breach area development for each cross section was plotted to compare the breach geometry at both the breach inlet and outlet. A characteristic frequently observed in the comparison of the breach trapezoidal area growth at both cross sections was the point at which uniformity in the rate of breach development at both C_{max} and W_m ceases (Figure 5.17). At this point, called the *branch point*, the development of C_{max} increases exponentially, deviating from W_m. The branch point has also been identified as a threshold condition for the onset of a higher rate of breach erosion apparent in both C_{max} and W_m profiles. This point may also represent a transition from dominantly vertical erosion to dominantly lateral erosion. From comparison of the breach area development at both profiles, three stages of breach erosion were identified, corresponding to two erosion regimes occurring before and after the onset of the branch point respectively (Table 5.5). Breach geometric evolution was also used to verify three erosional regimes (Table 5.6).

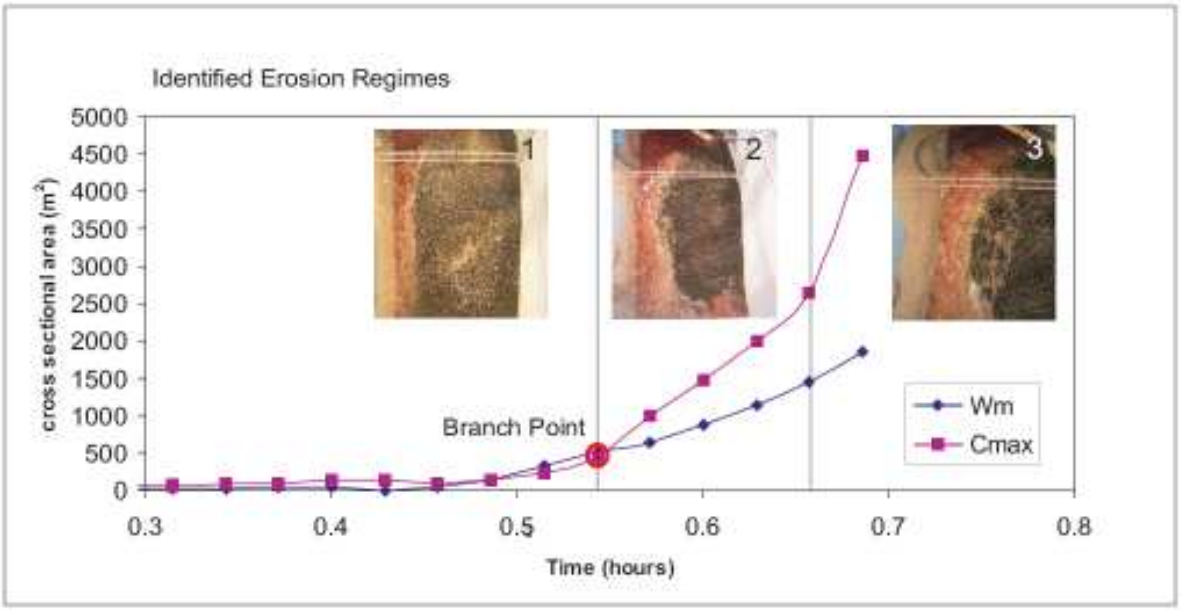

Figure 5.17. Idealised Erosional Regimes. The prototype cross sectional breach enlargement is presented with the breach morphology observed during testing of physical scale models.

Table 5.5 Erosional Regimes Identified for the Prototype Scale

Stage	*Erosion*	*Description*	*Duration (hrs)*
1	*Vertical*	*Overtopping surface flow, headcut development. Uniform rates of development at breach inlet and outlet.*	*0.1*
2	*Lateral*	*Increased development of breach inlet geometry*	*Carapace 0.12* *Non 0.06*
3	*Lateral*	*Enhanced development of breach inlet by side wall collapse*	*0.5*

High Inflows

Under high inflow rates, dams which displayed early occurrence of the *branch point* (transition to Stage 2 Erosion), recorded the highest outflow discharges. Under non saturated conditions, W_T develops at five times the observed rate of d_B, suggesting that lateral erosion controls breach development. Under saturated conditions, this rate of breach widening appears to halve. While the high inflow trials tended to produce parameter insensitivity due to the overpowering effect of the inflow condition, they do provide some verification of erosion trends identified specific to dam type.

Table 5.6 Use of breach geometry to identify stages of breach erosion at a prototype scale

	Erosion Stage I		***Erosion Stage II***		***Erosion Stage III***	
Parameter	*Area (m^2)*	*Time (hours)*	*Area (m^2)*	*Time (hours)*	*Area (C_{max}) (m^2)*	*Time (hours)*
DC	*-*	*0.45*	*500*	*0.54*	*2500*	*0.66*
DB	*-*	*0.1*	*500*	*0.19*	*1800*	*0.23*
SC	*-*	*0.4*	*500*	*0.51*	*1500*	*0.58*
SB	*-*	*0.1*	*1000*	*0.23*	*3000*	*0.31*

Low Inflows

Failure of rock avalanche dams under low inflow conditions have been identified by various researchers including Dunning *et al.,*, (2005a) and Hancox *et al.,*, (2005). Such inflow conditions are therefore considered appropriate for assessing parameter sensitivity in breach development. As indicated by Figures 5.18 and 5.19, the onset of Stage II erosion in the prototype appears to occur when the breach area exceeds 500m^2 under non saturated conditions and 1000 m^2 under saturated conditions. The slower rate of erosion in saturated materials, may be due to the apparent cohesion in the model (see section The second stage of erosion in carapace dams requires duration twice that of non-carapace dams, indicating the onset of channel armouring in resistance to vertical erosion of the breach channel bed. Comparison of DC and DB dam types in Figure 5.18 indicates that during Stage II erosion, the breach inlet cross section develops rapidly, promoting lateral erosion and successive sidewall collapse. Carapace material is then entrained and ejected from the breach under higher outflows resulting from the widened breach profile.

Comparison of breach development in C, STC and SC types (Figure 5.19) indicates that the second stage of erosion is characterised by several large side wall collapse events, temporarily blocking the breach outlet (represented by the W_m profile).

The occurrence of Stage II erosion was also found to correlate well with the formation of the steepest breach bed slope in non-carapace dams. As outlined in Table 5.6, the onset of Stage III erosion is less

well-defined but appears to occur when breach area at the C_{max} profile exceeds 1500 m^2 for carapace dams and 1800 m^2 for non carapace dams.

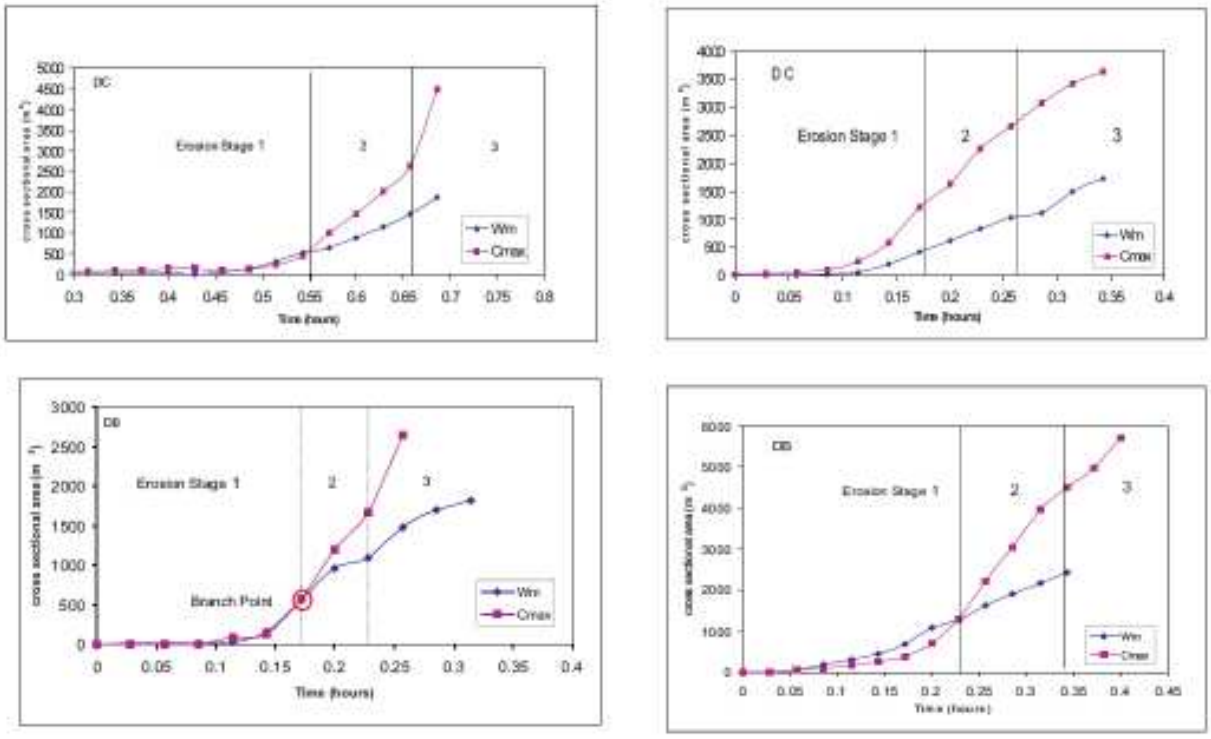

Figure 5.18. Breach Erosion stages identified for DC and DB dam types under low (left) and high (right) inflow conditions

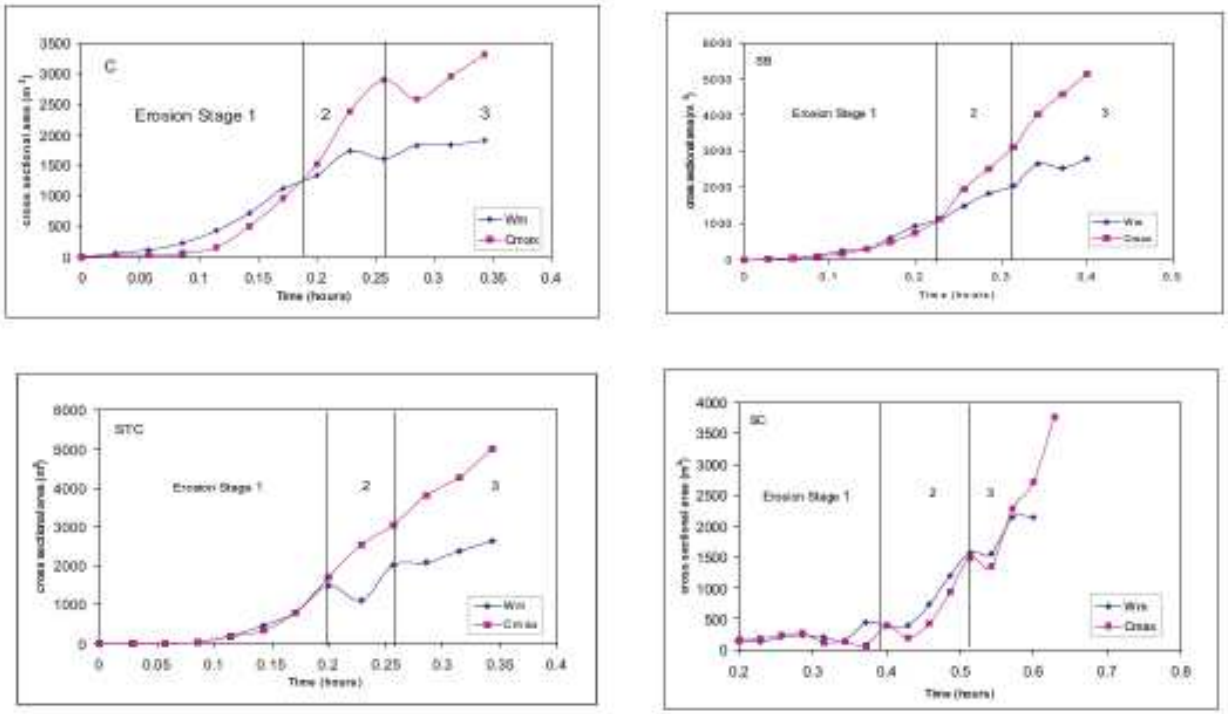

Figure 5.19. Breach Erosion stages identified for C, STC, SC and SB dam types under low inflow conditions

5.7.3 Breach Bed slope

The longitudinal profile of the breach slope was recorded to provide information on the protective influence the carapace may have in reducing breach incision and therefore the bed slope of the breach channel. Using video analysis each profile represents bed slope development at 5 second time intervals for the various dam structures under high and low inflow conditions (Figure 5.20-29).

5.7.3.1 Longitudinal Profiles of Breach Bed slope development under High Inflow

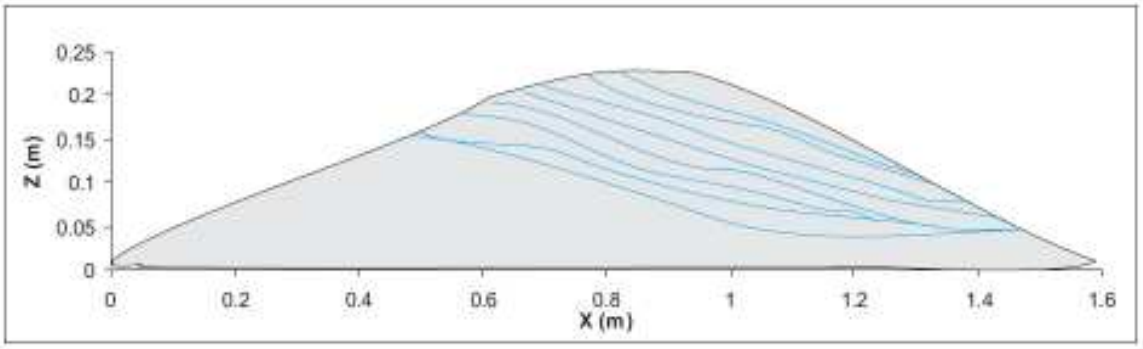

Figure 5.20.Homogeneous Carapace

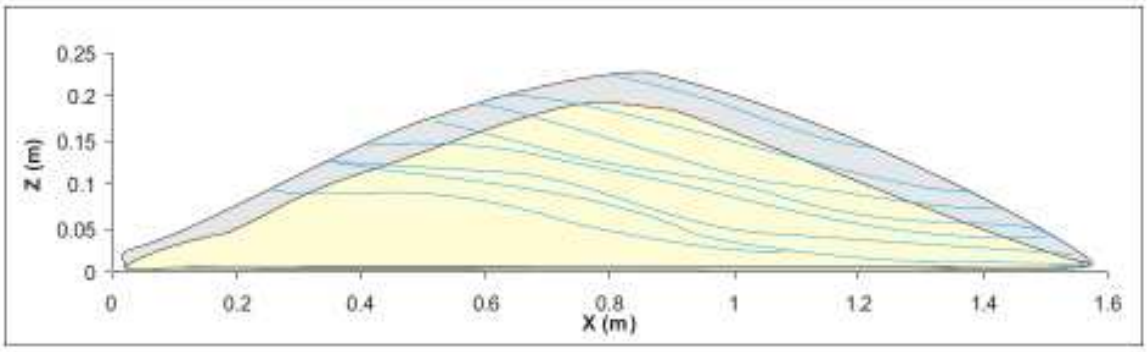

Figure 5.21.Unsaturated Carapace

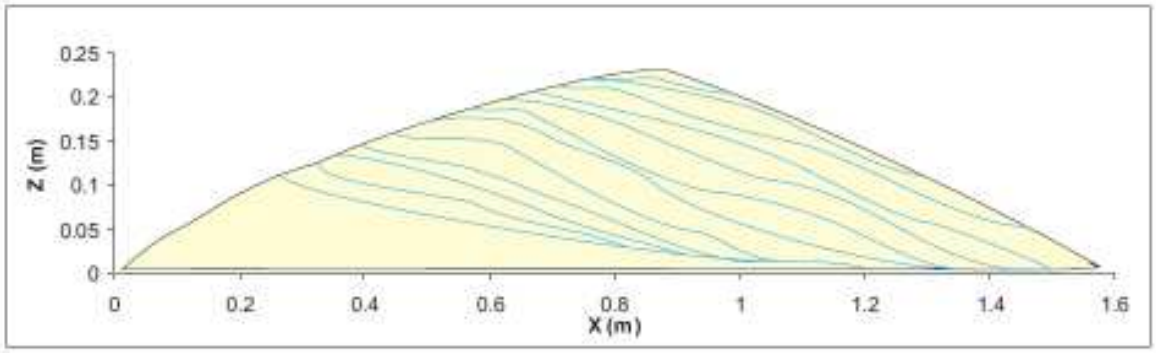

Figure 5.22.Unsaturated Body (Homogeneous)

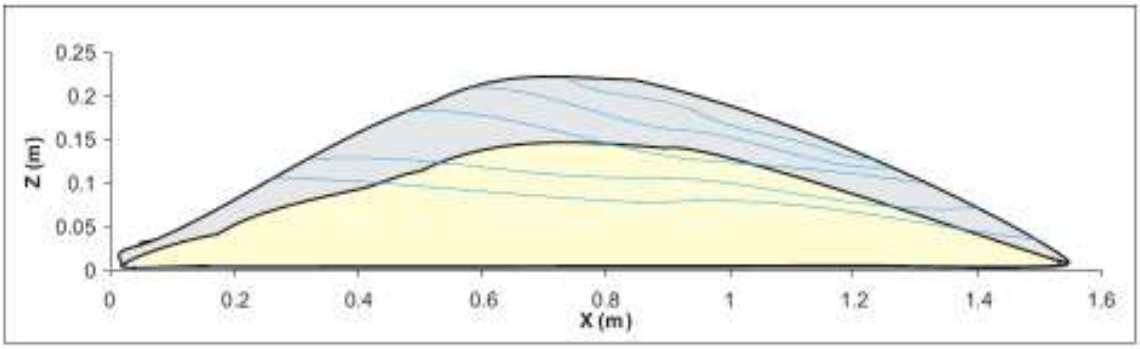

Figure 5.23.Saturated Thick Carapace

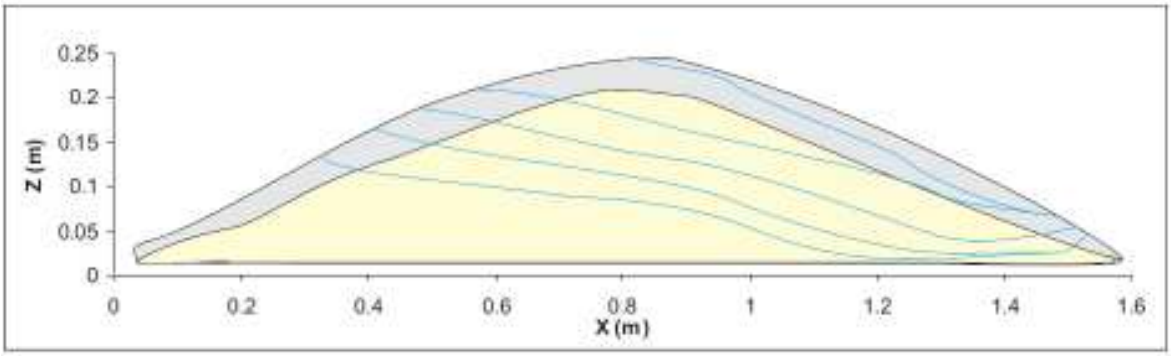

Figure 5.24.Saturated Carapace

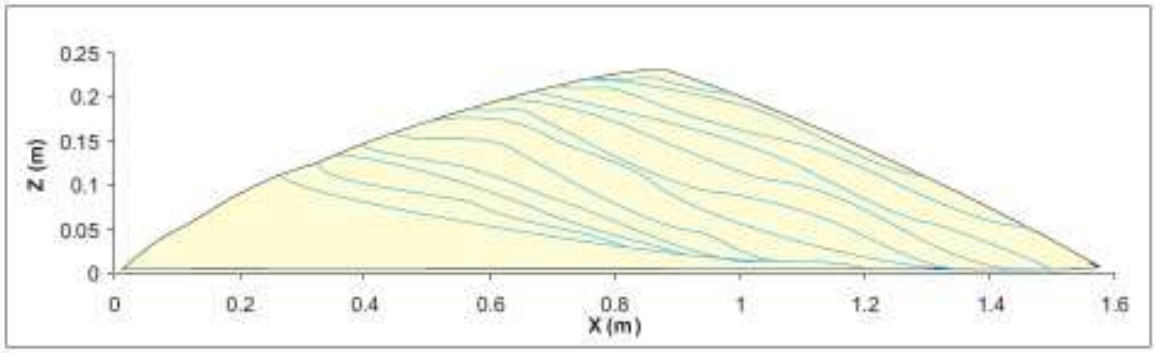

Figure 5.25.Saturated Body (Homogeneous)

5.7.3.2 Longitudinal Profiles of Breach Bed slope development under Low Inflow

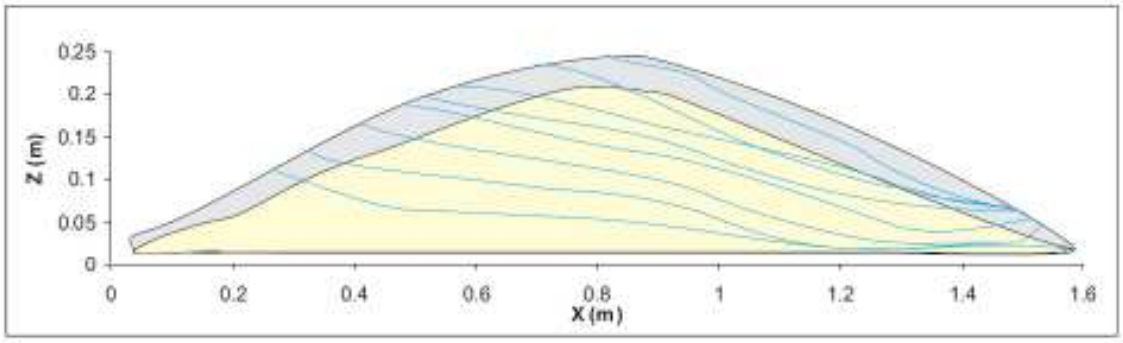

Figure 5.26.Unsaturated Carapace

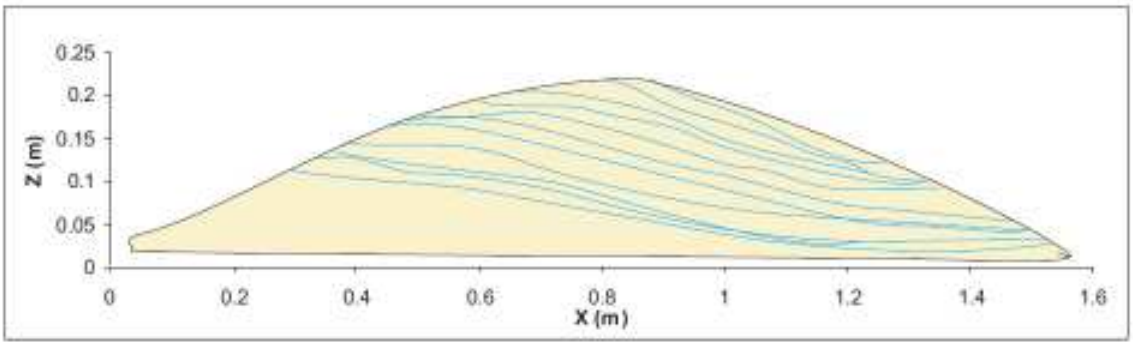

Figure 5.27.Unsaturated Body (Homogeneous)

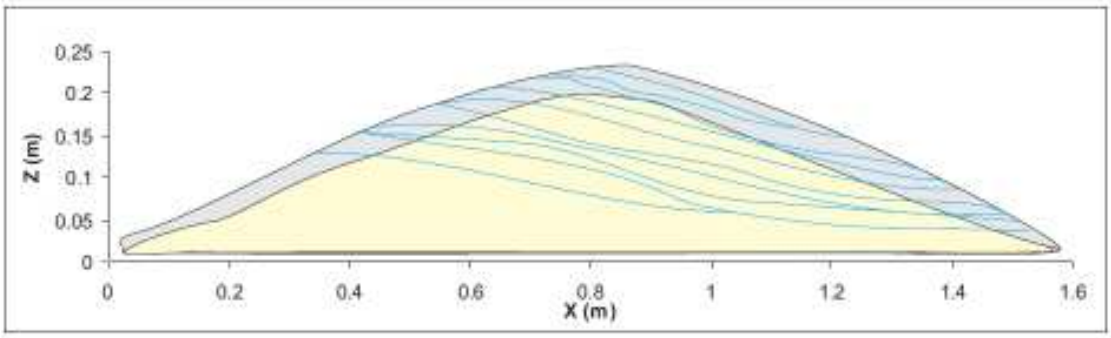

Figure 5.28. Saturated Carapace

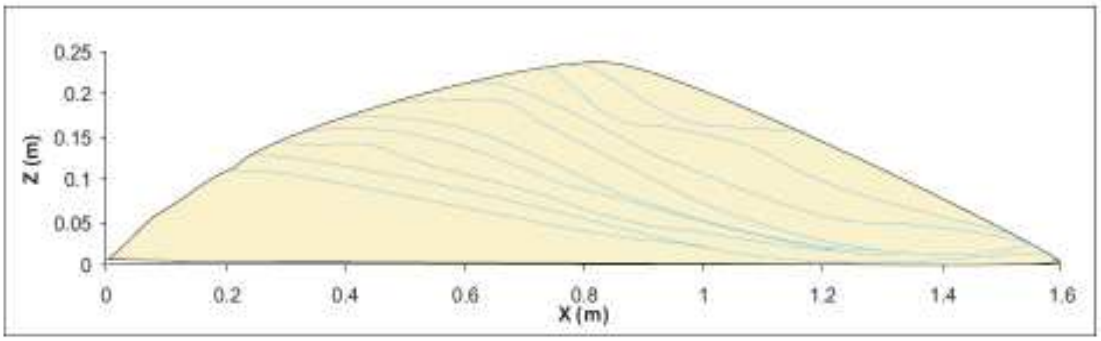

Figure 5.29.Saturated Body (homogeneous)

5.7.3.3 Average Breach Bed Slope

From Section 5.7.2 breach geometric evolution was identified to occur in three stages of erosion (Table 5.7). The evolution of the breach bed slope during breach enlargement was analysed relative to the three identified erosional regimes.

Table 5.7 Average Breach Bedslope (degrees)

		Erosion Stage		
Dam	***Inflow***	***I***	***II***	***III***
SC	*low*	*15*	*14*	*12.8*
	high	*15*	*15*	*10*
SB	*low*	*20*	*16.5*	*14.5*
	high	*20*	*17*	*11*
DB	*low*	*20*	*16*	*12*
	high	*23*	*19*	*16*
DC	*low*	*20*	*15*	*13*
	high	*20*	*15*	*15*
C	*high*	*15*	*13*	*10*
STC	*high*	*15*	*13*	*10*

Using the longitudinal profiles, the average bed slope angle at each erosional stage was calculated as outlined in Table 5.7. The larger, coarser carapace material reduces the gradient of the breach channel. Dams incorporating carapace material were observed to have average bed slopes ranging from 13-20° during Stage I-II from the armouring of the breach bed, through raveling of carapace towards the downstream toe. Comparatively, non carapace dams produced the steepest breach bed slopes ranging from 17-23° during stage I and II. The steepest bed gradients were recorded in homogeneous dams (excluding model C). In trials where a high volume of carapace material existed (STC and C), armouring of the channel reduced the breach bedslope erosion, maintaining a gradient between 10-15°. Saturation of dam structures appeared to lower gradients during stage I-II by approximately 3-4°. Bed slope was largely insensitive to inflow conditions, with low inflows producing bed slopes of marginally smaller gradient, than that of higher inflows.

One might expect the coarser material to give steeper bed slope, however as suggested from the results in Table 5.7, the body material (simulated using silica sand) offers little resistance to erosion and becomes deeply incised producing a very steep breach channel. The coarser carapace material provides resistance to erosion and inhibits incision until raveling takes place, thus maintaining a lower overall channel gradient.

5.8 Phreatic Migration

The migration of the phreatic front through both heterogeneous and homogeneous dams is a function of both inflow rate and the material properties of the dam. Phreatic contours are presented at 10 second intervals for the low inflow profiles (Figure 5.30-31) and 5 second intervals for high inflow profiles (Figure 5.32-33).

Under low inflow conditions the phreatic front propagates parallel to the downstream face. This condition was observed in both homogeneous and heterogeneous dam models, suggesting that the influence of the carapace is negligible in terms of velocity of migration of the phreatic front under conditions of slow reservoir filling. The phreatic profile (Figure 5.31) for carapace dams indicates that the carapace facies may in fact maintain inflow and outflow conditions below the critical flow velocity that initiates raveling on the downstream face. This characteristic of the carapace would allow it to act as a permeable spillway and resist overtopping, until a critical discharge was exceeded.

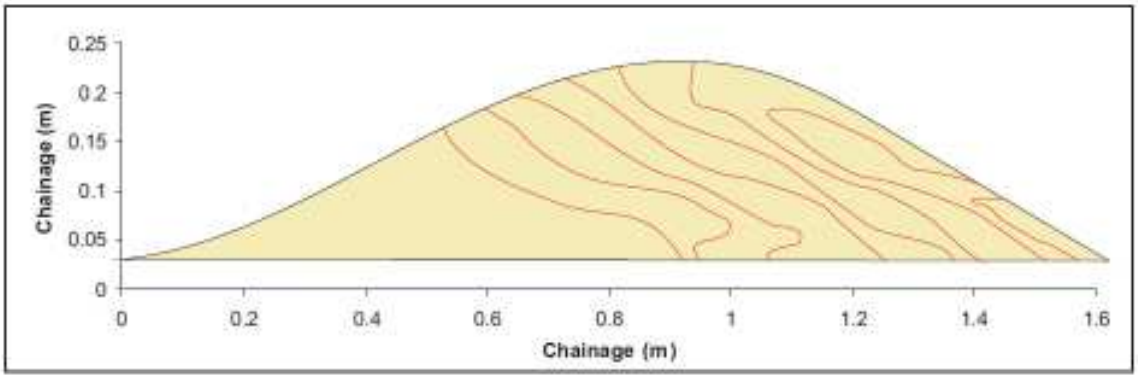

Figure 5.30. Phreatic migration through a homogeneous dam under Low Inflow

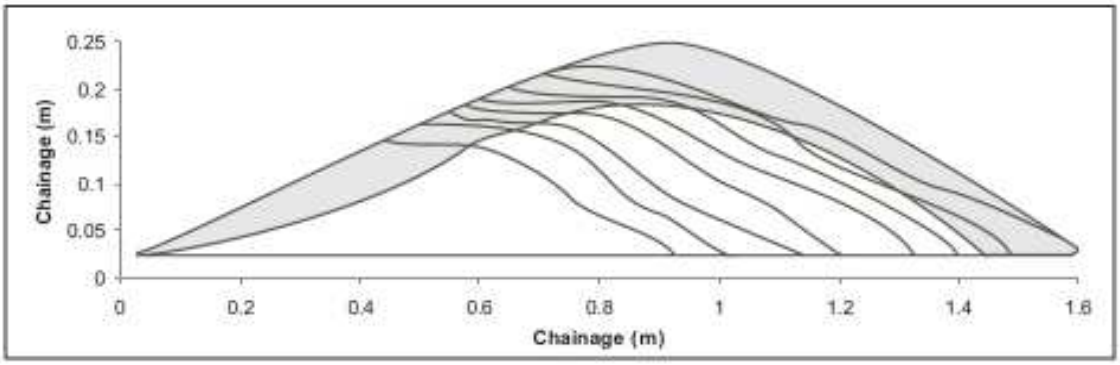

Figure 5.31. Phreatic Migration through heterogeneous dam under low inflows

At high inflows, the phreatic front propagates perpendicular to the dam base rather than parallel to the downstream face as observed at lower inflows. This difference must be related to the rate of reservoir filling, the only varied parameter. Under high inflows, seepage in the homogeneous dam increases when the reservoir level reaches the dam crest and overtopping commences (Figure 5.32). Once concentrated overflow has commenced on the surface of the downstream face, the phreatic front migrates downward from there toward the dam base.

The influence of the carapace is significant at high inflows. The phreatic front propagates perpendicular to the dam base, as observed in the homogeneous tests, but with more concavity as shown in Figure 5.33. The inclusion of the carapace results in an acceleration of the phreatic front at the interface between the body and carapace facies. The hydraulic conductivity of the carapace is approximately double that of the underlying body for the materials modelled. When the water surface reaches the dam crest, the phreatic front is driven beyond the facies interface, day-lighting in the lower third of the downstream face.

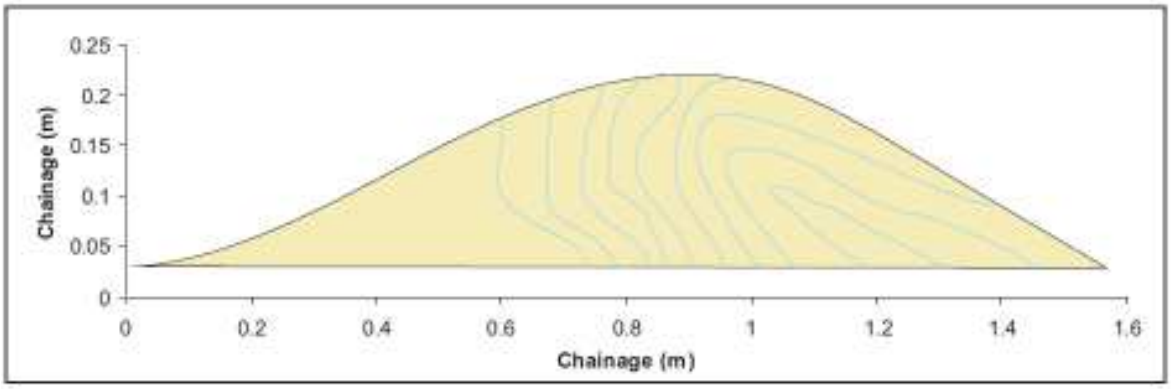

Figure 5.32. Phreatic migration through a homogeneous dam under High Inflow.

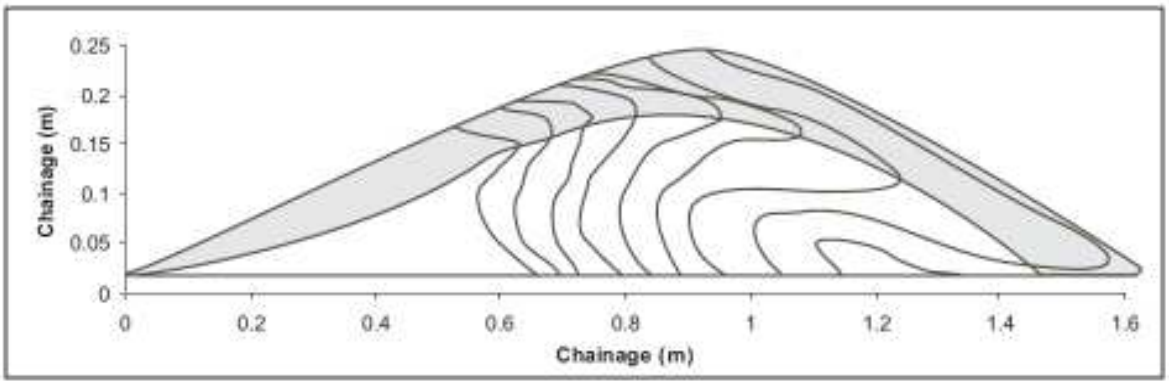

Figure 5.33. Phreatic migration through a heterogeneous dam under High Inflow

5.9 Failure Mechanism

5.9.1 Background

From analysis of the digital video data and outflow hydrographs, *five* stages of breach development were identified as characteristic of a rock avalanche dam failure. Because recent embankment dam research has addressed overtopping failure of homogeneous dams, only the failure sequence for carapace dams is presented herein. The failure sequences for carapace dams under saturated (Figure 5.34) and non saturated conditions (Figure 5.35) are presented to emphasise of the influence of higher hydrostatic pressures.

While breach geometry has been identified to evolve in three erosional stages (Section 5.7.2), the failure sequence is identified to occur toward the end of Stage I and terminate at the onset of Stage II.

Prior to breach initiation, seepage daylighting at the toe of the downstream face accelerates erosion. As overtopping flows accelerate down the downstream face, the highest flow velocity occurs at the base; the

point where the critical shear stress for external material is most likely to be exceeded by the flow. The seepage outflow induces regressive slope movements with a two-dimensional character, similar to a rotational slump.

The head scarp generated by slumping causes surface discontinuities on the downstream face, which act to concentrate flows and initiate erosion causing head cutting and upstream migration of a widening scour hole. The main breach forming event is the final slump which lowers the dam crest below the reservoir level and initiates the concentration of outflow on the scoured head cut section on the downstream face.

The failure of the carapace incorporates a process described in literature as *raveling* whereby the surficial coarse material is removed by rolling downslope due to the influence of gravity and the velocity of the overtopping flow.

5.9.2 Critical Discharges

Structural collapse of the dam due to the overtopping was identified to occur at four specific discharges, presented at the model scale in Table 5.8 below.

Table 5.8 Critical discharges for initiation of structural failure for a rock avalanche dam under low inflow

Time (secs)*	*Event*	*Q (L/s)*	*SE ± %*
0	*Weakening of rock armour*	*0.63*	*0.00*
10	*Partial saturation of the carapace*	*0.69*	*0.01*
15	*Seepage induced erosion of downstream toe*	*0.96*	*0.01*
20	*Main slope failure/ rotational slump*	*1.22*	*0.03*
25	*Breach Initiation (Carapace removed)*	*2.00*	*0.08*

** time from the lake level reaching dam crest*

5.9.2.1 Incipient Motion

At any point on the C_m (crest max) profile, the forces causing motion of a sediment particle are the tractive shear stresses from the flow, and the down slope gravity force components. The initiation of particle motion may be caused by shear stress developed by the breach flow; and the structural failure of destabilised bank material resulting in the collapse and deposition of sediment into the breach channel, to be rapidly entrained by breach flow.

Using coupling of PSM breach development and hydrograph data for carapace dams, the discharge at the time of carapace raveling was recorded (Table 5.9) and can be considered the critical discharge required for failure of the carapace armouring. Such results are only applicable to the dams constructed of the upscaled materials tested in this study.

Table 5.9 Critical discharge for failure of the carapace at model and prototype scales

	t^m (secs)	$Q^m(10^{-3}m^3/s)$	t^p (hrs)	Q^p (m^3/s)	q_c (%Q_p)*
DC	*70*	*0.63*	*0.38*	*2038*	*8*
SC	*45*	*0.17*	*0.25*	*544*	*3*
STC	*30*	*0.17*	*0.16*	*544*	*3*

** critical discharge presented as a percentage of peak discharge*

N.B. The Poerua Rock Avalanche Dam failed under an overflow < 1000 m^3/s

Critical velocity for incipient motion was calculated for carapace dams using Hartung and Scheulerin (1970) and Coleman and Andrews (2000) to give mean values ranging from 0.15 m/s to 0.38 m/s for an average bed slope of 0.21. Critical velocities in non carapace dams for an average bed slope of 0.26 were found to be 15% lower than that observed for carapace dams. Flow velocities at the time of breach enlargement for the prototype condition of the tested models vary from 0.15 m/s to 0.6 m/s. Therefore estimates of the critical velocity for incipient motion are considered reasonably accurate.

5.9.3 Photographic Failure Sequence for a Rock Avalanche Dam

Two photographic failure sequences are presented in Figure 5.34 and 5.35 detailing the average morphology observed on the downstream face for both DC and SC dam types under low inflow conditions.

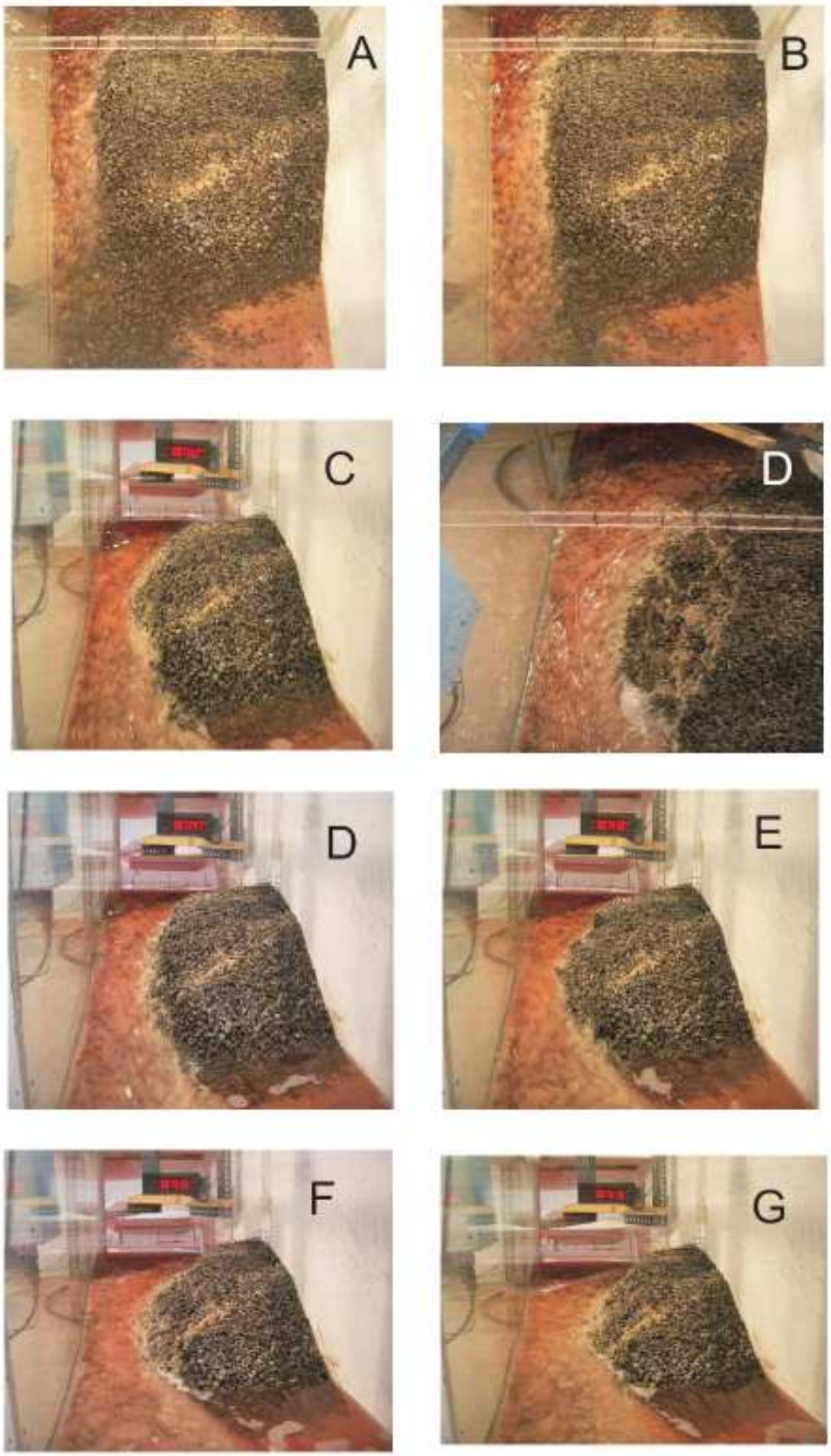

Figure 5.34. Failure Sequence for a saturated carapace dam

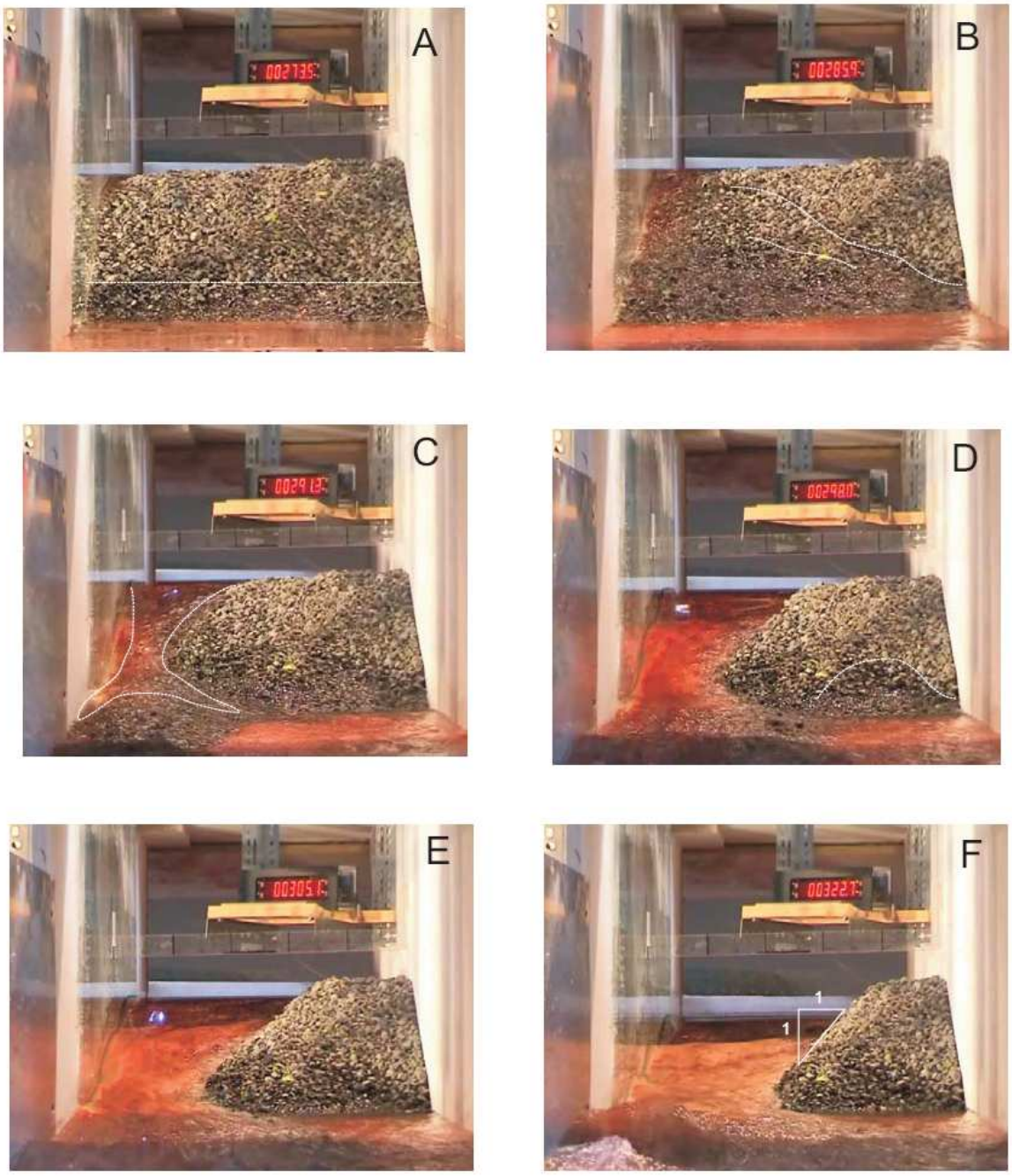

Figure 5.35. Failure Sequence for an unsaturated Carapace Dam

5.9.4 Qualitative Failure Sequence for a Rock Avalanche Dam

Each step refers to the corresponding photo in both Figure 5.34 and 5.35.

- The main failure mechanism required to initiate breach development commenced at a time equivalent to t=15 seconds ($0.2t_b$) and terminates at approximately t=25 seconds ($0.37t_b$).

- Upon the water level reaching the dam crest, the phreatic front propagates through the carapace, primarily concentrating seepage flow at the interface between the two materials, before day-lighting at the downstream toe (Figure 5.35A).

- At t=10 seconds ($0.14\ t_b$) the phreatic front moves up through the carapace, as the reservoir level rises until most pore spaces in the carapace are fully occupied by the inflow. The carapace becomes partially saturated, and *surface flow* becomes established within it.

- At t=15 seconds ($0.2\ t_b$) discharge from daylighting of the phreatic front on the lower toe increases to erode and destabilise the downstream base of the dam promoting a sudden major regressive slope movement (Figure 5.35B) along the longitudinal axis of the dam similar to a rotational slump/slide failure. The slumping/sliding of the downstream face reduces the dam crest level below the water surface level, increasing the flow overtopping the crest. Increasing the flow rate causes the breach to initiate.

- At 20 seconds ($0.28\ t_b$) the head scarp generated by slumping causes surface discontinuities on the downstream face, which act to concentrate flow and initiate erosion causing head cutting and upstream migration of a widening scour hole.

- A critical flow velocity (v_c) resulting from the free surface profile drives the erosion of the carapace through raveling (Figure 5.35C). With the breach discharge exceeding v_c the eroded crest carapace material is transported downstream and deposited as a fan of debris in the enlarging breach channel. This deposition obstructs the flow and stabilizes the dam toe, armouring the channel and reducing the bed slope gradient by 2-5°.

- At t=25 seconds ($0.35\ t_b$) both the breach inlet and outlet develop at a uniform rate (Stage 1 erosion). Vertical erosion is dominant due to the removal of the carapace and exposure of the more erodible underlying body facies (Figure 5.34A, B; 5.35C).

- Exposure of the toe at higher rates of vertical erosion enables the breach outlet to establish a trapezoidal geometry. Stabilisation at the dams toe (breach outlet), causes concentration of flow at the breach inlet causing extreme lateral erosion of breach inlet on the upstream face (Figure 5.34C, D).

- The enlarged breach geometry at the inlet enables a higher volume of escaping water to flow through the breach, and entrain and transport larger sized clasts.

- The deposit of carapace material at the breach outlet is removed, restoring the steep downstream face profile allowing rapid removal of the highly erodible body material (Figure 5.34E; 5.35D). The breach geometry now becomes defined by lateral and not vertical erosion, which proceeds downstream from the breach inlet.

- Breach development proceeds through enhanced lateral erosion causing undercutting, over-steepening and collapse of breach sidewalls initially at the breach inlet (Figure 5.34D,E; 5.35E). If the material is non saturated (DC), sidewall collapse will occur as a slide or flow, however due to the presence of surface tension forces, unsaturated materials (SC) are observed to slump (Figure 5.34D) or "topple" producing large tension cracks and head scarps visible in plan view.

- Carapace and body materials are then delivered to the breach floor, entrained and removed by the breach flow

- Sidewall destabilisation now appears to occur from lowering of the water surface, due to reservoir depletion, in addition to undercutting. Side wall failures become less frequent and sediment ejection from the breach channel slows (Figure 5.34E,F,G; 5.35F).

- As the flow rate through the breach increases rapidly the breach channel initially develops a funnel shape in plan view due to the rapid upstream migration of the crest from carapace raveling, but may stabilise to an hourglass shape as the reservoir becomes depleted (Figure 5.36).

Figure 5.36. Typical Hourglass channel profile

5.10 Final Breach Geometry

5.10.1 Importance of the Final Breach Profile

The geometry of the final breach is of critical importance because;

1. Peak discharge from large reservoirs is primarily a function of the breach final configuration (Walder and O'Connor, 1997).

2. Numerical models assume the evolution of breach development from the incipient shape of the breach until its final configuration.

The deposition of the carapace material immediately downstream of the dam has a stabilising effect, slowing the failure process – this is reflected mainly in the final breach depth which is about 80% of the dam height (in DC dam types). Using breach top width to depth ratios, the final breach geometry of carapace dams can clearly be distinguished from that of non-carapace dams (Table 5.10).

Table 5.10 Breach top width/ depth ratio

Dam	W_T / d_B
DC	*4.6*
SC	*4.5*
STC	*4.6*
DB	*3.5*
SB	*3.4*

5.10.2 Breach Planform

A curved planform of the breach channel mirrors the shape of a minimum energy loss channel suggesting that, during breaching, the channel tends to an equilibrium that is associated with minimum energy conditions and maximum discharge per unit width for the available specific energy (Grant, 1997).

Therefore the 'hourglass' profile is in fact a constant energy state, whereby flow in the breach is near-critical (i.e. 0.5 < Fr < 1.8) and the total head remains constant throughout the breach inlet as far as the throat (Chanson, 2005). Head losses occur downstream of the throat when the flow expands and separation takes place at the lateral boundaries (Figure 5.37).

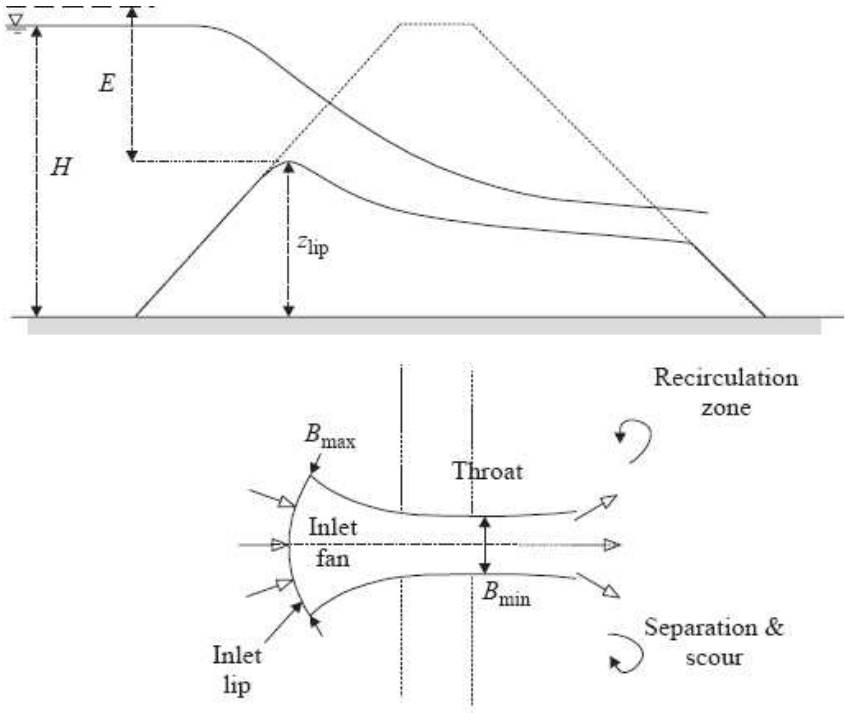

Figure 5.37. Definition sketch of embankment breach for non-cohesive material. Cross-section through the breach centre line and view in elevation of breach flow (Chanson, 2005).

The final breach planform for each dam type tested is presented in Figure 5.38. The final planform morphology and geometry for each dam type proved relatively insensitive to inflow conditions.

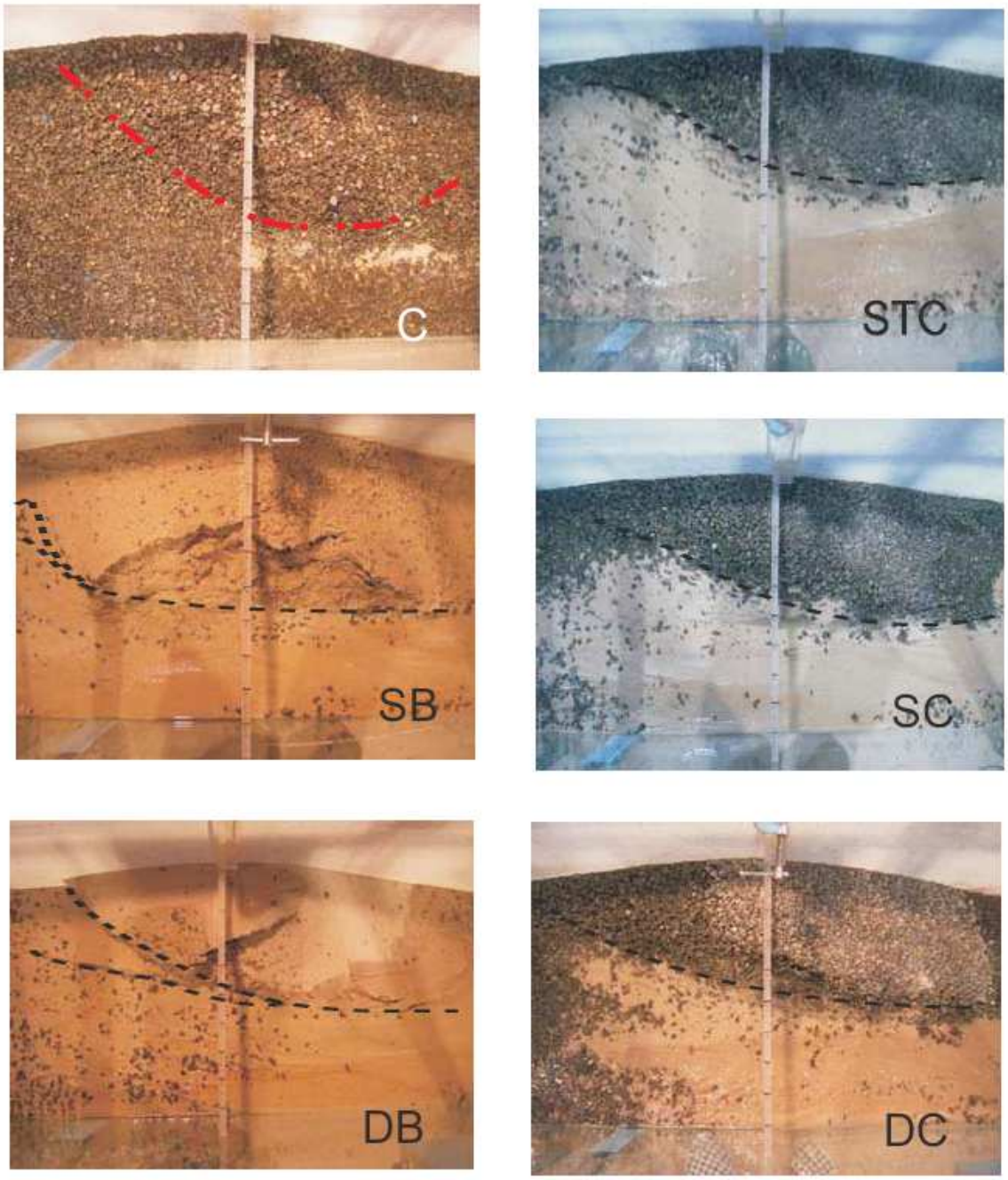

Figure 5.38. Planform Final breach profiles for carapace and non carapace dams

While the hourglass profile was observed initially during breach development, the final breach planform for all dams was observed to have a funnel profile, with an enlarged breach inlet and restricted outlet.

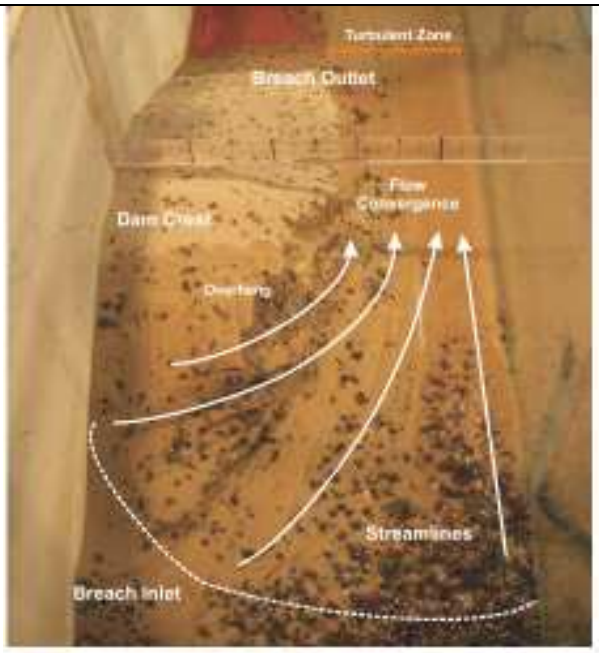

Figure 5.39. Streamline Flow through a half breach

5.10.2.1 Apparent Cohesion

Despite significant undercutting of the breach wall by the flow, high vertical sidewalls and overhangs were observed in non-carapace dams, caused by the apparent cohesion of soil-moisture tension. For this reason, the behaviour of the silica sand was that of a cohesive material and therefore the use of such sediment may correspond to that of a very cohesive material at the prototype scale. The silica sand used in modelling (d_{50} = 0.045 mm) is cohesionless when dry, with a friction angle of 33° with a standard slope stability, which would not permit overhang formation (Figure 5.39). Therefore such phenomena are non representative of the prototype condition.

A noticeable difference was observed in both the breach erosion mechanism and the shape of the resulting breach formation between carapace and non carapace dams. Non carapace dams produced breach channels with over-steepened sidewalls and dominantly vertical erosion, whereas carapace dams were observed to produce a breach with sidewall angles close to that of the material repose angle and evolving largely through lateral erosion. Therefore soil mechanical and geotechnical considerations must be included in the understanding of breaching processes.

5.10.2.2 Breach Hydraulics

Figure 5.39 shows the breach channel viewed from the breach inlet looking downstream after the depletion of the reservoir. Streamlines of the breach flow have been marked in Figure 5.39 to represent paths of equal flow transport. Yang (1996) defines a streamline as a line along which velocity vectors are

tangential. The following qualitative observations describe the hydraulic regime during breaching of carapace dams;

- The longitudinal velocity component is greatest at the breach centreline (represented by the flume wall in a half breach simulation)
- The flow spreads out leaving the breach, causing lateral erosion at the breach outlet and promoting the hourglass planform.
- Flow depth and velocity are greatest at the breach centreline

5.10.3 Post Failure Breach Channel Morphology

The experimental post failure downstream channel morphology was observed to be consistent with that reported in prototype events. Significant channel aggradation resulting from proximal deposition of the carapace material caused ponding at the downstream toe (Figure 5.40). The breach channel was also unusually lacking in coarse material, with significant scouring at the breach outlet. Terraces (caused by waves) on the upstream face indicated a temporarily static reservoir surface level and extent of lateral erosion. The observed downstream morphology did not however provide evidence of the failure mechanism or breach geometric evolution, but rather represented processes operating toward the end of the failure.

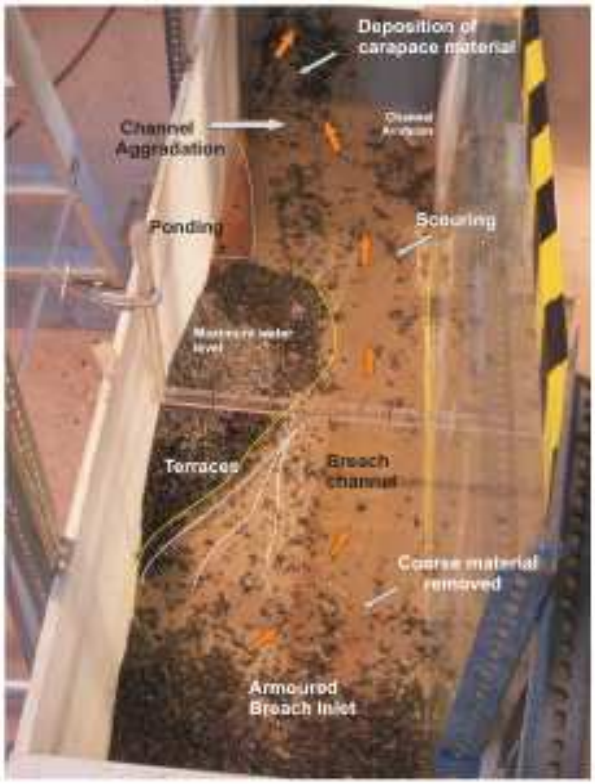

Figure 5.40. Characteristic Morphology observed for carapace dams during the PSM study

5.10.4 Final Breach Geometry

As outlined in section 5.7, breach dimensional growth can be constrained relative to a known parameter. All dams were constructed to a height of 0.25m. As dam height was held constant in each trial and is a readily identifiable parameter within the field, it can be used to describe the final breach geometry. Therefore the results presented herein are specific to the conditions and materials utilised in this investigation. The experiments reveal the following:

- The final breach cross section is best described as trapezoidal;
- The final top width of the breach is approximately 4.5 times the dam height for carapace (heterogeneous) dams, and 3.5 in homogeneous dams;
- The final average width of the breach is approximately 3.5 times the dam height;
- The average final breach depth for dams containing a carapace is approximately 75% of the dam height;
- The average final breach depth for dams without a carapace is approximately 90% of the dam height;
- The average depth development rate is ~50% of the average lateral erosion rate for carapace dams and ~ 0-33% for non carapace dams;
- The time to peak flow is between 36 -120s which corresponds to a time between 15 and 40 min in a prototype rock avalanche dam 100m in height.
- The breach side slopes are consistently greater than the angle of repose depending on the geotechnical properties of the dam construction material.
- The breach channel in final planform has a funnel shape (upstream, negative concavity; flow control section and inflection of positive concavity and downstream a negative concavity; deposition of carapace material)

5.11 Limitations to Accuracy

An important consideration in the use of physical scale modelling is the way in which the generated results can be interpreted. Any dataset should be analysed in the context of the methodology used in its compilation. During both experimental testing and parametric analysis stages of research, inaccuracies can affect the results, especially if used to explain prototype scale phenomena. As the measurement errors are probabilistic and non-correlated, they accumulate arithmetically as the square root of the sum of variances. The primary laboratory errors associated with the PSM dataset are outlined below and summarised in Table 5.11.

Dam Construction

The dam height, the variations of the water surface level and the use of digital imaging to obtain dimensional parametric data were identified as factors that could generate error in the geometry reported in the previous section. Relative error in the adherence to dam height during construction varied by 2%, (0.005m). Therefore outflow rate and peak discharge may have been incorrectly estimated in dams constructed with a height less than 0.245m due to a loss of reservoir storage.

Measurement of the change in water surface elevation

Fluctuation of the water surface level influences the reading of the rotcount (section 4.4) and therefore generates variation in the recorded height. Possible variations of the water surface level were assumed to be in the order of 0.002m (5 pulses ~ approximately 0.6%).

Hydraulic Conditions

Restriction to lateral erosion of the widening breach due to the physical limitations of flume width and the effect of the glass wall in the channel centre potentially generating non-representative hydraulic and erosive conditions to ultimately influence the development rate of breach width. Therefore breach width may have been overestimated to the order of 0.01m (2 %).

Image Recording

The writer regards the highest uncertainty to derive from the recording of dimensional data using the digital media (Section 4.9). The error associated with time was less than ±1/250 second (0.4%) and therefore the cumulative error over the duration of each trial is significantly smaller. Error from the overhead position of the initial breach width was ±0.001m. This correlates to a 2% error in the measurement of breach dimension from parallax effects. In the longitudinal profile, the error in the measurement of breach depth was set at ±0.002m, from a combination of turbulence and meniscus effects which produced an error of 4%. As the frontal camera was primarily used for verification of the failure mechanism, no error value is assigned.

Data Transfer

Digital movies were analysed frame-by-frame, with dimensions marked at 5 second intervals on transparent overlays; however the data acquisition and transfer technique is assigned an inaccuracy of 0.005m (1%).

Table 5.11 Laboratory Error associated with the PSM dataset

Variable	***Lab Error (%)***
Dam construction	*2*
Water level measurement	*0.6*
Flume hydraulic conditions	*2*
Time	*0.4*
Camera	*6*
Measurement of Breach Dimensions	*1*
Total Error	***7%***

Chapter 6 Dam Breach Modelling

6.1 Introduction

Breach formation and the resultant geometry have a fundamental control on the outflow hydrograph and downstream migration of the flood wave. Rapid analysis of the potential magnitude of a dam break flood is essential in mitigating loss of human life and infrastructure due to the rapid failure of many natural dams (Manville, 2001). Therefore a high level of accuracy in the simulation of outflow from a dam breach is required for effective hazard management.

Dam break research has focused on outburst flood magnitude prediction and the breach development time from initial overtopping to full breaching. A comprehensive understanding of the complex interaction between processes during overtopping- induced breaching of a rock avalanche dam requires an adequate database with information on key parameters before such dam breaks can be confidently simulated. The present study made use of physical scale modelling to develop a series of prototype events, from which new breach development data specific to landslide dams under representative inflow conditions could be obtained. Given the paucity of contemporary research in this field and a traditional reliance on embankment dam break technologies and inventories, these tests provide useful information on time dependent breach geometry in heterogeneous non-cohesive materials.

The two primary tasks in the analysis of a dam breach are the prediction of the reservoir outflow hydrograph and the routing of that hydrograph through the downstream valley. Predicting the outflow hydrograph can be further subdivided into predicting the breach characteristics (e.g. shape, depth, width, rate of breach formation) and routing the reservoir storage and inflow through the breach (Wahl, 1998); routing through the breach and downstream valley are accurately simulated in the majority of industry one-dimensional routing methods. However, the programs differ widely in their treatment of the breach simulation process.

6.2 Breach Parameter Estimation Methods

Breach simulation and breach parameter prediction contain the greatest uncertainty of all aspects of dam-break flood forecasting (Wurbs, 1987). Many models do not directly simulate the breach; rather, the user determines the breach characteristics independently and provides that information as input to the routing model. Methods for peak discharge determination vary from simple estimations based on empirical data from dam breach inventories, to complex numerical and mathematical techniques incorporating multiple

parameters (Fread, 1988; Manville, 2001). From the literature, models developed for simulating breach development in both constructed and natural dams can be classified into four categories:

Empirical Relationships - Estimate peak discharge from an empirical equation based on case study data and assume a reasonable outflow hydrograph shape.

Parametric models - Use case study information to estimate time to failure and ultimate breach geometry, then simulate breach growth as a time-dependent linear process and compute breach outflows using principles of hydraulics.

Dimensionless Models – Predict the breach growth rate and lake volume relative to the peak discharge, assuming that the fundamental physical mechanisms involved are the same for all dam-break flood events.

Physically based methods - Predict the development of a breach and the resulting breach outflows using an erosion model based on principles of hydraulics, sediment transport, and soil mechanics (ie. BossBREACH).

While the first three methods allow rapid analysis and an order of magnitude estimate of peak discharge, each approach is highly dependent on case study data (Wahl, 1998). Currently there is only a small amount of landslide dam failure data available to researchers, with few records for very high dams or very large storage volumes (Korup, 2002). Therefore selection of an appropriate empirical relationship requires similarity of boundary conditions between case study data and the dam under consideration.

6.3 Empirical Relationships

6.3.1 Peak Discharge

The simplest approach to estimating the peak discharge from dam breach events is to use empirically derived correlations, relating observed values of peak discharge to some characteristic of the lake or dam, such as lake depth and excess lake volume.

Empirically derived regression relationships have been widely used in the prediction of peak discharge, typically having the form of the power-law relationship;

$$Q_p = aX^b \qquad \textit{Equation 6.1}$$

where X is the lake or dam characteristic and *a* and *b* are empirical coefficients (Manville, 2001). The intrinsic variability in the source data reflects the disparity between data collection methods with discharge usually estimated well downstream of the actual breach, therefore requiring floodwave attenuation correction particularly in steep gradient or progressively widening river valleys. Similarly, extrapolation back to the dam site is complicated by bulking effects whereby sediment entrained into the flood may increase the volume (Pierson,1995, 1997).

Although empirically derived equations provide a rapid method of determining peak discharge from dambreak floods, such regression relationships produce estimates that vary by an order of magnitude and therefore cannot be confidently used to estimate peak discharge (Manville, 2001). A severe limitation of such an approach is that peak discharge is never a simple function of excess lake volume or breach depth (Manville, 2001). Walder and O'Connor (1997) conclude that such regression relations have limited predictive value because factors other than *lake volume* and *breach depth* commonly exert substantial control on peak discharge at the breach.

Empirical analysis has been widely used in estimating dam breach parameters from constructed dams (Table 6.1). A simple approach to estimating probable peak discharge Q_p at a dam breach is to develop regression relations between observed values of Q_p and measures of lake characteristics, typically *Hw*, the total drop in lake level during the flood, and *V*a, the volume of water released as the water level falls by the amount *Hw* (e.g. Kirkpatrick, 1977; Hagen, 1982; MacDonald and Langridge-Monopolis, 1984; Evans, 1986; Costa, 1988; Costa and Schuster, 1988).

Table 6.1 Empirical Relationships for estimation of Peak Discharge

Regression Equation	*Dataset*	r^2	*S.E. (%)*	*Reference*
$Q_p = 0.0184E_p^{0.42}$	26	0.75	91	Costa & Schuster 1988
$Q_p = 961(V_0/10^6)^{0.48}$	29	0.65	124	Costa 1985
$Q_p = 10.5d^{1.87}$	31	0.8	82	Costa 1985
$Q_p = 325(dV_o/10^6)^{0.42}$	29	0.75	95	Costa 1985
$Q_p = 13.4(d)^{1.89}$	28			Singh and Snorrason (1984)
$Q_p = 1.776(V_o/10^6)^{0.47}$	34			Singh and Snorrason (1984)
$Q_p = 0.72V_0^{0.53}$	22	0.84		Evans (1986)
$Q_p = 1.16V_0^{0.46}$	35	0.73		Walder & O'Connor 1997
$Q_p = 2.5d^{2.34}$	35	0.53		Walder & O'Connor 1997
$Q_p = 0.61dV_o^{0.43}$	35	0.76		Walder & O'Connor 1997
$Q_p = 2.297(d+1)^{2.5}$	21			Kirkpatrick (1977)
$Q_p = 65d^{1.85}$	13			U.S. Soil Conservation service 1981

Equation notations Q_p = peak discharge (m^3/s); Vo = volume of water released (excess lake volume, m^3);d = depth of lake (m); D =total drop in lake level during breach; E_p = potential energy (dam factor).

Although landslide dam failures are still frequently analysed as earthen dam failures, assuming similarity in breach development processes, empirical regression relationships specific to landslide dams have been formulated. As the accuracy of any empirical approach is a function of the number of historic events it draws upon to establish defining relationships, landslide dam inventories were created to provide better verification of defining parameters. Costa and Schuster (1988) and Walder and O'Connor (1997) developed several relationships for the prediction of peak discharge from landslide dam datasets (Table 6.2).

Table 6.2 Empirical relationships for estimation of peak discharge in landslide dams

Regression Equation	*Dataset*	r^2	*S.E. (%)*	*Reference*
$Q_p = 0.0158E_p^{0.41}$	*12*	*0.81*	*185*	*Costa & Schuster 1988*
$Q_p = 672(V_0/10^6)^{0.56}$	*10*	*0.73*	*142*	*Costa 1985*
$Q_p = 6.3d^{1.59}$	*10*	*0.74*	*147*	*Costa 1985*
$Q_p = 181(dV_0/10^6)^{0.43}$	*10*	*0.76*	*129*	*Costa 1985*
$Q_p = 1.6V_0^{0.46}$	*19*	*0.6*		*Walder & O'Connor 1997*
$Q_p = 6.7d^{1.73}$	*19*	*0.82*		*Walder & O'Connor 1997*
$Q_p = 0.99dV_o^{0.40}$	*19*	*0.7*		*Walder & O'Connor 1997*

Equation notations Q_p = peak discharge (m^3/s); Vo = volume of water released (excess lake volume, m^3); d = depth of lake (m); D =total drop in lake level during breach; ; E_p = potential energy (dam factor).

6.3.2 Prediction of Secondary Breach Parameters

Although peak discharge and its time of occurrence may provide the best indicators of potential flood magnitude, breach development time and breach width are important secondary breach parameters. From large databases on embankment dam failures (particularly in the US), several empirical relationships have been developed by various researchers. MacDonald and Langridge-Monopolis (1984) proposed a breach formation factor, defined as the product of the volume of breach outflow and the depth of water above the breach invert at the time of failure (Wahl, 1998). Froehlich (1987) developed nondimensional prediction equations for estimating average breach width, average side-slope factor, and breach development time. Von Thun and Gillette (1990) used the data from Froehlich (1987) and MacDonald and Langridge-Monopolis (1984) to develop guidance for estimating breach side slopes, breach width and time to failure. US Bureau of Reclamation (1988) also provided guidance for selecting ultimate breach width and time of failure to produce conservative, upper bound values introducing a factor of safety into the hazard classification procedure.

Four empirical relationships estimating t_b (Table 6.3) were selected for application to the PSM dataset. Empirical equations developed by Froehlich (1987; 1995b) have been recently used in landslide dam breach analysis (Manville, 2001; Ollett, 2001). Von Thun and Gillette (1990) developed two equations specific to the erodibility of dam materials for t_b based on average lateral erosion rates (the ratio of final breach width to t_b) versus depth of water above the breach invert. Consideration of the sedimentology of the rock avalanche deposit required use of the equation developed for *highly erosive materials* as presented in Table 6.3. Application of USBR guidelines will also provide indication as to the relevance and accuracy of safety guidelines for embankment dams.

Table 6.3 Empirical Equations for estimation of Breach Development

Breach Development Time Equation	*Dataset*	*Reference*
$t_b = 0.011B$	*40*	*USBR 1988*
$t_b = 0.8\,(V_r / H_w^2)^{0.5}$	*43*	*Froehlich (1987)**
$t_b = 3.84(V_o)^{0.364} d^{-0.9}$	*34*	*Froehlich (1995b)*
$t_b = B/(4H_w + 61)$	*36*	*Von Thun & Gillette (1990)*

Time (t_b computed in hours).

**SE = ± 70%*

6.3.3 Prediction of Breach Width

Empirical relationships have also been developed to predict breach width development for embankment dam failure (Table 6.4). Froehlich (1987) and USBR (1988) were used for similar reasons to those presented in section 7.3.4. Suitable ranges for estimates of breach width were presented by Johnson and Illes (1976) and Singh and Snorrason (1982) and their applicability to rock avalanche dams is uncertain. Therefore testing such empirical approaches against the PSM dataset will enable methods with higher uncertainty to be disregarded in hazard analysis.

Table 6.4 Empirical estimates for average breach width (Wahl, 1998)

Breach Width Equation	*Dataset*	*Reference*
$B = 3(H_w)$	80	USBR 1988
$B = 13.3(V_0H)^{0.25}$	43	Froehlich (1987)*
$0.5H < B > 3H$		Johnson & Illes (1976)
$2H<B>5H$	20	Singh & Snorrason (1982)

*SE = ± 54%

6.4 Parametric Models

Parametric approaches represent a complex method of dam break flood hydrograph forecasting, usually modelling the discharge through the evolving breach through the application of weir flow equations. Such models generally account for hydraulic constraints not reflected by regression relations, but commonly require the input of final breach dimensions (width, depth and sidewall angle) and breach development time; information that may be unavailable, especially for natural dams. The operator specifies the rate of breach development.

Most dam breaches are trapezoidal in final cross section (MacDonald and Langridge-Monopolis, 1984), and presumably may have this geometry during much of their development (Manville, 2001). Breach development in landslide dams, modelled hydraulically as broad crested weirs, may over-estimate breach discharge due to the breach channel being wide and not long enough for critical flow to develop.

Manville (2001) uses OUTFLOW3 (Appendix C; a numerical model of the growing breach) to calculate the discharge hydrograph. The model uses three alternate broad crested weir (Figure 6.1) equations to generate different values for the instantaneous peak discharge through a trapezoidal breach (ie the outflow that would occur if the breach attained its final size instantaneously when the reservoir was at the dam crest). Although this condition is unrealistic due to lake draw down, the technique constrains the potential upper maximum discharge likely during a dam break flood.

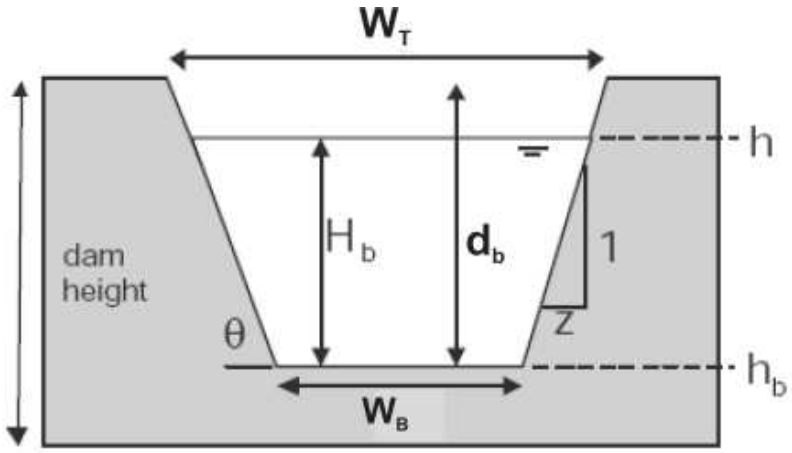

Figure 6.1. Definition sketch of a trapezoidal broad-crested weir (Manville,2001).

Assuming trapezoidal breach geometry throughout the duration of breaching, the trapezoidal form of the broad-crested weir equation should be used, given by Price *et al.,* (1977) as:

$$Q_b = \frac{8}{27} g^{0.5} H_b^{1.5} (0.4W_B + 0.6W_T) \qquad \textit{Equation 6.2}$$

Using Fread's (1996) alternative derivation of the broad-crested weir flow equation for a trapezoidal breach, Manville (2001, p.16) solves for the case of critical flow through a trapezoidal breach using head over the weir as a function of the unit discharge. Conversion of unit discharge to discharge though a breach yields:

$$Q_b = 1.7W_B(H_b)^{1.5} + 1.35z(H_b)^{2.5} \qquad \textit{Equation 6.3}$$

Manville (2001) presents a third equation for calculating the discharge through a trapezoidal breach as:

$$Q_b = 0.591C_d H_b^{1.5} (5W_B + 4zH_b) \qquad \textit{Equation 6.4}$$

Where the drag coefficient ($\boldsymbol{C_d}$) = 0.57 for a trapezoidal breach (Manville, 2001). Application of these three alternative broad-crested weir equations to the PSM study generates three different values for the instantaneous peak discharge (Manville, 2001). As such equations do not account for frictional and turbulent flow resistance in the outlet channel, actual peak discharges will be overestimated to produce a conservative prediction.

6.5 Dimensionless Analysis

Dimensionless analysis is a technique for investigating the relative importance of breach growth rate, lake volume and lake shape on the peak discharge of a dambreak flood (Walder and O'Connor, 1997). The method is based on the assumption that the fundamental physical mechanisms involved in dam breaching and lake drainage are the same for all dambreak flood events. The study conducted by Walder and O'Connor (1997) is significant because it points out the importance of the failure rate and process in determining the peak discharge of a dam failure. This set of procedures offers the advantage of a thoeretical foundation that accounts for the differences and limitations imposed by the large- and small-reservoir cases.

In addition to the uncertainty issue, with the exception of Walder and O'Connor (1997), the breach parameter prediction equations that have been developed do not address the rate of failure. Without the influence of tailwater at the breach outlet, the flow at the breach inlet will become critical (Fr=1) assuming the breach channel has sufficient length, causing the flow to behave hydraulically as a broad crested weir, where discharge at the outlet Q_o is given by Equation 2.5 (Chapter 2). Peak Discharge Q_p and lake volume V_o are then able to be recast as dimensionless variables according to

$$Q_p^* = \frac{Q_p}{g^{0.5} H_b^{2.5}} \qquad \textit{Equation 6.5}$$

$$V_o^* = \frac{V_o}{H_b^{3}} \qquad \textit{Equation 6.6}$$

The graphical representation of the relationship between these two dimensionless variables (Figure 6.2) yields a unique distinction between breach development processes for small and large reservoirs. Q_p* from large lakes ($V^*_o > 10^4$) displays a higher sensitivity to physical breach dimensions, with the breach typically forming before substantial drawdown of a lake can occur. Significant reductions in lake level during breaching cause Q_p* from small lakes to have a higher sensitivity to the breach development time.

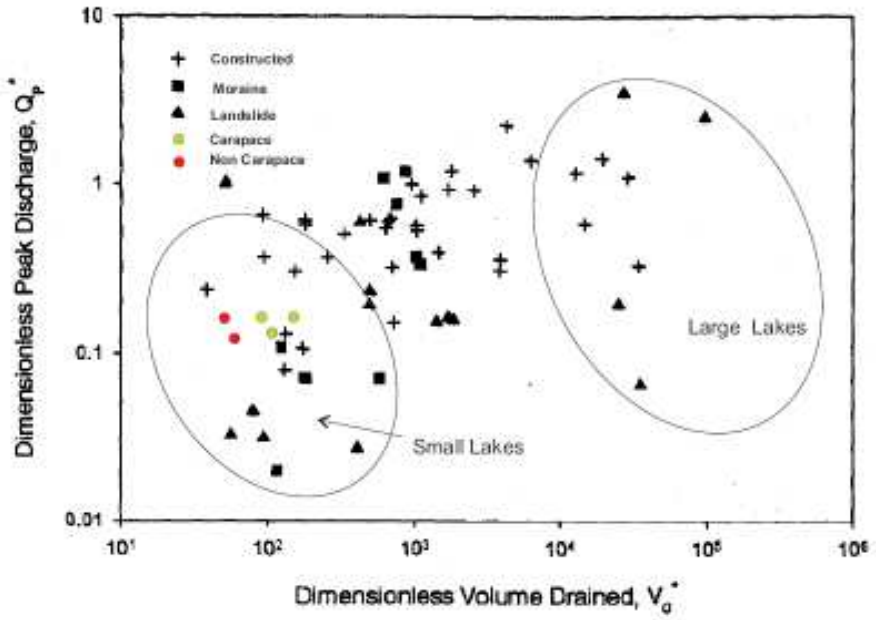

Figure 6.2. Plot of Q_p against V_o* (Walder and O'Connor, 1997) including the PSM study data*

From analysis of a simple, physically based model of dam breach formation Walder and O'Connor (1997) developed peak discharge parameter prediction equations based on the dimensionless parameter;

$$\eta = k^* V_o^* = \frac{k V_o}{g^{0.5} H_b^{3.5}}$$

Equation 6.7

k = mean vertical erosion rate of the breach,

k = dimensionless breach growth rate ($k^* = k/g^{0.5} H_b^{0.5}$).*

V_o = drained volume

V_o = dimensionless drained volume*

H_b = head

g = acceleration due to gravity.

They were thus able to make a distinction in types of reservoirs depending on whether $\eta < 1$ (slow breach formation relative to lake volume) or $\eta > 1$ (fast breach formation relative to lake volume). Physically, for values of $\eta < 1$, the peak outflow occurs before the breach reaches maximum depth of erosion, leading to significant draw down prior to full depth erosion of the breach. For values of $\eta >> 1$, the peak outflow occurs after the breach reaches maximum erosion depth but prior to any significant draw down of the reservoir.

Walder and O'Connor (1997) identified that physical characteristics of the lake in particular exert a significant control on the breach development and assumed that the hypsometric lake shape factor lies in the range m= 1-3 (Figure 6.3).

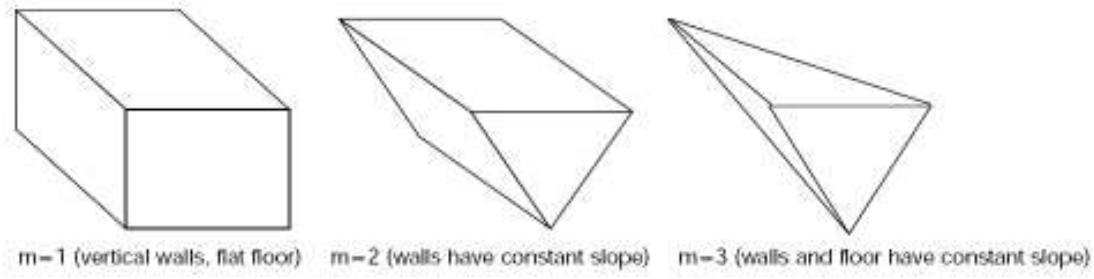

Figure 6.3. Hyposometric classification of potential lake shape

Due to the laboratory constraints of this research, only a hypsometric lake factor equivalent to m=1 could be simulated in the physical scale models, although the author the unrealistic nature of this condition is acknowledged, particularly in the context of rock avalanche dam formation

Calculation Steps

Stage 1

For the prediction of an approximate outflow hydrograph from a dam-breach, dimensionless analysis requires determination of η from realistic values of three parameters:

- The drop in lake level or breach depth ***d*** (typically 50-100% of the dam height ***H*** for rock avalanche dams)
- The water volume released V_o (constrained by ***d*** and some assessment of how the surface area of the lake varies with ***d***), and
- The vertical breach erosion rate ***k*** (typically 10-100 m/hr).

Stage 2

$$Q_p = 1.51(g^{0.5} d^{2.5})^{0.06} \left(\frac{kV_0}{d} \right)^{0.95}$$

When η < ~ 0.6 *Equation 6.8*

Stage 3

When $\eta >> 1$

$$Q_p = 1.94 g^{0.5} d^{2.5} \left(\frac{H}{d} \right)^{0.75}$$ *Equation 6.9*

Stage 4

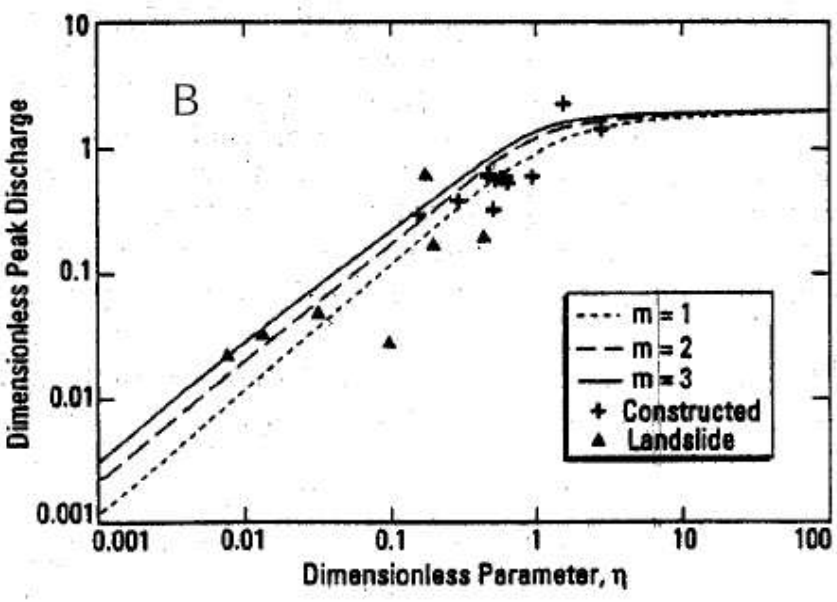

Figure 6.4. Dimensionless Peak Discharge with consideration of Lake hyposymetry

When $0.6 < \eta << 1$, the dimensionless peak discharge must be derived from the m=1 (lake hypsometry) curve from Figure 6.4 Q_p is then determined using:

$$Q_p = (1.94 g^{0.5} d^{2.5}) Qp*$$ *Equation 6.10*

This dimensionless technique is limited because there is no consideration of the role of breach width and it only assesses the sensitivity of the relationship between breach growth rate (as a proxy for breach development time) and lake volume (Manville, 2001). Consideration of breach width is best achieved using parametric methods such as OUTFLOW3.

6.6 Physically Based Breach Erosion Models

6.6.1 Background

Numerical modelling of dambreak flood outflows, usually relating breach development to the erosive capacity of the water flowing through the breach, has received much attention in the past four decades.

Most numerical models involve a computation process incorporating the development of a core algorithm such as that for the BREACH model. Key parameters describing the impoundment geometry (dam height, crest length and width, upstream and downstream face inclinations) and material properties (average grain size, cohesion, friction angle and unit weight) are initially required.

Computation of reservoir characteristics is often the next required input, typically describing the reservoir level and subsequent depletion as a series of 2D surface areas or layers. This enables lake volume to be calculated from the change in lake surface elevation. Inflow conditions and simulation duration are usually specified (particularly if a design storm, or variable inflow is being modelled).

The next step is specification of the initial breach geometry (pilot channel), with most models assuming a central crest breach position. Water flow through the breach is then simulated as a broad crested weir (Henderson, 1966) with conversion of flow depth over the weir to a volumetric discharge using the broad crested weir formula.

Computation of the erosion of the breach invert and sidewalls requires selection of an appropriate sediment transport formula. Such formulae usually require slope, average grainsize (d_{50}), and flow velocity, which can be calculated from the breach shape, discharge and water depth. Erosion of the material from the breach is then calculated as a rate (m/s).

A change in lake volume is calculated by multiplying the difference between the lake inflow and the breach outflow rates by a specific time increment. This volume change is used to calculate change in lake level through interpolation between the surface lake areas. As the breach erosion has been estimated, and the change in lake level determined, a new water depth can be calculated for the crest of the breach, giving a new breach outflow. From here, the process is iterated until some specified condition is reached, with data being recorded at each time increment.

6.6.2 Development of Physically Based Models

Cristofano (1965) proposed the first physically based dam breach model, relating the shear stress of the water through the breach to the shear strength of the material forming the dam, enabling the rate of erosion of the breach channel to be expressed as a function of the discharge rate (Wahl, 1998). The model assumed a trapezoidal breach of constant bottom width; side slopes of the breach were determined by the angle of repose of the material, and the bottom slope of the breach channel was equal to the internal angle of friction of the material. An empirical coefficient was critical to the model's performance (Fread, 1988).

Harris and Wagner (1967) applied the Schoklitsch sediment transport equation to dam breach flows, assuming breach erosion to begin immediately upon overtopping, and to proceed until the breach reached the bottom of the dam. Brown and Rogers (1977) presented a breach model, BRDAM, based on Harris and Wagner's work, which was applicable to overtopping and piping induced breaches.

The BEED (Breach Erosion of Embankment Dams) model developed by Singh and Scarlatos (1985) is a physically-based model simulating breach evolution, flood routing, and sediment routing. Erosion and sediment transport are computed using the equations of Einstein-Brown and Bagnold.

6.6.3 Physically Based Models currently in use

Concerted Action on Dambreak Modelling (CADAM), Report SR 571 (2000) for the European Commission, presents a comparison and assessment of currently available physically based breach prediction models in Table 6.5.

Model	Author	Breach Morphology	Flow Over The Dam	Sediment Transport	Geo-Mechanics Of The Breach Side Slope
Cristofano	Cristofano (1965)	Trapezoidal with constant bottom width.	Broad crested weir formula.	Cristofano's empirical formula.	None.
Harris-Wagner (HW)	Harris-Wagner (HW) (1967)	Parabolic with top width equals 3.75 depth.	Broad crested weir formula.	Schoklitsch formula.	None.
BRDAM	Brown & Rogers (1977/ 1981)	Parabolic with 45° side slopes.	Broad crested weir formula.	Schoklitsch formula.	Failure of the top wedge above pipe.
Ponce – Tsivoglou (PT)	Ponce – Tsivoglou (PT) (1981)	Top width flow rate relation.	Full St. Venant equations.	Exner equation with Mayer-Peter –Muller.	None.
Lou	Lou. (1981)	Most effective stable section (Cosine curve shape)	Full St. Venant equations.	1. Cristofano's empirical formula. 2. Duboy and Einstein formulae. 3. Lou's formula.	None.
Nogueira	Nogueira (1984)	Effective shear stress section (Cosine curve shape)	Full St. Venant equations.	Exner equation with Meyer-Peter / Müller	None.
BREACH	Fread (1988)	Rectangular and trapezoidal.	Broad crested weir formula for over topping and orifice for piping.	Meyer-Peter / Müller modified by smart.	1. Breach side slope stability. 2. Top wedge failure during piping or overtopping.

Table 6.5 Physically Based Models currently used in Industry (Source CADAM SR 571)

Model	Author	Breach Morphology	Flow Over The Dam	Sediment Transport	Geo-Mechanics Of The Breach Side Slope
BEED.	Singh et al (1986 / 1988)	Trapezoidal.	Broad crested weir formula.	Einstein-Brown.	Breach side slope stability.
Sites	NRCS (US) (1998)	3 stages failure: 1. Cover failure. 2. Headcut formation. 3. Headcut erosion.	Principles of hydrology and hydraulics to produce spillway flow-stage curve.	For stage 1 and 2 a detachment model was used. For stage 3 an energy dissipation equation was used.	Spillway exit channel stability.
NCP-BREACH	Coleman et al (1998)	Parabolic	Empirical formula.	Empirical formula.	None.
EDBREACH	Loukola & Huokuna (1998)	Trapezoidal	Broad crested weir formula.	Meyer-Peter / Müller	Top wedge failure during piping.
BRES	Visser (1998)	5 stages failure	Broad crested weir formula.	Four sediment formulae can be used: 1. Bagnold – Visser. 2. Engelund – Hanssen. 3. Van Rijn. 4. Wilson.	None.
DEICH_N2	Broich (1998)	From solution of 2D Exner equation	2D full St Venant equation	Nine different formulae or combinations: 1 Meyer-Peter / Müller (bed load) 2 Engelund / Hansen (suspended load) 3 Bagnold (total load) 4 Smart (bed load) 5 Smart / Bagnold (combined total)	None

6.6.4 Selection of a Physical Model

Despite the different geometric and material properties observed in rock avalanche dams, breaching from such impoundments is still frequently studied using embankment failure technology. Therefore any numerical model used for the simulation of breach development from a landslide dam should be applied with caution. Based on the available models outlined in Table 6.5, selection of an appropriate physically based model to simulate the failure of a landslide dam must consider the following;

Breach Geometry- The breach enlargement should be simulated using a trapezoidal geometry in cross sectional profile.

Sediment Transport- The average bedslope during breaching is steep, producing unsteady, critical to supercritical flow. Most existing sediment transport equations were derived for steady state, subcritical flow conditions, for specific types of sediment, and for a certain range of sediment diameters, making them inapplicable to a dam breach scenario. Therefore breach erosion can only be accurately simulated using the Meyer-Peter and Müller formula modified by Smart (1984) and the Schoklitsch formula (Schoklitsch, 1962) which both were calibrated against steep gradient beds with unlimited sediment supply.

Heterogeneous Composition- The model should enable specification of two average grainsizes to account for material heterogeneity in the rock avalanche deposit.

Most numerical dam breach models rely on bed-load erosion formulae that imply assumptions of gradually varied flow and relatively large flow depth in comparison to the size of roughness elements. Singh (1996) emphasises that little is known about the mechanics of heterogeneous sediment transport especially under highly dynamic conditions, and therefore researchers rely on experience from alluvial streams. The bed load formulae based on the tractive force theory assume that sediment transport is a function of excess bed shear stress. Most of these conditions are likely to be violated during the breaching process since conditions are typically unsteady, supercritical flow, and with a wide variety of grain sizes in landslide dams.

The only numerical erosion model found to fully satisfy the above conditions was Boss BREACH™. BossBREACH™ is presently the only model identified which enables specification of two different materials. The following section outlines the background theory to this model.

6.7 BossBREACH™.

To study the effects of the heterogeneity of the landslide material on the erosion of the breach, the BossBREACH code, the most widely used breach modelling software within the industry, was used to simulate the breaching of the scaled physical models tested in this study.

Boss BREACH™ is a mathematical model developed by Fread (1987) at the US National Weather Service, used to simulate the failure of earthen dams. The model predicts breach characteristics (dimensions, geometry, and rate of development) from the physical properties of the dam material and the characteristics of the lake. The model couples the breach outflow with the sediment-transporting capacity of the unsteady uniform flow along the erosional channel cut through the dam (Manville, 2001).

6.7.1 Input Parameters

The BREACH model uses the principles of soil mechanics, hydraulics, and sediment transport to simulate the bed and side wall erosion processes that occur during breach enlargement (Fread, 1996). A range of input parameters is used in the computation of the outflow hydrograph (Figure 6.5).

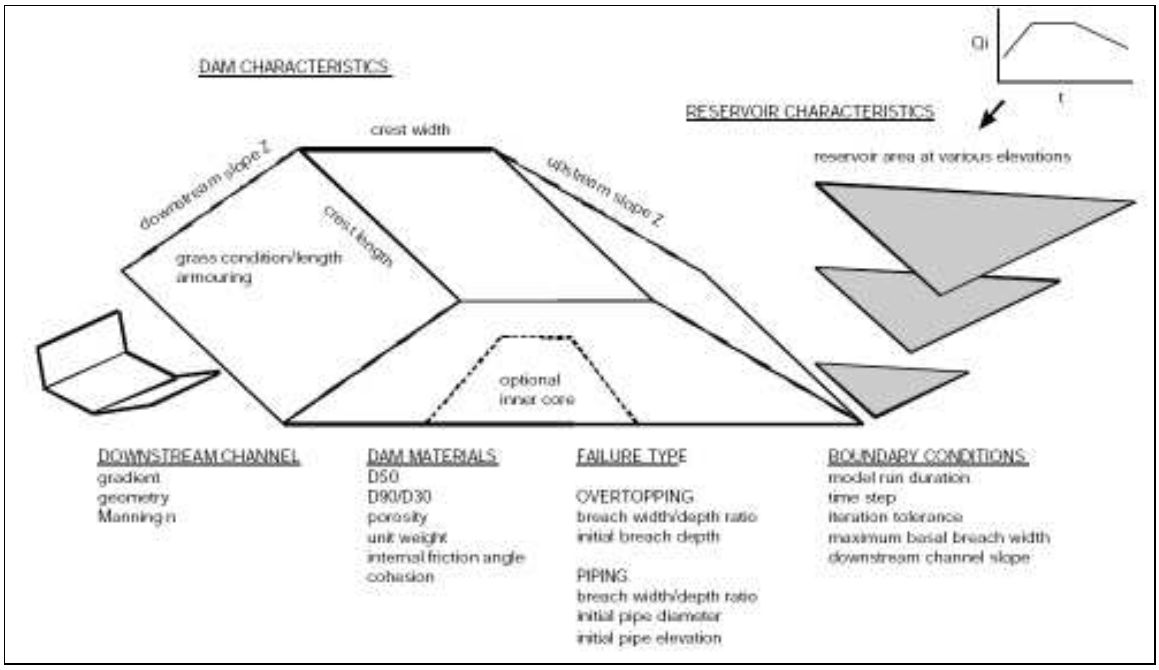

Figure 6.5. Schematic representation of input parameters and components of Boss BREACH (Manville, 2001)

6.7.2 Calculation of Breach Parameters

Calculation of breach parameters involves the following methods;

1. The reservoir surface elevation is calculated using a specified reservoir inflow hydrograph and spillway overflow.

2. Overtopping and breach flow are simulated using a broad crested weir flow equation.

3. Breach width is simulated as a function of the optimal channel hydraulic efficiency*, evolving from rectangular to trapezoidal geometry through sidewall collapse when breach depth exceeds the stability limits for the dam material.

4. Breach erosion is assumed to be uniform along both the channel bed and side, but is suspended upon sidewall collapse until the fallen material is ejected from the breach at the pre-collapse erosion rate (Manville, 2001).

5. The rate of breach erosion is dependent on the transport capacity of breach outflow, calculated using the Meyer-Peter and Müller sediment transport relation, as modified by Smart (1984) for steep channels as outlined in section 2.10.

6. Iteration of calculations is required as the flow into the breach is dependent on breach dimensions. Breach enlargement is therefore also dependent on erosion depth which is controlled by the sediment transport capacity of the breach flow, which is itself a function of the breach size and flow (Manville, 2001). An estimated incremental erosion depth is used at each time-step to start an iterative solution that accounts for the mutual interdependence of the flow, erosion, and breach properties (Manville, 2001).

6.7.3 Application of the Model

The dam-break may occur by overtopping, by piping, or by sudden structural collapse due to hydrostatic pressure. Manville (2001) outlines the following conditions that can be modelled using Boss BREACH™;

- An inner core of different composition and properties to the outer parts of the dam (useful for rock-fill cored earthen dams).

---

* *The ability of a hydraulic structure or element to conduct water with minimum energy loss*

- The development of an initial erosion gully on the downstream face of the dam prior to the formation of a through-going breach that penetrates the full thickness of the dam crest.

- Armouring of the downstream face of the dam by grass or coarse rip-rap.

- Breach enlargement by sudden structural collapses through the hydrostatic pressure exerted by the reservoir exceeding the shear and cohesive strength of the dam.

- Breach enlargement by failure of over-steepened breach walls, calculated from slope stability rules.

- Initiation of the breach by piping flow followed by development of free-surface breach flow.

6.8 BREACH analysis of the Prototype Condition

A key objective of this research was to assess the ability of breaching models to predict breach development and peak outflows in rock avalanche dams. A series of physical models representing rock avalanche sedimentology was tested to investigate peak discharge and breach development time under overtopping flow. Using Froude scale modelling, the laboratory tests were scaled up to prototype size using a linear scaling factor of $\lambda = 400$ (see Section 3.4). The scaled prototype parameters were used as inputs to simulate the breaching of a 100m high, 416m wide dam with a heterogeneous structure in BossBREACH (Figure 6.6).

A low inflow condition of 0.001m^3/s was sufficient to reliably initiate failure, without overwhelming the intrinsic behaviour of the failing dam. Due to the nature of the scaling factor, the low inflow condition of 0.001m^3/s in the laboratory is represented by an inflow of 3200 m^3/s in the prototype. This is extremely conservative and of low probability, representing a 10 year flood or alternately a 100 year rainfall event within a 100 km^2 catchment, produced by inundation of the catchment with >100 mm falling in 24 hours. The scaled high inflow condition of 10,000 m^3/s was only representative of a condition whereby multiple landslide dams had formed in a river valley and a cascading outburst flow had been generated from an upstream collapse. Therefore only the low flow condition was simulated using Boss BREACH™.

Unsaturated Carapace Dam
Breach filenames DC2
OVERTOPPING

INFLOW		RESERVOIR		LAKE VOLUME	
time (hrs)	inflow (m3/s)	initial level (m)	100	elevation (m)	area (km2)
0	3200	dam base (m)	0	100	0.5
3	3200	dam top (m)	100	50	0.4
		spillway elev (m)		0	0
		crest length (m)	416		
		crest width (m)	2		
		breach width/flow depth	2		
		initial breach width (m)	4		

INNER CORE		OUTER CORE	
D50 (mm)	1	D50 (mm)	100
D90/D30	10	D90/D30	1000
porosity	0.45	porosity	0.6
unit weight (N/m3)	15713	unit weight (N/m3)	20000
Manning		Manning	
friction angle (deg)	33	friction angle (deg)	42
cohesion (N/m2)		cohesion (N/m2)	
av. Clay plasticity		Z upstream	1:05
		Z downstream	1:05
		downstream D50 (mm)	100
		downstream D90/D30	1000
		grass length (cm)	
		grass condition	
		max grass velocity (m/s)	

OUTFLOW			
spillway	all blank		
channel	elevation (m	width (m)	Manning
	0	416	0.04
	50	416	0.04
	100	416	0.04

BOUNDARY CONDITIONS	
model duration (hrs)	3
time step (hrs)	0.01
iteration tolerance (%	0.1
max Bw (m)	200
channel slope (m/m)	0

RESULTS	
computation	OK
time of failure (hrs)	0.28
duration of rising limb (hrs)	
peak outflow (m3/s)	**21301**
at (hrs)	0.29
Breach top width (m)	132
Breach bottom width (m)	24
Side wall (degrees)	47
Breach depth (m)	96

Figure 6.6.Input Parameters for the BREACH simulation of the DC dam.

Six dam types, both homogenous and heterogeneous in composition, were simulated using the model input parameters listed in Figure 6.6. The dam materials were modelled as a poorly sorted and unconsolidated mass of rock fragments, with d_{50} ranging from 0.045 mm to 1mm within the inner core (modelled to represent the body), to 100-1000 mm in the outer core (modelled to represent the carapace). For the simulation of unsaturated sediments (DB, DC, C models), materials were considered cohesionless, however due to surface tension a small degree of cohesion was observed in saturated materials. Therefore the prototype condition of SC, SB and STC models were simulated using cohesion = 30N/m^2. Saturation of materials in the prototype condition was simulated through a 25% reduction in porosity and 15% increase in internal friction angle. The decision to use such values was influenced by reported prototype values in Kojan and Hutchinson, (1979); Dunning *et al.*, (2005) and Hancox *et al.,* (2005).

The body material was simulated with a friction angle ranging between 27-33 degrees, while the carapace material was simulated with a friction angle ranging from 40-45 degrees. Guidance as to the use of appropriate values was found in the geotechnical evaluations of the Montaro landslide dam (Kojan and Hutchinson, 1979). The upstream and downstream dam faces were defined with a slope of 1 in 5 to

maintain numerical stability in the model (a serious limitation); true values were closer to 1 in 3.0 downstream and 1 in 4.8 upstream (25 and 15 degrees respectively). A Manning roughness coefficient of 0.04 (characteristic of steep gradient hydraulics as observed in mountain streams, floored with gravels, cobbles and boulders) was used, with the tail water gradient assumed to be approximately 0.1m/m. The simulation duration was set to 3 hours, to allow full development of the falling limb in the outflow hydrograph.

6.9 Parameter Sensitivity

All models selected (empirical, parametric, dimensional and physical) have a degree of sensitivity to the geometric and material properties of a dam. Sensitivity analysis was conducted for each modelling technique.

6.9.1 Sensitivity Analysis for BossBREACH

Simulations of the DC physical model were used to test the sensitivity of peak discharge and the time to peak outflow to the material properties of the dam (Figure 6.7).

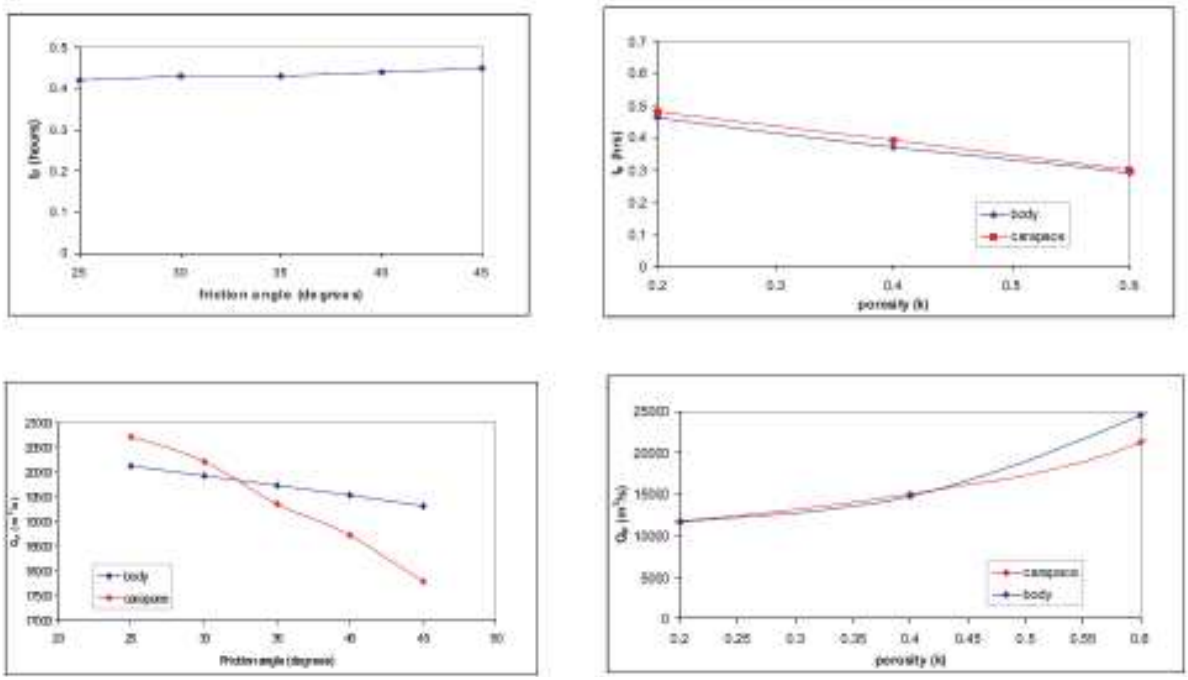

Figure 6.7. Sensitivity analysis for peak discharge using BossBREACH

Peak discharge was sensitive to the internal friction angle of the dam material. Variation of the friction angle in the body is unlikely to exceed ±10° causing a ± 2% change in Q_p. Variation in the carapace

friction angle, although also unlikely to exceed ± 10° alters Q_p by ± 8%. The time to peak outflow appeared to be insensitive to friction angles.

Q_p and t_p are also sensitive to dam material porosity. Porosity is a critical parameter controlling the migration of the phreatic front through the upstream face on filling of the lake behind the impoundment. Porosity of the body was simulated with a void ratio of 45%, while the carapace was modelled as having void spacing of >50%, indicative of the larger spacing between larger angular clasts. Estimates of porosity could vary by 15%, yielding an uncertainty of ±25% in Q_p.

The average grain size (d_{50}) varied between 0.045mm in the body to 1000mm in the carapace. Sensitivity analysis of peak discharge to average grain size (d_{50}) revealed that a critical threshold exists for outflow conditions conducive to breach formation and entrainment of clasts (Figure 6.8). Q_p was found to reduce by 84%, when d_{50} exceeded 250mm. t_p was also sensitive to variance in d_{50}; t_p increased by an order of magnitude as d_{50} increased from 100mm to 200mm.

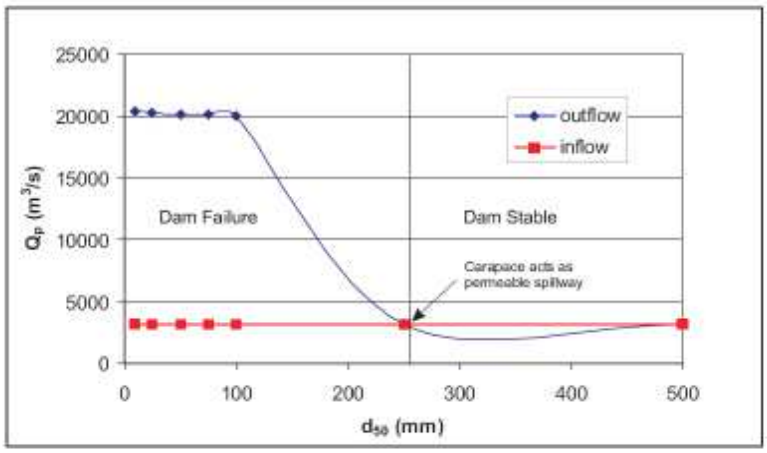

Figure 6.8. Sensitivity analysis for peak discharge to average grainsize for a carapace dam reveals the grain size at which a dam remains stable in the BREACH simulation.

Conversely, both peak discharge and time to peak are insensitive to variation in the crest width and cohesion over 2 orders of magnitude.

6.9.2 Sensitivity Analysis for Empirical Methods

Empirical Models (Costa 1985; Walder and O'Connor, 1997) only require dam height/lake depth and or volume of water released (lake volume). As these parameters are usually well constrained no uncertainty is assigned.

6.9.3 Sensitivity Analysis for Parametric Methods

The main uncertainty associated with parametric model OUTFLOW3 (Manville, 2001) surrounds the assumption of breach dimension and development time. Conservative estimates of the peak outflow should be based on maximum probable breach dimensions and minimum breach development times. As both temporal and dimensional data inputs were sourced from the PSM, the main uncertainties relate to the method of data acquisition as outlined in section 4.10.

Sensitivity analysis of OUTFLOW3 suggests that the greatest uncertainty is associated with the constraint of the breach development time. Alteration in t_b from 10 to 20 minutes can generate a 50% reduction in Q_p. Breach depth and lake surface area have linear relationships with outflow discharge and are better constrained than other parameters.

6.9.4 Sensitivity Analysis for Dimensional Methods

Dimensionless analysis has a limited amount of uncertainty, but places a high reliance on the reservoir volume and water depth at the dam face. The model is also highly sensitive to the breach width/ breach depth ratio.

Chapter 7 Testing of Models

7.1 Introduction

A primary objective of this investigation was to estimate the uncertainty associated with the four types of models used (empirical, parametric, dimensional and physical). As outlined in Section 5.11, the limits of accuracy in the dataset acquired from physical scale modelling can be related to parameter and component uncertainty, or the uncertainty associated with assumptions made regarding the physical process of breach development. Component uncertainty compared the performance of the empirical, parametric and numerical models to the observed results from the physical scale model (PSM) of variable dam sedimentologies. This method also enabled the identification of parameters used in the modelling process that cannot be estimated accurately, to provide indication of the overall uncertainty. The sensitivity of various parameters to peak discharge is represented within the error assigned to *model performance* for each model. The combined error associated with each dam breach modelling technique is presented as the sum of both model performance and laboratory uncertainty errors.

7.2 Model Performance

7.2.1 Overview

While prediction of peak discharge is the most critical parameter for dam breach prediction, various researchers have derived empirical relationships and parametric models (BREACH, OUTFLOW3) to link lake/dam characteristics with time to peak breach discharge, total breach development time and breach geometry (presented in Section 6.2) for a variety of natural and constructed dam types, including landslide dams (Fread, 1988; Costa 1985; Costa and Schuster 1988; Walder and O'Connor 1997).

Based on the dataset obtained from physical scale modelling and the use of identical parametric inputs, the four models (empirical, parametric, dimensional and physical) were assessed on their ability to simulate the breach development process observed in the PSM. Specific empirical methods, while simplistic, were found to predict critical breach parameters to a higher accuracy than other methods and are therefore recommended as an appropriate first order assessment.

7.2.2 Peak Discharge

Peak discharge provides the best indicator of potential flood magnitude (impact) and is therefore the principal parameter required for dam break analysis. While all four models demonstrated the ability to

constrain peak discharge to the same order of magnitude as PSM data, the empirical method using Walder and O'Connor's Equation 7.1 (Table 7.1), which is derived from a landslide dam dataset, predicted Q_p to an accuracy of ± 7% in carapace dams and ± 25% in non carapace dams. Parametric modelling techniques are also considered suitable for application to landslide dams, predicting peak discharge to an accuracy of ± 37% in carapace dams and ± 34% in non carapace dams. The results from simulation of PSM data for each dam type are presented in Table 7.2. The combined uncertainty associated with estimation of peak discharge is presented for both carapace dams (Table 7.3) and non carapace dams (Table 7.4).

Table 7.1 Empirical Relationships for Q_p estimation (PSM 19200 m^3/s < Q_p> 25600 m^3/s)

Regression Equation	*Dataset*	*r^2*	*S.E. (%)*	*Q_p (m^3/s)*	*Reference*
$Q_p = 0.0158E_p^{0.41}$	12	0.81	185	6605	Costa & Schuster 1988
$Q_p = 672(V_0/10^6)^{0.56}$	10	0.73	142	6163	Costa 1985
$Q_p = 6.3d^{1.59}$	10	0.74	147	9535	Costa 1985
$Q_p = 181(dV_o/10^6)^{0.43}$	10	0.76	129	7189	Costa 1985
$Q_p = 1.6V_0^{0.46}$	19	0.6		5684	Walder & O'Connor 1997
$Q_p = 6.7d^{1.73}$ *	19	0.82		19323	Walder & O'Connor 1997
$Q_p = 0.99dV_o^{0.40}$	19	0.7		7640	Walder & O'Connor 1997
		landslide - average		8877	+/- 4772

* Equation 7.1

Table 7.2 Simulation Results for estimation of Q_p

Model	*PSM*	*Empirical*		*Parametric*		*BREACH*		*Dimensional* [b]	
	Q_{out}	Q_{out} [a]	Error	Q_{out}	Error	Q_{out}	Error	Q_{out}	Error
	(m^3/s)	(m^3/s)	(%)	(m^3/s)	(%)	(m^3/s)	(%)	(m^3/s)	(%)
DC	22400	19323	14	15605	30	21301	5	35858	60
SC	19200	19323	1	15360	20	9433	51	35093	83
DB	25600	19323	25	35344	38	13302	48	58417	128
SB	25600	19323	25	26880	5	12800	50	41726	63

[a] Empirical method using Equation 1

[b] Dimensional method uses Equation 6.2 (Fread,1996)

Table 7.3 Combined Uncertainty associated with the estimation of Q_p from Carapace Dams. Value is the arithmetic mean, with error bars at one standard deviation.

Model	*Lab Uncertainty*	*Model Performance*	*Combined Uncertainty*	*Total Failure (m^3/s)*
				Carapace
Empirical	*±7%*	*± 7%*	*± 14 %*	*19323 ± 2705*
Parametric	*±7%*	*± 25%*	*± 32 %*	*15483 ± 4955*
BREACH	*±7%*	*± 27%*	*± 34%*	*15367 ± 5225*
Dimensionless	*±7%*	*± 71%*	*± 78%*	*35476 ± 27671*

Table 7.4 Combined Uncertainty associated with the estimation of Q_p from Non Carapace Dams. Value is the arithmetic mean, with error bars at one standard deviation.

Model	*Lab Uncertainty*	*Model Performance*	*Combined Uncertainty*	*Total Failure (m^3/s)*
				Non Carapace
Empirical	*±7%*	*± 25%*	*± 32 %*	*19323 ± 6183*
Parametric	*±7%*	*± 22%*	*± 29 %*	*31112 ± 9022*
BREACH	*±7%*	*± 50%*	*± 57%*	*13051 ± 7439*
Dimensionless	*±7%*	*± 95%*	*± 102%*	*50072 ± 51073*

7.3.3 Time to Peak Discharge

Estimations of time to peak discharge provide indication of available response times from calculation of flood peak arrival times at downstream locations. BREACH predicted t_p to an adequate degree of accuracy (Table 7.5).

Table 7.5 Uncertainty in Time to Peak Outflow estimates

	Carapace		*Non-Carapace*	
Model	*Performance*	*$t_{p\ *hrs)}$*	*Performance**	*$t_{p*(hrs)}$*
Parametric	*±48%*	*0.21-0.61*	*±40%*	*0.12-0.28*
BREACH	*±26%*	*0.32-0.54*	*±17%*	*0.18-0.25*

**Includes lab uncertainty (±7%)*

7.3.4 Breach Development Time

Unlike time to peak discharge, breach development time reflects the physical controls on the development of breach geometry, such as lake volume, dam volume and inflow conditions. Rapid breach development times may indicate peak outflow occurs when the breach reaches maximum depth prior to any significant drawdown of the reservoir, which will initiate different geomorphic impacts to that observed from slow development.

The empirical approach presented by Froehlich (1987) provided the most accurate prediction of breach development time in carapace dams, but proved to be inappropriate for use in non carapace dams (Table 7.6).

Table 7.6 Uncertainty in Breach Development Time estimates

	Carapace		*Non-Carapace*	
Model	***Performance***	$t_{b*(hrs)}$	***Performance***	$t_{b*(hrs)}$
Froehlich (1995b)	*±63%*	*0.15-0.66*	*±63%*	*0.07-0.32*
Von Thun & Gillette (1990)	*±9%*	*0.42-0.51*	-	-
Froehlich (1987)	*±5%*	*0.49*	*±76%*	*0.06 - 0.33*
BREACH	*±22%*	*0.24-0.37*	*±20%*	*0.23-0.35*

**Includes lab uncertainty (±7%)*

7.3.5 Breach Width

The ultimate breach width and the rate of breach width expansion can dramatically affect the peak discharge and resulting inundation levels downstream from the dam. Empirical approaches accurately predicted breach width (Tables 7.7-7.9) and should be used for rapid first order assessment of potential breach geometry.

Table 7.7 Uncertainty in estimation of Breach Top Width

	Carapace		*Non carapace*	
	Performance	W_T *	***Performance***	W_T *
Froehlich (1987) [a]	*± 7%*	*242-278m*	-	-
BREACH	*± 38%*	*81-180m*	*± 37%*	*74-162m*

**Includes lab uncertainty (±7%).* [a] *Assumption of 45° sidewalls*

Table 7.8 Uncertainty in estimation of Breach Base Width

	Carapace		*Non carapace*	
	Performance	***W_B****	***Performance***	***W_B****
Froehlich (1987) [a]	*± 18%*	*86-123m*	-	-
BREACH	*± 90%*	*1-19m*	-	-

**Includes lab uncertainty (±7%)* [a] *Assumption of 45° sidewalls*

Table 7.9 Uncertainty in estimation of Average Breach Width (B)

	Carapace		*Non carapace*	
	Performance	***B***	***Performance***	***B***
USBR (1988)	*± 9%*	*155-186m**	*± 5%*	*198m**
Johnson & Illes (1976)	-	*40-240m*	-	*45-270m*
Singh & Snorrason (1982)	-	*160-400m*	-	*180-450m*

**Includes lab uncertainty (±7%)*

7.4 Discussion of Model Analysis

7.4.1 Empirical regression analysis

Application of empirical relationships (Table 7.1) derived for landslide dams (Costa 1985; Costa and Schuster 1988; Walder and O'Connor, 1997) to the physical scale model (PSM) data yielded a wide range of estimates in peak discharge. Of seven equations presented, only Equation 7.1 predicted Q_p for the given dataset within the correct order of magnitude. Total failure was modelled to characterise the observed final breach configuration as well as to represent the low dam:lake volume ratio.

Application of Equation 7.1 to the both carapace and non carapace dam types under variable conditions of saturation produced mean values are in the range 12173–26472 m^3/s for non carapace dams and 15652-22994 m^3/s for carapace dams. The higher accuracy in the prediction of Q_p for carapace dams is expected given the dataset Equation 7.1 was derived from.

A single empirical regression relationship was used to describe the known values of Q_p from the extremely rapid failure condition observed in the PSM (representative of the worst case scenario). Other studies including Manville (2001) and Hancox *et al.,* (2005) have also used single regression equations in

retrospective analysis of the Poerua event. While such an approach has been used to assess the inherent uncertainty associated with such equations, the use of empirical methods as predictive tools for first order magnitude forecasting must consider the worst case scenario of extremely rapid failure.

Use of multiple empirical relationships derived from landslide dam data sets may help constrain estimates of peak discharge to an upper and lower limit. Using the mean value from empirical methods presented by Manville (2001), the accuracy of peak discharge prediction falls within ±60%.

The use of empirical relationships linking dam geometry and lake volume to breach development time for constructed dam types reveals a broad range of estimates, when applied to the PSM data (Table 7.2). The empirical relationships developed by Von Thun and Gillette (1990) and Froehlich (1987) estimate t_b for carapace dams extremely accurately, but appear to be unsuitable for estimation in non carapace dams. Application of Froehlich (1987) to the PSM data produced mean values in the range of 0.49 hours in carapace dams (Table 7.6). Mean values in a similar range (0.42-0.51 hours) were found using Von Thun & Gillette (1990) for highly erosive conditions. Unlike Von Thun and Gillette (1990) which uses B and H_w to estimate t_b, Froehlich (1987) is considered more appropriate because it incorporates input parameters which can be assessed prior to failure for the landslide dam, such as H and V.

Breach top width (Table 7.7) and base width (Table 7.8) were calculated using the empirical relationship for average breach width for constructed dam types after Froehlich (1987) for two separate sidewall conditions, relative to the friction angle of the controlling material present. In non carapace dams, W_T was accurately estimated using a trapezoid with high angle sidewalls, generating mean values in the range 264-356m. As outlined in Table 7.8, W_B is approximately constrained using Froehlich (1987) indicating that the angle that the breach wall makes with the breach bed should be modelled as steeper than the angle of repose.

Empirical relationships for the estimation of average breach width for constructed dam types produced results in agreement with the PSM data (Table 7.9). The USBR equation estimated average breach width with less uncertainty for non carapace dams producing mean values for B in the range 155-198m.

Empirical relationships defining the dimensional limits to average breach width were also considered for the PSM dataset (Table 7.9). Comparison of three documented relationships revealed Johnson and Illes' (1976) limits to average breach width are most applicable to the landslide dam breach geometry observed for the PSM dataset.

Empirical relationships, while useful for approximation of both breach outflow and resultant geometry, provide no information about downstream conditions, particularly in relation to the effects of bulking, sediment entrainment and attenuation.

7.4.2 Dimensional

Walder and O'Connor (1997) indicate that peak discharge is primarily a function of the lake volume and breach erosion rate, so that only three parameters; breach depth (d_B),volume released (V_o) and rate of vertical breach erosion (k) are required to predict the full outflow hydrograph. Breach development times of 0.25 - 0.66 hours generated peak breach discharges of 6031- 64921m^3/s for carapace dams and 0 - 103649m^3/s for non carapace dams (Table 7.4). Figure 7.1 displays the plot of dimensionless peak discharge against dimensionless volume drained, incorporating the PSM data into the dataset used by Walder and O'Connor (1997).

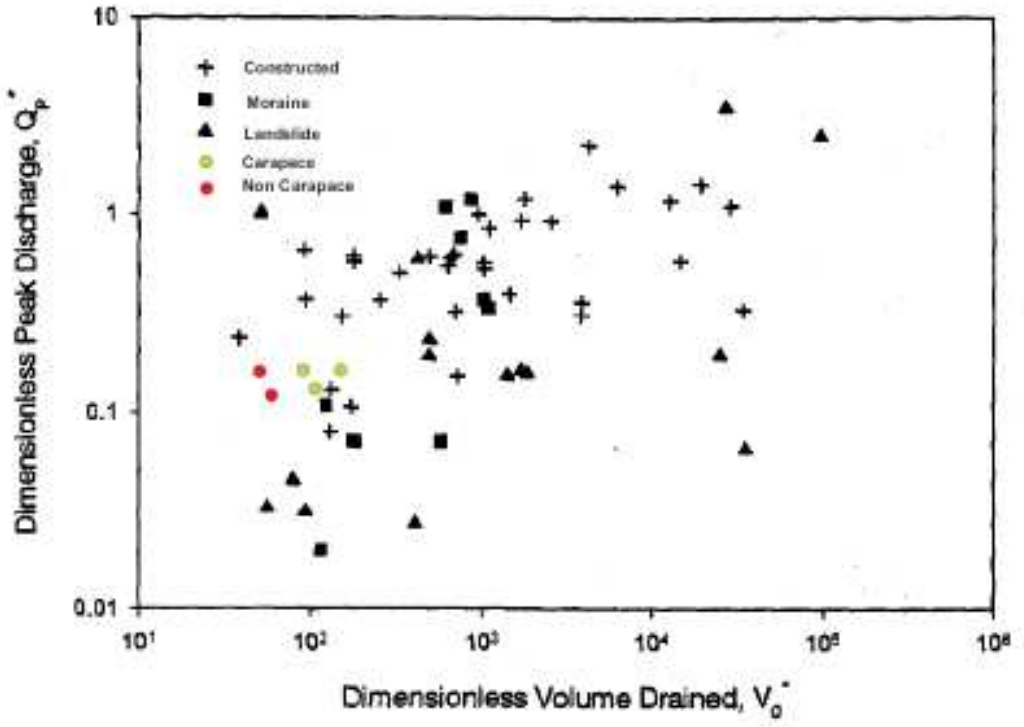

Figure 7.1. Plot of Dimensionless Peak Discharge and Drained Volume including PSM data (Walder and O'Connor, 1997).

The large excess lake volume used in the PSM made the peak discharge sensitive to breach geometry, particularly the ratio of breach width to breach depth. Dimensional modelling of the PSM dataset overestimated Q_p in carapace and non carapace dams by 80% (excluding lab error), making it unreliable as a predictive tool to assess Q_p for rock avalanche dams. Dimensional analysis did however correctly

predict the disparity between erosion rates for carapace and non carapace dams, due to channel armouring in carapace dams reducing erosion rates by 50%.

7.4.3 Parametric analysis

The parametric approach forecasts dam-break flood hydrographs by modelling the discharge through an evolving breach using standard weir flow equations. These place physical constraints on the rate at which water can pass through a breach of defined geometry and size. The parametric approach is limited by reliance on uncertain input parameters (final configuration breach geometry, and t_b), however realistic values for such parameters can be estimated from analogous case studies. The OUTFLOW3 parametric model was applied to the PSM dataset using a trapezoidal breach with a top width 3.5 times the depth for non carapace dams and 4.5 times the depth for carapace dams (i.e., sidewall slope is equal to friction angle of the body or carapace material c.33° – 45°). The parametric approach was found to underestimate peak breach discharges from carapace dams generating mean values ranging between 9755-21211 m^3/s, but served as the most accurate method for estimation of peak discharge from non carapace dams, producing mean values within the range 20534-41690 m^3/s. Although the parametric approach also has the capacity to estimate t_p, results from application to the PSM dataset (Table 7.6) suggest that such an approach cannot constrain t_p to the required accuracy to justify its use as a predictive tool.

The parametric approach simulates peak discharge from the lake as occurring before t_b and therefore before the breach has reached its maximum dimensions. Termination of breach development prior to peak outflow as modelled using the parametric approach is not consistent with observations made during the PSM study. It does however suggest that the duration of the observed rising limb of a hydrograph (at a downstream site) may under-estimate the actual breach development time for carapace type dams.

7.4.4 BREACH Analysis

Choice of the BREACH model to simulate the PSM dataset was based on its ability to account for heterogeneous dam composition, steep slope sediment transport and non linear breach growth. Simulations using BREACH predicted peak discharge to ± 39% in carapace dams and ± 62% in non carapace dams.

Unlike the empirical relationships presented, BREACH estimates t_b relatively accurately for both dam types. BREACH constrains t_b to 0.27-0.61 hours in carapace dams and 0.31-0.51 hours in non carapace dams, thereby correctly addressing the disparity in breach development rates due to breach armouring in carapace dam types. BREACH estimates may be used as an approximate value for prediction of t_p in non carapace type dams.

Furthermore, BREACH struggles to simulate extremely rapid dam failures (t_p <1 hour) such as those documented for the PSM dataset, given the large reservoir size. The simulation duration for the BREACH model had to be increased from 0.6 hours (as recorded in the PSM) to 3 hours to produce representative results. Increasing the simulation time was not observed to influence Q_p, t_p, or t_b.

Overall, the BREACH analysis of the PSM dataset showed a number of features observed during testing. BREACH correctly simulated the termination of breach development prior to the peak discharge in the SC dam type and the continuation of breach development after peak discharge in DC, DB and SB dam types. BREACH correctly simulated steeper side wall angles in the saturated non carapace dam types.

BREACH estimates of breach geometry were inaccurate and problematic. BREACH frequently underestimated W_T by 43% for all dam types, making the BREACH approach significantly less reliable as a predictive tool than the empirical relationship presented by Froehlich (1987). The error associated with the BREACH estimation of W_B in rock avalanche dams was unacceptable (Table 7.8).

7.5 Critical Assessment of BossBREACH

7.5.1 Introduction

The BREACH code is widely used as a modelling tool, so comparison of the geometric enlargement of the breach between the BREACH model and the PSM dataset is useful for assessing the applicability of BREACH to model breach development in rock avalanche dams.

The BossBREACH model allows consideration of multiple parameters, notably reservoir, geotechnical and outflow channel conditions. Despite the detail of input data, BREACH outputs were found to poorly represent the PSM dataset. As the BREACH output is presented at each specified time step, the disparity between breach geometric development in the BREACH simulation and the PSM study can be examined in detail.

The PSM dataset reflects breach development until the occurrence of peak discharge and therefore does not address evolution to the final breach configuration. The following section presents results from the BREACH simulation of the PSM dataset, presenting the temporal development of the parameters describing breach enlargement; ***outflow discharge, trapezoidal cross sectional area, breach top width and breach depth.*** Breach enlargement rates from the PSM study and BREACH simulation are compared (Figures 7.2-7.5) using the development of the breach channel inlet (C_{max} cross sectional profile) and breach channel outlet (W_m cross sectional profile).

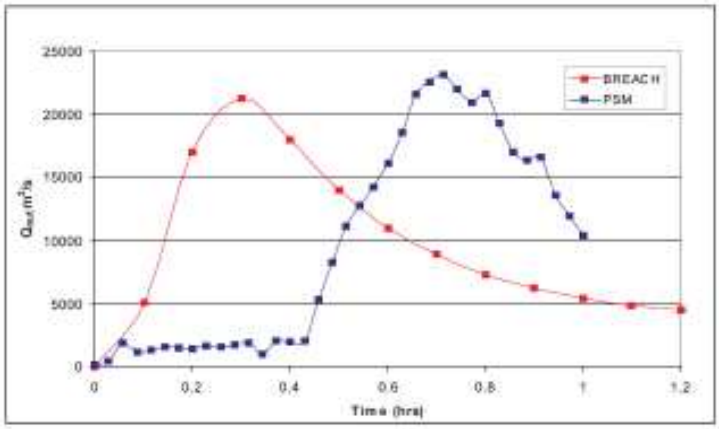

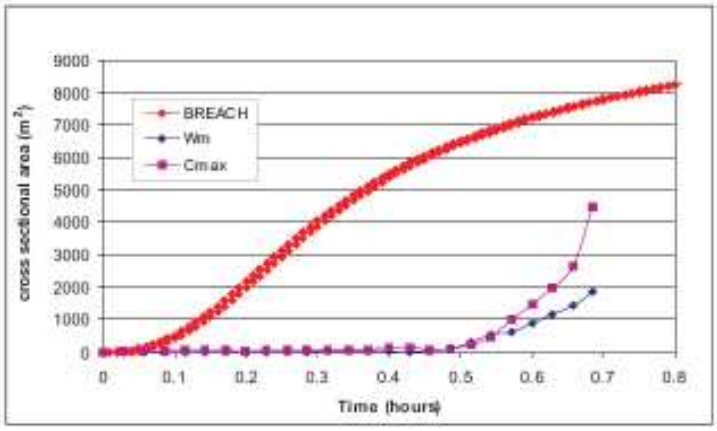

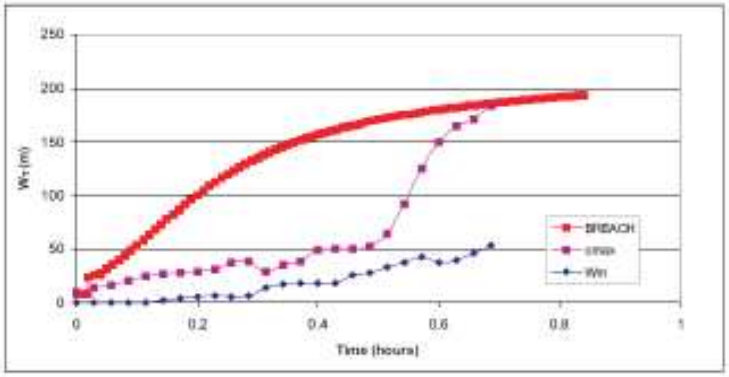

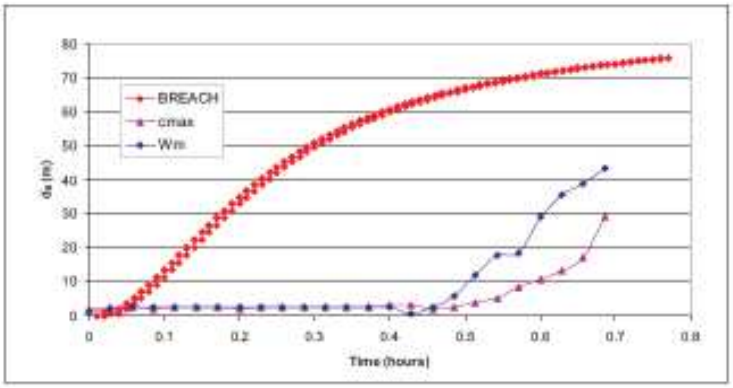

Figure 7.2(a-d) Breach Development in DC type dams

7.5.2 DC Dam types

Comparison of the BREACH and PSM hydrographs in Figure 7.2a clearly indicates that while BREACH accurately simulates Q_p, failure is simulated without consideration of dam crest armouring by the carapace, resulting in significant underestimation of t_p and t_b. Therefore BREACH outflow hydrograph for DC type dams appears to poorly represent the observed physical behaviour in the PSM.

Comparison of PSM data to the BREACH simulation of breach geometry development in DC dams indicates the following;

- BREACH is unable to account for the carapace armouring at the dam crest, providing resistance to erosion, to act as a permeable spillway before a critical discharge initiates raveling, entrainment and detachment at 0.49 hours (Figure 7.2a-b)

- Breach depth and width do not develop uniformly as simulated by BREACH, but rather breach growth initially proceeds through lateral erosion at the breach inlet and vertical erosion at the breach outlet (Figure 7.2c-d).

- BREACH predicts W_T at peak discharge reasonably accurately despite simulating the development at an incorrect rate by not accounting for armouring. (Figure 7.2c).

- The failure of BREACH to simulate the progressive enlargement of B_w is a severe limitation of the model. BREACH overestimates the rate of breach development in the DC model, due to the sudden growth of the B_w from an overflow condition concentrated to 8 m on the downstream face, to erosion on the upstream face and the terminal dimension of 24 m at only 0.02 hours (Figure 7.2b). Comparatively the same B_w dimension occurs at 0.19 hours at the inlet and 0.61 hours at the outlet in the PSM.

- Although BREACH inaccurately simulates the breach development process, for estimations of potential breach geometry at peak outflow BREACH may be considered representative to ±38% (Figure 7.2b).

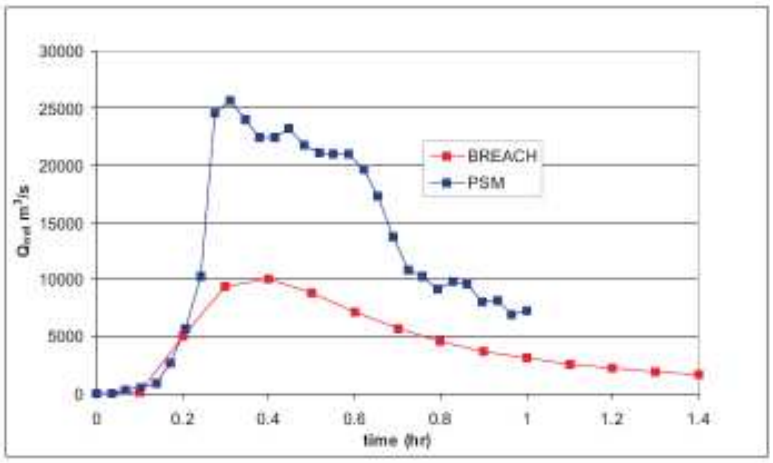

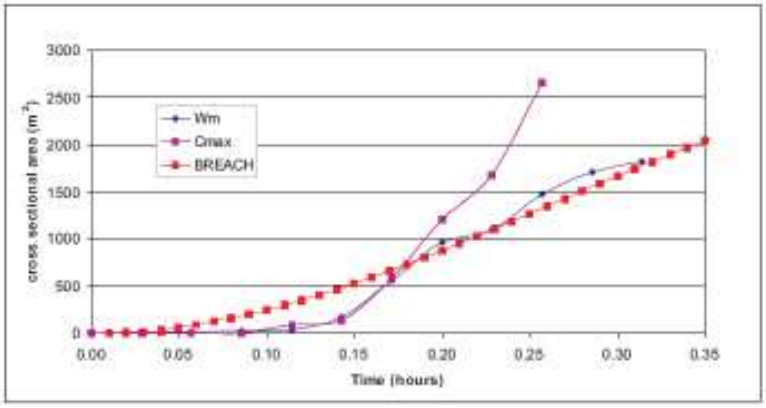

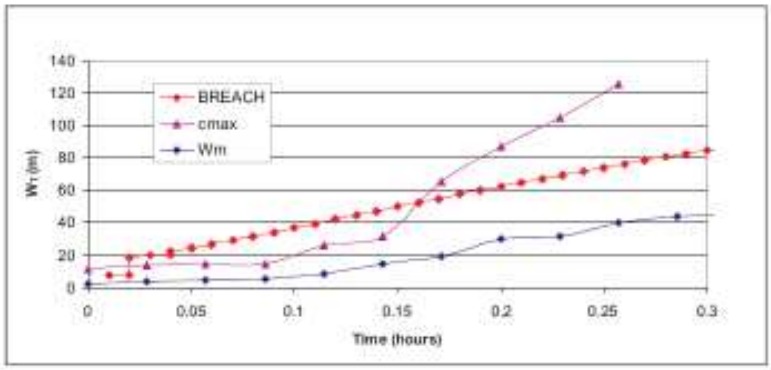

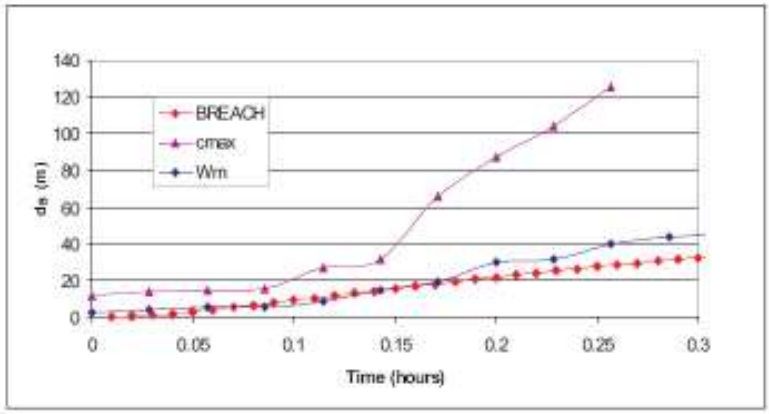

Figure 7.3(a-d) Breach Development in DB type dams

7.5.3 DB Type Dams

Non carapace dams incorporated carapace material in a matrix of fine sediment. Detailed input parameters are outlined in Appendix G. Comparison of the BREACH and PSM hydrographs in Figure 7.3a demonstrates that BREACH significantly underestimates Q_p by 60%, but accurately estimates t_p.

Despite being specifically designed for embankment dams, BREACH performed only moderately in the simulation of overtopping failure in non carapace dams composed of a homogeneous material. Comparison of PSM data with the BREACH simulation of breach development in DB dams indicates the following;

- At the onset of stage 2 erosion, the outlet breach area (W_m profile) develops at the same rate as the BREACH simulation (Figure 7.3b).

- BREACH correctly simulates the depth development in the breach outlet, but models breach width development at approximately 50% the observed rate for the breach outlet after the onset of stage 2 erosion at 0.17 hours (Figure 7.3c-d).

- From Figures 7.3c and 7.3d, BREACH fails to account for the non uniform development of the breach inlet, which evolves displaying characteristics of the two initial erosion stages; breach formation (0.08-0.15 hours) and breach enlargement (0.16-0.25 hours).

- BREACH significantly underestimates the depth development (vertical erosion) at the breach outlet after the onset of stage 2 erosion at 0.14 hours (Figure 7.3d).

- BREACH predicts breach width and depth development at peak discharge reasonably accurately for the outlet position of non carapace dams, but fails to simulate the non uniform development of the inlet position (Figure 7.3c-d).

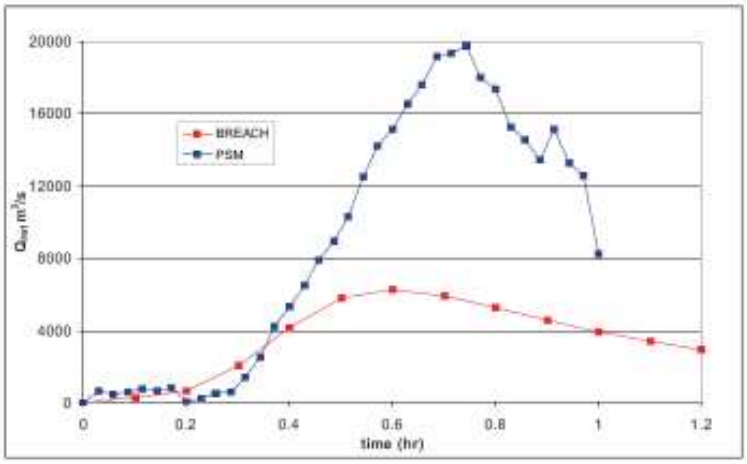

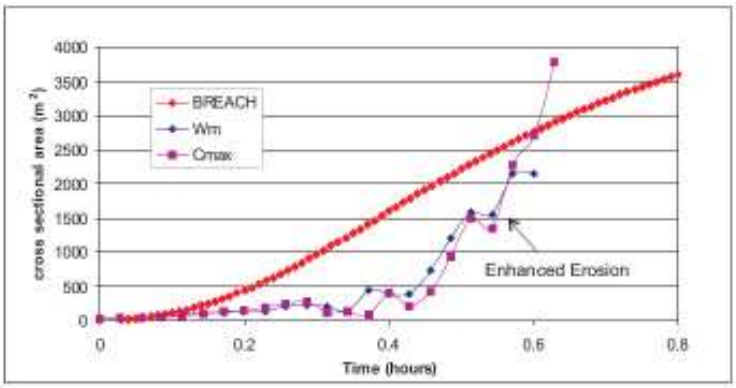

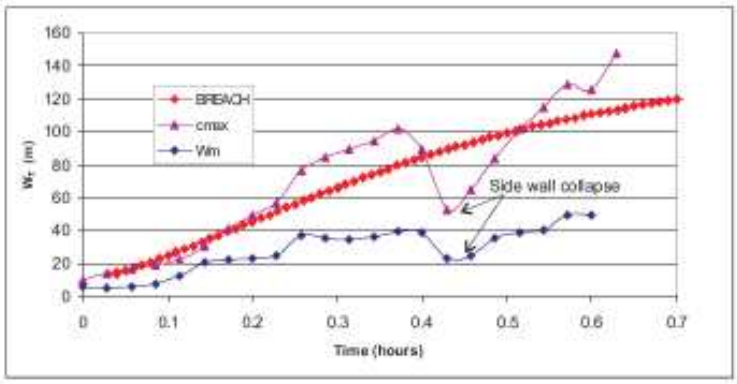

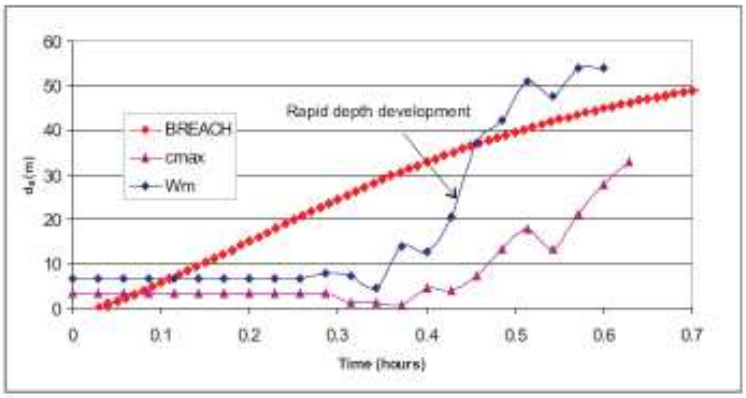

Figure 7.4(a-d) Breach Development in SC type dams

7.5.4 SC Type Dams

Carapace dams constructed with saturated materials were modelled in BREACH through reduction of the material porosity input value to 75% of that used for dry materials. Comparison of the BREACH and PSM hydrographs in Figure 7.4b indicates that BREACH approximates t_p, but significantly underestimates Q_p. This result contrasts with the behaviour of BREACH in the simulation of non saturated carapace dams.

Comparison of PSM data to the BREACH simulation of breach development in SC dams indicates the following;

- The BREACH simulation of breach trapezoidal area development for the PSM data indicates that BREACH correctly estimates breach area, inlet width and outlet depth at peak discharge, despite failing to simulate armouring, as observed in the DC dam types (Figure 7.4b).

- As identified in DC type dams, BREACH inaccurately models B_w in SC dams as a static dimension throughout breach enlargement (Figure 7.4b).

- Significant side wall collapses, which enhance lateral development of the breach at the inlet (visible at 0.43 hours in Figure 7.4c) also contribute to the onset of rapid vertical erosion at the outlet (Figure 7.4b).

- Although BREACH fails to simulate the armouring of the carapace, for estimations of potential breach geometry at peak outflow BREACH may be considered representative to ±54%.

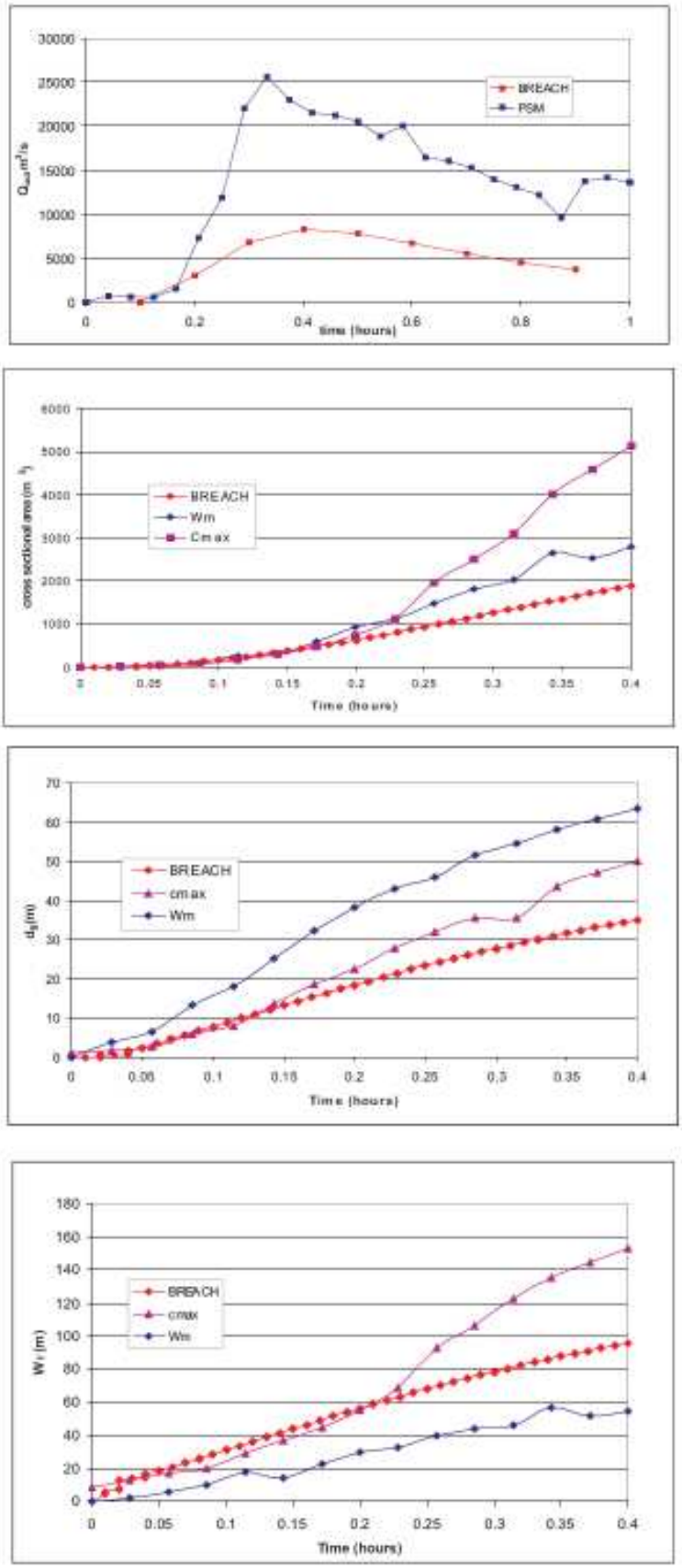

Figure 7.5(a-d) Breach Development in SB type dams

7.5.5 SB Type Dams

Non carapace dams used saturated materials in construction, incorporating carapace material in a matrix of fine sediment. Input parameters are outlined in Appendix G. Comparison of the BREACH and PSM hydrographs in Figure 7.5a demonstrates that while BREACH significantly underestimates Q_p by 54%, it approximately matches t_p.

As in the simulation of DB structures, BREACH accurately models the observed breach development rate for the W_m profile, but appears to underestimate the development of the breach width in the C_{max} profile after the onset of stage 2 erosion (0.23 hours). Comparison of PSM data to the BREACH simulation of breach development in SB dams indicates the following;

- BREACH simulation of saturated materials reduces the resultant breach area by approximately 20%, while enhancing the development of the breach inlet (C_{max}) by approximately 50% and the outlet (W_m) by 13% (Figure 7.5b).

- At the onset of stage 2 erosion (0.2hours), the inlet breach area (C_{max} profile) deviates from the both the outlet development rate and the BREACH simulated rate (Figure 7.5b).

- BREACH underestimates the growth of the breach outlet area by approximately 20% resulting from underestimation of breach width and depth development at the breach outlet by approximately 50% (Figure 7.5c-d).

- Unlike the DB model, the BREACH simulation appears to closely resemble breach development at the inlet and not outlet position, as observed for the carapace models which indicate BREACH simulates breach growth by primarily lateral and not vertical erosion.

- As observed in the DB model, BREACH fails to account for the non uniform development (enhanced lateral erosion) at the breach inlet at the onset of stage 2 erosion at 0.23 hours (Figure 7.5b-c).

- The SB structure was the only trial whereby initial uniformity was observed for breach area development rate in both the physical scale model and BREACH.

7.5.6 Comparative Studies of Model Uncertainty

The breach models used in this study were based upon methods used in the retrospective analysis of the Poerua River event (Hancox *et al.,* 2005), enabling comparison between uncertainty predictions. Modelling of the Poerua breach as a partial failure (representative of the prototype condition) indicated that uncertainty could be up to ±60% of the predicted peak discharge. Uncertainty quoted for the BREACH model was in agreement with the PSM value, while uncertainty for other models was within ±20% of PSM values. As observed in the PSM study, empirical estimates recorded the lowest uncertainty, while dimensional methods, despite their derivation from natural dam studies, recorded the highest uncertainty. Therefore uncertainty estimates for the PSM study can be considered both representative and appropriate.

7.5.7 BREACH Applications

BREACH analyses of catastrophic and gradual landslide dam failures are sparse within literature. The BREACH software package presents two landslide dam case studies as template simulations; the overtopping failure of the Mantaro River landslide, Peru, 1974 and the potential piping failure of Spirit Lake, US, 1982. Manville (2001) applies BREACH to the retrospective analysis of the Poerua River landslide dam failure, New Zealand 1999, in addition to a variety of other dam breach technologies for process verification, including physical scale modelling. Corrado *et al.,* (2006) used BREACH to model landslide dams of homogenous composition and variable boulder content, implementing new components to the software to improve its application to landslide dams. In addition to these studies, work by Almeida *et al.,* (2005) comparing the performance of BREACH against the RoDaB model in the simulation of rockfill dam breaching is also considered important in the verification of BREACH as a suitable tool for breach analysis in rock avalanche dam failures.

7.5.7.1 Mantaro River Landslide Dam

BREACH accurately modelled both Q_p and t_p from the Mantaro failure to within ±5% of observed conditions, with both parameters highly sensitive to cohesion, but insensitive to friction angle (Fread, 1988). Furthermore, BREACH appears to simulate armouring of the dam crest during the Mantaro failure, permitting a stable discharge for 17 hours prior to rapid failure. PSM prototype (scaled) dams were simulated in BREACH using similar geotechnical properties and hydraulic conditions to those used in the Mantaro simulation, however the inability to correctly simulate the influence of armouring may result from the significant disparity between temporal scales and dam geometry. Comparatively, the duration of the Mantaro event was simulated as 200 hours, while PSM protoype events ranged from 0.28-0.66 hours. The low gradient of the Mantaro dam geometry enabled accurate BREACH simulation, without exceeding the $z_u z_d$=1 limitation of the model, as encountered in the PSM prototype dam simulations. The Mantaro dam was modelled using only an outer core, with no consideration of a carapace facies mantling

a finer body material with significant disparity between the geotechnical properties of the modelled materials as simulated for the PSM prototype dams. BREACH also significantly underestimated the Mantaro breach geometry, modelling the breach as pseudo-triangular at peak discharge and in final configuration, with dimensions W_T = 126m B_w = 1.9m, when in reality the Mantaro breach was observed be trapezoidal with W_T = 243 B_w = 30m. This suggests that BREACH may be a representative tool for Q_p and t_p prediction, but not breach geometry.

7.5.7.2 Poerua River Landslide Dam

Hancox *et al.,* (2005) utilised several dam-break technologies, including BREACH, in the retrospective analysis of the Poerua landslide dam. BREACH was documented as the only model to simulate the observed partial breach, producing estimates of Q_p, t_p and t_b which '*did not conflict with the available observations'* (Hancox *et al.,*2005). Physical laboratory modelling of the Poerua landslide dam indicated the occurrence of peak outflow before full breach development and a relatively short time-to-peak. Physical scale modelling of the Poerua event conducted by Donadini and Kunz*,* (2002), tested variable dam geometries, including the geometry used for the current PSM dataset (but with a much smaller lake volume). Comparison of the Poerua (1:150) physical scale model for a landslide dam with geometry of 15us/25ds to the BREACH simulation of the Poerua event, yields similar results to the BREACH simulation of DB and SB dam types in the current PSM study. The Poerua physical scale model was modelled as a homogeneous dam, with different behaviour to that observed for carapace dams, primarily through the rapid onset of erosion without the armouring of the carapace facies.

The disparity between Q_p estimates for the Poerua event using the PSM presented by Davies *et al.,* (2002) and BREACH is evident in Figure 7.6. While Hancox *et al.,*(2005) considers the BREACH model to accurately simulate the observed behaviour of the prototype event, Davies PSM (with similar geometry), over estimates both peak discharge by 32% and time to peak by 38%. This result highlights the individual strengths of both numerical and physical modelling techniques and validates their independent use at specific stages in the analysis. The inability of BREACH to simulate the observed Q_p and t_p to better than ±50% in the current PSM study and ±35% the PSM presented by Davies *et al.,*(2002) indicates BREACH may simulate the breach initiation phase as a tractive-force erosion problem, which conflicts with the erosion mechanics observed in laboratory testing (Wahl, 1998).

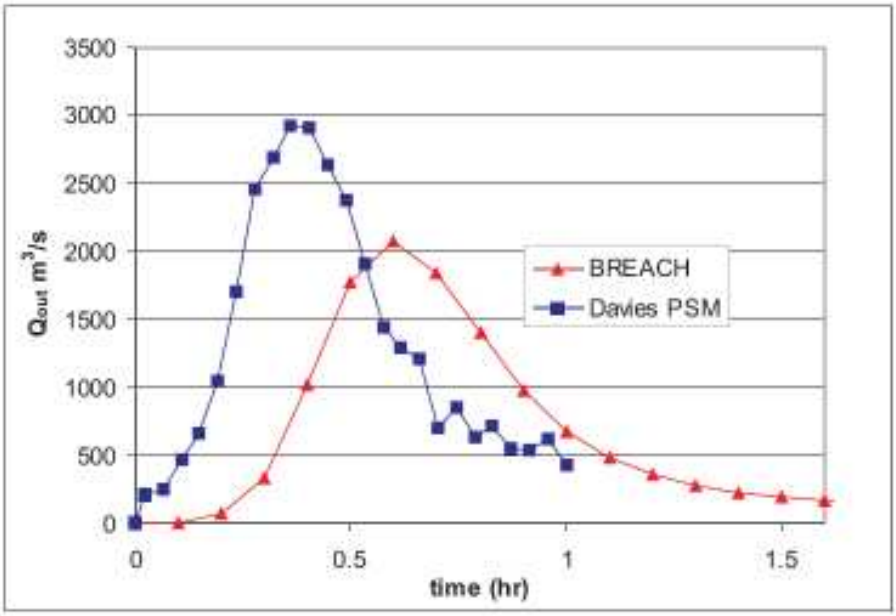

Figure 7.6.Poerua Outflow hydrographs

7.5.6.3 RoDaB Model

RoDaB was developed by Almeida *et al.,*(2005) to address the issue of overtopping failure in rockfill dams with a homogeneous body and an impervious layer on the upstream slope. While such a model cannot be applied to landslide dams, comparison of the BREACH against RoDaB for simulation of overtopping failure of rockfill dams revealed that BREACH generates a time to peak 0.69 hours before the simulated t_p in the RoDaB. The time to peak discharge in an earth dam of similar geometry is about 15% of the time corresponding to the rockfill dam. Furthermore BREACH estimates peak discharge 65% higher than RoDaB for rockfill dam and 15% higher than the BREACH earth dam. Therefore BREACH appears to be restricted in its ability to accurately model the influence of large grain sizes on Q_p.

Almeida *et al.,* (2005) concluded that BREACH significantly underestimates the influence of armouring due to the inadequacy of the Smart sediment transport formula and is therefore more appropriate for the simulation of an earth dam breach.

7.6 Modification of the BREACH model

From retrospective modelling of the Valderchia landslide dam, Italy 1997, Corrado *et al.,*(2006) considered BREACH to inaccurately represent material transport over a poorly sorted landslide deposit given the use of the Smart-Jaeggi bed-load transport formula, derived from flume experiments where $d_{90}/d_{30} < 10$. Corrado *et al.,*(2006) question the use of the Shields stress, to evaluate entrainment thresholds in Smart's revision of the Meyer-Peter-Muller equation (Smart, 1984) claiming accurate

assessment of water depth under turbulent flow conditions to be problematic. Corrado *et al.,*(2006) overcome the requirement for depth assessment by using the Schoklitsch equation (Schoklitsch, 1964) which instead considers discharge per unit width and not depth as a critical parameter. Selection of the Schoklitsch equation is also attributed to its development and testing under field and not laboratory conditions (Corrado *et al.,* 2006).

Corrado *et al.,*(2006) also claim that the use of a single d_{50} for both the inner and outer core in the BREACH model is not representative of a real granulometric class and could result in overestimation of breach erosion and the outflow hydrograph.

Corrado *et al.,*(2006) implemented BREACH with a new procedure that calculates two granulometric curves, one for each mode of the original distribution, and evaluates transport of the landslide material separately. Results of the analysis indicate that the model is very sensitive to the bed-load equation and that the procedure implemented to consider the eventual bimodal distribution of the dam material simulates the armouring phenomenon (frequently observed in carapace dams for this PSM study).

Consideration of material bimodality in the Corrado *et al.,*(2006) modified BREACH model indicates the original BREACH model may overestimate peak outflow by ~60% for a homogeneous dam composed of 10-20% boulders by volume. When the composition of the landslide deposit was simulated to have a boulder content >30% by volume, peak outflow was overestimated by 90% and the breach erosion observed to terminate after the time of peak discharge. The modified model also produces a significantly reduced breach channel depth both at the peak flow and in final configuration; armouring causes erosion at the breach base to cease, due to the increase in relative frequency of the boulders in the breach bed.

The peak discharge values are constant for d_{50} ranging from 0.045 to 15 mm using either the Schoklitsch or the Smart equation Corrado *et al.,*(2006). Entrainment within the breach outflow of clasts with a median diameter of 47-256mm is also constant using either the Schoklitsch or the Smart equations. Corrado *et al.,*(2006) however claim that inflow conditions conducive to breach formation and entrainment of clasts >256 mm in the Schoklitsch or the Smart equations vary by 2 orders of magnitude (i.e. Schoklitsch formula, 15.4 m^3/s compared to Smart formula 3,000 m^3/s). Linear scaling of the critical discharge (presented in section 5.8.2) using $\lambda = 400$ reveals a discharge of 2038 m^3/s is required for entrainment of carapace materials in the prototype condition of the DC dam type. Linear scaling of flow velocities during initial breach enlargement produce values ranging from 0.15 m/s-0.6 m/s. Such values are within a similar range to the critical velocities obtained using formulae developed by Coleman *et al.,* (2002) and Scheuerlein and Hartung (1970).

Rock avalanche deposits as documented by Dunning (2005) are classed as very poorly sorted with a mean grainsize of -2.63 Phi (10mm). Detailed sampling at five rock avalanche deposits by Dunning (2005) revealed the mean absolute range in grain size to lie between -0.82 - 3.69 Phi (1-200mm) and therefore well within the range for clast entrainment simulated by the original BREACH model. Given the scaling ratio of 1:400 used in this PSM study, the required inflow condition for clast entrainment using the Smart equation is also met.

From detailed field investigation of the post formation development of landslide dams in the North-West Nelson region, Nash (2003) reported dam materials with block sizes > 250mm to correspond to relative dam stability. Therefore the BREACH model appears appropriate in its simulation of landslide dam stability when the d_{50} > 250mm (see Figure 6.8). Although individual blocks within the carapace facies have been observed in the field to range from 100 to > 1000mm in size (*Davies pers comm.*), BREACH should be able to accurately simulate breach erosion and development for approximately 85% deposit materials (< 256mm), but may underestimate breach outflow due to the use of tractive-force erosion modelling.

Given the lack of geotechnical data available for sampling during their investigation, Corrado *et al.,* (2006) model the Valderchia landslide as a homogenous deposit with variable boulder composition within a fine matrix. While such a condition may be representative of rock type mass movements with low volumes (< 10^6 m^3) and runout distances or even the body facies as modelled in DB and SB dam types, rock avalanches have a distinctly different morphology with a heterogeneous fabric composed of unique facies with contrasting geotechnical properties (as outlined in section 2.2.6).

The carapace facies, therefore cannot be correctly simulated by the bimodal distribution of the new BREACH procedure assuming a specific boulder content. The writer suggests that this is the main reason for the disparity between BREACH simulations from the PSM study and that presented by Corrado *et al.,*(2006). Furthermore, the modified BREACH model was not available for application to the PSM dataset in this study and therefore its performance relative to the original model cannot be assessed.

The PSM study confirms a number of the physical assumptions made by Corrado *et al.,*(2006). The volume of boulders (within the carapace) and the spatial distribution significantly influence peak discharge by selective erosion of fine particles leading to the creation of an armour on the breach bed, which does not permit the incision of the breach. This leads to the formation of a smaller breach section area and to a consequent smaller peak outflow.

The PSM study (incorporating carapace and non carapace dams) also confirms that the increase in percentage of boulders determines (at the time of peak discharge) a substantial decrease in the section area and a decrease in the breach depth.

7.7 Limitations of the BREACH model

Physically-based numerical models such as BREACH offer the potential to provide more detailed information regarding breach dynamics but are recognised as having limited accuracy. Several deficiencies have recently been identified in critical reviews of the model by Manville (2001) and Mohamed *et al.*,(2005). The implications for practical application are that flood hazard areas identified by hydrodynamic modelling of the dam breach wave may have large error margins particularly in proximal downstream regions where risk to life is greatest.

As presented in the preceding sections, the BREACH model has been applied to a variety of dam breach case studies for both natural and artificial dams proving to have variable accuracy as a predictive tool. From BREACH analysis of the PSM dataset, limitations were observed in the model's ability to accurately simulate overtopping failure, regardless of dam composition (homogeneous or heterogeneous) or type of emplacement (constructed or natural). The following principal limitations are identified for the model.

1. Inability to simulate armouring induced by carapace material despite sensitivity analysis indicating that dam stability occurs when d_{50} exceeds 250mm

2. Incorrectly simulates the rate of breach enlargement for the outer core condition modelled with the geotechnical properties of a carapace.

3. The model requires unrealistic inflow conditions for the entrainment of carapace material with a median diameter of >250mm.

4. The model was found to be particularly sensitive to the dam geometry, requiring slope angles to be restricted to $z > 5$ to maintain numerical stability(Manville, 2001) Dams with high angle slopes ($z < 5$) are simulated to be stable, while reducing the slope ($z > 5$) was found to trigger failure. Such conditions are obviously contrary to reality. The use of high Z_u/Z_d values also produces unrealistic estimates of Q_p (Figure 7.7)

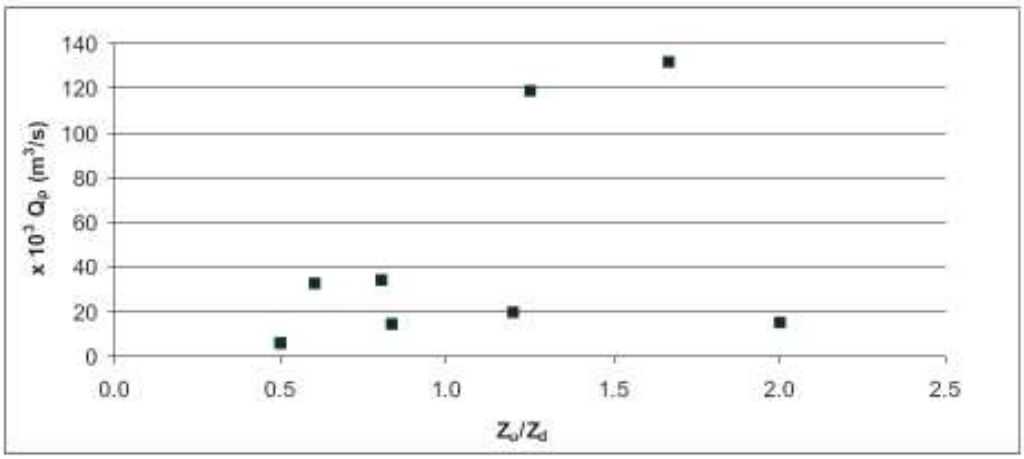

Figure 7.7. Q_p sensitivity to variation in Z_u/Z_d angle

5. BREACH inaccurately models B_w in carapace dams as a static dimension throughout breach enlargement

6. Manville (2001) further identified that when simulating low dams impounding relatively large lakes, breach growth (both lateral and vertical) is terminated upon reaching the dam base, while the discharge increases. This restricts the model's ability to accurately evaluate breach dimensions at Q_p.

7. d_{50} is the only granulometric parameter used by the base model to calculate the breach erosion.

Further criticism of BREACH relates to its reliance on sediment transport relations that are untested in the regime of flow conditions applicable to a dam breach. Both Almeida *et al.,* (2005) and Corrado *et al.,* (2006) consider the use of the Smart bed-load transport equation, (which may not be appropriate for all stages of the breach process) to limit the application of BREACH to large unsorted sediments typical of those observed in rock avalanche deposits.

The use of the Smart bed-load transport equation is therefore only valid if used specific to the conditions from which it was derived (ie. $d_{90}/d_{30} < 10$). Comparatively the d_{90}/d_{30} values used in the BREACH simulation of PSM prototype dams ranged from 100-1000, which may have contributed to the significant underestimation of peak discharge in most dam types. Graf and Altinakar (1998) claim 28.6 mm to be the maximum grain size diameter for which the original Meyer-Peter-Muller formula was established.

The reliance of BREACH on tractive force erosion is also not consistent with the mechanics of the breaching process as observed in several laboratory and field studies (Wahl, 1998). While tractive stresses on the downstream face are very high, and changes in slope or surface discontinuities can concentrate

stresses and initiate erosion, analyses based on such mechanics apply only until initiation of erosion after which surface discontinuities and observed headcutting behaviour make tractive stress analyses questionable (Wahl, 1998). BREACH is also criticised by Hahn *et al.,* (2000) for its inability to correctly model headcut-type erosion processes in cohesive embankments.

Overall, however, the BREACH analysis of the PSM dataset, predicted a number of physical features observed during testing. BREACH correctly simulated the termination of breach development prior to the peak discharge in the SC dam type and the continuation of breach development after peak discharge in DC, DB and SB dam types. BREACH correctly simulated steeper side wall angles in the saturated non carapace dam types.

Although the BREACH model is data intensive with an overall error margin of ±50%, the detail provided in the output file enables consideration of all principal breach parameters and physical characteristics associated with failure. The assumption of linear breach development, though shown to be incorrect by the PSM, still adequately represents the breach process without causing consistent error in predictions. The modified BREACH model developed by Corrado *et al.,* (2006) may however be more applicable to modelling breach development in rock avalanche dams and therefore should be the focus of future research.

7.8 Physical Scale Modelling as a Predictive Tool

The use of a PSM also allowed observation of several features unaccounted for by the empirical and computer based models, including dam crest and breach channel armouring, the slumping failure mechanism, the formation of a debris fan at the toe of the breach outlet and the disparity between breach development at the inlet and the outlet. The PSM also indicated that downstream geomorphic features were produced by outflow conditions during the final stages of breach erosion and cannot be used to infer probable breach development rates or failure mechanisms.

Application of PSM phenomena to prototype observations assists in understanding the accuracy associated with the use of this modelling technique. The role of carapace armouring in prolonging time to failure was identified as a key characteristic distinguishing between carapace and non carapace (homogeneous) dams. The results of the PSM study appear to contrast those of Dunning (2004) who used SLOPE/W and SEEP/W Geoslope™ software to model the influence of the carapace facies on time to dam failure (outlined in Section 2.4). Dunning *et al.,* (2005a) reported time to failure in homogeneous dams to be 88% greater than carapace dams for the same geometry under normal inflow conditions. Results from the PSM however indicated that the time to failure in carapace dams was 57% greater than

homogeneous dams for the same geometry and inflow, probably due to armouring. The value of physical scale modelling to verify computer simulation is therefore realised in this study.

Preliminary breach trials conducted prior to the PSM study found that non carapace dams would fail under a condition of zero inflow, whereas carapace dams require a minimum inflow of 1 litre/second. This suggests that the failure mechanism for both dam types is also different, however only the failure of carapace dams was investigated in this study.

Reported carapace armouring for prototype conditions are in agreement with PSM behaviour. Both the Poerua (1999) and La Josefina (1993) landslide lakes were reported to overtop their respective barriers approximately 6 days before breach failure was initiated (Hancox *et al.,* 2005; Plaza-Nieto, 1990). Both landslide dams were observed to contain coarse material up to 1-2 m diameter at the dam crest, representative of a carapace facies. Therefore the armouring properties and resistance to erosion offered by the carapace as observed in the PSM are qualitatively comparable to the short term stability observed in prototype scenarios under semi-static inflow conditions. Under such conditions the carapace may act as a permeable spillway, maintaining inflow and outflow in equilibrium, before a critical discharge induces instability on the downstream face. Equilibrium behaviour was documented for the Tsatichhu landslide dam failure in Bhutan (2004), with seepage outflow ranging between 0.53 - 5 $m^3 s^{-1}$ to reduce the lake level at dam crest by 3m (Dunning *et al.,*2005).

Consideration of armouring as a characteristic of prototype scale failures requires verification using a wider dataset. The New Zealand landslide dam dataset plot for volume against time to failure (Figure 7.8) reveals a population of landslide dams which display stability for a period ranging from 1-100 days (marked band). While it must be emphasised that this dataset includes landslide dams derived from a broad spectrum of mass movements, rock avalanches and rockslide/fall derived landslide dams make up approximately 50% of the data. Furthermore, Korup (2004) reported 38% dams to be derived from an unknown blockage mechanism. Therefore, the high concentration of dams (volume > $10^6 m^3$) with a time to failure between 10-100 days may be indicative of armouring related stability for impoundments incorporating large grainsizes comparable to a carapace facies.

As documented for both the Poerua and Tsatichhu landslide dam failures (Hancox *et al.,* 1999; Dunning *et al.,* 2005), a critical change in conditions caused by rainfall was required to initiate failure. Reported observations of actual failure at a prototype scale are sparse in literature due to the tendency for such events to occurr during conditions of poor visibility. Observations of the failure of the Tsatichhu landslide dam, incorporating dam-face saturation, progressive seepage and slumping (Dunning *et al.,*2005) are consistent with failure mechanisms observed in the PSM.

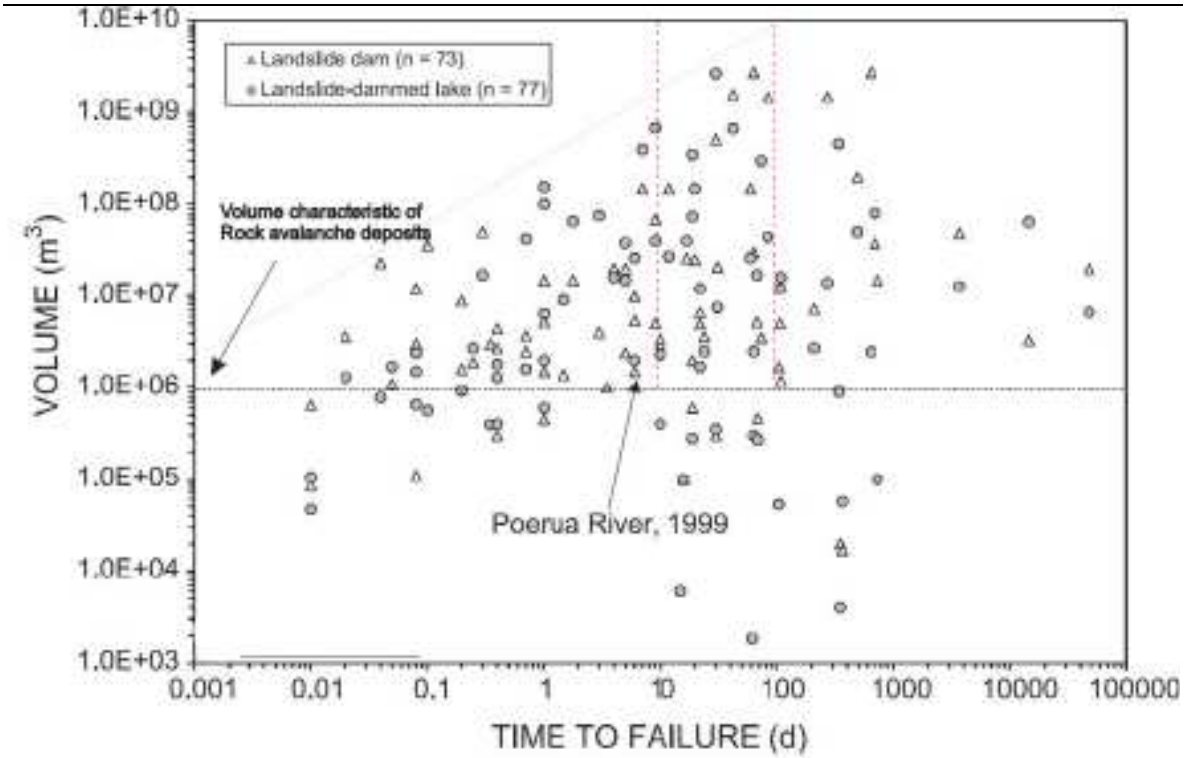

Figure 7.8. Identification of the armouring phenomena at a prototype scale using the New Zealand landslide dam dataset. The marked band represents a population of landslide dams with volumes > $10^6 m^3$ for which time to failure ranges between 10- 100 days. (Source Korup, 2004)

Chapter 8 Hazard Management

8.1 Introduction

The formation and failure of rock avalanche dams are common geomorphic processes in mountain regions throughout the world, causing a series of geomorphic hazards such as catastrophic outburst floods, debris flows, backwater ponding, up-and downstream aggradation, and channel instability. The hazard posed by such failures is often much greater than that posed by the initial landslide event.

While outburst floods or debris flows following rapid landslide dam failure are usually the focus of hazard management, the 1999 Poerua event demonstrated the profound geomorphic and social impact of sustained post-flood downstream aggradation of landslide-derived sediment. Therefore management of the hazard must also consider the longer term geomorphic impact such failures have for an extensive distance downstream of the dam breach.

The use of a physical scale model in this study, to quantify the influence of representative rock avalanche sedimentology on the prediction of critical breach parameters, provides new insights into rapid response management of landslide dam hazards, primarily through;

1. Identification of physical features and specific conditions which may be used as indicators of potential dam stability/instability and outburst flood magnitude.

2. Identification of contemporary dam breach modelling technologies which can be applied to rock avalanche dams for the accurate assessment of the outburst flood hazard.

8.2 Future Hazard Management

Risk management is decision making based on available data and precedent. The 1999 Poerua River event was a timely example of the hazard posed by landslide dams, providing evidence of the spatial and temporal nature of the associated geomorphic impacts from outburst flooding.

Management of landslide dam hazards requires identification of catchments prone to landslide damming, primarily through geomorphic investigation. The response time for the implementation of effective management will depend on the availability of the following;

- precipitation and lake level data
- dambreak modelling data for various scenarios in the affected catchment; peak discharge, breach development time, inundation plans etc.
- information on potential inundation, land use, centres of population, infrastructure etc. (GIS/DEM)
- geomorphic maps
- response plans; evacuation routes

Identification of catchments susceptible to dam-break flooding will enable effective management to reduce the hazard of future landslide dams. While the annual probability of a landslide dam-break flood in an identified catchment is usually very small ($< 10^{-2}$), the risk to inhabited areas proximal to the exit of the downstream gorge is significantly greater than to inhabited areas further downstream due to short response time and minimal attenuation of the flood wave. Appropriate response planning requires integration of all emergency services. Increased public awareness through education and distribution of appropriate information to the public will also enable more efficient response to hazard warnings.

8.3 Flood Impact on Structures and Infrastructure

The economic impact of outburst flooding will be a function of (a) peak outflow discharge/ downstream attenuation and (b) the type of infrastructure located in the downstream valley (i.e. high value structures such as dams, or lifeline infrastructure such as transport, water supply, communication and electrical facilities). While peak discharge is a useful measure of outburst flood magnitude, it leaves the spatial and temporal range of geomorphic impact unspecified. Furthermore, at a critical distance downstream the flood wave peak discharge becomes independent of the magnitude of the discharge at the dam site.

As at Poerua the long term downstream impact of channel avulsion and aggradation may also be greater than that of the initial flood. The geomorphic response depends on the size and nature of the dam, and the size of the river and its ability to breach the dam and redistribute the debris downstream (Korup, 2002).

8.4 Rapid Response Hazard Management

8.4.1 Importance of Rapid Response Hazard Management

Scenario based hazard assessments are beneficial for development of emergency response plans, but the complexity of such geomorphic phenomena (i.e. the Mt Adams landslide had no triggering mechanism) and their consequential impacts are difficult to assess prior to occurrence. Furthermore, given the scarcity of both historic and quantitative geomorphic data for a specific region, such hazards may also occur outside those catchments identified as “at risk”.

Formation of a large landslide dam near a gorge exit presents the greatest risk to downstream populations given the limited response time available before the arrival of the flood wave. A landslide dam could form and fail in only a few hours, before local authorities became aware of the hazard. Rapid hazard assessment and response primarily require quantification of the potential magnitude of the outburst flood. The critical breach parameter, peak discharge (Q_p) provides the best indicator of magnitude (Hancox *et al.,* 2005). From estimation of Q_p, t_p may be calculated using flood routing methods to define the critical response time (arrival of the downstream flood wave), which will also be a function of proceeding meteorologic and/or seismic conditions. Threatening meteorologic and/or seismic conditions will also affect the surveillance of the dam condition prior to failure. Investigation and analysis should be focused toward consideration of a worst case scenario (rapid failure) and mitigation of potential impacts which will extend for a significant distance both up and downstream of the point of blockage.

Aerial observation (of the upstream catchment, landslide scarp, landslide dam and resultant lake) is imperative to obtain a full understanding of the hazard and collect key parametric data. It also allows identification of variables which may compound to the existing hazard potential, such as multiple upstream blockages or activation of further slips on the existing scarp.

Use of a high inflow condition in the PSM (comparable to cascading collapse of multiple dams upstream at the prototype scale) indicated that in such a scenario peak discharge at the subject dam would be 35-50% higher than that observed from single failure. Due to the overwhelming inflow, the carapace would offer no resistance to failure (armouring) reducing the time to peak outflow by 60%. Future slope failures into the dammed lake might generate displacement waves, which could induce overtopping failure of the dam.

8.4.1.1 Critical Indicators identified through the PSM

The PSM study suggests that rock avalanche dam stability will depend on (a) the geotechnical characteristics of the carapace and (b) the critical lake level on the upstream face (affected by inflow rate) at which seepage flow becomes concentrated at the interface between the carapace and body facies. Inspection of the downstream toe to monitor springs or seepage induced erosion is a critical indicator of dam *stability* under constant low or reducing lake inflow, and *instability* if inflow is likely to increase. The observation of tension cracks, headscarp development, slumping or headward migration of seepage on the downstream face are indicators of imminent failure (they will cause rotation of the downstream face, to lower the breach inlet below the reservoir level). Appearance of such features should imply immediate evacuation of the downstream areas at risk of inundation.

8.4.2 Primary Response

In order to rapidly estimate peak discharge to within ±30% of real values, the writer recommends the use of empirical analysis as a first order assessment for the worst case scenario. The empirical method is extremely efficient due to the reliance of most regressional relationships on parameters such as dam height and lake volume that are easily obtained from aerial and indirect observation (DEM methods). Furthermore, as outlined in section 7.4, empirical relationships verified against the PSM dataset (indicative of realistic sedimentology) were able to estimate Q_p to ±19%, t_b to ±17% and W_T to ±24%. Given the accuracy of the empirical prediction of Q_p as the principal parameter from which event magnitude can be assessed, this approach is considered the *primary response*. Such an approach is especially relevant to conditions conducive to rapid failure, but should always be utilised despite forecasting of conditions associated with minimal perceived risk as outlined in Figure 8.1. With provision of the probable event magnitude through the empirical method, downstream routing of the outburst flood enables indication as to the likely response time for required action.

Previous studies (e.g. Manville, 2001) have emphasised a consensus approach for the estimation of the potential flood magnitude, using parametric, dimensional and physical methods for refinement of initial regression analysis predictions. Results from this study indicate that the higher uncertainties associated with dimensional, parametric and physical predictions limit their ability to refine and increase the precision of empirical peak discharge estimates.

While parametric and physical models may not be applicable to rapid first order assessment of potential magnitude, they produce an outflow hydrograph which can be used for downstream routing of the outburst flood, to provide a more accurate determination of more distal hazards. Physical models such as BREACH can provide useful information on sediment bulking and entrainment potential in the downstream channel. BREACH also was found to accurately predict physical features associated with the dam failure, including partial breach and maximum breach development prior to peak outflow.

Due to the requirement for extensive data collection and operator familiarity, increasing processing time, parametric and physical models are a *secondary response* which may be used to qualify specific temporal and spatial characteristics of the outburst flood on the downstream valley. The secondary response is not however an alternative approach to the primary response, but rather a complementary analysis which relates specific impacts (both social and geomorphic) to a predicted magnitude.

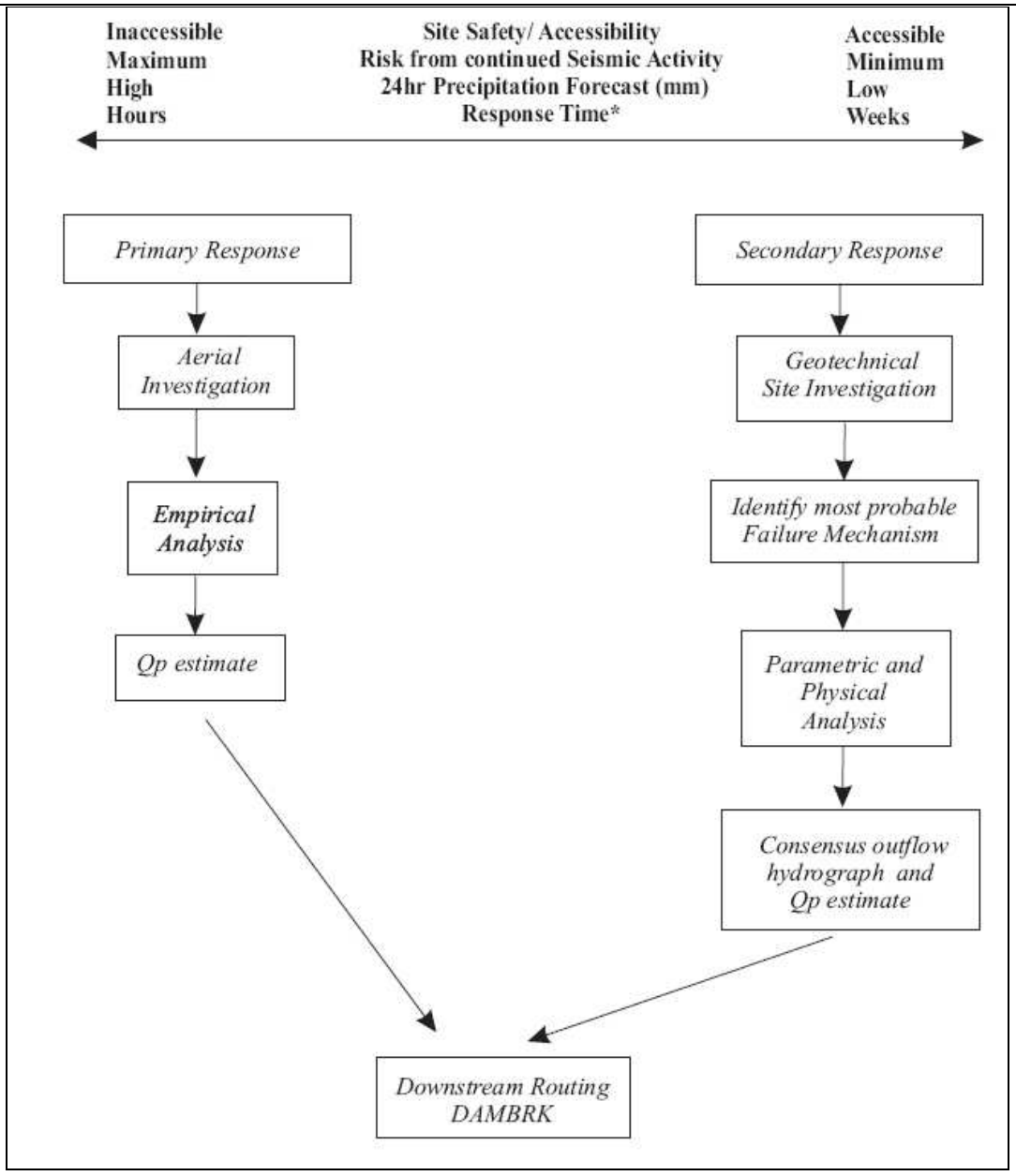

Figure 8.1. Recommended Rapid Response methodology after the identification of a Landslide dam

**Response time is generated from the primary response empirical analysis for first order assessment of magnitude. It is presented as a clarifying condition under which further use of the secondary response system might be considered feasible.*

8.4.3 Secondary Response

Where seismic and meteorlogic conditions are conducive to conducting a site investigation, a detailed assessment of geotechnical parameters should be undertaken. Specification as to the exact parametric data required for the use of secondary response models is presented in detail in Section 2.3.7. A brief summary of the principal data required from site investigation is presented below.

8.4.3.1 Data Collection

Lake Inflow

The rate of inflow into the impounded lake enables constraint to be placed on dam stability in the estimation of lake infill time (or time to overtopping). Rapid changes in lake level are critical to both dam and valley wall stability. Installation of monitoring equipment such as a radio-linked water-level recorder, will allow remote assessment of critical lake conditions to provide sufficient alert to the affected population and precise inflow inputs in secondary response models.

Carapace

The size of the material occupying the dam crest and downstream face will provide some indication as to the potential resistance to overtopping offered by the carapace (armouring) or its ability to transmit flow and act as a permeable spillway. Investigation as to the assemblage of the deposit and whether the carapace is clast or matrix supported will significantly influence estimations of potential dam stability. The PSM study provided clear indication that rock avalanche dams, despite having a very different sedimentology, produce a peak discharge comparable to that observed for failure of homogeneous dams .

Sediment Transport

Consideration of the landslide dam volume will indicate the potential debris requiring delivery downstream, and may be used to forecast geomorphic impact. Estimation of dam volume may also assist in modelling the dambreak flood as a hyperconcentrated or debris flow. Evidence from the Poerua event suggests that the initial flood wave may be laden with vegetative debris, increasing the destructive potential of the flow.

Attenuation

Assessment of the downstream channel and valley characteristics will enable estimation of the likely downstream attenuation and bulking of the flood. If the downstream channel is steep, a significant increase in the peak discharge may occur without attenuation if a large volume of sediment is eroded and transported as bed load by the outburst flood. Significant sediment debulking due to attenuation of the floodwave on the alluvial fan will also cause the mouth of the gorge to become a locus for geomorphic impacts.

Failure Mechanism

Investigation of the potential failure mechanism (if not apparent), should consider the potential for overtopping from a landslide induced displacement wave or cascade collapse from multiple dam failures

upstream. Identification of bedrock abutments which may act as natural spillways and lead to instability of the downstream toe, due to flow concentration effects is also paramount.

Breach Characteristic

The PSM study indicates that the maximum breach cross sectional area will occur shortly after the time of peak discharge through the breach and be trapezoidal in form with sidewall angles slightly higher than the angle of repose for carapace material.

Consideration of all parameters listed above is required to simulate representative failure conditions in both parametric and physical models.

8.4.3.2 Secondary Response Models

The parametric model (OUTFLOW3) was verified against the PSM dataset providing estimates of Q_p to ±37% and tp to ±53% for carapace dams. Use of the parametric model will enable sensitivity analysis of the peak discharge to breach development time and breach dimensions to help quantify the rate of breach development (Manville, 2001).

The physical model (BossBREACH) was verified against the PSM dataset (indicative of realistic sedimentology) but could only estimate Q_p to ±50%, tb to ±27%, W_T to ±43% and tp to ±32% for carapace dams. The assumption of linear breach development in BREACH, though shown to be incorrect from direct comparison to the PSM rates, *may* be applicable to model breach development in materials with a $d_{50} < 250$mm. The writer however recommends the use of a modified BREACH model (Corrado *et al.,*2006) to specifically model the armouring influence of a carapace under low inflow conditions.

8.4.4 Model Outputs

The results of the primary and secondary (if required) response systems may then be presented (in the context of their limitations) along with field inspection evidence (if applicable) to allow the authorities to decide on appropriate action. The first order magnitude assessment used in the primary response may be coupled with the secondary response to identify potential downstream impacts and social/economic vulnerability. The appropriate action will depend on the response time available for either relocation of the downstream population or physical modification to the dam to reduce the risk of catastrophic failure.

The value of conducting scenario based hazard analyses is evident in the immediate need for specific information from which hazard management decisions can be made. Inundation simulation and mapping to identify zones of highest susceptibility will assist in effective planning for evacuation of affected populations and future residential development.

Chapter 9 Summary and Conclusions

9.1 Basis for Investigation

The formation and failure of landslide dams are common geomorphic processes in mountain regions throughout the world, generating a series of indirect hazards such as catastrophic outburst floods, debris flows, backwater ponding, up- and downstream aggradation, and channel instability. River blockages formed by rock avalanches often pose a higher hazard potential than other landslide dams, given the extreme runout distances and volumes of rock avalanche deposits. Recent research has identified rock avalanche deposits to have a unique internal sedimentology consisting of a surficial, coarse material (carapace) and a fragmented interior (body). As such dams are reported to fail rapidly by overtopping; the influence of the carapace material at the dam crest was proposed to be of critical importance to rock-avalanche dam stability, potential breach development and the resultant peak discharge of the outburst flood.

9.2 Experimental Study

Physical scale modelling of overtopping failure and breach development in rock avalanche dams under variable inflow was used to quantify the influence of representative sedimentology on critical breach parameters and their prediction using existing embankment dam breach technologies.

9.3 Critical Breach Parameters

9.3.1 Peak Discharge

Results from the PSM indicated that the carapace has minimal influence on Q_p under a range of inflow conditions: rock avalanche dams produce Q_p values similar to homogeneous dams. Although carapace dams recorded Q_p values 9-13% lower than homogeneous dams for the same geometry and inflow condition, such variation can be considered negligible in the context of the precision of embankment dam breach modelling technologies.

9.3.2 Time to Peak Discharge

The influence of the carapace on t_p depends on inflow conditions. The carapace acts to reduce t_p by ~30% under high inflow, but increases it by ~60% under low inflow (due to crest armouring) when compared to homogenous dams of the same geometry. The time to peak flow observed in the models was between 36 - 120 seconds corresponding to 15 - 40 minutes in a prototype rock avalanche dam 100m high.

9.3.3 Breach Development

Breach formation in carapace dams was identified to be initiated by concentration of subsurface flow at the interface between carapace and body facies, causing seepage to daylight at the toe of the downstream face. At a critical discharge defined as 40-60% of the low inflow condition used in this study, the carapace armouring properties were exceeded and carapace material becomes entrained in the outflow. The breach is then enlarged by regressive slope movement along the longitudinal axis of the dam, lowering the dam crest below the reservoir level and initialising complete removal of the carapace material to form a debris fan at the breach outlet. The time required for the maximum breach geometry to develop (complete failure) in rock avalanche dams (under low inflow) is approximately twice that observed for homogeneous dams due to the armouring properties of the carapace.

Breach erosion and geometry was observed to evolve in three distinct stages identified through the comparison of breach development rates at the breach inlet and outlet. The initial stage is characterised by rapid vertical erosion (channel incision) after the removal of the carapace, while later stages were dominated by lateral erosion at the breach inlet through successive sidewall collapse. In comparison to homogeneous dams, presence of carapace materials appeared to reduce breach depth by 10-15% but enhance width development by 8-12% to produce a funnel shape in plan form, possibly indicative of maximum sediment transport efficiency. Armouring of the breach bed by carapace materials, prevented incision, and maintained a low angle bed slope in the breach channel, leading to the formation of a smaller breach section area and to a consequent smaller peak discharge. The maximum breach cross sectional area was observed to occur within ± 5% of t_p and be trapezoidal in form with sidewall angles slightly higher than the angle of repose for the carapace material.

9.4 Breach Development Simulation in Rock Avalanche Dams

Based on the dataset obtained from physical scale modelling and the use of identical parametric inputs, four models (empirical, parametric, dimensional and physical) were assessed to estimate the uncertainty associated with their prediction of critical breach parameters. BossBREACH (a physically based model) was also tested to evaluate its relevance to breaching in rock avalanche dams, through comparison of simulated breach development rates with those observed in the PSM.

Uncertainty analysis (which considered laboratory error, sensitivity analysis and model performance against the PSM dataset) indicated that typical modelling uncertainty could range from ±19% to ±107% of the predicted peak discharge. Despite the range of uncertainty observed, empirical, parametric and physical models performed consistently for carapace and non carapace dams, generating uncertainty values in agreement with reported value ranges from similar studies. Empirical estimations of peak

discharge, while simplistic, recorded the lowest uncertainty (±19%). Higher uncertainties were associated with parametric and physical model predictions, (± 35-50%) due to a dependence on multiple input parameters, however the uncertainty associated with estimates using dimensional models was considered unacceptable.

The BREACH simulation of linear breach development is moderately consistent with the observed breach development in rock avalanche deposits with a carapace facies. BREACH was unable to simulate armouring using the Smart sediment transport equation, despite sensitivity analysis indicating breach discharges to be insufficient to entrain materials with a d_{50} > 250mm; a block size verified by field investigation to equate to landslide dam stability. Recent modification to the original BREACH model by Corrado *et al.,* (2006) to incorporate a new procedure that considers the bimodal distribution of dam material and uses the Schoklitsch equation to model sediment transport, may be more appropriate to simulate the armouring properties of the carapace. Further research is required to test such a model.

9.5 Rapid Response Hazard Management

Formation of a large landslide dam proximal to a gorge exit presents the greatest risk to downstream populations given the limited response time available before the arrival of the flood wave. Rapid hazard assessment and response primarily requires quantification of the peak discharge to indicate the potential magnitude of the outburst flood.

Empirical methods are therefore recommended for first order assessment of magnitude due to their reliance on parameters that are easily obtainable from aerial and indirect observation. Higher uncertainties associated with parametric and physical model predictions were found to limit their ability to refine empirical estimates, as previous studies have recommended. Parametric and physical models could be incorporated into a secondary response as such methods produce an outflow hydrograph which can be used for downstream routing of the outburst flood, to provide a more accurate determination of more distal hazards. Such models are limited by the requirement for detailed parametric data, often only obtainable by geotechnical site investigation. The value of conducting scenario-based hazard analyses is evident in the immediate need for specific information from which hazard management decisions can be made. Recognition of the hazard posed by landslide dams in New Zealand and abroad, requires guidelines for acceptable societal risk to be incorporated into, and enforced by legislation to provide effective hazard management.

9.6 Scope for Future Research

Due to the complexity of breach development research, this study was only able to address the influence of sedimentology on critical breach parameters. Therefore it is recommended that future research should address;

- probability, magnitude and frequency analysis for catchments whereby the downstream risk of a landslide dam break proximal to a gorge mouth is deemed unacceptable.
- the long term geomorphic influence of landslide dams on confined channel reaches; particularly those incised in deep valleys which evolve into unconfined semi braided systems at the mouth of a gorge.
- steep channel sediment transport during and after landslide dam breaching
- the hydraulics of the armouring process
- the ability of the modified BREACH model developed by Corrado *et al.*,(2006) to simulate the process of armouring through application to an actual rock avalanche dam event
- the influence of lake hyposymetry on breach development processes

References

AS/NZS 1170.0: 2002 Structural Design Actions

Abt, S.R., R.J. Wittler, J.F. Ruff, D.L. LaGrone, M.S. Khattak, J.D. Nelson, N.E. Hinkle, and D.W. Lee, 1988. *Development of Riprap Design Criteria by Riprap Testing in Flumes Phase II. Followup Investigations*, U.S. Nuclear Regulatory Commission, NUREG/CR-4651, ORNL/TM-10100/V2

Adams, J.E. 1981a: Earthquake-dammed lakes in New Zealand. *Geology,* 9:215–19.

ANCOLD 1998, *ANCOLD Guidelines on Risk Assessment*. Position paper for revised criteria for acceptable risk to life. Australian National Committee On Large Dams (ANCOLD) Working Group on Risk Assessment.

Andrews, D. P. 1998.*Embankment failure due to overtopping flow*. ME thesis, University of Auckland, Auckland, New Zealand.

Almeida A.B., and Franca M. 2004. A Computational Model of Rockfill Dam Breaching Caused by Overtopping (RoDaB), *Journal of Hydraulic Research*, 42(2):197-206

Al-Qaser, G.N. 1991. *Progressive failure of an overtopped embankment*. Unpublished PhD Dissertation. Colorado State University. Fort Collins, CO.

Bagnold, R.A., 1966. An Approach to the Sediment Transport Problem from General Physics, *Geological Survey Professional Paper* 422-I, GPO, Washington, DC.

Bathurst, J.C. and Ashiq, M. 1998. Dambreak flood impact on mountain stream bedload transport after 13 years. *Earth Surface Processes and Landforms* 23:643–49.

Bathurst, J.C., Graf, W.H. and Cao, H.H.1996. Bed load discharge equations for steep mountain rivers, in: Sediment Transport In Gravel Bed Rivers, eds. C.R. Thorne and J.C. Bathurst (Wiley, New York).

Brown, R J. and Rogers D.C, 1977.A Simulation of the Hydraulic Events During and Following the Teton Dam Failure," *Proceedings of the Dam-Break Flood Routing Workshop*, Water Resources Council, pp. 131-163

Casagli, N. and Ermini, L. 1999. Geomorphic analysis of landslide dams in the northern Apennine. *Transactions of the Japanese Geomorphological Journal*, 20 (3):219-249.

Casagli, N., Ermini, L., and Rosati, G. 2003. Determining grain size distribution of the material composing landslide dams in the Northern Apennines: sampling and processing methods. *Engineering Geology*, 69: 83-97.

Chanson, H. 1999. *The hydraulics of open channel flow, an introduction*, Wiley, New York, 495pp.

Chanson, H.2005. Modelling a Washout of Dams. *Journal of Hydraulic Research* 43(4):435-438

Chow, V.T. 1959. *Open Channel Hydraulics*. McGraw-Hill, New York, 680pp.

Coleman, S. E., Jack, R. C, and Melville, B. W. 1997. "Overtopping breaching of noncohesive embankment dams". *Proc, 27th Congress of the Int. Association for Hydraulic Research,* San Francisco, D42-D47.

Coleman, S.E. and Andrews, D.P. 2000. *Overtopping breaching of noncohesive homogeneous embankments*. Department of Civil and Resource Engineering, University of Auckland, Auckland.

Coleman, S.E, Andrews, D.P. and Webby, M.G. 2002. Overtopping breaching of noncohesive homogeneous embankments. *Journal of Hydraulic Engineering*, 128: 829-838.

Corrado, C., Andrea, F., Ivan, M., Mara, N., and Paolo, T. 2006. "Some considerations about the simulation of breach channel erosion on landslide dams." *Computational Geosciences*, 10(2): 201-219.

Costa, J.E. 1985. *Floods from dam failures,* U.S. Geological Survey Open-File Report 85-560, Denver, Colorado, 54pp.

Costa, J. E., and Schuster, R. L. 1988. Formation and Failure of Natural Dams. *Geological Society of America Bulletin*, 100(7): 1054-1068.

Costa, J.E. and Schuster, R.L. 1991. Documented historical landslide dams from around the world. *U.S. Geological Survey Open-File Report* 91–239, 486pp.

Costa, J.E. 1988. Floods from dam failures. In Baker, V.R., editor, *Flood Geomorphology*. Chichester: Wiley, pp.439–69.

Cristofano, E.A., 1965. *Method of Computing Erosion Rate for Failure of Earthfill Dams*, U.S. Bureau of Reclamation, Denver, Colorado.

Cruden, D.M. and Hungr, O. 1986. The debris of the Frank Slide and theories of rockslide-avalanche mobility. *Canadian Journal of Earth Sciences*, 23(3):425-432.

Cruden, D.M. and Lu, Z.Y. 1992. The rockslide and debris flow from Mount Cayley, BC, in June 1984. *Canadian Geotechnical Journal* 29:614–26.

Davies, T.R.H. and Scott, B.K. 1997. Dambreak flood hazard from the Callery River, Westland, New Zealand. *Journal of Hydrology New Zealand* 3: 361–13.

Davies, T. R., and McSaveney, M. J. 1999. Runout of dry granular avalanches.*Canadian Geotechnical Journal*, 36(2):313.

Davies, T.R. 2002. Landslide-dambreak floods at Franz Josef Glacier township, Westland, New Zealand: a risk assessment. *Journal of Hydrology (New Zealand)*, 41(1): 1-17.

Davies, T. R., and McSaveney, M. J. 2002. Dynamic simulation of the motion of fragmenting rock avalanches. *Canadian Geotechnical Journal*, 39(4): 789.

Davies, T.R. & McSaveney, M.J. 2004, in press. Rock-avalanche size and runout- implications for landslide dams. In Evans, S.G., Hermanns, R, Scarascia, Mugnozza, G. and Strom, A.L. (eds) *Security of Natural and Artificial Rock-slide Dams*; *NATO Science Series IV Earth and Environmental Sciences*. Dordrecht: Kluwer Academic Publishers.

Dodge, Russell A., 1988. *Overtopping Flow on Low Embankment Dams — Summary Report of Model Tests*, REC-ERC-88-3, U.S. Bureau of Reclamation, Denver, Colorado, August 1988, 28 pp.

Donadini, L. and Kunz, M. 2001. Laboratory model of the Poerua landslide dambreak in 1999 in Westland, New Zealand. Dissertation for the Diploma in Environmental Engineering, VAW, ETH-Zentrum, Zürich, Switzerland, 36pp.

Dunning, S.A. 2004, unpublished. Rock Avalanches in High Mountains. PhD Thesis, University of Luton, United Kingdom.

Dunning SA 2004.The grain-size distribution of rock avalanche deposits. In: Abdrakhmatov K, Evans

S.G, Hermanns R.L, Scarascia Mugnozza G, Strom AL (eds) Security of natural and artificial rockslide dams. Kluwer, Dordrecht, pp. 38–43.

Dunning, S.A., Petley, D.N., and Strom, A.L. 2005. the morphologies and sedimentology of valley confined roc-avalanche deposits and their effect on potential dam hazard. *In* Hungr, O, Fell, R, Couture, R. & Eberhardt, E. (eds) Landslide Risk Management. A.T. Balkema, Amsterdam, pp.691-704.

Dunning, S.A., Rosser, N.J., Petley, D.N. & Massey, C.J. 2005, in review. The formation and failure of the Tsatichhu rock-avalanche dam, Bhutan.

Dunning S.A, Petley D.N, Strom A.L 2005a, unpublished. The morphologies and sedimentology of valley confined rock -avalanche deposits and their effect on potential dam hazard.

Dunning SA, McSaveney MJ, Davies TR, Petley, DN 2005b. Significance of the fractal grain-size distributions of rock-avalanche deposits. Abstracts Volume, 6th International Conference on Geomorphology, Zaragoza, September 7–11, 2005, Francisco Guti´errez, Mateo Guti´errez, Gloria Desir, Jes´us Guerrero, Pedro Lucha, Cinta Mar´ın, Jos´e Mar´ıa Garc´ıa-Ruiz (eds).

Dunning SA, Armitage PJ (2005) The grain-size distribution of rock-avalanche deposits: implications for natural dam stability. In: Abdrakhmatov K, Evans SG, Hermanns RL, Scarascia Mugnozza G, Strom AL (eds) Security of natural and artificial rockslide dams. NATO Science Series IV: Earth and Environmental Sciences, Dordrecht

Eisbacher, G.H. 1979. Cliff collapse and rock avalanches (sturzstroms) in the Mackenzie Mountains, north-western Canada. *Canadian Geotechnical Journal*, 16:309-334.

Ermini, L. & Casagli, N. 2003. Prediction of the behaviour of landslide dams using a geomorphological dimensionless index. *Earth Surface Processes and Landforms*, 28:31-47.

Evans, S.G., 1986.The Maximum Discharge of Outburst Floods Caused by the Breaching of Man-Made and Natural Dams," *Canadian Geotechnical Journal*, vol. 23, August 1986

Evans, S.G. 1989. Rock avalanche run-up record. *Nature* 340: 271.

Finley, P.J. and Fell, R. 1997. Landslides: risk perception and acceptance. *Canadian Geotechnical Journal*, 34: 169-188.

Fread, D.L., 1988 (revised 1991), *BREACH An Erosion Model for Earthen Dam Failures*, National Weather Service, National Oceanic and Atmospheric Administration, Silver Spring, Maryland.

Fread, D. L., 1996. Dam-Breach Flood, *in* Singh, V. P., ed., *Hydrology of Disasters*, Kluwer, pp.85-126

Froehlich, D.C., 1987. Embankment-Dam Breach Parameters, *Hydraulic Engineering*, Proceedings of the 1987 ASCE National Conference on Hydraulic Engineering pp. 570-575.

Froehlich, D.C., 1995a. Peak Outflow from Breached Embankment Dam, *Journal of Water Resources Planning and Management*, vol. (121)1: 90-97.

Froehlich, D. C., 1995b. "Embankment Dam Breach Parameters Revisited," *Water Resources Engineering*, Proceedings of the 1995 ASCE Conference on Water Resources Engineering, San Antonio, Texas. pp. 887-891

Galland, J. and Morris, M. 1999. CADAM European Concerted Action on Dam-break Modelling. *Proceedings of the 28th Congress of the Int. Association for Hydraulic Research,* Graz, Austria.

Geo-Slope Office .2003. SLOPE/W, SEEP/W, QUAKE/W. Geo-Slope International, Calgary.

Graf, W.H. and Altinakar, M.S. 1998. *Fluvial Hydraulics-Flow and Transport Processes in Channels of Simple Geometry*. JohnWiley and Sons, Sussex.

Grant, G. E. 1997. Critical flow constrains flow hydraulics in mobile-bed streams; a new hypothesis. *Water Resources Research*., 33: 349–358

Hagen, V. K., 1982. Re-evaluation of design floods and dam safety: Fourteenth ICOLD Congress, Rio de Janiero.

Hahn, W., G.J. Hanson, and K.R. Cook. 2000. Breach morphology observations of embankment overtopping tests. *Proceedings of the 2000 Joint Conference of Water Resources Eng., Planning, and Management*, ASCE. Minneapolis,10pp.

Hancox, G. T. 1999. Mt Adams rock avalanche of 6 October 1999 and the subsequent formation and breaching of a large landslide dam in Poerua River, Westland, New Zealand, Institute of Geological and Nuclear Sciences, Lower Hutt, N.Z.

Hancox, G. T., McSaveney M.J., Manville V., Davies T.R., 2005. The October 1999 Mt Adams rock avalanche and subsequent landslide dam-break flood and effects in Poerua River, Westland, New Zealand. *New Zealand Journal of Geology & Geophysics, 2005,* (48): 683–705.

Hanson, G. J., K.R. Cook, W. Hahn, and S. L. Britton. 2003. Observed erosion processes during embankment overtopping tests. ASAE Paper No. 032066.

Hartung, F. and H. Scheuerlein, 1970. "Design of Overflow Rockfill Dams," in *Proceedings*, International Commission on Large Dams, Tenth International Congress on Large Dams, Q.36, R.35, Montreal, Canada, June 1-5, 1970, pp. 587-598.

Henderson, F.M., 1966. Open channel flow: New York, MacMillan, 522 pp.

Hewitt, K. 1999. Quaternary Moraines vs Catastrophic Rock Avalanches in the Karakoram Himalaya, Northern Pakistan. *Quaternary Research*, 51: 220-237.

Hewitt, K. 2001. Catastrophic rockslides and the geomorphol-ogy of the Hunza and Gilgit River Valleys, Karakoram Himalaya, *Erdkunde*, Band 55.

Hungr, O. 1999. Landslide/debris flow runout prediction for risk assessment, Forest Renewal BC.

Hungr, O., Evans, S.G., Bovis, M. and Hutchinson, J.N., 2001. Review of the classification of landslides of the flow type. *Environmental and Engineering Geoscience*, (7): 221-238

Hutchinson, J.N., 1988. General Report; Morphological and geotechnical parameters of landslides in relation to geology and hydrology, in Bonnard, ed., Landslides, Proceedings, 5th International Symposium on Landslides, Lausanne, (1): 3-35

Hsu, K.J 1978. Albert Heim; Obersvations on landslides and relevance to modern interpretations. In Voight B (ed) *Rockslides and avalanches*. 1. Natural phenomena, 71-93. Elsevier, New York.

Jack, R. 1996. The mechanics of embankment failure due to overtopping flow. ME thesis, University of Auckland, New Zealand.

Jarrett, R. D. 1984. Hydraulics of high-gradient streams, *Journal of. Hydraulic Engineering.110*: 1519–1539

Jarrett, R. D. 1988. Hydrologic and hydraulic research in mountain rivers. *IAHS Publication (International Association of Hydrological Sciences)* (190): 107-119.

Johnson, F. A., and Illes, P. 1976. Classification of Dam Failures. *International Water Power and Dam Construction*, 28(12): 43-45.

Kaliser, B. N., and Fleming, R. W. 1983. Landslide dam at Thistle, Utah. Seattle, WA, USA. pp.59-83.

Kilburn, C.R.J., and Sorensen, S.A., (1998), Runout lengths of Sturzstroms: the control of initial conditions and of fragment dynamics: *Journal of Geophysical Research*, (103) :17877-17884.

Kirkpatrick, Gerald W., 1977. "Evaluation Guidelines for Spillway Adequacy," *The Evaluation of Dam Safety*, Engineering Foundation Conference, Pacific Grove, California, ASCE, pp. 395-414

King, J., Loveday, I. and Schuster, R.L. 1989. The 1985 Bairaman landslide dam and resulting debris flow, Papua New Guinea. *Quarterly Journal of Engineering Geology (*22): 257–70.

Kollgaard Eric B. and Wallace L. Chadwick, 1988. "Development of Dam Engineering in the United States, Prepared in commemoration of the sixteenth congress (of ICOLD) by the United States Committee on Large Dams, Pergamon.

Kojan, E., and Hutchinson, J. N., 1979. Maynumarca rockslide and debris flow, *in* Voight, B., ed.,Rockslides and avalanches 1:Developments in Geotechnical Engineering, Elsevier, pp. 315-361.

Korup, O. 2002. Recent research on landslide dams a literature review with special attention to New Zealand. *Progress in Physical Geography*, (26): 206-235.

Korup, O. 2004. Geomorphometric characteristics of New Zealand landslide dams. *Engineering Geology*, (73): 13-35.

Korup, O. 2005. Geomorphic hazard assessment of landslide dams in South Westland, New Zealand: fundamental problems and approaches. *Geomorphology*, 66(1-4): 167-188.

Li, T. 1989. Landslides extent and economic significance in China. In Brabb, E.E. and Harrod, B.L., editors, *Landslides. Extent and economic significance. Proceedings 28th International Geological Congress Symposium on Landslides*, 17 July, Washington, D.C. Rotterdam: Barkema, pp.271–87.

Lou, W.C., 1981. *Mathematical Modelling of Earth Dam Breaches*. Unpublished PhD Thesis, Colorado State University, Fort Collins, Colorado.

Loukola E.P, Reiter, S. Chonggang and P. Shubio 1993. Embankment Dams and Their Foundations: Evaluation of Erosion; International Workshop on Dam Safety Evaluation Vol 4., ICOLD Switzerland, pp.17-46

Manville, V., 2001. *Techniques for evaluating the size of potential dam-break floods from natural dams.* Institute of Geological and Nuclear Sciences SR 2001/28.

Macchione, F., and B. Sirangelo, 1988, "Study of Earth Dam Erosion Due to Overtopping," *Proceedings of the Technical Conference on Hydrology of Disasters*, WMO, Geneva, Switzerland, pp. 212-219.

MacDonald, T.C., and J. Langridge-Monopolis, 1984. "Breaching Characteristics of Dam Failures," *Journal of Hydraulic Engineering*, (110)5 :567-586.

McSaveney,M.J., 2002. Recent rockfalls and rock avalanches in Mount Cook National Park, New Zealand: Reviews in Engineering Geology: Catastrophic Landslides: effects, occurrence, and mechanisms.(15): 35-71.

McSaveney, M.J. and Davies, T.R.H. *in press* 2003. Rapid rock-mass flow with dynamic fragmentation. *In* Evans, S.G., Martino, S.(eds) NATO Advanced Research Workshop: *Massive rock slope failure New Models for hazard assessment*. Celano, Italy, 2002.

Melosh, H.J., 1987. The mechanics of large rock avalanches. *Rev Eng Geol* VII, 41-49.

Meyer, W., Schuster, R. L., and Sabol, M. A. 1994. Potential for seepage erosion of landslide dam. *Journal of Geotechnical Engineering*, 120(7): 1211-1229.

Mohamed, M., Samuels, P. G., and Morris, M. W. Uncertainties in dam failure modelling with the US NWS BREACH model. Cardiff, United Kingdom.

Morris M. 2000.Concerted Action on Dambreak Modelling (CADAM). Report SR 571.

Nash, T. R. 2003. Engineering geological assessment of selected landslide dams formed from the 1929 Murchison and 1968 Inangahua earthquakes. MSc thesis. University of Canterbury, Christchurch, New Zealand.

Novak, P. and Cábelka, J. 1981. *Models in Hydraulic Engineering,* Pitman, London, 459 p.

New Zealand Society on Large Dams. 2000. *New Zealand Dam Safety Guidelines.* NZSOLD Report

Okura, Y., Kitahara, H. Sammori, T. Kawanami, A 2000. The effects of rock fall volume on runout distance: *Engineering Geology*, (58):109-124

Ollett, P.P. 2000. Landslide dambreak flooding in the Callery River, Westland. Unpublished M.Eng. (Nat. Res.) thesis, Lincoln University, 90 pp.

Peakall, J. Ashworth J., Best J**.** 1996. Physical modelling in fluvial geomorphology: principles, applications and unresolved issues In: Rhoades, B.L. and Thorn, C.E. (eds) *The Scientific Nature of Geomorphology,* Wiley and Sons, Chichester, pp.221-253

Peakall J, Warburton J. 1996. Surface tension in small hydraulic river models – the significance of Weber number. *Journal of Hydrology (NZ)* 35(2): 199–212.

Pierson, T. C., 1995. Flow characteristics of large eruption-triggered debris flows at snow-clad volcanoes: constraints for debris-flow models: *J. Volc. Geoth. Res.*, (66): 283-294.

Pierson, T. C., 1997. Transformation of water flood to debris flow following the eruption-triggered transient-lake breakout from the crater on 19 March 1982, *in* Pierson, T. C., ed., Hydrologic consequences of hot-rock/snowpack interactions at Mount St. Helens volcano, Washington, 1982-84, United States Geological Survey.

Plaza-Nieto, G. and Zevallos, O. 1999. The La Josefina rockslide, in The 1993 La Josefina rockslide and Río Paute landslide dam. In K. Sassa, *Landslides of the world,* Japan Landslide Soc., Kyoto Univ. Press, pp. 355-358.

Ponce, V. M., and A.J. Tsivoglou, 1981. "Modelling Gradual Dam Breaches," *Journal of the Hydraulics Division, Proceedings of the ASCE*, vol. 107 (7):829-838.

Powledge, G. R., D.C. Ralston, P. Miller, Y.H. Chen, P.E. Clopper, and D.M. Temple, 1989a. "Mechanics of Overflow Erosion on Embankments. I: Research Activities," *Journal of Hydraulic Engineering*, (115) 8: 1040-1055.

Powledge, G.R., D.C. Ralston, P. Miller, Y.H. Chen, P.E. Clopper, and D.M. Temple, 1989b. "Mechanics of Overflow Erosion on Embankments. II: Hydraulic and Design Considerations," *Journal of Hydraulic Engineering*, vol. 115 (8): 1056-1075.

Price, J. T., Lowe, G. W., and Garrison, J. M., 1977. Unsteady flow modeling of dam-break waves: Proceedings Dam-break flood routing workshop, Bethesda, Maryland. U.S. Water Resources Council, Washington D.C., pp. 90-130

Pugh, C.A., 1985. *Hydraulic Model Studies of Fuse Plug Embankments*, REC-ERC-85-7, U.S. Bureau of Reclamation, Denver, Colorado, December 1985, 33 pp.

Ralston, D. C. 1987. Mechanics of embankment erosion during overflow. Proceedings of the 1987 National Conference on Hydraulic Engineering, Hydraulics Division of ASCE. pp.733-738.

Rathgeb, A. 2000. http://www.iahr.org/membersonly/grazproceedings99/doc/000/000/438.htm

Rickenmann, D. 1991. "Hyperconcentrated flow and sediment transport at steep slopes." *Journal of Hydraulic Engineering*, 117(11): 1419-1439.

Sammis, C., King, G. & Biegel, R. 1987. The kinematics of gouge formation. *Pure and Applied Geophysics*.125 (5): 777-812.

Schoklitsch, A. 1962 Handbuch des Wasserbaues (Springer, Wien).

Schuster, R.L. 1993. Landslide dams – a worldwide phenomenon. *Proceedings Annual Symposium of The Japanese Landslide Society, Kansai Branch*, 27 April, Osaka, pp.1–23.

Schuster, R.L.2000. Outburst debris flows from failure of natural dams. *Proceedings 2nd International Conference on Debris Flow Hazard Mitigation*, 16–20 August, Taipeh, pp.29–42.

Skoglund M. and Solvik O. 1995, External and Internal Erosion in Rockfill Dams, Hydropower and Dams, May, pp.44-77

Smart, G. M., and Jaeggi, M. 1983.. Sediment transport in steilen Gerinnen. Sediment transport on steep slopes. Mitteilung Nr. 64 der *Versuchsanstalt für Wasserbau, Hydrologie und Glaziologie*, ETH, Zürich.

Smart, G.M., 1984. "Sediment Transport Formula for Steep Channels," *Journal of Hydraulic Engineering*, vol. 110 (3): 267-276.

Singh, V.P., and P.D. Scarlatos, 1985. *Breach Erosion of Earthfill Dams and Flood Routing BEED Model*, Research Report, Army Research Office, Battelle, Research Triangle Park, North Carolina, 131 pp.

Singh, V.P., and P.D. Scarlatos, 1988. "Analysis of Gradual Earth-Dam Failure," *Journal of Hydraulic Engineering*, (114)1: 21-42.

Singh, V. P. 1996. *Dam breach modelling technology*, Kluwer Academic Publishers, Dordrecht ; Boston.

Smith, G. M. 2003. The coseismicity and morphology of the Acheron rock avalanche deposit in the Red Hill valley, New Zealand : a thesis submitted in fulfillment of the requirements for the degree of Master of Science in Engineering Geology at the University of Canterbury.

Strom, A.L., 1999. The morphology and internal structure of large rockslides as indicators of their formational mechanisms. *Dolkady Earth Sciences*, 369(8): 1079-1081.

Strom, A.L. & Pernik, L.M. 2004. Utilization of the data on rockslide dams formation and structure for blast-fill dams design. In Abdrakhmatov, K., Evans, S.G., Hermanns, R., Scarascia Mugnozza, G. & Strom, A.L. (eds) *Security of Natural and Artificial Rockslide Dams, extended abstracts volume, NATO Advanced Research Workshop, Bishkek, Kyrgyzstan, June 8 – 13*, *2004*, pp.177-182.

Trieste, D.J. 1992. Evaluation of supercritical/ subcritical flows in high gradient channels, *J. Hydraul. Eng*., (*118*): 1107–1118,

U.S. Bureau of Reclamation, 1988. *Downstream Hazard Classification Guidelines*, ACER Technical Memorandum No. 11, Engineering and Research, Denver, Colorado, December 1988, 57 pp.

Varnes, D.J., Cruden. D.M., 1996. Landslides: investigation and mitigation. Turner, K., Schuster, R.L., (ed) Special Report (National Research Council (U.S) Transportation Research Board 673.

Visser, P.J. 1998. Breach Growth in Sand-Dikes. Communications on Hydraulic and Geotechnical Engineering. Report no. 98-1. Hydraulic and Geotechnical Engineering Division. Faculty of Civil Engineering and Geosciences. Delft University of Technology.

Voight, B., 1978. Rockslides and Avalanches: an introduction, in Voight, B., ed., Rockslides and Avalanches.1.Natural Phenomena, Volume 1, Elsevier, Amsterdam.

Von Thun, J. Lawrence, and David R. Gillette, 1990. *Guidance on Breach Parameters*, unpublished internal document, U.S. Bureau of Reclamation, Denver, Colorado, March 13, 1990, 17 pp.

Walder, J.S. and O'Connor, J.E. 1997. Methods for predicting peak discharge of floods caused by failure of natural and constructed earthen dams. *Water Resources Research (*33): 237–48.

Wahl, T.L. 1998. *Prediction of embankment dam breach parameters A literature review and needs assessment*. DSO-98-004. Dam Safety Office, Water Resources Research Laboratory, U.S. Bureau of Reclamation. Denver, CO.

Wahl, T. L. 2004. Uncertainty of predictions of embankment dam breach parameters. *Journal of Hydraulic Engineering*, 130(5): 389-397.

Webby, M. G., and Jennings, D. N. 1994. ''Analysis of dam break flood caused by failure of Tunawaea landslide dam.'' *Proc, Int. Conf. on Hydraulics in Civil Engineering,* Brisbane, Australia, pp.163-168.

Whitehouse, I.E. 1983. Distribution of large rock avalanche deposits in the central Southern Alps, New Zealand. *New Zealand Journal of Geology and Geophysics (*26): 272–79.

Whitehouse, I.E. and Griffiths, G.A. 1983. Frequency and hazard of large rock avalanches in the central Southern Alps. *Geology* (11): 331–34.

Wurbs, Ralph A., 1987. Dam-Breach Flood Wave Models. *Journal of Hydraulic Engineering*, (113).

Yalin, M.S. 1971. *Theory of Hydraulic Models.* Macmillan, Oxford.

Yang C.T. 1996. Sediment Transport Theory and Practise, McGraw-Hill.

Young, W.J and Warburton, J. 1996. Principles and practice of hydraulic modelling of braided gravel-bed rivers. *Journal of Hydrology (NZ)* 35(2):175–198.

Zaslavsky, Y. and Shapira, A., 2000. Experimental study of topographic amplification using the Israel seismic network, *Journal of Earthquake Engineering*, (4)1:43-65

Appendices

Appendix A

Importance level	Comment	Examples
1	Structures presenting a low degree of hazard to life and other property	Farm buildings, isolated structures, towers in rural situations Fences, masts, walls, in-ground swimming pools
2	Normal structures and structures not in other importance levels	Hotels, offices, and apartments less than 15 storeys high Car parking buildings Shopping centres less than 10 000 m^2 gross area
3	Structures that as a whole may contain people in crowds or contents of high value to the community or pose risks to people in crowds	Emergency medical and other emergency facilities not designated as post-disaster Airport terminals, principal railway stations, correctional institutions, schools, colleges, universities Structures over 15 storeys high of the following types: (a) Hotels and motels (b) Apartment buildings (c) Offices Public assembly buildings of more than 1000 m^2 Public museums and art galleries of more than 1000 m^2 Shopping centres with covered malls with over 10 000 m^2 gross area excluding parking Grandstands for more than 10 000 people
4	Structures with special post-disaster functions	Major infrastructure facilities, e.g., power stations, substations Air traffic control installations Designated civilian emergency centres, medical emergency facilities, emergency vehicle garages and their fuel supplies and ambulance, fire and police stations, etc. Ancillary installations necessary for the operation of Importance level 4 structures (emergency power, phone, radio, etc.)
5	Special structures (outside the scope of this Standard—acceptable probability of failure to be determined by special study)	Structures that have special functions or whose failure poses catastrophic risk to a large area (e.g. 100 km^2) or a large number of people (e.g. 100 000) Dams, extreme hazard facilities

Appendix A-1 Importance Levels For Building Types - NZ Structures (AS/NZS 1170.0 2002)

Importance level	Annual probability of the design event for safety		
	Wind	Snow	Earthquake
1	1/100	1/50	1/100
2	1/500	1/150	1/500
3	1/1000	1/250	1/1000
4	1/2000	1/500	1/2500

Appendix A-2 Reference Probability of Exceedance (AS/NZS 1170.0 2002)

Appendix B Legislation

1) Resource Management Act 1991

Section 5 Purpose

1. The purpose of this Act is to promote the sustainable management of natural and physical resources.
2. In this Act, "sustainable management" means managing the use, development, and protection of natural and physical resources in a way, or at a rate, which enables people and communities to provide for their social, economic, and cultural well being and for their health and safety while:

   (a) Sustaining the potential of natural and physical resources (excluding minerals) to meet the reasonably foreseeable needs of future generations; and

   (b) Safeguarding the life-supporting capacity of air, water, soil, and ecosystems; and

   (c) Avoiding, remedying, or mitigating any adverse effects of activities on the environment.

Section 24 Functions of Minister for the Environment

The Minister for the Environment shall have the following functions under this Act:

(a) The recommendation of the issue of national policy statements under section 52:

(b) The recommendation of the making of regulations under section 43:

(c) The call-in of projects for decision under section 140:

(d) The recommendation of the approval of an applicant as a requiring authority under section 167 or a heritage protection authority under section 188:

(e) The recommendation of the issue of water conservation orders under section 214:

(f) The monitoring of the effect and implementation of this Act (including any regulations in force under it), national policy statements, and water conservation orders:

(g) The monitoring of the relationship between the functions, powers, and duties of central government and local government under this Part, and the functions, powers, and duties of the Hazards Control Commission under Part XIII:

(h) The consideration and investigation of the use of economic instruments (including charges, levies, other fiscal measures, and incentives) to achieve the purpose of this Act:

(i) Any other functions specified in this Act.

Section 30 Functions of regional councils under this Act

(1) Every regional council shall have the following functions for the purpose of giving effect to this Act in its region:

(a) The establishment, implementation, and review of objectives, policies, and methods to achieve integrated management of the natural and physical resources of the region:

(b) The preparation of objectives and policies in relation to any actual or potential effects of the use, development, or protection of land, which are of regional significance:

(c) The control of the use of land for the purpose of:

(i) Soil conservation;

(ii) The maintenance and enhancement of the quality of water in water bodies and coastal water;

(iii) The maintenance of the quantity of water in water bodies and coastal water;

(iv) The avoidance or mitigation of natural hazards;

(v) The prevention or mitigation of any adverse effects of the storage, use, disposal, or transportation of hazardous substances;

(d) In respect of any coastal marine area in the region, the control (in conjunction with the Minister of Conservation) of:

(i) Land and associated natural and physical resources;

(ii) The occupation of space on lands of the Crown or lands vested in the regional council, that are foreshore or seabed and the extraction of sand, shingle, or other natural material from that land;

(iii) The taking, use, damming, and diversion of water;

(iv) Discharges of contaminants into or onto land, air, or water and discharges of water into water;

(v) Any actual or potential effects of the use, development, or protection of land, including the avoidance or mitigation of natural hazards and the prevention or mitigation of any adverse effects of the storage, use, disposal, or transportation of hazardous substances;

(vi) The emission of noise and the mitigation of the effects of noise;

(vii) Activities in relation to the surface of water;

(e) The control of the taking, use, damming, and diversion of water, and the control of the quantity, level, and flow of water in any water body, including:

(i) The setting of any maximum or minimum levels or flows of water;

(ii) The control of the range, or rate of change, of levels or flows of water;

(iii) The control of the taking or use of geothermal energy;

(f) The control of discharges of contaminants into or onto land, air, or water and discharges of water into water;

(g) In relation to any bed of a water body, the control of the introduction or planting of any plant in, on, or under that land, for the purpose of:

(i) Soil conservation;

(ii) The maintenance and enhancement of the quality of water in that water body;

(iii) The maintenance of the quantity of water in that water body;

(iv) The avoidance or mitigation of natural hazards;

(h) Any other functions specified in this Act;

(2) The functions of the regional council and the Minister of Conservation in subsection (1) (d) (i) do not apply to the control of the harvesting or enhancement of populations of aquatic organisms, where the purpose of that control is to conserve, enhance, protect, allocate, or manage any fishery controlled by the Fisheries Act 1983.

Section 31 Functions of territorial authorities under this Act

Every territorial authority shall have the following functions for the purpose of giving effect to this Act in its district:

(a) The establishment, implementation, and review of objectives, policies, and methods to achieve integrated management of the effects of the use, development, or protection of land and associated natural and physical resources of the district;

(b) The control of any actual or potential effects of the use, development, or protection of land, including the implementation of rules for the avoidance or mitigation of natural hazards and the prevention and mitigation of any adverse effects of the storage, use, disposal, or transportation of hazardous substances;

(c) The control of subdivision of land;

(d) The control of the emission of noise and the mitigation of the effects of noise;

(e) The control of any actual or potential effects of activities in relation to the surface of water in rivers and lakes;

(f) Any other functions specified in this Act.

2) Civil Defence Emergency Management Act 2002

Part 3

Civil defence emergency management planning and civil defence emergency management duties (Section 31 to 65).

Section 37

- Groups and Director must not act inconsistently with national civil defence emergency management strategy

- A Civil Defence Emergency Management Group must ensure that its actions in exercising or performing its functions, duties, and powers under this Act are not inconsistent with any national civil defence emergency management strategy that is for the time being in force.

- The Director must ensure that his or her actions in exercising or performing his or her functions, duties, and powers under this Act are not inconsistent with any national civil defence emergency management strategy that is for the time being in force.

Section 48 ***Civil defence emergency management group plans***

Every Civil Defence Emergency Management Group must prepare and approve a civil defence emergency management group plan.

Section 53

Civil defence emergency management group plan must not be inconsistent with national civil defence emergency management strategy and must take account of Director's guidelines, codes, or technical standards

A civil defence emergency management group plan must not be inconsistent with the national civil defence emergency management strategy in force when the plan is approved.

A civil defence emergency management group plan must take account of the guidelines, codes, or technical standards issued by the Director under this Act.

3) Building Act 2004

Part 2 Building (section 15 to 168)

Section 153; Meaning of dangerous dam

A dam is dangerous for the purposes of this Act if the dam—

(a) is a high potential impact dam or a medium potential impact dam; and
(b) is likely to collapse—

(i) in the ordinary course of events; or
(ii) in a moderate earthquake (as defined in the regulations); or
(iii) in a moderate flood (as defined in the regulations); or

(c) is a leaky dam.

Section 161; Regional authority must adopt policy on dangerous dams

(1) A regional authority must, within 18 months after the commencement of this Part, adopt a policy on dangerous dams within its district.

(2)The policy must state—

a) the approach that the regional authority will take in performing its functions under this Part; and
b) the regional authority's priorities in performing those functions; and
c) how the policy will apply to heritage dams.

Appendix C OUTFLOW3.xls (Manville, 2001)

This Microsoft Excel 97™ spreadsheet incrementally calculates the breach outflow from a reservoir using user-specified parameters of final breach dimensions, breach development time, and the surface area of the reservoir at the start and end of the run. The model accounts for a reservoir whose surface area decreases with falling level, and declining hydraulic head and effective breach top width as the lake level falls during drainage. Three alternative broad-crested weir equations (discussed in section 3) are utilised on the different sheets, with their respective answers collated on the first sheet for comparison.

Four key assumptions are made:

1. The lake is shaped like a funnel, with a constant side-slope
2. The rate of breach growth is linear, i.e. top width, basal width, and breach depth all increase simultaneously
3. The lake is full to the top of the dam when failure occurs, failure is by overtopping.
4. Mean discharge for each time-step is calculated from the average of the discharges at the end of the current and the previous time step. This is multiplied by the duration of the time-step to obtain the volume of outflow during that interval.

This parametric method is a rapid means of testing the sensitivity of the peak discharge to variations in the breach size and development time. Experimenting with different values of breach size and development time is a way of constraining the peak discharge estimates generated by other methods in this report.

Using the spreadsheet:

1. Open OUTFLOW3.xls
2. Enter user-specified values for the final breach dimensions, breach development time, and the surface area of the lake at the top of the dam and at the base of the final breach.
3. The spreadsheet automatically calculates the evolving breach outflow hydrograph over a period of 100 time-steps, and then the lake outflow hydrograph over an additional 100

time-steps using three alternative forms of the broad-crested weir equation for trapezoidal breaches.

4. Time-series plots of breach discharge (i.e. the outflow hydrograph), lake level, breach base level, and

effective head are generated automatically. The vertical scales of these graphs may need adjusting by the user, depending on the range of dam crest and breach base elevations.

5. Values for the peak discharge, the time of peak discharge, and the lake elevation at this time are extracted from the spreadsheet.

Digital Appendices

Appendix D Outflow Hydrograph Calculation

Appendix E Summary of Breach Discharges

Appendix F Breach Geometry Calculation

Appendix G Model Testing

Appendix H BossBREACH Output Files

Appendix I Sensitivity Analysis for BossBREACH

Appendix J Digital Video Data for Dam Trials (DVD)